Università degli Studi di Padova

Dipartimento di Scienze Chimiche

SCUOLA DI DOTTORATO DI RICERCA IN SCIENZE MOLECOLARI

Indirizzo SCIENZE CHIMICHE

Ciclo XXVIII

Functionalized short peptides and polypeptides: from organic reactions, through secondary structure control, to supramolecular applications

Direttore della Scuola: Ch.mo Prof. Antonino Polimeno

Coordinatore d'indirizzo: Ch.mo Prof. Antonino Polimeno

Supervisore: Prof. Alessandro Moretto

Dottorando: Daniela Mazzier

INDEX

ABSTRACT

Short helical peptides

Peptides with a well-defined helical conformation were examined with the aims of reinforcing their secondary structure or using their rigid conformation to control asymmetric induction over long distances.

In the first example, two consecutive *i*, *i*+4 intramolecular side chain-to-side chain macrocyclization reactions of different type, carried out on a preformed, partially helical linear peptide resulted in a double stapled, overlapping, bicyclic oligopeptide system. A detailed CD and NMR conformational study revealed that the mixed 3_{10}/α-helical conformation exhibited by the original linear peptide is converted into a fully-developed α-helix in the bicyclic peptide. In parallel, both the helix overall content and stability are significantly increased. In the second part, an achiral Aib-based helical foldamer was appropriately functionalized with the photoswitchable fumaramide/maleamide linkage, thus obtaining a system in which a screw sense preference may be activated by the absorption of UV light. The *trans* configuration in the fumaramide linkage holds the chiral residue away from the achiral portion of the oligomer, preventing the induction of a conformational preference. However, after photoisomerization, the *cis* configuration of the maleamide brings the chiral and achiral portions into proximity, generating a pronounced preference for one of the two possible, helical screw senses. In conclusion, we showed that it is feasible to use light to switch on and off the ability of the molecules to react strereoselectively in a chain extension reaction, or to modulate helix-to-helix communication.

Functionalized helical polypeptides

The well-known, rod-like α-helical polypeptide poly(γ-benzyl-L-glutamate) (PBLG) was selected for this study. The possibility to create self-assembled microstructures with different characteristics, shapes and functions from different PBLG-conjugates was explored.

Mono- and *bis*-fullerene (C_{60})-PBLG conjugates were obtained by one-pot thiol-ene chemistry. These systems showed the propensity to self-assemble in water creating precise bulky microstructures of toroidal or vesicular shape. In a second part, we reported the synthesis of star-shaped carbon quantum dots (CQDs)-PBLG conjugates that self-assemble into microstructures and retain the characteristic emission properties of the native dots. CQDs, prepared by microwave-assisted carbonization of Arg and 1,2-ethylendiamine in water, were

used either as initiators to afford a daisy-like peptide-polymer structure, or as capping agents towards more elaborated hybrid nanostructures that self-assemble into supramolecular aggregates of spherical shape. Finally, smart microstructures with photoresponsive behavior was obtained by the insertion of azobenzene-containing α-amino acids in PBLG systems. We created two systems, with either C_2- or C_3-symmetry, that self-assemble in spherical structures. The change in their 3D-structure after light irradiation is followed by a variation in the morphology of the aggregates.

Self-assembling short peptides

The synthesis and self-assembly properties of two different peptide systems were studied. The first series of compounds contain the photoswitchable α-amino acid *bis*[*p*-(phenylazo)benzyl]glycine, which undergoes a reversible *cis-trans* isomerization upon exposure to light at the appropriate wavelengths. Derivatives and short peptides containing this α-amino acid are able to promote the formation of well-ordered supramolecular structures. Interestingly, the morphological transition observed after UV-light irradiation proved to be reversible due to the presence of the two side-chain azobenzene groups.

In the second part, we investigated the hydrophobic, terminally-protected dipeptide Boc-L-Cys(Me)-L-Leu-OMe that it is able to hierarchically self-assemble producing nano-, micro- and macroscale complex architectures, including hollow rods, under appropriate conditions. Our results suggested that its self-assembly properties might be related to the occurrence in its single crystal structure of a supramolecular sixfold helix motif. Subsequently, we decided to chemically modify the molecule to obtain a diacetylene derivative. This final compound is able to form an organogel or spherical aggregates, which undergo a topochemical polymerization under UV-light irradiation.

RIASSUNTO

Peptidi elicoidali corti

In questo lavoro di tesi sono stati studiati diversi peptidi caratterizzati da una ben definita conformazione elicoidale con lo scopo di stabilizzarne la struttura secondaria oppure di sfruttare la loro conformazione rigida come mezzo per controllare l'induzione asimmetrica su lunghe distanze.

Il primo esempio, un sistema oligopeptidico biciclico doppiamente stabilizzato, è stato ottenuto tramite due reazioni di macrociclizzazione che hanno coinvolto le catene laterali dei residui in posizione *i* e *i*+4 di un peptide lineare. Un'indagine conformazionale dettagliata, condotta utilizzando le spettroscopie CD ed NMR, ha rivelato che la conformazione mista 3_{10}/α-elica, osservata per il peptide lineare, risulta completamente convertita in una struttura ad elevato contributo α-elicoidale nel peptide biciclico. In parallelo, sia il contenuto totale di elica sia la stabilità risultano significativamente aumentati. Nel secondo caso, un foldamero achirale elicoidale a base di Aib è stato opportunamente funzionalizzato con il gruppo fotoisomerizzabile fumarammide/maleammide contenente un residuo chirale. In questo modo è stato ottenuto un sistema in cui è stato possibile influenzare il senso di spiralizzazione dell'elica grazie all'uso di luce ultravioletta. La configurazione *trans* nella fumarammide, infatti mantiene il residuo chirale lontano dal segmento achirale dell'oligomero, rendendo impossibile l'induzione di una conformazione preferenziale. Tuttavia dopo l'isomerizzazione, la configurazione *cis* della maleammide consente alla parte chirale e a quella achirale di essere spazialmente vicine, con conseguente induzione di chiralità e adozione di un senso preferenziale di spiralizzazione. Sfruttando questo principio è stato quindi possibile utilizzare la luce per accendere o spegnere la capacità del sistema di reagire stereoselettivamente, oppure di modulare la comunicazione di chiralità tra due segmenti elicoidali.

Polipeptidi elicoidali funzionalizzati

Con lo scopo di ottenere tramite *self-assembly* microstrutture con differenti caratteristiche, forme e funzioni sono stati sintetizzati diversi sistemi coniugati a base di poli(γ-benzil-L-glutammato) (PBLG). Sistemi polipeptidici contenenti una o due unità di fullerene sono stati ottenuti tramite reazione tiol-ene *one-pot*. Questi due polimeri hanno mostrato una diversa propensione ad auto-assemblarsi in ambiente acquoso, formando microstrutture di forma toroidale oppure di tipo vescicolare. Come ulteriore esempio è stata riportata la sintesi di

sistemi coniugati a base di PBLG e *carbon quantum dots*. I CQDs, preparati per trattamento in microonde a partire da una soluzione acquosa di arginina e 1,2-etilendiammina, sono stati usati come iniziatore, ottenendo una struttura polimerica a forma di stella, oppure come agente cappante, portando alla formazione di microstrutture più complesse. I sistemi ottenuti sono in grado di autoassemblarsi formando aggregati supramolecolari di forma sferica che mantengono le caratteristiche proprietà di emissione dei *dots* originali. Infine, microstrutture *"smart"* con comportamento fotoresponsivo sono state ottenute inserendo amminoacidi a base di azobenzene all'interno del sistema polipeptidico. Sono state quindi sintetizzate due strutture polipeptidiche con simmetria C_2 e C_3 che hanno evidenziato la formazione di strutture sferiche tramite *self-assembly*. Il cambiamento della loro struttura tridimensionale in seguito ad irraggiamento è accompagnato da una variazione nella morfologia degli aggregati.

Peptidi corti auto-assemblanti

In questo ultimo capitolo sono discusse la sintesi e le peculiari proprietà di self-assembly mostrate da due diversi sistemi peptidici. La prima serie di composti contiene l'amminoacido fotoisomerizzabile *bis*[*p*-(fenilazo)benzil]glicina, che è in grado di isomerizzare reversibilmente tra le due forme *cis*/*trans* in seguito ad irraggiamento con luce di adeguata lunghezza d'onda. Derivati e peptidi corti contenenti questo amminoacido sono in grado di promuovere la formazione di strutture supramolecolari ordinate. Inoltre, grazie alla presenza delle due unità di azobenzene sulle catene lineari, la transizione morfologica osservata in seguito ad irraggiamento si è dimostrata essere reversibile.

Nella seconda parte di questo studio è stato esaminato il comportamento del dipeptide idrofobico protetto Boc-L-Cys(Me)-L-Leu-OMe. La formazione di nano-, micro- e macro-architetture complesse, tra cui bacchette caratterizzate da una cavità interna, è stata osservata in diverse condizioni sperimentali. I risultati ottenuti suggeriscono che le proprietà di *self-assembly* sono correlate all'organizzazione delle molecole nel cristallo singolo in cui è stata osservata la presenza di una particolare struttura supramolecolare elicoidale formata da sei molecole. Successivamente è stato deciso di modificare il dipeptide in modo da ottenere un derivato diacetilenico. Questo derivato è in grado di formare un organogel o delle strutture sferiche che possono subire polimerizzazione topochimica per irraggiamento UV.

Abbreviations

(αMe)Val	=	C^{α}-methylvaline
Ac	=	acetyl
Ac_2O	=	acetic anhydride
AcOH	=	acetic acid
AFM	=	atomic force microscopy
Aib	=	α-amino*iso*butyric acid
AIBN	=	2,2′-Azobis(2-methylpropionitrile)
Ala	=	alanine
Aloc	=	allyloxycarbonyl
Arg	=	arginine
BLG	=	γ-benzyl-L-glutamate
Boc	=	*tert*-butyloxycarbonyl
Boc_2O	=	di-*tert*-butyl dicarbonate
CD	=	circular dichroism
CF	=	carboxyfluorescein
COSY	=	correlation spectroscopy
CQDs	=	carbon quantum dots
Cys	=	cysteine
DBU	=	1,8-diazabicyclo[5.4.0]undec-7-ene
DIC	=	N,N'-di*iso*propylcarbodiimide
DIPEA	=	N,N-di*iso*propylethylamine
DLS	=	dynamic light scattering
DMAP	=	4-dimethylaminopyridine
DMF	=	N,N-dimethylformamide
DMPA	=	2,2'-dimethoxy-2-phenylacetophenone
DMSO	=	dimethylsulphoxyde
DPPA	=	diphenylphosphoryl azide
EDC	=	N-ethyl-N'-(3-dimethylamino)propyl-carbodiimide
ESI	=	electrospray ionization
Et_2O	=	diethyl ether
EtOAc	=	ethyl acetate
EtOH	=	ethanol
Fmoc	=	(9*H*-fluoren-9-yl)methoxycarbonyl
FT-IR	=	Fourier transform infrared spectroscopy
Gly	=	Glycine

HATU	=	*O*-(7-aza-1,2,3-benzotriazol-1-yl)-N,N,N',N'-tetramethyluronium hexafluorophosphate
HFIP	=	1,1,1,3,3,3-hexafluoro-2-propanol
HOAt	=	1-hydroxy-7-azabenzotriazol
HPLC	=	high performance liquid chromatography
Lys	=	Lysine
MALDI	=	Matrix-Assisted Laser Desorption/Ionization
MeOH	=	methanol
M_w	=	molecular weight
NCA	=	*N*-carboxyanhydride
NMR	=	nuclear magnetic resonance
NOESY	=	nuclear Overhauser effect spectroscopy
OMe	=	Methoxy
O*t*Bu	=	*tert*-butoxy
PBLG	=	poly(γ-benzyl-L-glutamate)
PDI	=	polydispersity index
Phe	=	phenylalanine
RCM	=	ring-closing metathesis
ROP	=	ring opening polymerization
SEC	=	size exclusion chromatography
SEM	=	scanning electron microscopy
SPPS	=	solid phase peptide synthesis
TEA	=	trimethylamine
TEM	=	transmission electron microscopy
Tfa	=	trifluoro acetyl
TFA	=	trifluoroacetic acid
TGA	=	thermogravimetric analysis
THF	=	tetrahydrofuran
TIS	=	triisopropylsilane
TMEDA	=	N,N,N′,N′-Tetramethylethylenediamine
$TMSCHN_2$	=	(Trimethylsilyl)diazomethane
TOCSY	=	total correlation spectroscopy
Trt	=	triphenylmethyl
UV-Vis	=	ultraviolet-visible spectroscopy
Val	=	valine
XPS	=	X-ray photoemission spectroscopy

Project aims

The main purpose of this Ph.D. project was the development of new families of peptides and peptide-based microstructures, based on chemically modified peptides and peptide hybrid-organic polymers. In recent years, peptides have found a growing interest in various scientific areas not only for their intrinsic biological functions, but also for their potential innovative applications in materials science. In this context, peptides may offer attractive features related to their ability to fold into precise structures also when appropriately linked to other functional molecules. Moreover, under suitable conditions peptides possess an enormous potential as smart materials, due to their ability to self-assemble into nano- and microscale ordered structures through non-covalent interactions.

The final results discussed in this Thesis were obtained by combining knowledge of organic synthesis, peptide science and supramolecular chemistry.

1. Introduction

1.1 Peptides helical structures: α- and 3_{10}-helix

The helix is a central structural motif found in numerous biopolymers, including DNA and proteins, which play a fundamental role in living systems. Therefore, taking inspiration from nature, research on artificial helical molecules has found application in various areas, not only to mimic biological helices and functions but also for their potential applications in different fields such as materials science.

The classical α-helix is the most common secondary structure of peptides and proteins (Figure 1.3 A). Another helical structure that occurs in peptides is the 3_{10}-helix (Figure 1.3 B). These helical conformations differ by the number of residues per turn, the pitch, the φ, ψ, ω torsion angles (as defined in Figure 1.1) in the peptide backbone[1] (Table 1.1), and the number of the atoms in the *pseudo*-cycle formed by the C=O···H-N intramolecular H-bonds (Figure 1.2).

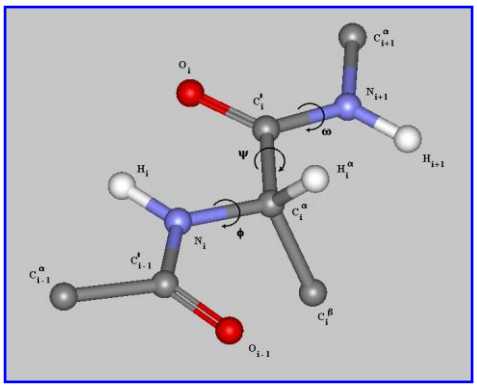

Figure 1.1 Representation of a segment of polypeptide chain in the fully-extended conformation ($\varphi_i = \psi_i = \omega_i = 180°$).

The α-helix is characterized by 3.63 residues per turn and it is stabilized by intramolecular H-bonds between the carbonyl group of a residue at position *i* and the N-H group at the *i* + 4 position, forming the *pseudo*-cycle of 13 atoms (α-turn or C_{13}-structure) (Figure 1.2 A).[2]

The 3_{10}-helical structure has 3.24 residues per turn. The *pseudo*-cycle is formed between the residues at position *i* and *i* + 3 and is composed of 10 atoms (β-turn or C_{10}-structure) (Figure 1.2 B). The sets of ϕ, ψ torsion angles of the α- and 3_{10}-helices do not differ significantly, but the latter helix is more tightly bound and more elongated than the α-helix (Figure 1.2).

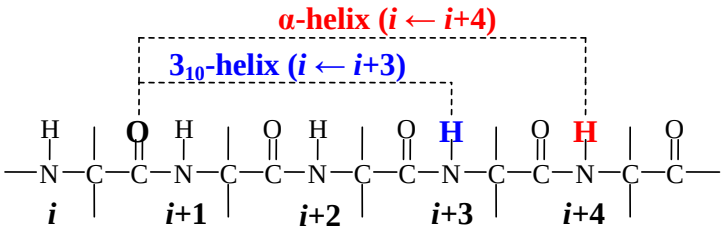

Figure 1.2 Intramolecular (backbone) C=O···H–N (backbone) H-bonds: $i \leftarrow i+3$ for the 3_{10}-helix and $i \leftarrow i+4$ for the α-helix.

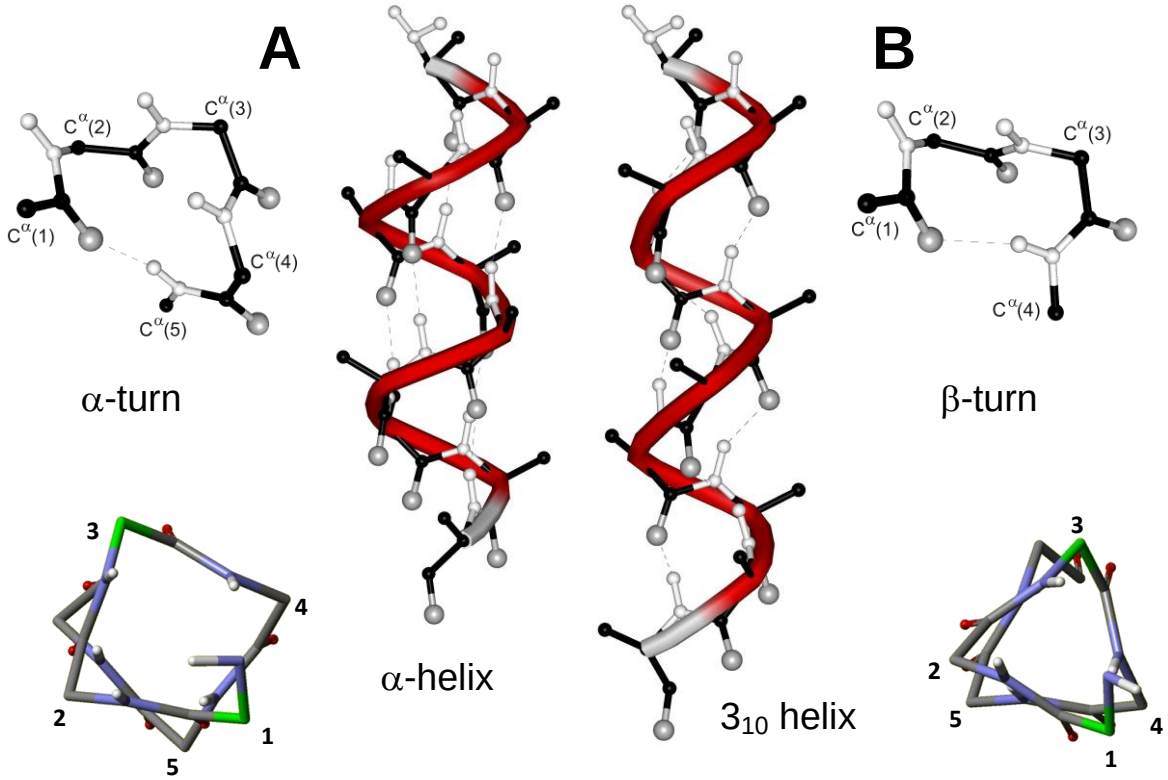

Figure 1.3 (**A**) The α-helix and its basic unit, the helical α-turn and view along helix axis. (**B**) The 3_{10}-helix and its basic unit, the helical type-III β-turn and view along helix axis.

Table 1.1 Structural parameters for the α- and 3_{10}-helical conformations.[2]

Parameter	α-helix	3_{10}-helix
Φ	-63°	-57°
Ψ	-42°	-30°
number of residues per turn	3.63	3.24
pitch	5.67 Å	6.29 Å

In a long polypeptide chain based on C^{α}-trisubstituted (e.g. protein) α-amino acid residues, the 3_{10}-helix is less stable than the α-helix due to the larger distortion of the H-bonds and some unfavorable van der Waals interactions.[3] In contrast the C^{α}-tetrasubstituted α-amino acids are extremely strong promoters of 3_{10}-helical structures. C^{α}-tetrasubstituted amino acids differ from protein amino acids by the substitution of the hydrogen at the α-carbon atom by an alkyl or an aryl group (Figure 1.4). The noticeable sterical hindrance induced by these substituents drastically limits the N-C^{α} and C^{α}-C' (φ and ψ torsion angles, respectively) bond rotations.[4]

Figure 1.4 Chemical structures of C^{α}-tri- (a) and (b) tetra-substituted amino acids.

The simplest C^{α}-tetrasubstituted α-amino acid, found in natural antibiotic peptides,[5] is the achiral α-amino*iso*butyric acid (Aib). The presence of α,α-dimethyl substituents severely restricts its conformational freedom compared to less congested residues. Oligomers of Aib have a strong preference for adopting helical conformations.[6] and in particular its homopeptides typically form 3_{10} helices.[7] In the case of peptides containing Aib and protein amino acids as well, in the crystal state only helical structures of the α-, 3_{10}- or α/3_{10}-"mixed" type were found.[8] Many factors govern the peptide conformational preference toward a specific type of helix including the length of the polypeptide chain, the Aib content, and the amino acid sequence. In general, the α-helix formation tends to be favored when the main chain is lengthened and the number of Aib residues is decreased.[6]

1.2 Polypeptides

Poly(α-aminoacids) are a class of bio-inspired synthetic polymers derived from naturally occurring amino acids. In comparison with other synthetic polymers, polypeptides have several potential advantages that inherit from proteins such as excellent biocompatibility, biodegradability, versatile structures and functionalities, and unique hierarchical assembly property.[9] Typically polypeptides adopt well-defined secondary structure, α-helix and β-sheet have been found both in solution phase and in solid state. Vastly different functions can be originated from a wide choice of α-amino acid monomers which provide a variety of reactive groups ranging from hydroxyl, carboxyl, thiol, to amino groups, rendering the polypeptides particularly appealing in design and development of multi-functional materials.

Polypeptides are mainly synthesized by α-aminoacid *N*-carboxyanhydrides (NCA) ring opening polymerization (ROP).[10] NCA-ROP allows large-scale preparation of high molecular weight polypeptides with no detectable racemization at the chiral centers.

In the past decade a remarkable progress has been made in controlled NCA polymerization, thus polypeptide and hybrid materials with various architectures (block copolymers, graft copolymers, random copolymers, star-shaped polymers, and dendrimers), secondary structures and functionalities have been achieved using NCA monomers.[10,11]

The most widely used method for the preparation of the NCA involves the direct phosgenation of side-chain protected α-amino acids in inert polar solvents (such as EtOAc, dioxane, THF, and CH_3CN) (Fuchs-Farthing method).[12] Pure NCA monomers with good yields and no racemization can be easily obtained with this synthetic method. Hydrochloride scavengers like α-pinene and limonene were proved effective in preventing byproducts formation, especially in the large scale synthesis.[13]

Depending on the relative nucleophilicity and basicity of initiator, NCA polymerizations have been reported to follow mainly two polymerization mechanisms: i) normal amine mechanism (NAM) and ii) activated monomer mechanism (AMM).[11a,b,14]

Nucleophiles such as primary amines, secondary amines and alcohols, that display stronger nucleophilicity than basicity, promote NCA polymerization most likely via an NAM mechanism (Scheme 1.1). After the nucleophilic attack, ring opening of NCA results in the release of one molecule of carbon dioxide and exposure of a primary amine, which behaves as the active species to open the next NCA monomer and the repetition of this step finally generates the polypeptides. Primary amines are generally excellent initiators, in fact they are more nucleophilic than the ω-amino group of the propagating chain leading to polypeptides with low polydispersity index (PDI), since initiation is faster than propagation.

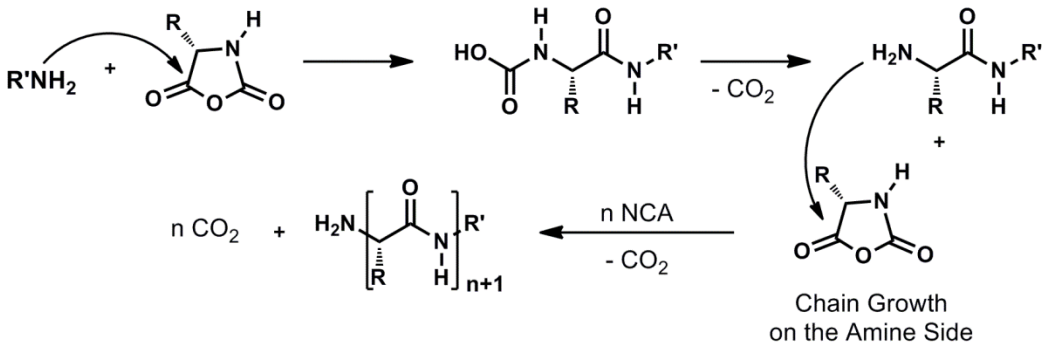

Scheme 1.1 Mechanism for NCA-ROP initiated by nucleophilic amines (NAM).[14b]

In the case of initiators such as metal alkoxides and tertiary amines, which show stronger basicity than nucleophilicity, NCA polymerization most likely proceeds via an AMM mechanism. These kind of initiators can easily abstract the acidic N–H proton of NCA and generate negatively charged NCA molecules that are sufficiently nucleophilic to attack another NCA monomer and initiate polymerization (Scheme 1.2). Polypeptides with very large PDI values and uncontrolled molecular weights are generally produced via AMM because initiation is slower than propagation and both AMM and NAM occur simultaneously.

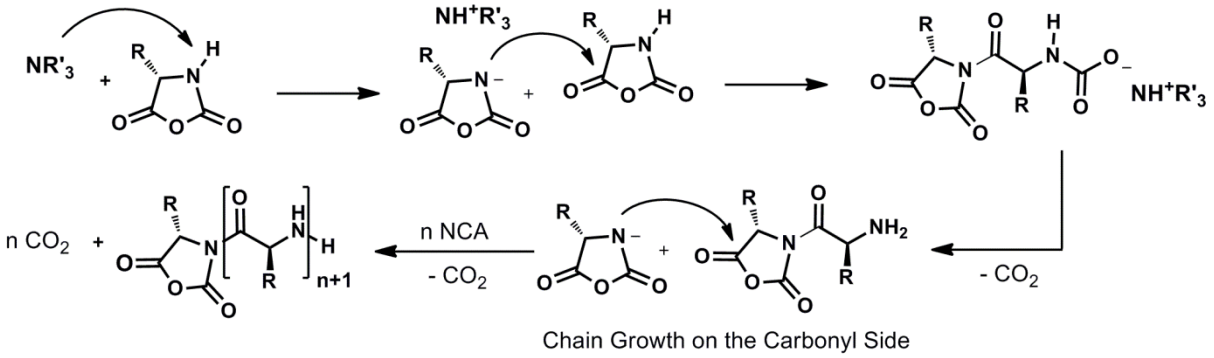

Scheme 1.2 Mechanism for NCA-ROP initiated by activated monomer (AMM).[14b]

Other methods to obtain poly(amino acid)s with controlled molecular weight and low polydispersity by NCA-ROP have been obtained using as initiator other species such as transition metal complexes[11a,15], organosilicon reagent derivatives[16] and primary amine hydrochloride.[17]

1.3 Supramolecular chemistry and self-assembly process

The supramolecular chemistry, commonly referred as the "chemistry beyond the molecule", was introduced by Lehn (Nobel Laureate 1987), who defined it as the "chemistry of molecular assemblies and of the intermolecular bonds".[18] As in the molecules atoms are connected by covalent bonds, in supramolecular systems molecules are bonded by additive and cooperative noncovalent interactions. The power of supramolecular chemistry lies in the combination of a number of weak interactions, relatively insignificant alone, but that are able to held together small molecules forming very complex systems.

There are a number of noncovalent interactions that can be utilized for the construction of supramolecular structure, which include:[19]

- electrostatic interactions [ion-ion (100-350 kJ/mol), ion-dipole (50-200 kJ/mol), dipole-dipole (5-50 kJ/mol)];
- hydrogen bonds (4-120 kJ/mol);
- π-π stacking interactions (2-50 kJ/mol);
- van der Waals forces (< 5 kJ/mol).

Electrostatic interactions are based on the Coulombic attraction between opposite charges and tend to be relatively strong. Ion-ion interactions are comparable in strength to covalent bonding. Ion-dipole and dipole-dipole interactions result from an electrostatic attraction between an ion and a neutral molecule with a dipole or two molecules with dipoles, respectively.

A hydrogen bond can be describe as an attractive interaction between a hydrogen atom attached to an electronegative atom (or electron withdrawing group) and a neighbouring dipole on an adjacent molecule or functional group. In general, hydrogen bonds, commonly represented as D-H···A, involve a hydrogen atom attached to an electronegative atom such as O or N as the donor (D) and a similarly electronegative atom, often bearing a lone pair, as the acceptor (A). Hydrogen bonds are ubiquitous in living systems and considered as the 'masterkey interaction in supramolecular chemistry".[20] In fact they have a relatively strong and highly directional nature, making them especially attractive to molecular designers.

The π-π stacking forces occur between systems containing aromatic rings, often in situations where one is relatively electron rich and one is electron poor. These interactions commonly occur in a-face-to-face or edge-to-edge manner, although a wide variety of intermediate geometries are known.

Van der Waals interactions occur when instantaneous dipoles in the electron clouds around each molecule interact favorably, resulting in a weak electrostatic attraction. They are nondirectional and hence possess only limited scope in the design of specific interacting molecules.

Another aspect that is worth considering for the creation of supramolecular system is the hydrophobic effect. The hydrophobic effect is the specific driving force for the association of apolar binding partners in polar solvent, in particular in aqueous environment. Essentially, the strong inter-solvent interactions between the water molecules give rise to the exclusion from the solvent of the apolar molecules and the formation of aggregates.

The self-assembly process, defined as the "spontaneous assembly of molecules into structured, stable, noncovalently joined aggregates",[21] has emerged as a powerful approach to create novel multi-nanometer scale structures and systems. Self-assembly allows access to unprecedented and very complex molecular architectures that are inaccessible using traditional multi-step synthesis. Novel molecular architectures can be produced by combination of appropriately designed sub-units, which contain all information necessary to spontaneously organize.

The fabrication of new materials through self-assembly of natural building blocks, including proteins and peptides, has become a subject of major interest.[22] In particular peptides can spontaneously self-assemble into nanospheres, nanotubes, nanofibrils, nanotapes and other ordered structures.[23] In addition, peptides have drawn significant attention due to their simple structure, diversity in functions and shapes, biocompatibility and well-establish synthetic methods permit to obtain them in large scale.[24]

References

[1] (a) G.N. Ramachandran, V. Sasisekharan, *Adv. Protein Chem.*, **1968**, *23*, 283-438; (b) IUPAC-IUB, *Biochemistry*, **1970**, *9*, 3471–3479.

[2] C. Toniolo, E. Benedetti, *Trends Biochem. Sci.*, **1991**, *16*, 350-353.

[3] (a) J. Donohue, *Proc. Natl. Acad. Sci. USA*, **1983**, 39, 470-478; (b) G.N. Ramachandran, C. M. Venkatachalam, S. Krimm, *Biophys. J.*, **1966**, *66*, 849-872; (c) E. N. Baker, R. E. Hubbard, *Progr. Biophys. Mol. Biol.*, **1984**, *44*, 97-179.

[4] (a) G. N. Ramachandran, R. Chandrasekaran, *Indian J. Biochem. Biophys.*, **1972**, *9*, 1-11; (b) A.W. Burgess, S. J. Leach, *Biopolymers*, **1973**, *12*, 2599-2605.

[5] C. Toniolo, H. Brückner *Peptaibiotics: Fungal Peptides Containing α-Dialkyl α-Amino Acids*. **2009**, Zürich, Switzerland: Verlag Helvetica Chimica Acta, Weinheim, Germany: Wiley-VCH.

[6] I. L. Karle, P. Balaram, *Biochemistry* **1990,** *29*, 6747-6756.

[7] F. Formaggio, M. Crisma, P. Rossi, P. Scrimin, B. Kaptein, Q. B. Broxterman, J. Kamphuis, C. Toniolo, *Chem. Eur. J.*, **2000**, *6*, 4498-4504.

[8] (a) V. Pavone, B. Di Blasio, A. Santini, E. Benedetti, C. Pedone, C. Toniolo, M. Crisma, *J. Mol. Biol.*, **1990**, *214*, 633-635; (b) C. Toniolo, M. Crisma, G. M. Bonora, E. Benedetti, B. Di Blasio, V. Pavone, C. Pedone, A. Santini, *Biopolymers*, **1991**, *31*, 129-138.

[9] (a) C. Deng, J. Wu, R. Cheng, F. Meng, H.-A. Klok, Z. Zhong, *Progr. Polym. Sci.*, **2014**, *39*, 330-364; (b) Y. Shen, X. Fu, W. Fu, Z. Li, *Chem. Soc. Rev.*, **2015**, *44*, 612-622.

[10] (a) H. R. Kricheldorf, *Angew. Chem. Int. Ed.*, **2006**, *45*, 5752-5784; (b) G. J. M. Habraken, M. Peeters, C. H. J. T. Dietz, C. E. Koning, A. Heise, *Polym. Chem.*, **2010**, *1*, 514-524; (c) H. Lu, J. Wang, Z. Song, L. Yin, Y. Zhang, H. Tang, C. Tu, Y. Lin, J. Cheng, *Chem. Commun.* **2014**, *50*, 139-155.

[11] (a) N. Hadjichristidis, H. Iatrou, M. Pitsikalis, G. Sakellariou, *Chem. Rev.* **2009**, *109*, 5528-5578; (b) T. J. Deming, *Adv. Polym. Sci.*, **2006**, *202*, 1–18; (c) H. Tian, Z. Tang, X. Zhuang, X. Chen, X. Jing, *Prog. Polym. Sci*., **2012**, *37*, 237–280.

[12] (a) A. C. Farthing, R. J. W. Reynolds, *Nature*, **1950**, *165*, 647–657; (b) D. Coleman, A. C. Farthing, *J. Chem. Soc.*, **1950**, 3218–3222.

[13] N. M. B. Smeets, P. L. J. van der Weide, J. Meuldijk, J. Vekemans, L. A. Hulshof, *Org. Process Res. Dev.*, **2005**, *9*, 757-763.

[14] (a) N. Hadjichristidis, H. Iatrou, M. Pitsikalis, G. Sakellariou, *Chem. Rev.*, **2009**, *109*, 5528–5578; (b) J. Cheng, T. J. Deming, *Top. Curr. Chem.*, **2012**, *310*, 1–26; (c) H. Lu, J. Wang, Z. Song, L. Yin, Y. Zhang, H. Tang, C. Tu, Y. Lin, J. Cheng, *Chem. Commun.*, **2014**, *50*, 139–155.

[15] (a) J. P. Collman, L. S. Hegedus, J. R. Norton, R. G. Finke, *Principles and applications of organotransition metal chemistry*, **1987**, 2nd ed. University Science, Mill Valley; (b) T. J. Deming, *Adv. Mater.*, **1997**, *9*, 299–311; (c) T. J. Deming, *J. Am. Chem. Soc.*, **1997**, 119, 2759–2760; (c) T. J. Deming, *Nature*, **1997**, *390*, 386-389.

[16] H. Lu, J. Cheng, *J. Am. Chem. Soc.*, **2007**, *129*, 14114–14115.

[17] I. Dimitrov, H. Schlaad, *Chem. Commun.*, **2003**, 2944-2945.

[18] (a) J. M. Lehn, *Pure Appl. Chem.*, **1978**, *50*, 871-892; (b) J. M. Lehn, *Angew. Chem. Int. Ed.*, **1988**, *27*, 89-112.

[19] (a) J. W. Steed, J. L. Atwood, *Supramolecular Chemistry*, **2009**, 2nd ed., John Wiley & Sons, Ltd; (b) J. W. Steed, P. A. Gale, *Supramolecular Chemistry: From Molecules to Nanomaterials*, **2012**, Wiley.

[20] J. M. Lehn, *Supramolecular Chemistry*, **1995**, 1st ed., VCH: Weinheim.

[21] G. M. Whitesides, J. P. Mathias, C. T. Set, *Science*, **1991**, *254*, 1312–1319.

[22] (a) S. Zhang, *Nature Biotechnology*, **2003**, *21*, 1171-1178; (b) R. de la Rica, H. Matsui, *Chem. Soc. Rev.*, **2010**, *39*, 3499-3509.

[23] (a) E. Gazit, *Chem. Soc. Rev.*, **2007**, *36*, 1263-1269; (b) R.V. Ulijin, A.M. Smith, Chem. Soc. Rev. **2008**, *37*, 664-675.

[24] (a) X. Zhao, F. Pan, J. R. Lu, *Prog. Nat. Sci.*, **2008**, *18*, 653-660; (b) D. Mandal, A. Nasrolahi Shirazib, K. Parang, *Org. Biomol. Chem.*, **2014**, *12*, 3544-3561; (c) E. De Santis, M. G. Ryadnov, *Chem. Soc. Rev.*, **2015**, *44*, 8288-8300.

2. Short helical peptides: synthesis and secondary structure control

There is great interest in developing molecules which can mimic α-helices since this motif has been found at the binding interface between two proteins and is involved in the protein-protein interactions.[1] In medicinal chemistry, the ability to selectively inhibit protein-protein interactions may enable therapeutics to be developed against a wide range of diseases.

It is not surprisingly that peptides received the greatest deal of attention since they offer a great variety and the intrinsic ability to fold in stable conformations. For these reasons, synthetic methods for modifying peptides with the aim of reinforcing their native helical conformation have been investigated.[1b,2] In particular, it is hoped that these modifications on peptide molecules will display significantly improved pharmacological properties, including bioactivity, receptor binding selectivity, metabolic stability, cell permeability, and rapid clearance *in vivo*. One of the most established methods for generating helical conformations is peptide stapling in which naturally occurring or appropriately modified amino acid side chains are covalently linked together forming a macrocycle.[3]

In this context, the group where I carried out my PhD previously applied this approach in 3_{10}-helical peptide sequences containing the strongly helicogenic α-aminoisobutyric acid (Aib). The selected intramolecular cross-linking reactions between the side chains of residues *i* and *i*+3, namely the ring-closing metathesis (RCM)[4] or the photo induced Paternò-Yang-macrocyclization reaction,[5] did not modify the regularity of the 3_{10}-helix backbone. Moreover, we further exploited intramolecular macrocyclization reactions with the aim to obtain an *i*, *i*+4 intramolecularly double stapled, overlapping, bicyclic oligopeptide system with α-helical conformation.[6] The results obtained will be presented in the first part of this chapter.

Furthermore, since the helical conformation is intrinsically chiral, helices have been considered also as potential conveyors of stereochemical information. Helical foldamers,[7] which are synthetic molecules that likewise adopt well-defined conformations, have been successfully used as rigid medium to achieve asymmetric induction over long distances.[8]

Oligomers of Aib are achiral peptides that typically adopt stable 3_{10} helical conformations, but left- and right-handed screw sense conformations are equally populated in the absence of an external chiral influence.[9] This ratio of conformers can be biased by the incorporation of a

single stereogenic center into the peptide chain, e.g. by the insertion of a chiral amino acid at the N-terminus,[10] or at the C-terminus.[11]

Recently, it has been shown that helical Aib peptides with an induced preferred screw-sense, even if remotely induced by the incorporation of a single chiral residue at the N-terminus, exhibit enantioselectivity in their chain-extension reactions at the C-terminus.[12]

In order to exploit stereochemical reactions in Aib oligomers, I had the opportunity to spend a research period of six months as a Visiting Student in the group of prof. J. Clayden, (School of Chemistry, University of Manchester, UK) during the third year of my Ph.D. work.

In this period, I worked on the functionalization of Aib oligomers with the photoswitchable fumaric/maleic linkage with the aim of developing a system in which the stereoselectivity of a reaction can be controlled using light. The work described in the second part of this chapter started in UK and it was then continued in Italy during the last months of the third year.

2.1 Stapled peptide

We focused our attention on the realization of a bicyclic peptide system in which a reaction covalently joining the side chain of residue **1** of a linear nonapeptide to the side chain of residue **3**, is combined with a macrocyclization from residue **2** to residue **4** (Figure 2.1).
The resulting bicyclic peptide is overlapping, with an amino acid stretch in common between the two ring systems. Furthermore both macrocyclizations are of the *i*, *i*+4 class appropriate for an α-helix peptide substrate. Also, these reactions are orthogonal, in fact a sulphydryl *bis*-alkylation is followed by an RCM reaction.

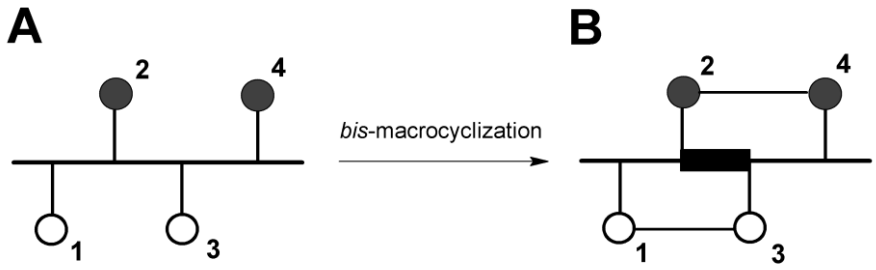

Figure 2.1 (**A**) Representation of a completely preformed linear peptide with four reactive side chains (**1**, **2**, **3**, and **4**) numbered starting from the N-terminus of the backbone. (**B**) Representation of the resulting, overlapping, peptide motif after the two macrocyclizations **1**-to-**3** and **2**-to-**4**. The backbone segment of the peptide product highlighted in bold is in common between the two ring systems.

The sequence of the linear peptide **1** [Ac-Aib^{1}-Cys^{2}-Aib^{3}-Lys(Aloc)^{4}-Aib^{5}-Cys^{6}-Aib^{7}-Lys(Aloc)^{8}-Aib^{9}-NH_2], shown in Figure 2.2, was designed: (*i*) to generate a model which would exhibit a considerable level of α-helicity as it contains five helicogenic Aib residues and (*ii*) to precisely locate the two amino acid dyads, Cys^{2}/Cys^{6} and Lys(Aloc)^{4}/Lys(Aloc)^{8} at relative positions *i*, *i*+4 in the internal part of the sequence. Peptide **1** was synthesized *via* SPPS and Fmoc chemistry, using a Rink-amide resin as solid support and following the conventional HOAt/HATU/DIPEA C-activation protocol.[13] Acetylation at the N-terminus was accomplished with a large excess of acetic anhydride. In the last step, the peptide was removed from the resin by use of TFA in the presence of TIS as scavenger. Then, nonapeptide **1** was purified by reverse-phase *semi*-preparative HPLC.

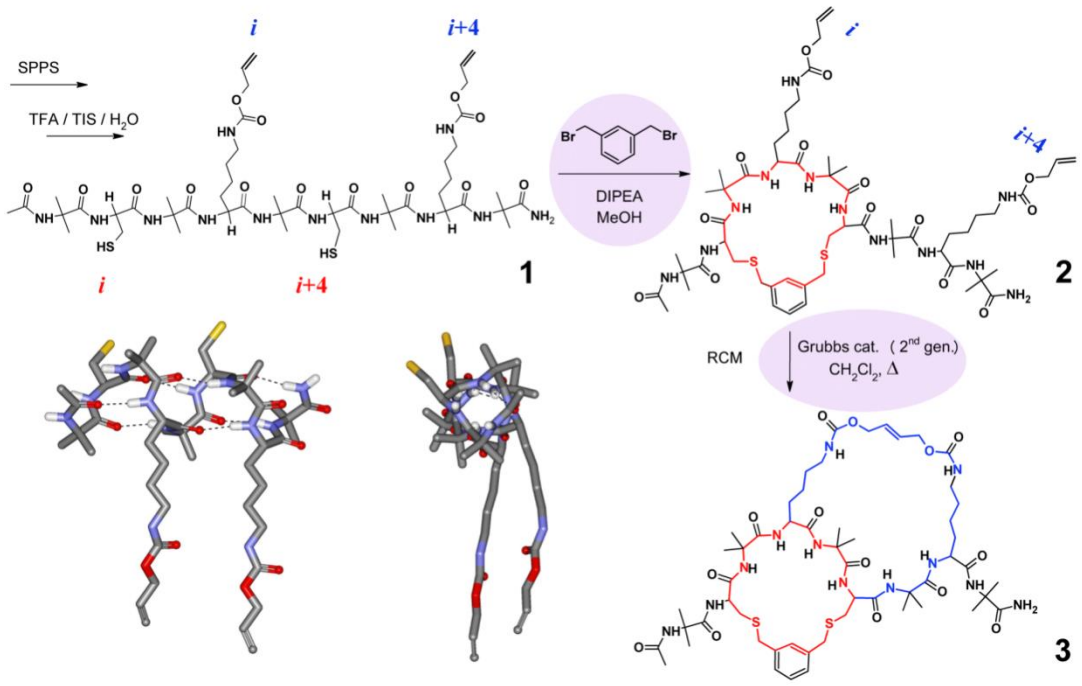

Figure 2.2 Syntheses and chemical formulas of peptides **1**-**3**. The *i*, *i*+4 intramolecularly cross-linked side chains connecting Cys^2 to Cys^6 (red) and $Lys(Aloc)^4$ to $Lys(Aloc)^8$ (blue) are shown. In peptide **3**, the -CO-Aib^5-NH- backbone segment is in common between the two macrocycles. Lower part, left: Perpendicular and axial projections of the linear peptide **1**. This 3D-model was computer generated using a regular α-helical backbone.

The first conformational restriction of peptide **1** was achieved by converting it into peptide **2** *via* double Cys alkylation. Recently, from screening a library of potential intramolecular cross-linkers, the *meta*-xylyl group was carefully demonstrated to be an excellent *bis*-Cys spacer.[14] Indeed, it was found optimal to match the inter-thiol distance of two Cys side chains placed at relative positions *i*, *i*+4 in an α-helical peptide. To perform the "template-constrained thioeher cyclization",[14] we initially reacted a small volume of a diluted (0.45 mmolar) solution of peptide **1** in MeOH with a slight excess (1.1 eq.) of 1,3-*bis*(bromomethyl) benzene in the presence of DIPEA (Figure 2.2). These conditions were designed to increase the rate of intramolecular cyclization over those of intermolecular *bis*-alkylations. However, the progress of the reaction was extremely slow. An HPLC-mass spectrometry analysis of the crude after four hours revealed the presence of only a small amount of the desired cyclized product **2**, accompanied by various types of monoalkylated and non-cyclic *bis*-alkylated peptides. Then, we decided to repeat this procedure with a larger volume of the same solution of peptide **1**, but adding slowly and dropwise an increasing excess (to 4:1) of the cross-linker over a period of two hours. In this case, it was gratifying to find that the yield of the purified, monocyclized peptide **2** was satisfactory (60%). We believe

that this result is mainly related to the marked α-helical content of the starting linear compound **1**, which in turn is responsible for directing the two Cys^2 and Cys^6 side chains outwards from the same face of the peptide backbone.

In the second step, peptide **2** (1.8 mmol) was treated with the 2nd-generation Grubbs catalyst in CH_2Cl_2 solution. Under these conditions, the $Lys(Aloc)^4$ and $Lys(Aloc)^8$ residues of macrocyclic peptide **2** underwent a rapid RCM reaction to afford the bicyclic [31,22,5] ene peptide **3** in an almost quantitative yield (Figure 2.2). The completeness of the reaction was monitored by HPLC by following the disappearance of the starting material (peptide **2**). After each synthetic step, peptides **2** and **3** were purified by flash chromatography. Obtaining pure peptide **3** without any catalyst contamination required an extensive chromatographic treatment which, unfortunately, reduced its overall yield to 31%. In Figure 2.3 (left) the analytical HPLC chromatograms and ESI-ToF mass spectra of peptides **1-3** are shown. In the mass spectra, peaks as intense as those for the correct peptides and consistent with a deficiency of 17.0 Da are seen. We associated them to loss of ammonia from the protonated, labile, C-terminal primary amide functionality.

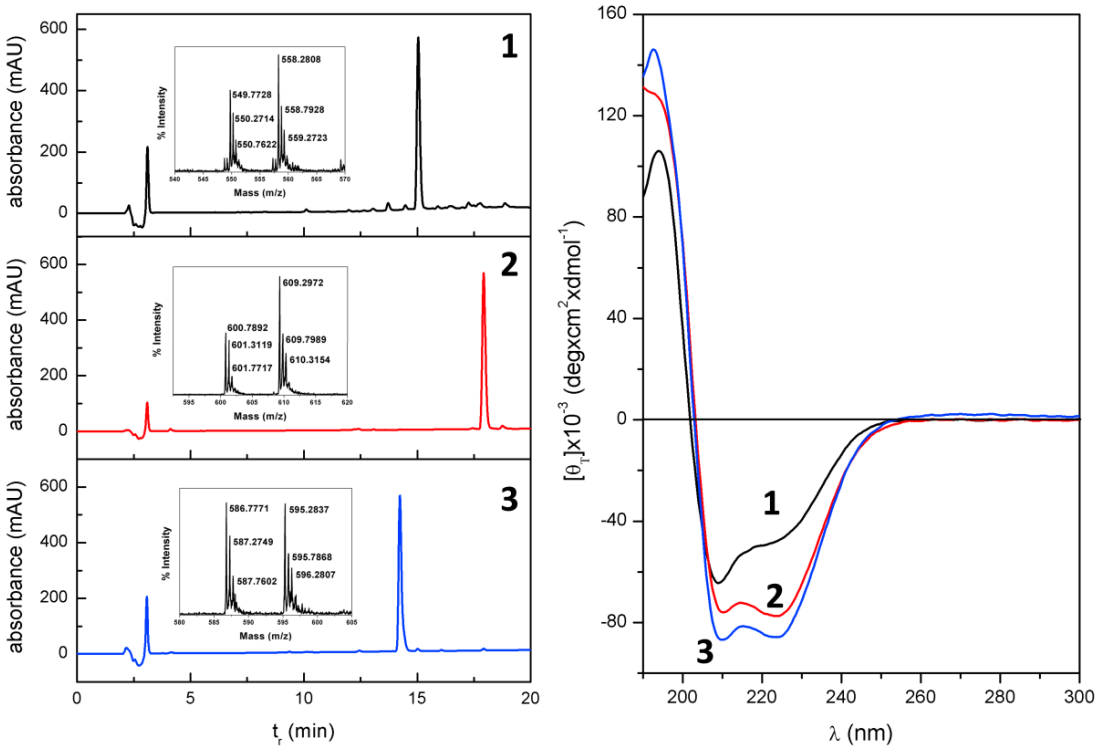

Figure 2.3 Left: Analytical HPLC profiles of the purified peptides **1-3**. Inset: Corresponding ESI-ToF mass spectra where the $[M+2H]^{2+}$ ions are visible. Right: Far-UV ECD spectra of peptides **1-3** recorded in MeOH solution at 20°C (concentration: 1 x 10^{-3}*M*).

The analysis of the ellipticity ratio (*R*) between the negative Cotton effects at 223 nm (peptide n → π* transition) and near 210 nm (parallel component of the split peptide π → π* transition)[15] allows the discrimination between the 3_{10}- and α-helix structures by circular dichroism (CD).[16] A value of 0.15-0.35 for *R* is considered diagnostic of an extensively developed 3_{10}-helix, while a value close to the unity is typical of an α-helix. Based on these considerations, peptides **1**-**3** were analyzed by CD (Figure 2.3, right). Peptide **1** exhibits an *R* value of 0.76, which indicates that a mixed 3_{10}-/α-helix conformation (with a considerable α-helical amount) is that preferred for this compound. In contrast, both monocyclic peptide **2** and bicyclic peptide **3** are characterized by an *R* value close to one, which suggests a complete α-helix folding for these two compounds. Moreover, a comparison of the ellipticity values at 222 nm highlights a significant helix enhancement (37% and 43%, respectively) for both the single (**2**) and double (**3**) macrocyclized motifs as compared to that of the linear peptide **1**.

^{1}H-NMR and 2D-NMR spectra (the latter carried out using DQF-COSY,[17] TOCSY[18] and NOESY experiments) were recorded for the **1**-**3** peptide series in DMSO-d_6 solution. From a comparison of the ^{1}H-NMR spectra, we found a number of variations in the chemical shift and signal shape characterizing the protons directly involved in or spatially located near the sites of the macrocyclization. In particular, the two Cys residues of the monocyclized peptide **2**, alkylated with the *meta*-xylyl moiety, show a downfield shift of their αCH protons with respect to the corresponding protons of peptide **1** (Figure 2.4 A). Concomitantly, new signals, assigned to the protons of the aromatic (Ar) *meta*-xylyl group, are seen in the 3.8-3.5 ppm and 7.3-7.1 ppm regions of peptide **2** (Figures 2.4 A-B). In the amide NH spectral region (Figure 2.4 B) we observed a larger spread in the chemical shifts not only for the Cys NH protons, but for those of the αNH protons of the Lys residues as well, suggesting that peptide **2** is more conformationally constrained than peptide **1**.

After the RCM reaction and the accompanied loss of the ethylene molecule, the signals at 5.24 and 5.14 ppm of peptides **1** and **2**, corresponding to the terminal alkene protons (Figure 2.4 A), are missing in the spectra of bicyclic peptide **3**. Moreover, the complex signal at 5.85 ppm of the –CH=CH– ethylene bridge of peptide **3** appears as a broad singlet (Figure 2.4 A), and the εCH_2 and ζNH protons of the Lys^4 and Lys^8 residues are more spread (Figure 2.4 B).In addition, the generally broad ^{1}H-NMR spectrum of peptide **3** at 25 °C (Figures 2.4 A-B and 2.5) indicates the simultaneous occurrence of *more than one conformer*, due to the large number of atoms in the Lys^4/Lys^8macrocyclic system. Indeed, after heating from 25 to 65 °C all broad peaks, including that at 5.85 ppm, become sharper (Figure 2.5).

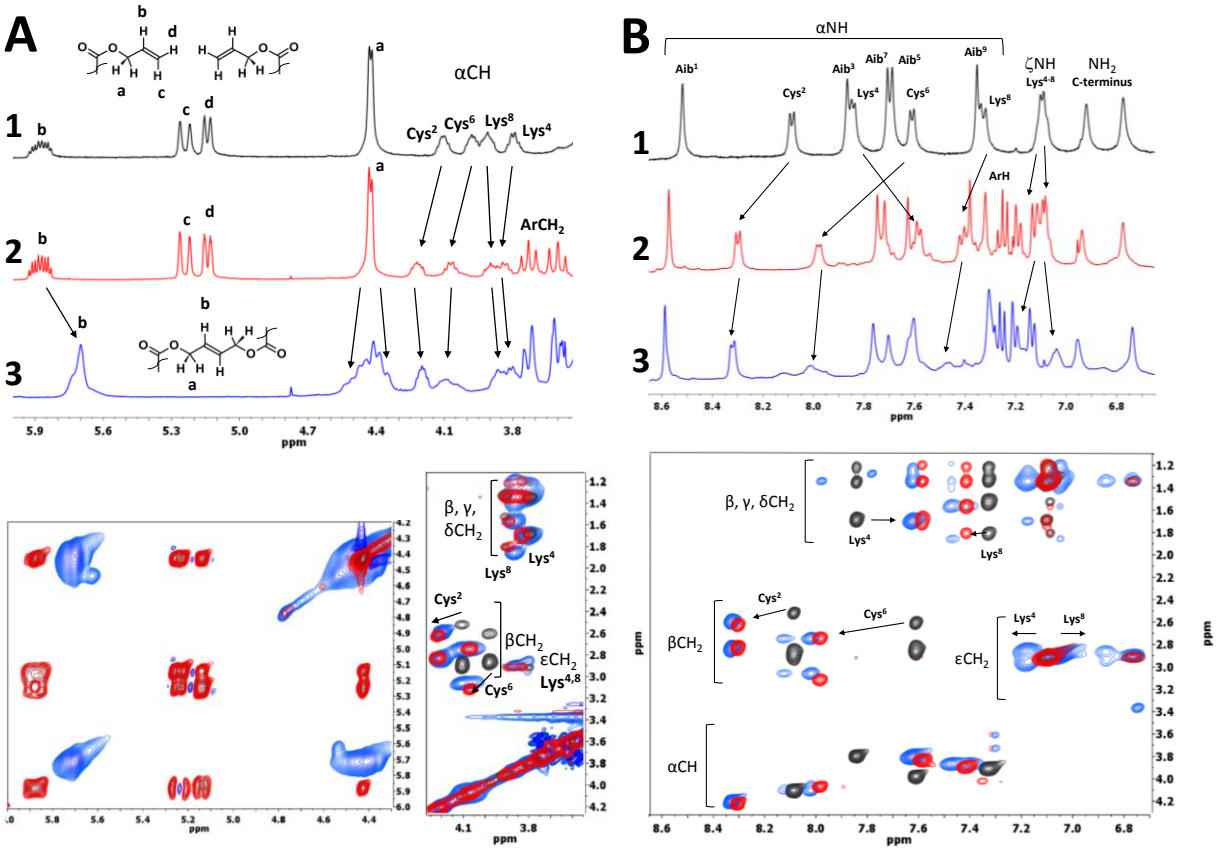

Figure 2.4 (**A**) Overlap of the ^{1}H-NMR and TOCSY 2D-NMR spectra for the alkene (allyl) and αCH regions of peptides **1** (black), **2** (red), and **3** (blue) recorded in DMSO-d_6 solution at 25°C (concentration: 1 x 10^{-3}*M*). Insets: Effects of macrocyclizations and proton assignments. (**B**) Overlap of the ^{1}H-NMR and TOCSY 2D-NMR spectra for the NH region of peptides **1** (black), **2** (red), and **3** (blue) under the same experimental conditions as above. Insets: Effects of macrocyclizations and proton assignments.

Interestingly, in the spectra recorded at the two highest temperatures (55 and 65 °C), we observe a major peak (5.76 ppm) which we assign to the protons of the –CH=CH– ethylene bridge[4] of the *major configurational isomer* that is formed. Moreover, another peak (indicated in Figure 2.5 by an arrow), albeit very small (less than 10% of the major peak after integration), is clearly visible at 5.67 ppm. We assign it to the same type of protons of the *minor configurational isomer*. We attribute the major peak to the *E* isomer on the basis of literature data (in particular, NMR chemical shifts, *E*/*Z* ratio values, and ring size) on the RCM reaction where strictly similar (helical peptides)[4] or related[19] substrates were used. More specifically, the 2nd generation Grubbs catalyst employed in the present work was shown to produce large-sized cyclic compounds (as the one synthesized here) in very good yields and high *E*-selectivities.[19] Unfortunately, our NMR attempts to confirm this *configurational* assignment *via* COSY phase-sensitive and J-resolved experiments at different frequencies (500 and 600 MHz) failed to give a clear-cut information, most probably because

of the complexity of the hyperfine system (the –CH=CH– moiety is coupled to the nearby –CH_2– protons) under the peak.

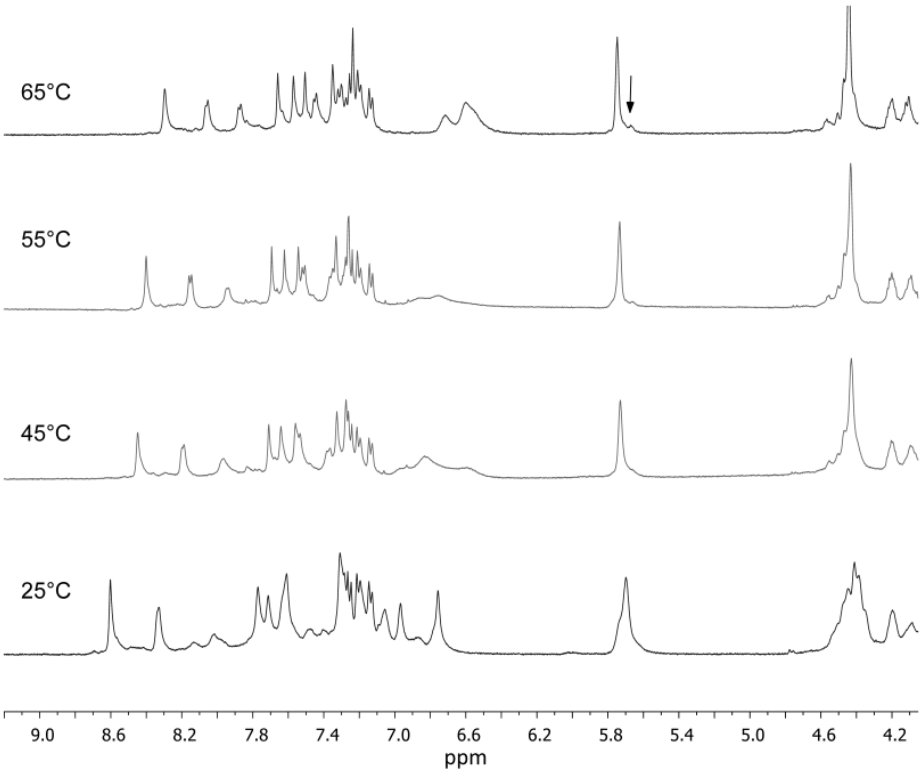

Figure 2.5 Partial ^{1}H-NMR spectrum of peptide **3** recorded in DMSO-d_6 solution as a function of heating (from 25 to 65 °C).

Furthermore, from a comparison of the spectral region of the Aib βCH_3 protons (1.5-1.3 ppm), we noted a greater dispersion of the resonances for peptide **3** as compared to those for peptides **1** and **2**. This finding might be taken as an evidence for a more structured bicyclic peptide **3**.

All sequential αNH(*i*)→αNH(*i*+1) connectivities, characteristic of a well-developed helical conformation,[20] are seen in the NOESY spectra of peptide **1** and **3** in DMSO-d_6 solution (Figure 2.6). Additional information was obtained from the large number of sequential αCH(*i*)→αNH(*i*+1) connectivities observed, along with some long-range NOE signals, which further support the presence of an helical structure (Figure 2.7). When an αCH is not present in the amino acid (in correspondence to the Aib residues), we looked at the βCH_3(*i*)→αNH(*i*+1) connectivities: these parameters are exhibited by all three peptides (not shown). As a further test of peptide helicity, we determined the temperature coefficients of the αNH protons. Although there is not a big difference in the behavior of the three peptides, we noticed that the Aib^1 and Lys^4 residues (near the N-terminus) of peptide **1** are more mobile than the corresponding residues of peptides **2** and **3** (not shown).

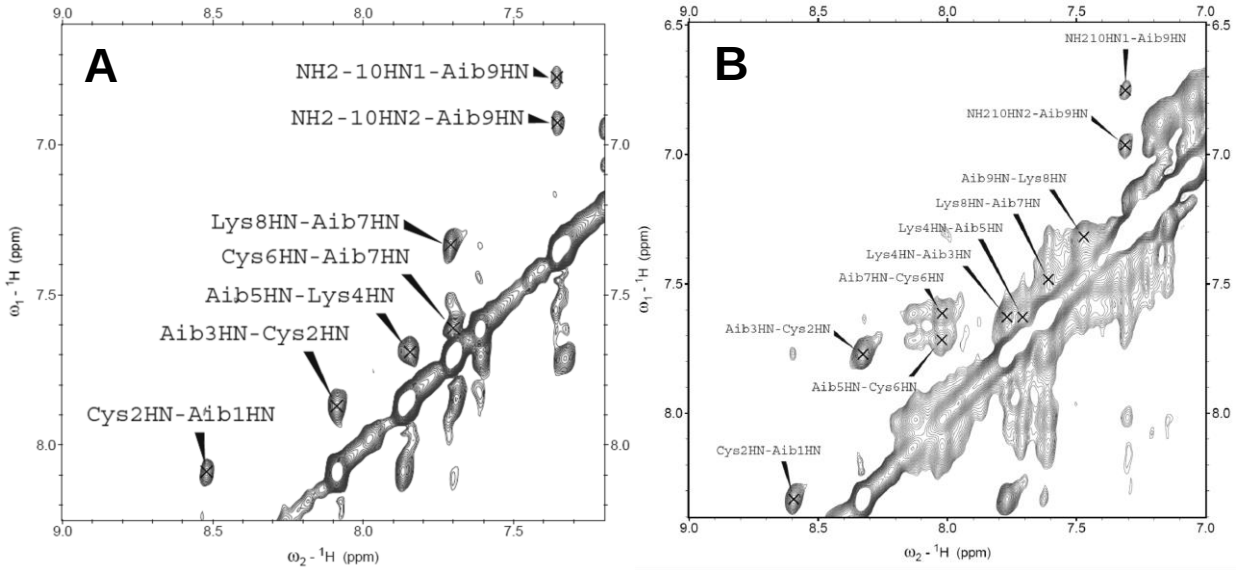

Figure 2.6 NH→NH region of the NOESY spectra of peptides **1** (**A**) and **3** (**B**) in DMSO-d_6 solution at 25 °C.

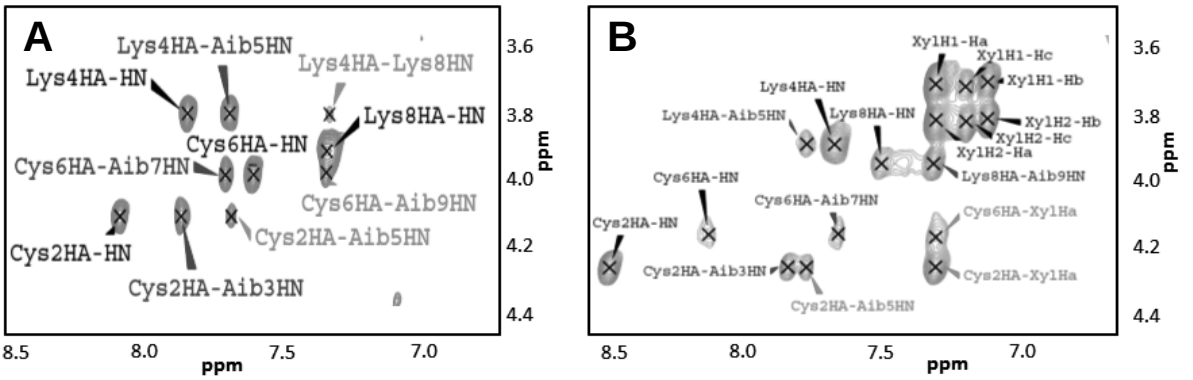

Figure 2.7 αCH→NH region of the NOESY spectra of peptides **1** (**A**) and **3** (**B**) in DMSO-d_6 solution at 25 °C.

In general, for the three peptides all other residues are significantly fixed, except Cys^2. We also measured the $J_{\alpha NH\text{-}\alpha CH}$ coupling constants for the four non-Aib (two Cys and two Lys) residues. For all three peptides the experimental values are compatible with helical structures,[20] as they range between 5.0 and 7.0 Hz. However, these values are only slightly affected by the temperature increment.

In addition, peptide **3** displays NOE cross-peaks between the αCH protons of Cys^2 and Cys^6 and the H^a aromatic proton of the *meta*-xylyl moiety in their vicinity (Figure 2.8 A). The proximity of Aib^5 to the two Cys residues constrained by formation of the *meta*-xylyl ring structure is highlighted by NOE cross-peaks between the αCH protons of Cys^2/Cys^6 and the βCH_3 protons of Aib^5 (Figure 2.8 B).

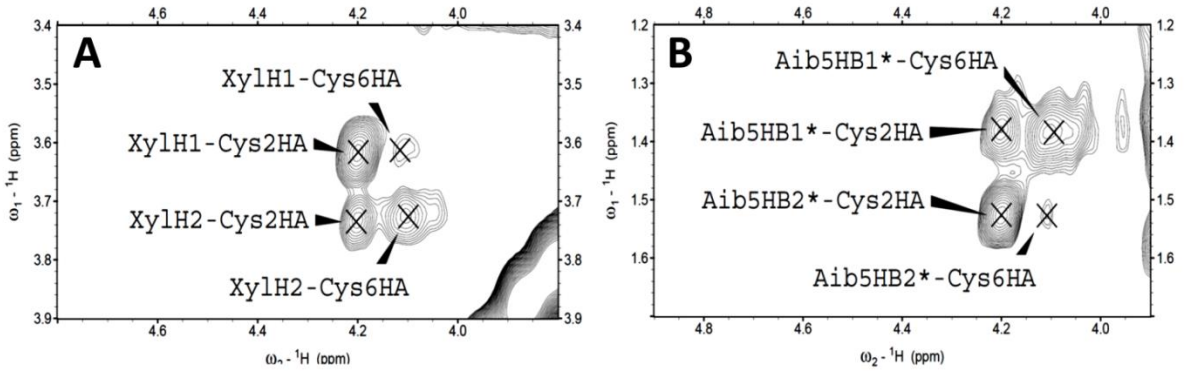

Figure 2.8 NOESY spectrum of peptide **3** in DMSO-d_6 solution at 25 °C. (**A**) Cross-peaks between the αCH protons of Cys^2/Cys^6 and H^a proton of the *meta*-xylyl moiety. (**B**) Cross-peaks between the αCH protons of Cys^2/Cys^6 and the βCH_3 protons belonging to Aib^5.

Next, to understand the role played by the double stapled[21] motif on the stability of the helical structures, we recorded a series of CD curves for peptides **1-3** in MeOH at different temperatures (Figure 2.9). After heating at 60 °C, both the linear peptide **1** and the monocyclic peptide **2** underwent a 37-38 % loss of their original helical contents (as referred to the measurement at 20 °C). In contrast, peptide **3** did not display any significant change in its CD spectrum during an identical heating process. These results suggest a remarkable thermal stabilization effect on the α-helix induced by the second cyclization, which affords the bicyclic [31,22,5](*E*)ene motif of **3**.

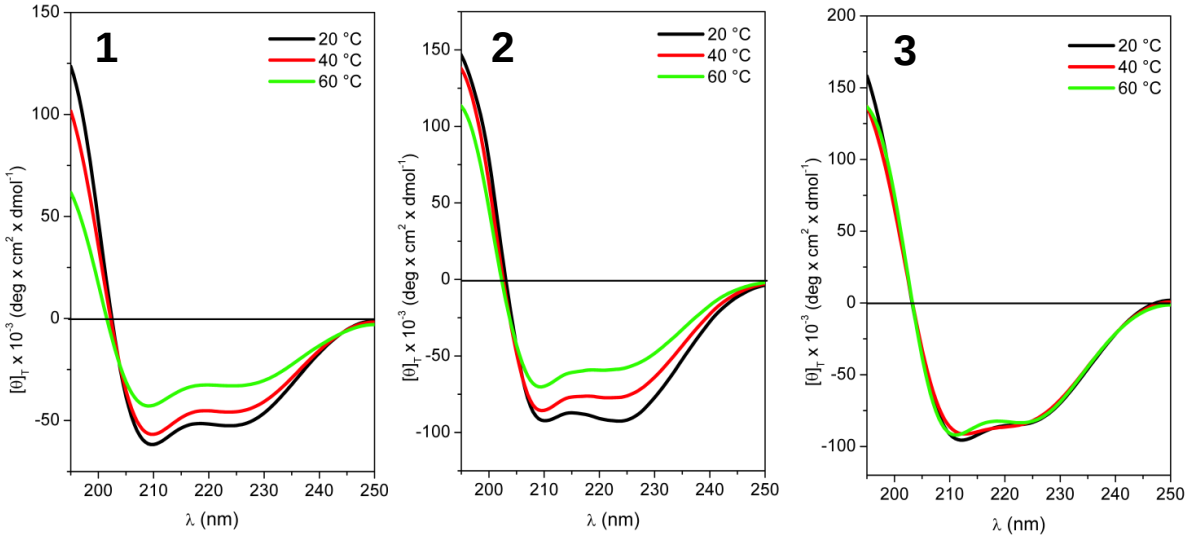

Figure 2.9 Far-UV CD spectra of peptides **1-3** recorded in MeOH solution at 20 °C (black), 40 °C (red) and 60 °C (green) (concentration: 1 x 10^{-3}*M*).

Conclusions

We reported the synthesis of an *i*, *i*+4 intramolecularly double stapled, overlapping, bicyclic oligopeptide system generated by two side chain-to-side chain macrocyclization reactions of different type on a completely preformed sequence. Moreover, by use of NMR and CD spectroscopies, the resulting final 9-mer peptide (**3**) was characterized in detail. Upon bicyclization, the mixed 3_{10}/α-helical conformation exhibited by the original linear peptide **1** is converted into a fully developed α-helix in peptide **3**. In parallel, both the helix overall content and stability are significantly increased.

2.2 Light-mediated modulation of screw sense communication in helical foldamers

The light-induced isomerization between a fumaramide (*E*-isomer) and a maleamide (*Z*-isomer) linkage was successfully employed in the field of molecular machines, in particular as a switchable component of peptido[2]rotaxanes.[22] The isomerization between this pair of diamides can be obtained using light at different wavelengths, from *E* to *Z* at 254 nm and for the reverse process, *Z*→*E*, at 312 nm.[23]

By taking advantage from this system, we decided to opportunely introduce the fumaramide linkage by stepwise amide bond formation on one side to a chiral residue capable of inducing a conformational preference and on the other to a series of achiral Aib oligomers. Our aim was to create a molecular system in which conformational induction is restored or interrupted as a result of a photochemical switch. In our studies, we choose as chiral inducers the amino acids L-valine (L-Val) and L-α-methylvaline [L-(αMe)Val]. In particular, we expected that the incorporation of L-(αMe)Val would maximize the chances to induce a high degree of preference for the right-handed screw-sense,[10a] since this chiral quaternary residue is compatible with the 3_{10}-helical structure of Aib oligomers.[10i,16a]

Thus *mono*ethyl fumarate was coupled with H-L-(αMe)Val-O^{t}Bu and H-L-Val-O^{t}Bu under standard coupling conditions (EDC/HOAt) (Scheme 2.1). After basic hydrolysis, the carboxylic acids **5a** and **5b** were recovered in quantitative yield.

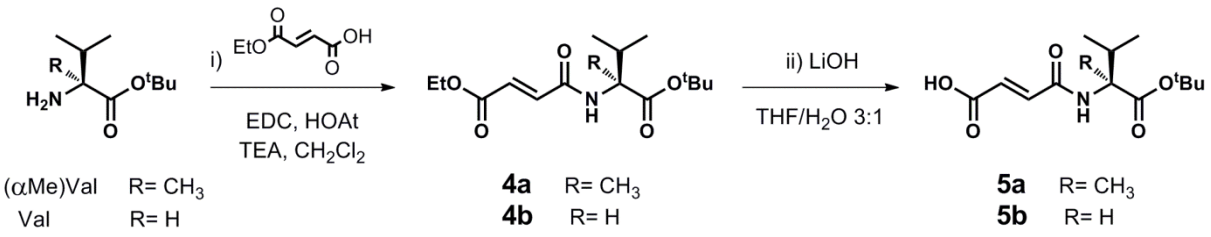

Scheme 2.1 Synthesis of fumaric acid derivatives **4a**-**b** and **5a**-**b**. Reagents and conditions: i) *Mono*ethyl fumarate, EDC, HOAt, TEA, CH_2Cl_2, r.t.; ii) LiOH, THF/H_2O 3:1, r.t., 1 h.

The synthetic strategy used to synthesize Aib homopeptides for this study is based on the well-established solution-phase, iterative coupling procedure [10b] *via* azido acyl chloride.[24] The achiral Aib oligopeptides were built up from the C-terminal protected ester (H-Aib-O*t*Bu) by acylation with α-azido*iso*butyryl chloride (Azib-Cl) followed by catalytic hydrogenation of the azide (Scheme 2.2).[10b] Repetition of the procedure gave fully protected Aib fragments. Selective functionalisation can be subsequently achieved at the N-terminus by reduction of its azido group, or at the C-terminus after removal of the orthogonal *tert*butyl ester protection.

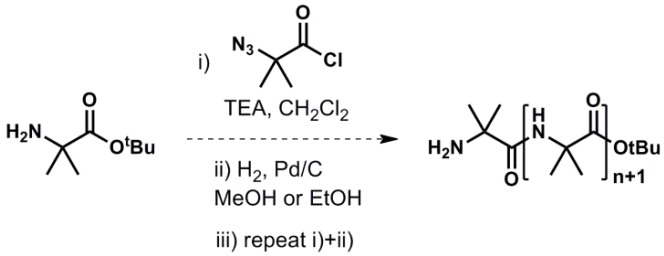

Scheme 2.2 Iterative coupling procedure applied in the synthesis of Aib homopeptides.

Functionalized Aib oligomers **6a-c** were obtained by reaction of **5a** (containing L-(αMe)Val) or **5b** (containing L-Val) with H-Aib$_n$GlyNH$_2$ (n= 4, 8) under standard coupling conditions (EDC/HOAt) (Scheme 2.3). The fumaramide peptides **6a-c** were converted to their maleamide *Z* isomers **7a-c** by irradiation (UV-light at 254 nm) of solutions in MeOH.

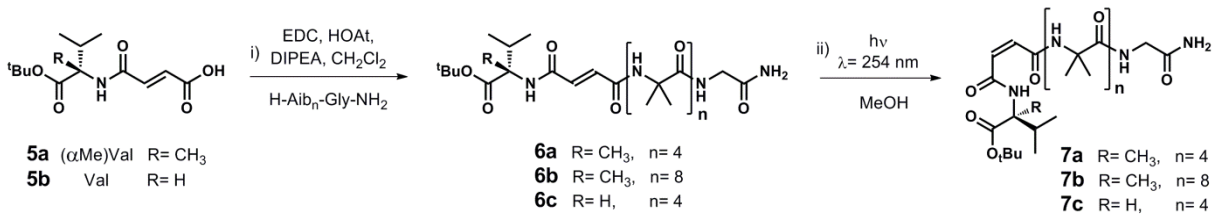

Scheme 2.3 Synthesis of the series of fumaramides **6a-c** and conversion to maleamide isomers **7a-c**. Reagents and conditions: i) H-Aib$_n$-GlyNH$_2$, EDC, HOAt, DIPEA, CH_2Cl_2, r.t.; ii) hν 254 nm, MeOH, 1 h.

Compounds **6a-c** and **7a-c** contain a C-terminal glycinamide residue to provide an NMR reporter of screw-sense preference.[10c,25] The quantification of the chemical shift separation (Δδ) between the anisochronous peaks arising from diastereotopic protons of glycinamide (αH^a and αH^b) allows the determination of relative screw-sense control in helical foldamers.[10a,10e] The ^{1}H NMR in CD_3OD of **6a**, that contains L-(αMe)Val, was recorded before irradiation (Figure 2.10, blue line) and after irradiation at 254 nm for different times (1h, green line and 3h, red line). The isomerization of **6a** to **7a** was almost quantitative in an hour (> 97%).

The inversion of double bond geometry has significant consequences for the conformational preference of the Aib$_4$ portion of the oligomer. Concurrent with the change in the olefinic region of the ^{1}H NMR spectrum as **6a** was converted into **7a**, the 2H singlet arising from the glycinamide methylene group became split into an AB system, with a chemical shift separation of 218 ppb. (Figures 2.10 A-B). Because the screw sense conformers of the Aib helix are in fast exchange on the NMR timescale, and the chiral influence is remote from the

glycinamide residue, this change in chemical shift separation indicates that the level of screw sense control transmitted through the oligomer increases from zero in the *E* derivative **2a** (Δδ = 0 ppb) to 41% helical excess in the *Z* derivative **3a** (Δδ = 218 ppb) (calculated as outlined in ref. 10e).

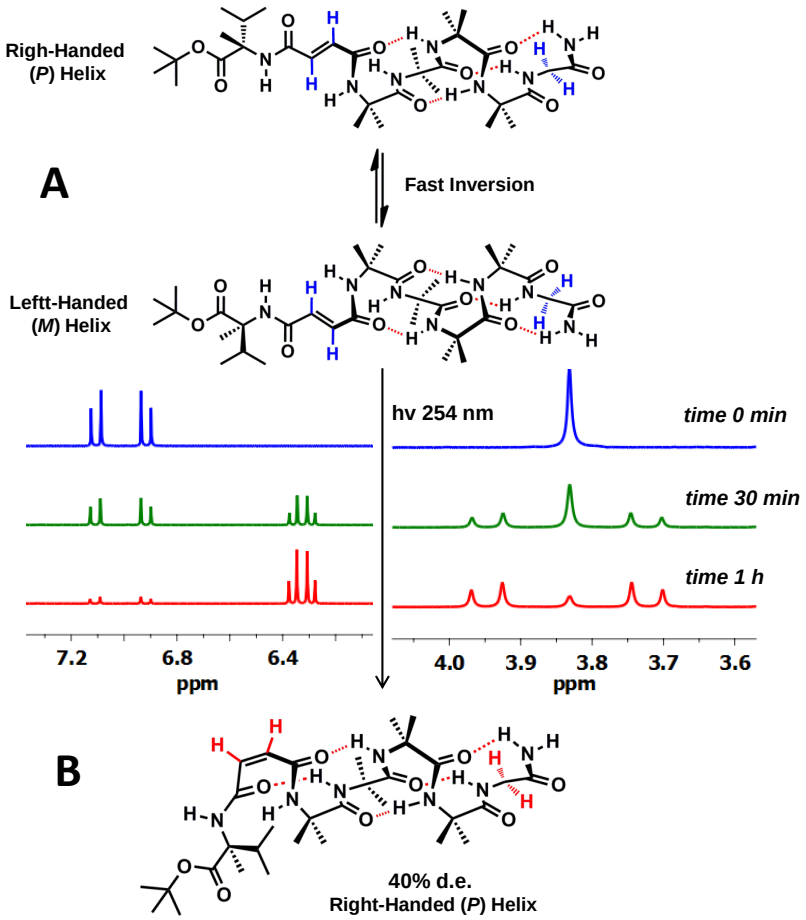

Figure 2.10 (**A**-**B**) Details of the ^{1}H NMR spectra of **6a** before irradiation (blue line) and after irradiation at 254 nm for different times (30 min, green line and 1h, red line), showing (left) the olefinic signals and (right) the glycinamide methylene signals.

The configuration around the double bond evidently plays a key role in the induction of the helical preference on Aib oligomers. The same behaviour was also observed in the glycinamide signals of the longer oligomers **6b**, which indicated no helical screw-sense preference, and **7b**, in which a chemical shift separation Δδ = 145 ppb indicated a helical excess of 27% (Table 1). Conversely, the compounds containing L-Val (**6c** and **7c**) showed lower level of control (Table 1). We found a small chiral induction also in the fumaramide derivative **6c** (Δδ = 16 ppb, 3% helical excess), and a slightly larger value for the maleamide isomer **7c** (Δδ = 67 ppb, 13% helical excess).

Table 1. Anisochronicity in the terminal CH_2 group of **6a-c**, before [$\Delta\delta_{(E)}$] and after [$\Delta\delta_{(Z)}$] photo-isomerization.

compound	amino acid	R	n	$\Delta\delta_{(E)}$ ppb	$\Delta\delta_{(Z)}$ ppb
6a	L-(αMe)Val	Me	4	0	218
6b	L-(αMe)Val	Me	8	0	145
6c	L-Val	H	4	16	67

The consequences of isomerizing the *E* double bond of **6a** to the *Z* double bond of **7a** were further studied using ^{1}H and 2D-NMR (NOESY) experiments in CD_3CN. Comparison of the two ^{1}H NMR spectra (Figure 2.11) reveals significantly different chemical shifts for the NH signals of Aib^2 and L-(αMe)Val in the two isomers. In particular, the Aib^2 NH signal of **6a** moves to higher chemical shift when isomerized to the *Z* isomer **7a** (from 7.14 to 8.61 ppm). This suggests that the *E* to Z photo-switch allows a new intramolecular H-bond to form, involving the NH of Aib^2 residue and the carbonyl of the maleamide unit adjacent to the L-(αMe)Val residue (Figure 2.11, right part).

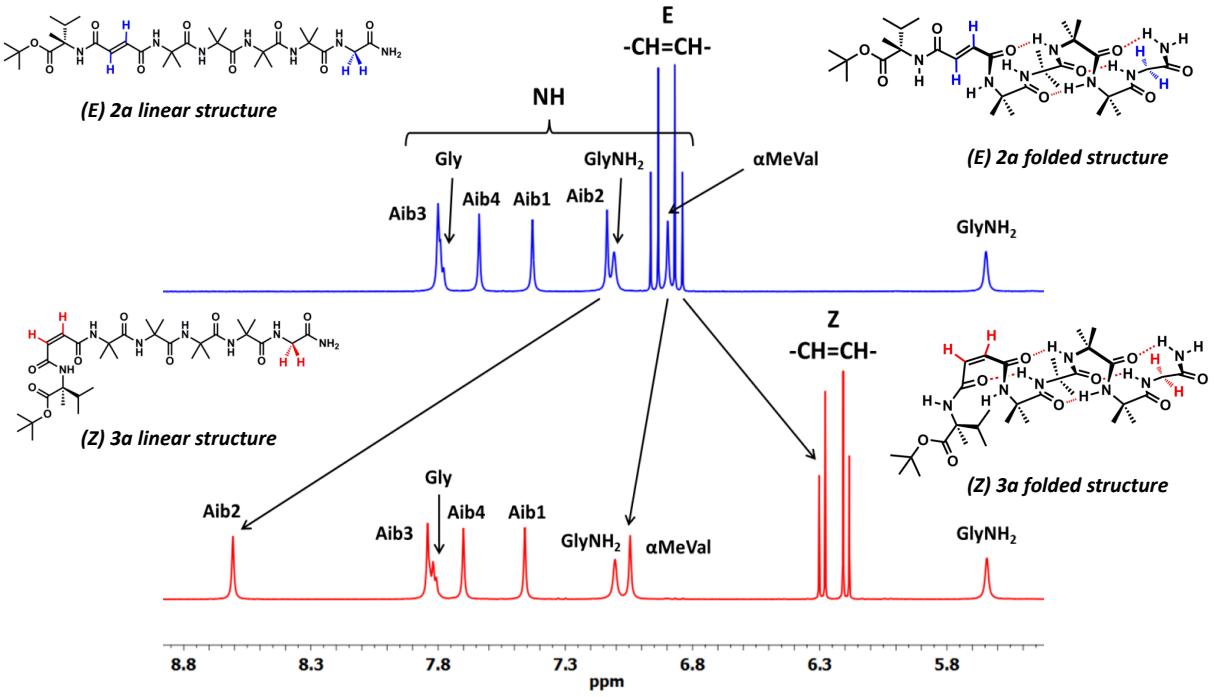

Figure 2.11 ^{1}H NMR spectra (500 MHz in CD_3CN) and assignments showing the NH and olefinic signals of *E* isomer **6a** (red line) and *Z* isomer **7a** (pure sample isolated by HPLC, blue line). Right, representation of the two different H-bond networks occurring (as hypothesis) for isomers *E* and *Z*.

Moreover sequential αNH(*i*)→αNH(*i*+1) and βCH$_3$(*i*)→αNH(*i*+1), and some medium range βCH$_3$(*i*)→αNH(*i*+2) connectivities, characteristic of a well-developed helical conformation,[20] are seen in the NOESY spectra of peptides **6a**/**7a** (Figures 2.12-2.14). These findings suggest that the Aib$_4$ segment is folded in a helical conformation, which is not modified by the isomerization.

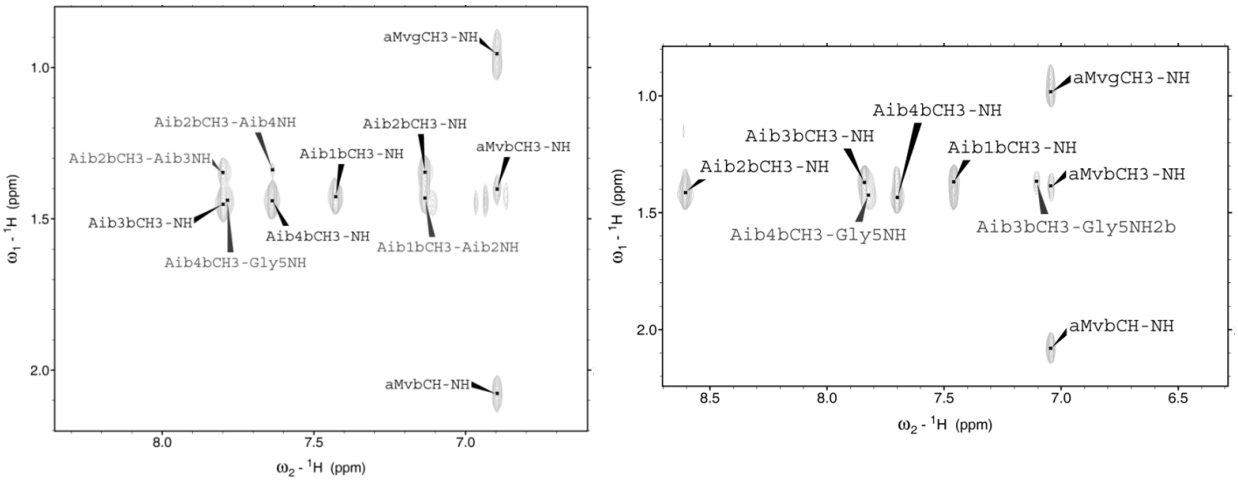

Figure 2.12 βCH$_3$ → αNH region of the NOESY spectra (500 MHz, CD$_3$CN) of peptides **6a** (**A**) and **7a** (**B**). Sequential (*i* → *i*+1) and medium-range (*i* → *i*+2), diagnostic of the presence of a 3$_{10}$-helical structure are visible in both spectra.

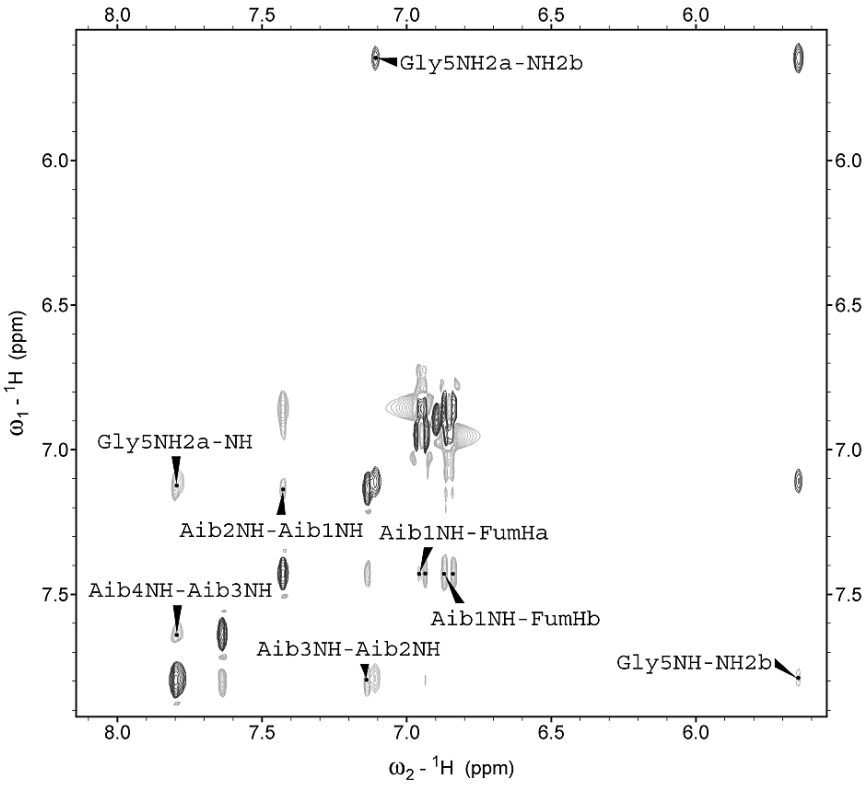

Figure 2.13 Amide region of the NOESY spectrum (500 MHz, CD$_3$CN) of **6a**. Sequential αNH(*i*)→αNH(*i*+1) are assigned in the spectrum.

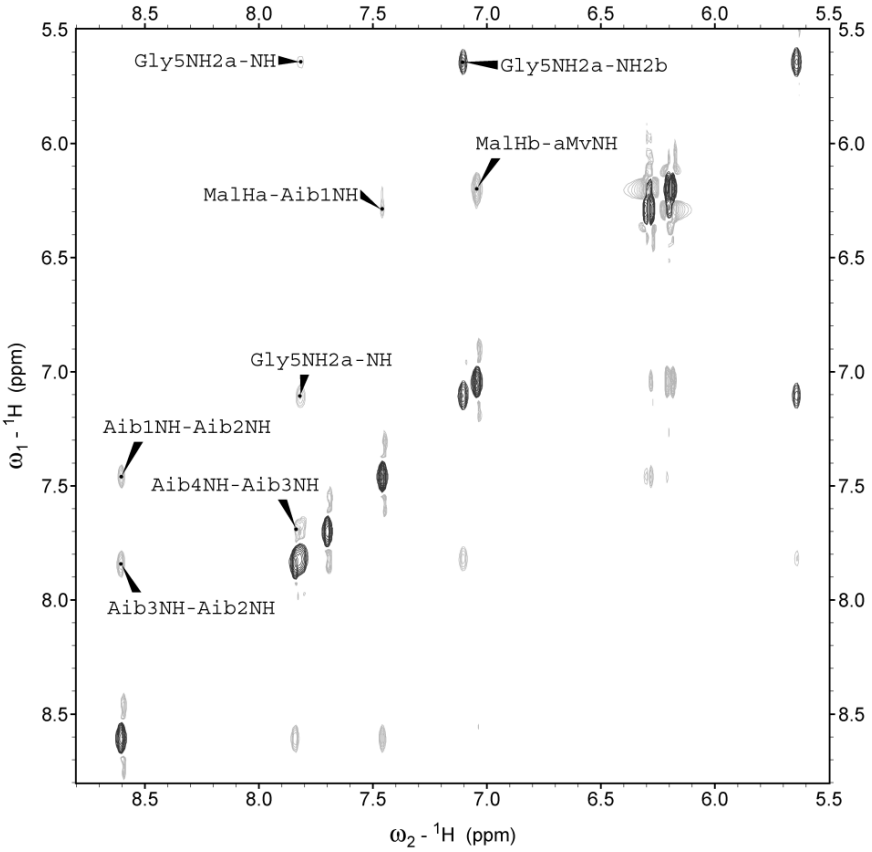

Figure 2.14 Amide region of the NOESY spectrum (500 MHz, CD_3CN) of **7a**. Sequential αNH(*i*)→αNH(*i*+1) are assigned in the spectrum.

The molecular structure of **6a** was also determined by single crystal X-ray diffraction analysis (Figure 2.15). All of the amide and ester bonds are found in the usual *trans* disposition, none of them deviating by more than ±9.0° from the ideal *trans*-planarity (180°). The conformation adopted by L-(αMe)Val is right-handed helical [ϕ,ψ = -58.4(3)°, -47.9(3)°], as expected, and its isopropyl side chain is found in the common tg^- disposition.[16a,26] The value of the torsion angle about the double bond of the fumaric acid unit (C1F-C2F-C3F-C4F) is -174.6(3)°. Both fumaramide carbonyl oxygen atoms are in a *cisoid* arrangement relative to the double bond, the values of the torsion angles O1F-C1F-C2F-C3F and C2F-C3F-C4F-O2F being -17.5(5)° and -11.4(5)°, respectively. As a result, the two oxygen atoms are slightly displaced from the average plane defined by the C1F, C2F, C3F and C4F atoms, namely O1F by 0.229(3) Å while O2F by 0.122(2) Å.

The -Aib_4- segment is folded in a right-handed 3_{10}-helix, stabilized by four intramolecular H-bonds involving the NH groups of Aib^3, Aib^4 and Gly as the donors, and the carbonyl oxygen atoms O2F, O1, and O2, respectively, as the acceptors. The average values of the ϕ,ψ backbone torsion angles for the -$(Aib)_4$- segment are -55°,-32°. The C-terminal Gly residue adopts a *semi*-extended conformation with the sign of the ϕ torsion angle opposite with

respect to that of the preceding Aib residues, thus precluding the C-terminal primary amide moiety from being involved in any intramolecular H-bond.

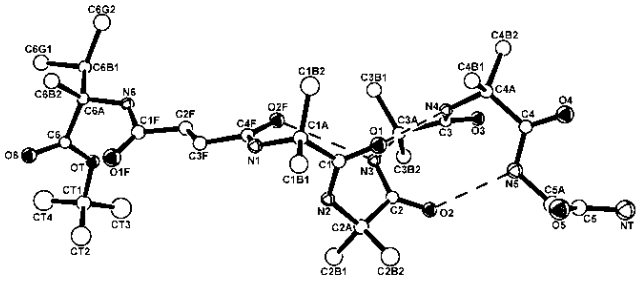

Figure 2.15 X-Ray structure of (*E*) **6a** with atom numbering. H-bonds are indicated by dashed lines.

The distance between the C^{α} atoms of L-(αMe)Val (the only chiral center) and Aib^{1} is 8.54 Å. There is no obvious reason why the chiral information should be transferred across the fumaramide linkage to the helical -Aib_4- segment. Indeed, although in this structure the -Aib_4- segment is right-handed helical, a model built by reversing the sign of all torsion angles from Aib^{1} to the C-terminal primary amide clearly showed that a left-handed helix is fully compatible with the occurrence of an L-(αMe)Val residue at the other end of the fumaramide spacer.

The secondary structure of peptides **6a-b** and **7a-b** were explored further using UV-Vis and CD measurements in MeOH solution (Figure 2.16). The chromophores of **6a** and **7a** have distinctively different UV-Vis spectra. **6a** is characterized by a more intense UV-Vis profile with a maximum absorption located at 200 nm and a pronounced shoulder located at 260 nm (Figure 2.16 A). With regard to far-UV CD analyses, *E* isomer **6a** displayed a moderately intense negative band with maximum at 212 nm followed by two weak bands of opposite sign, one positive at 238 nm and one negative at 255 nm, respectively (Figure 2.16 B, blue line). Conversely, the *Z* isomer **7a** displayed a very different CD profile (Figure 2.16 B, red line). In this case the far-UV CD profile is characterized by an intense negative maximum at 228 nm (having a shoulder at 212 nm) followed by a weak band of opposite sign at 265 nm. The compounds **6b** and **7b** displayed similar CD profiles (Figure 2.16 C).

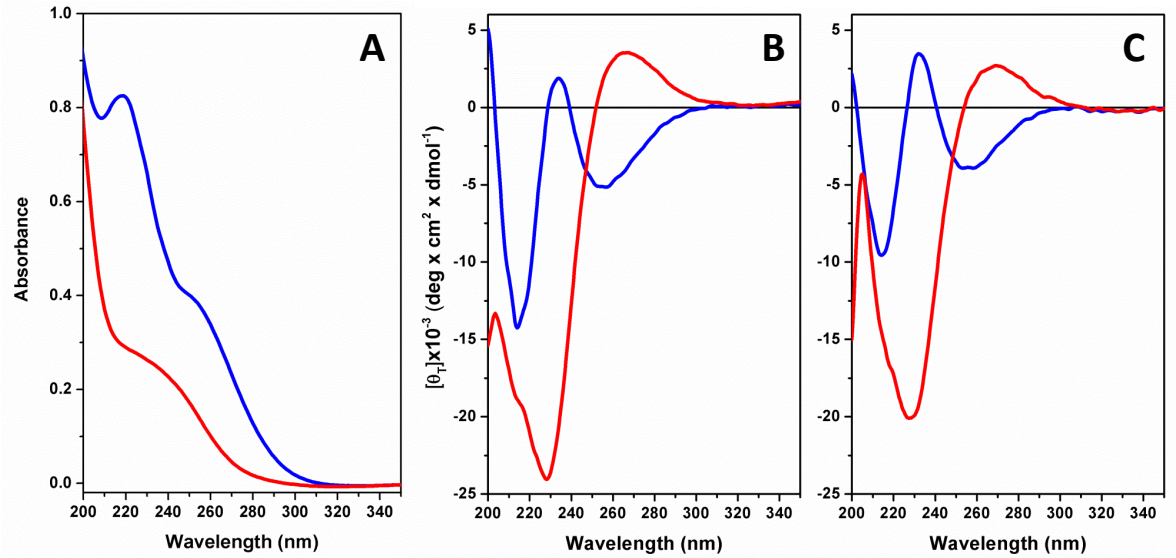

Figure 2.16 (**A**) UV-Vis spectra of (*E*) **6a** (blue line) and (*Z*) **7a** (red line) in MeOH solution. (**B**) Far-UV CD spectra of (*E*) **6a** (blue line) and (*Z*) **7a** (red line) in MeOH solution (0.3 mM). (**C**) CD spectra of **6b** in MeOH before irradiation (blue line) and after irradiation (red line) at 254 nm (0.2 mM).

In order to rationalize the CD spectra of **6a-b** and **7a-b**, we synthesized a second group of compounds (**8a-d**) which provides a series of Aib homo-peptides methyl esters of increasing length (1, 2, 4 or 8 residues, Scheme 2.4). Fumaramide peptides **8a-d** were converted to their corresponding maleamide (*Z*) isomers **9a-d** by UV-light irradiation of solutions in MeOH.

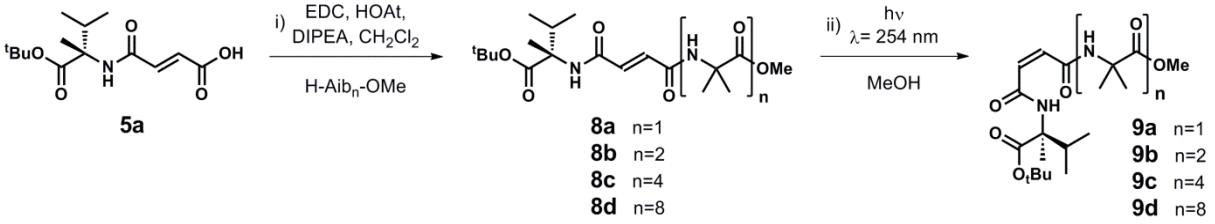

Scheme 2.4 Synthesis of compounds **8a-d** and conversion to their isomers **9a-d**. Reagents and conditions: i) H-Aib$_n$-OMe, EDC, HOAt, DIPEA, CH_2Cl_2, r.t.; ii) hν 254 nm, MeOH, 1 h.

Surprisingly, UV-light photoisomerization gave only 65% conversion of **8a** (*E*) to **9a** (*Z*). **9a** was consequently synthesized directly by reaction with the maleic acid derivative ***Z*5a** (Scheme 2.5). ***Z*5a** was obtained by one pot reaction between maleic anhydride and L-(αMe)Val under basic conditions and then coupled to H-Aib-OMe obtaining **9a**.

In order to characterize the influence of the fumaramide and the maleamide chromophores in the CD spectra we initially compared the spectra of the two shortest analogues **8a** and **9a**, lacking a helical tail (Figure 2.17 A).

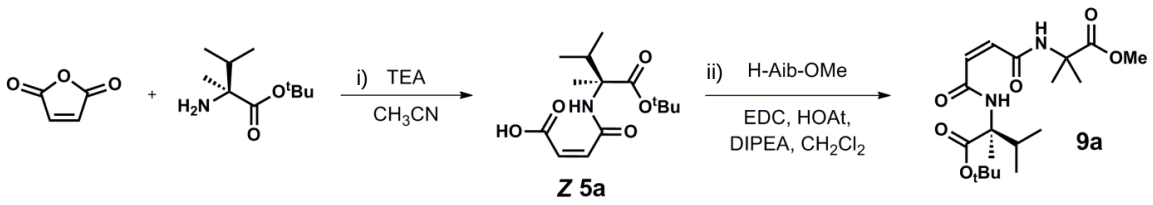

Scheme 2.5 Synthesis of maleamide derivatives ***Z*5a** and **9a**. Reagents and conditions: i) TEA, CH3CN, r.t., overnight; ii) H-Aib-OMe, EDC, HOAt, DIPEA, CH_2Cl_2, r.t.

Compound **8a** presents a CD signature comparable to those of **6a-b**, while **9a** displays a very weak CD signal, comparable in profile to that of its *E*-isomer **8a**. The CD spectra of the series of *E* configured Aib peptide methyl esters **8b-d** are all similar to the spectra recorded both for **6a-b** and the non-helical homologue **9a** (Figures 2.17 B-D, red lines). Their *Z* configured homologues **9b-d** (formed by photoisomerization) provided more interesting information. In the case of **9b** (with only two Aib residues, Figure 2.17 B, blue line) the resulting spectrum, even resembling in shape those of **7a-b**, showed intriguing features. It reveals a negative maximum at 208 nm followed by a pronounced shoulder at 227 nm and a positive maximum at 270 nm. The CD spectrum of **9c** (with four Aib residues, Figure 2.17 C, blue line) shows two intense negative maxima characterized by similar intensity located at 209 and 228 nm (and preserve the positive maximum at 260-270 nm). Finally compound **9d** (with eight Aib residues, Figure 2.17 D) displays a CD signature almost superimposable with the curve shown by **6b**. We can conclude that the CD signature of the *E* isomers containing more than two Aib residues arises from the adoption of a preferred helix screw-sense, which is induced by the fumaramide-to-maleamide photoisomerization.

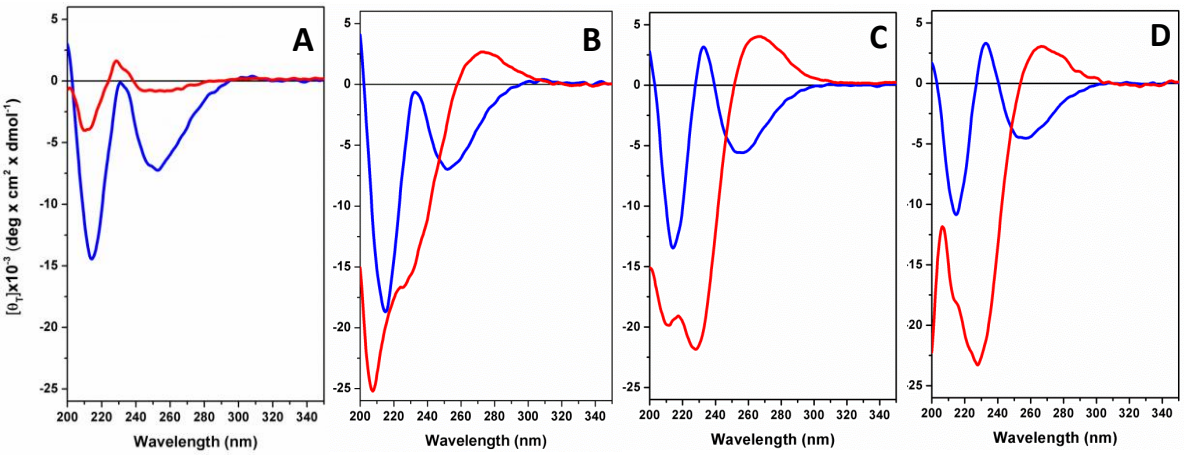

Figure 2.17 CD spectra in MeOH (0.3 mM) of **8a** and **9a** (**A**, blue and red line respectively); **8b** and **9b** (**B**, blue and red line respectively); **8c** and **9c** (**C**, blue and red line respectively); **8d** and **9d** (**D**, blue and red line respectively).

^{1}H-NMR and 2D-NMR spectra (NOESY experiment) were recorded also for the **8a-c** and **9a-c** peptide series in CD_3CN (Figures 2.18-2.20). From a comparison of the ^{1}H NMR spectra, we found a number of variations in the chemical shift of NH signals after photoisomerization. In the case of the shortest compounds **8a**/**9a**, both NH [Aib and (αMe)Val] signals possess higher chemical shift in the spectrum of the *Z* isomer **9a** (Figure 2.18). Similar behavior was observed for **8b**/**9b** but the variation of chemical shift was less pronounced (Figure 2.19). The spectra of **8c**/**9c** resemble in shape those of **6a**/**7a**, in which only the Aib^2 and (αMe)Val NH signals revealed significantly different chemical shifts (Figure 2.20).

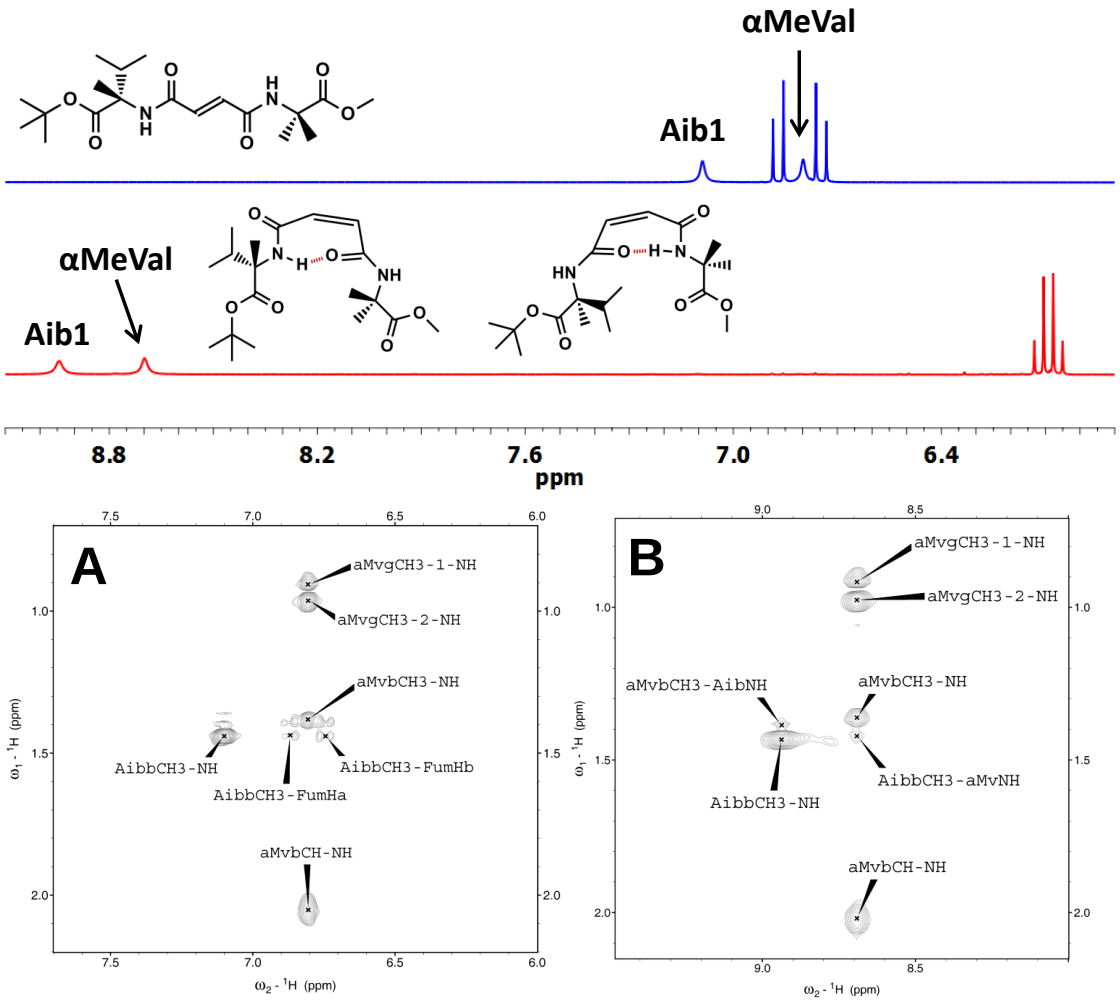

Figure 2.18 Upper part: ^{1}H NMR spectra (500 MHz, CD_3CN) of **8a** and **9a**. $\beta CH_3 \rightarrow \alpha NH$ region of the NOESY spectra of peptides **8a** (**A**) and **9a** (**B**).

Additional information was obtained from the NOESY spectra, in which different connectivities are seen for fumaramide and maleamide isomers (Figures 2.18 A-B). We found the sequential connectivities $\beta CH_3(i) \rightarrow \alpha NH(i+1)$ in the NOESY spectra of **8b** (Aib^1 →Aib^2)

and **8c** (Aib[1] → Aib[2], Aib[2] → Aib[3]). Coversely only in the spectra of Z isomers **9b-c**, we observed a cross-peak between Aib[2] NH and (αMe)Val γCH_3, which suggests the close spatial proximity of these residues after isomerization. All sequential αNH(*i*)→αNH(*i*+1) connectivities are visible in the NOESY spectra of peptides **8c**/**9c**, confirming the presence of a well-developed helical conformation throughout the –Aib_4- segment (Figure 2.18).

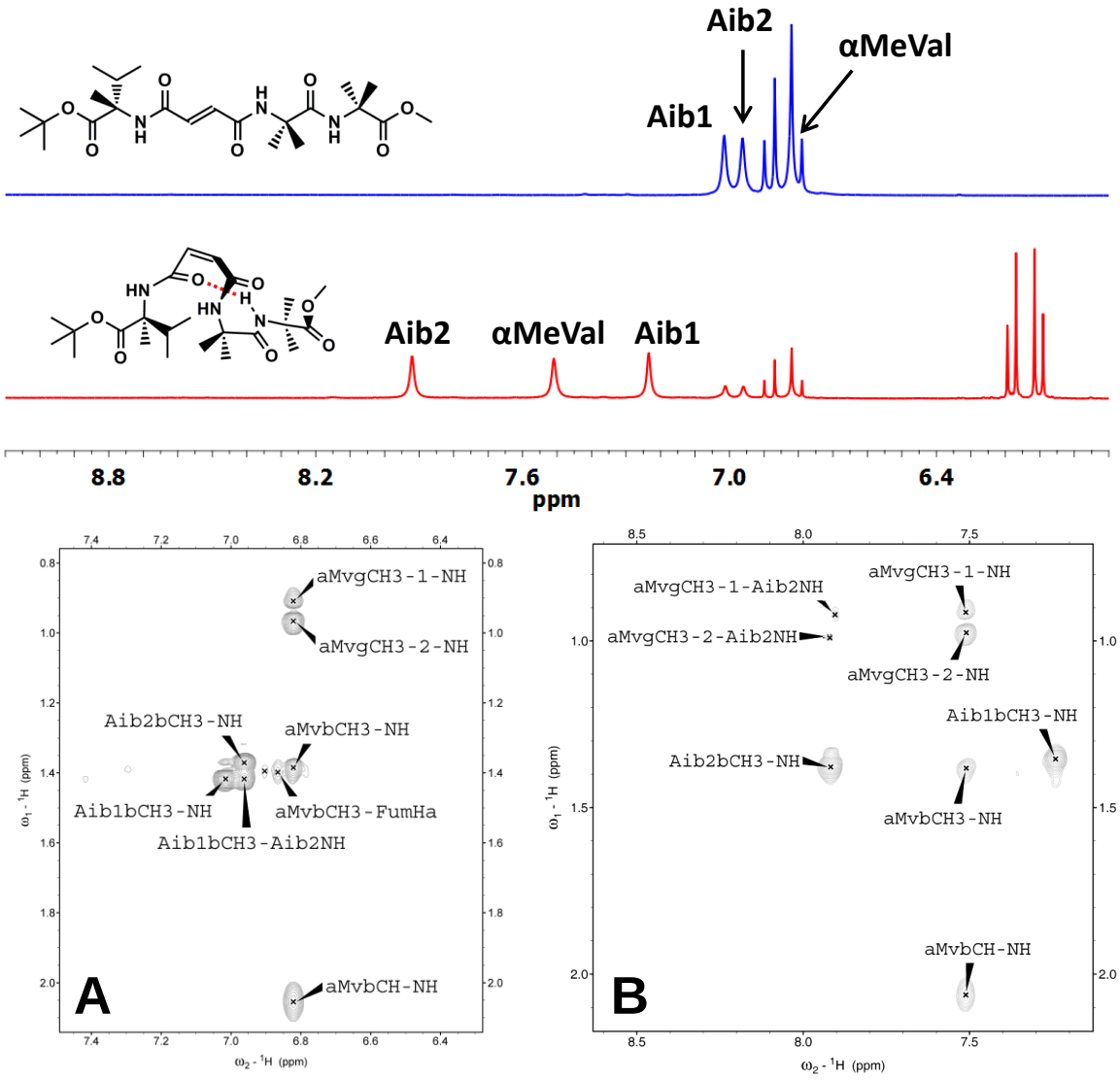

Figure 2.19 Upper part: ^{1}H NMR spectra (500 MHz, CD_3CN) of **8a** and **9a**. βCH$_3$ → αNH region of the NOESY spectra of peptides **8b** (**A**) and **9b** (**B**).

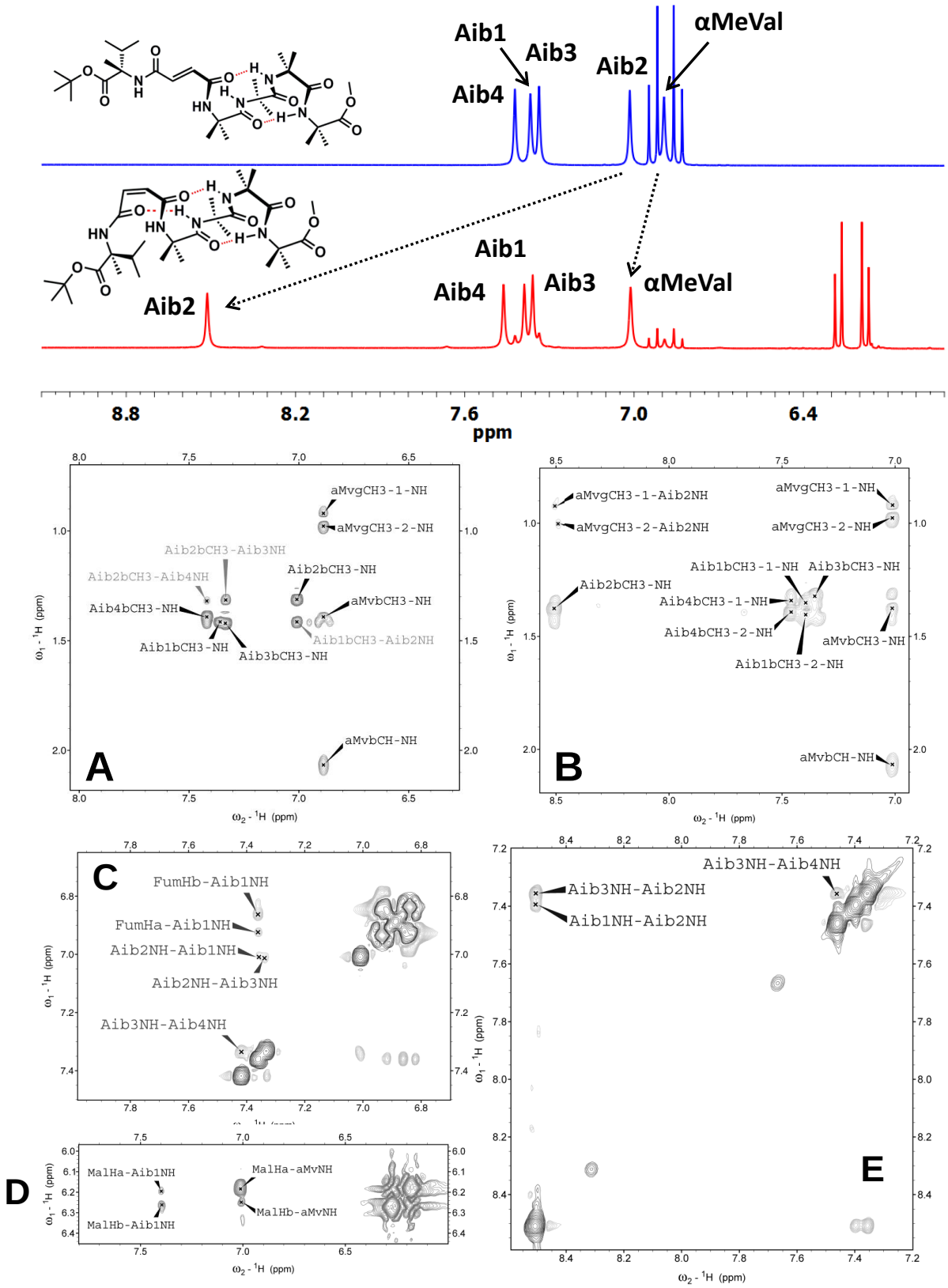

Figure 2.20 Upper part: ^{1}H NMR spectra (500 MHz, CD_3CN) of **8c** and **9c**. $\beta CH_3 \rightarrow \alpha NH$ region of the NOESY spectra of peptides **8c** (**A**) and **9c** (**B**). NH → NH region of the NOESY spectra of peptides **8c** (**C**) and **9c** (**D**,**E**).

As previously reported in literature, the secondary structure plays a key role in the enantioselective chain extension reactions of helical peptides.[12,27] Induction of a globally chiral secondary structure in an achiral peptide chain by a single remote chiral residue at the N terminus, is on its own sufficient to allow enantioselective chain extension at the C terminus.[12] To demonstrate the potential of our system in which a helical screw sense preference can be turned on or off using light, we exploited 5(*4H*)oxazolones (azlactones) from the *tetra*- and *octa*-Aib peptides **8c** and **8d** as activated compound for chain extension reactions. To this end, peptides **8c** and **8d** were hydrolyzed under basic conditions to the corresponding *E* configured carboxylic acids **10a-b** (Scheme 2.6). The corresponding (*Z*) isomers **11a-b** were easily formed on irradiation with UV light.

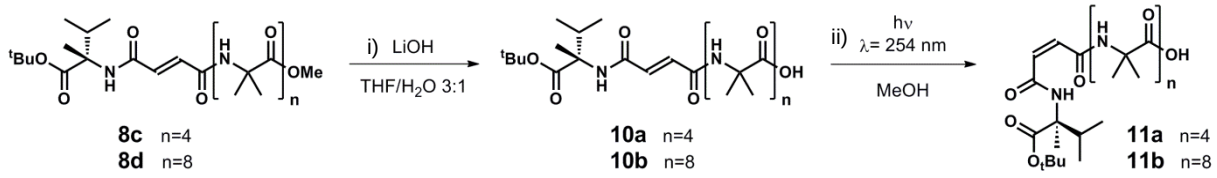

Scheme 2.6 Synthesis of the carboxylic acids **10a-b** and **11a-b**. Reagents and conditions: i) LiOH, THF/H_2O 3:1, 40-60 °C, 24 h; ii) hν 254 nm, MeOH, 1 h.

The peptide oxazolones **12a-b**, **13a-b** were synthesized by reaction with EDC in an appropriate solvent. To run the diastereoselection experiments, the oxazolones **12a-b** and **13a-b** were allowed to react with a large excess (8 equiv.) of H-D,L-Val-OMe (Scheme 2.7).

The ratios of the pairs of diastereoisomers formed were quantified by reverse phase HPLC. A first set of experiments was performed in acetonitrile at different temperatures (20, 40 and 70 °C). In no case was stereoselectivity observed: the pairs of diastereoisomers (**14a**/**c** or **14b**/**d**, **15a**/**c** or **15b**/**d**) were formed in a 50:50 ratio. The reactions were repeated in CH_2Cl_2 (at 20 °C, 35 °C and under reflux). Interestingly, we found that only **13b** (*Z* isomer, 8 Aib residues) showed a remarkable stereoselectivity in chain extension reaction by incorporating preferentially L-Val-OMe (Figure 2.21). Moreover, in this solvent we found a kinetic control, as we observed an increase of diastereoselection ratio with decreasing temperature (Table 2).

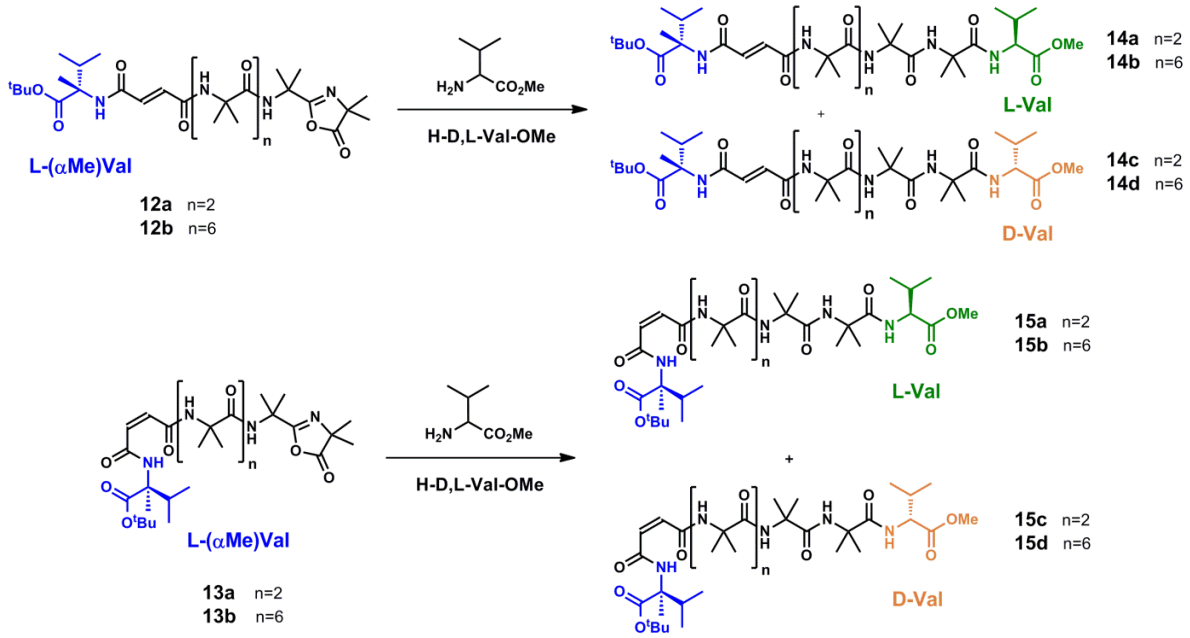

Scheme 2.7 Diastereoselection experiments of peptide oxazolones (*E*) **12a-b** (**A**) and (*Z*) **13a-b** (**B**) with H-D,L-Val-OMe.

Table 2. Diastereoselection experiment of (*Z*) **13b** with H-D,L-Val-OMe. Reaction conditions (solvent and temperature) and ratio between the two diastereoisomers, calculated as the relative peak areas % from HPLC trace.

solvent	*temperature*	**9b : 9d**
CH_2Cl_2	20 °C	74 : 26
CH_2Cl_2	35 °C	62 : 38
CH_2Cl_2	reflux	57 : 43
CH_3CN	20 °C	51 : 49

These findings are in agreement with previous results on related systems which demonstrated that low polarity solvent and low temperature markedly favor a higher stereoselectivity.[27c] Additionally, as it was stated above, only (*Z*) **13b** was able to give a diastereoselection and this critical main-chain length suggests that only at the octamer level the C-terminal oxazolone is "buried" enough to be affected by the overall chirality of the system, and this means that the helical structure is stabilized in a preferred screw-sense by a sufficient number of intramolecular H-bonds. Importantly, the solvent effect may be rationalized on the basis on the H-bonding competition. A polar solvent such as CH_3CN, in contrast to CH_2Cl_2, can be considered as a moderately competitive H-bonding acceptor and for this reason may have a

critical effect on the stabilization of the overall constrained structure, thus facilitating helix screw-sense inversion.

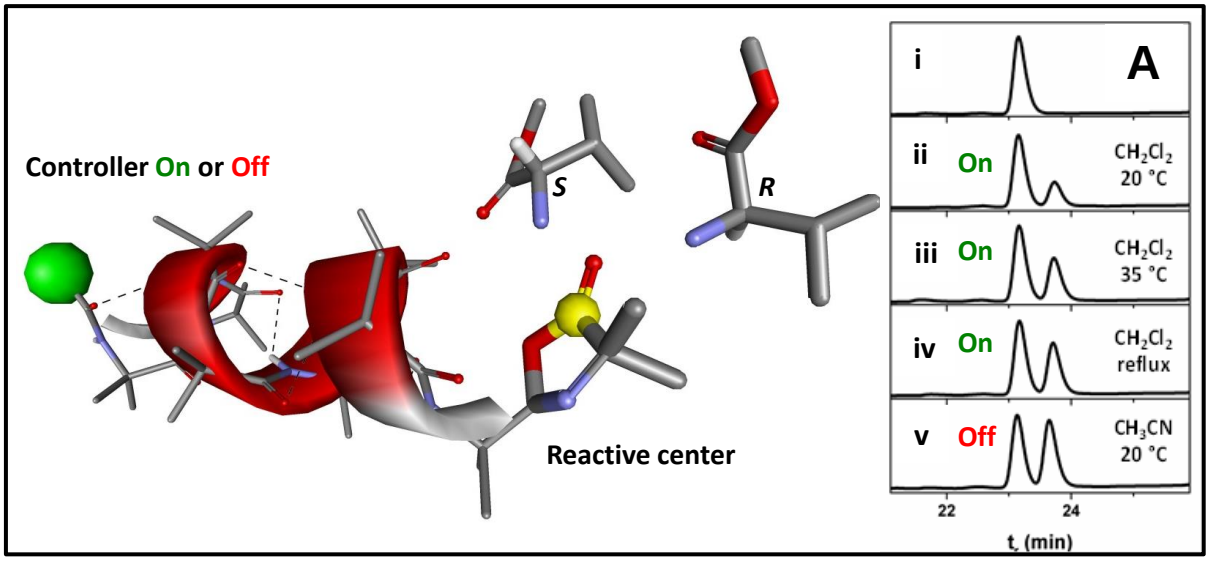

Figure 2.21 Scheme of diastereoselection experiments of peptide oxazolone (*Z*) **13b** with H-D,L-Val-OMe; (**A**) HPLC traces of (**i**) an authentic sample of (*Z*) **15b**; (**ii**) reaction mixture of **13b** with H-D,L-Val-OMe in CH_2Cl_2 at 20 °C, at (**iii**) 40 °C and (**iv**) under reflux; (**v**) reaction mixture of **13b** with H-D,L-Val-OMe in CH_3CN at 20 °C.

Finally we investigated the behavior of a more complex system in which the photoswitchable linker serves as a means of conducting or insulating conformational communication between two helical Aib_4 domains linked head-to-head (N-terminus to N-terminus) (Scheme 2.8). A chiral inducer (L-Ala-O^{t}Bu and a glycinamide NMR reporter were each located at the C-terminus of the Aib_4 domains. L-Ala can participate in a 3_{10} helical structure and as its ester derivative induces high levels of left-handed screw-sense control when located at the C-terminus of an Aib oligomer.[11]

*Mono*ethyl fumarate was coupled to the N-terminus of H-Aib_4GlyNH$_2$ and the free carboxylic acid **16** was recovered after basic hydrolysis (Scheme 2.8). H-L-Ala-O^{t}Bu was linked at the C-terminus of N_3-Aib_4-OH, catalytic hydrogenation yielded **17**. Compound **18** was obtained by coupling the two fragments **16** and **17**. **18** was converted to its corresponding maleamide (*Z*) isomer **19** in 85% selectivity by irradiation (UV light 254 nm).

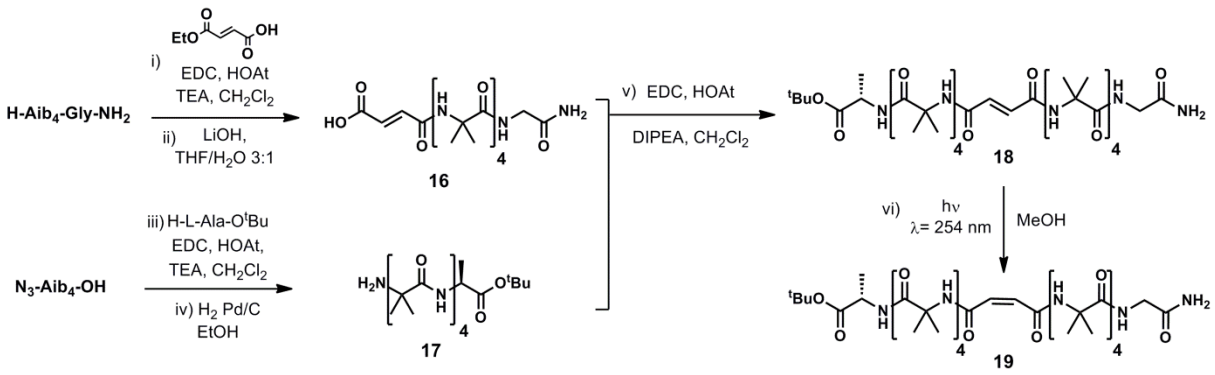

Scheme 2.8 Synthesis of compounds (*E*) **18** and (*Z*) **19**. Reagents and conditions: i) *Mono*ethyl fumarate, EDC, HOAt, TEA, CH_2Cl_2, r.t.; ii) LiOH, THF/H_2O 3:1, r.t., 1 h; iii) H-L-Ala-O*t*Bu, EDC, HOAt, TEA, CH_2Cl_2, r.t.; iv) H_2, Pd/C, EtOH, 24 h; v) EDC, HOAt, DIPEA, CH_2Cl_2, r.t.; vi) hν 254 nm, MeOH, 2 h.

The far UV CD spectrum of (*E*) **18** recorded in MeOH solution revealed some preliminary interesting information (Figure 2.22). Despite the spatial separation of the fumaramide chromophore and the chiral inducer (Ala), the spectrum shows a CD signature from the fumaramide characterized by two maxima (one positive located at 212 nm, and one negative located at 235 nm) of equal intensity. Comparison with **6a-b** and **8c-d** (the four longest homopeptide sequences Figures 2.16 and 2.17) reveals similar profiles but opposite sign. In the case of **18**, the fumaramide chromophore is affected by the chiral environment imposed by the left-handed helix originating from the C-terminal L-Ala-OMe residue.[11] In the CD spectrum of the *Z* isomer **19** the positive band around 210 nm is markedly less intense than that observed for the corresponding *E* isomer, while the intensity of the negative band around 235 nm is only slightly modified.

The details of ^{1}H NMR spectra of **18** illustrate the signals due to the glycinamide methylene group before (blue) and after (red) irradiation at 254 nm (Figura 2.22). A singlet for **18** indicates no induction of screw sense preference, but the chemical shift separation $\Delta\delta$ = 31 ppb indicates that in the case of **19** the maleamide communicates conformational information from the left-handed helical domain adjacent to the L-Ala residue to the more remote helical domain carrying the Gly residue.

The CD spectra of both **18** and **19** show that a preferred screw sense preference pass from the chiral inducer (L-Ala) to the unsaturated moiety, NMR shows that only the maleamide communicates this conformational information further, to the GlyNH_2 residue. Despite this, the CD signal of **19** is *less* intense than that of **18**, suggesting that in the case of the (*Z*) **19** isomer the screw sense induced in the remote helical domain is of opposite chirality to that in

the domain adjacent to the L-Ala residue. Because of the chemical differentiation of the two helical parts is slight (L-Ala vs. Gly) the two helices of opposite screw-sense tend towards a pseudo-meso structure, leading to the less intense CD spectrum of the (*Z*) **19** isomer.

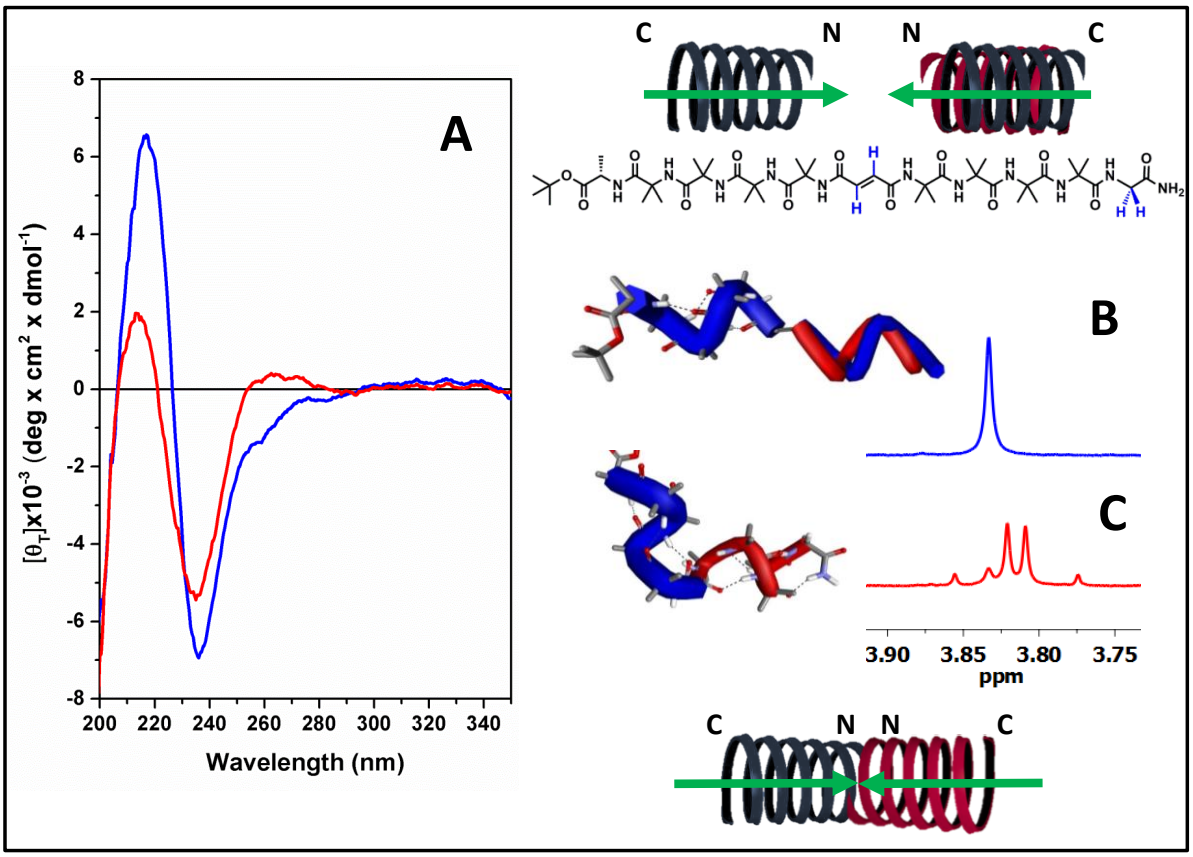

Figure 2.22 (**A**) CD spectra of **18** before (blue) and after (red) irradiation at 254 nm. Center: schematic view of the photo-induced molecular rearrangement occurring for **19**. (**B** and **C**) Details of the ^{1}H NMR spectra glycinamide signals before (blue) and after (red) irradiation at 254 nm.

Conclusions

To summarize, we presented a novel approach to control asymmetric induction over long distances (up to 20Å, and up to 30 covalent bonds) by using helical molecules in which a screw-sense preference may be activated by the absorption of UV light. In the molecules we presented here, a *trans* configuration in the fumaramide linkage holds the chiral residue away from the achiral portion of the oligomers, preventing the induction of a conformational preference. However, after photoisomerization, the *cis* configuration of the resulting maleamide brings the chiral and achiral portions into proximity, and results in a pronounced preference for one of the two possible, helical screw senses. As a result, we showed that it is

possible to use light to switch on or off the ability of the molecules to react stereoselectively in a chain extension reaction. Finally, we reported an example of helix-to-helix communication of conformational preference modulated by the absorption of light.

2.3 Experimental Section

Instruments and Methods

High-Performance Liquid Chromatography. The HPLC measurements were performed using an Agilent 1200 apparatus (Palo Alto, CA), equipped with a UV detector at 226 nm and a column Agilent Extend-C_{18} (stationary phase). Eluants: A= 9:1 H_2O/CH_3CN, 0.05 % TFA; B= 1:9 H_2O/CH_3CN, 0.05 % TFA.

Nuclear Magnetic Resonance. ^1H NMR and 2D-NMR spectra (DQF-COSY, TOCSY and NOESY experiments) were recorded at 25, 45 and 65 °C on a Bruker Avance 400 or 500 MHz instruments. ^1H and ^{13}C spectra were referenced relative to the solvent residual peaks and chemical shifts (δ) reported in ppm downfield of tetramethylsilane ($CDCl_3$ δ H: 7.26 ppm, δ C: 77.16 ppm; CD_3OD δ H: 3.31 ppm, δ C 49.05 ppm, CD_3CN δ H: 1.94 ppm, δ C: 118.26 ppm). The multiplicity of a signal is indicated as br, broad; s, singlet; d, doublet; t, triplet; m, multiplet. Where ^1H NMR spectra were run in MeOD exchangeable protons (NH, OH) are reported only where observed.

Mass Spectrometry. High-resolution (HR) mass spectra by electrospray ionization (ESI), collected in the positive mode, were performed on two different instruments:

i) Perseptive Biosystem Mariner ESI-ToF5220 spectrometer (Foster City, CA);

ii) Thermo Finnigan MAT95XP (data were recorded by staff at the University of Manchester and are accurate to ± 0.001Da).

Circular Dichroism. CD measurements were carried using a Jasco J-715 spectropolarimeter at different temperatures (20, 40 and 60°C) and a thermostatic system to control the temperature of the sample. Fused quartz cells of 0.2-mm and 1-mm path length (Hellma, Müllheim, Germany) were used. The value are expressed in terms of $[\theta]_T$, the total molar ellipticity (deg x cm^2 x $dmol^{-1}$).

Fourier Transform-Infrared Spectroscopy. FT-IR absorption spectra were recorded with a ATi Perkin Elmer Spectrum RX1 FT-IR spectrometer. The $\bar{\upsilon}$ maxima for the main absorption bands are given.

Melting point. Mps were determined on a GallenKamp apparatus and are uncorrected.

Single cristal X-Ray diffraction. Single crystals of **6a** were grown by slow evaporation from CH_3CN. Relevant crystal data, structure refinement parameters and details specific to the individual structures are given below (Tables S1-3).

X-Ray diffraction data were collected with a Gemini E four-circle kappa diffractometer (Agilent Technologies) equipped with a 92 mm EOS CCD detector, using graphite monochromated Cu Kα radiation (λ = 1.54178 Å). Data collection and reduction were performed with the CrysAlisPro software (version 1.171.36.28, Agilent Technologies). A semi-empirical absorption correction based on the multi-scan technique using spherical harmonics, implemented in the SCALE3 ABSPACK scaling algorithm, was applied. The structure was solved by ab initio procedures of the SIR 2014 program,[28] and refined by full-matrix least-squares on F^2, using all data, by application of the SHELXL-2014 program,[29] with anisotropic displacement parameters for all of the non-H atoms. H-Atoms were calculated at idealized positions and refined using a riding model.

UV lamp. A handheld UV Lamp (mineralight lamp, Model UVG-54) with wavelength of 254 nm (6W) was used in the photoisomerization experiments.

Materials

Protected amino acids Fmoc-Aib-OH and Fmoc-Cys(Trt)-OH, and 1-hydroxy-7-aza-1,2,3-benzotriazole (HOAt) were purchased from GL Biochem (Shanghai). Fmoc-Lys(Aloc)-OH and Rink amide resin (loading 0.65 mmol/g) were obtained from Iris Biotech (Germany).

O-(7-aza-1,2,3-benzotriazol-1-yl)-N,N,N',N'-tetramethyluronium hexafluorophosphate (HATU) was purchased from Novabiochem (San Diego, CA). H-L-(αMe)Val-OH, H-L-Val-OMe and H-D,L-Val-OMe were obtained from Bachem.

Grubbs (2^{nd}-generation) catalyst [1,3-bis-(2,4,6-trimethylphenyl)-2-(imidazolidinylidene) (dichlorophenylmethylene)(tricyclohexylphosphine) ruthenium], piperidine, N,N-diisopropylethylamine (DIPEA), triisopropylsilane (TIS), trifluoroacetic acid (TFA), *mono*ethyl fumarate, LiOH, triethylamine (TEA), *tert*butyl acetate, H-L-Val-O*t*Bu·HCl, $HClO_4$, *tert*-butyl *α*-bromoisobutyrate, α-bromo*iso*butyric acid, Pd/C catalyst (10% wt. loading), 1-Ethyl-3-(3-dimethylaminopropyl)carbodiimide hydrochloride (EDC·HCl), sodium azide, $SOCl_2$, H-Gly-NH_2·HCl, solution of $TMSCHN_2$ 2M in hexane were obtained from Sigma-Aldrich. The deuterated solvents DMSO-d_6, $CDCl_3$, MeOH-d_3 and MeOD-d_4 were purchased from Euriso-Top (France).

a) Stapled peptide

Ac-Aib-Cys-Aib-Lys(Aloc)-Aib-Cys-Aib-Lys(Aloc)-Aib-NH_2 (**1**). Linear compound (**1**) was prepared using standard solid-phase peptide synthesis (SPPS) and Fmoc chemistry on a Rink amide resin. The dry resin was swelled with DMF for 30 min before use. In each step, the Fmoc protecting group was removed by treatment with a piperidine/DMF (2:8) solution for 10 min (2x), then washed with DMF and CH_2Cl_2. For all of the amino acid couplings, we used the following protocol: 5.0 eq. (relative to the resin loading) of Fmoc-protected amino acid were activated with 4.9 eq. of HATU,4.9 eq. of HOAt and 15 eq. of DIPEA in DMF (2.5 mL/mmol of amino acid). This mixture was then added to a flask containing the resin-bound peptide and mixed for 2 h under a N_2 flux. The resin was then drained and rinsed with DMF and CH_2Cl_2, and then allowed to dry. For the last coupling reaction, a mixture of Ac_2O, DIPEA and DMF (1:1:3) was used and allowed to react for 20 min. For the cleavage step, the resin was prepared by washing with DMF and CH_2Cl_2, then drying under high vacuum. Cleavage from the resin and simultaneous removal of Cys side-chain protecting groups (Trt) were performed by stirring with a mixture of TFA, water and TIS (90:5:5) for 2 h. The resin was removed by filtration and washed with CH_2Cl_2. The filtrate was then evaporated under reduced pressure. The residue was dissolved in MeOH and precipitated by the addition of cold diethyl ether. The mixture was centrifuged and settled to obtain the crude peptide. Finally, the linear peptide was purified *via semi*-preparative reverse-phase HPLC and lyophilized to give a solid material (overall yield 65%).

^{1}H-NMR (400 MHz, 25 °C, DMSO-d_6) δ 8.52 (s, 1H, NH Aib^1), 8.08 (d, 1H, NH Cys^2), 7.87 (s, 1H, NH Aib^3), 7.84 (d, 1H, NH Lys^4), 7.71 (s, 1H, NH Aib^7), 7.69 (s, 1H, NH Aib^5), 7.61 (d, 1H, NH Cys^6), 7.35 (s, 1H, NH Aib^9), 7.31 (d, 1H, NH Lys^8), 7.02 (m, 2H, ζNH Lys^{4,8}), 6.92 (s, 1H, C-terminal NH), 6.77 (s, 1H, C-terminal NH), 5.88 (m, 2H, Hb Aloc^{4,8}), 5.24 (d, 2H, Hc Aloc^{4,8}), 5.14 (d, 2H, Hd Aloc^{4,8}), 4.42 (d, 4H, CH_2 Aloc^{4,8}), 4.10 (m, 1H, αCH Cys^2), 3.98 (m, 1H, αCH Cys^6), 3.91 (m, 1H, αCH Lys^8), 3.79 (m, 1H, αCH Lys^4), 2.91 (m, 4H, εCH$_2$ Lys^{4,8}), 2.90 (m, 1H, βCH Cys^6), 2.86 (m, 1H, βCH Cys^6), 2.60 (m, 1H, βCH Cys^2), 2.53 (m, 1H, βCH Cys^2), 1.92 (s, 3H, CH_3 Ac), 1.81 (m, 1H, βCH Lys^8), 1.69 (m, 2H, βCH$_2$ Lys^4), 1.53 (m, 1H, βCH Lys^8), 1.47 (s, 3H, βCH$_3$ Aib^5), 1.41 (s, 6H, 2 βCH$_3$ Aib^3), 1.40 (s, 6H, 2 βCH$_3$ Aib^7), 1.38 (s, 3H, βCH$_3$ Aib^5), 1.37 (s, 6H, 2 βCH$_3$ Aib^9), 1.36 (s, 6H, 2 βCH$_3$ Aib^1), 1.33 (m, 4H, δCH$_2$ Lys^{4,8}), 1.22 (m, 4H, γCH$_2$ Lys^{4,8}). HRMS (ESI+) *m*/*z* calcd. for $C_{48}H_{82}N_{12}O_{14}S_2$ 1114.5515; found 1115.5588 $[M+H]^+$, 558.2808 $[M+2H]^{2+}$.

Ac-Aib-Cys(X)-Aib-Lys(Aloc)-Aib-Cys(X)-Aib-Lys(Aloc)-Aib-NH_2 (**2**, X, *meta*-xylyl). A solution of α,α′-dibromo-*meta*-xylene (96 mg, 0.36mmol) and DIPEA (125 µL, 0.72 mmol) in MeOH (50 mL) was added slowly and dropwise during 2 h to a solution of linear peptide (**1**) (100mg, 0.09 mmol) in MeOH (200 mL). The mixture was stirred at r.t. for additional 4 h and the conversion of the starting material was monitored by HPLC. Then, the solution was evaporated under reduced pressure and the residue purified by flash chromatography (silica gel) with a CH_2Cl_2/MeOH eluant mixture, by increasing the polarity from 95:5 to 9:1. The material recovered after evaporation of the solvent mixture was suspended in hot ethyl acetate and precipitated by addition of petroleum ether. The solid compound was filtered and rinsed with petroleum ether. The monocyclic product was recovered in 60% yield (65 mg).
^{1}H-NMR (400 MHz, 25 °C, DMSO-d_6) δ 8.58 (s, 1H, NH Aib^1), 8.30 (d, 1H, NH Cys^2), 7.98 (d, 1H, Cys^6), 7.75 (s, 1H, NH Aib^3), 7.72 (s, 1H, NH Aib^7), 7.63 (s, 1H, NH Aib^5), 7.59 (d, 1H, NH Lys^4), 7.40 (d, 1H, NH Lys^8), 7.38 (s, 1H, NH Aib^9), 7.32 (s, 1H, Ar-*H m*-xylyl), 7.20 (m, 1H, Ar-*H m*-xylyl), 7.25 (m, 1H, Ar-*H m*-xylyl), 7.12 (d, 1H, ζNH Lys^4), 7.09 (d, 1H, ζNH Lys^8), 6.94 (s, 1H, C-terminal NH), 6.78 (s, 1H, C-terminal NH), 5.87 (m, 2H, Hb Aloc^{4,8}), 5.24 (d, 2H, Hc Aloc^{4,8}), 5.14 (d, 2H, Hd Aloc^{4,8}), 4.42 (d, 4H, CH_2 Aloc^{4,8}), 4.22 (m, 1H, αCH Cys^2), 4.07 (m, 1H, αCH Cys^6), 3.89 (m, 1H, αCH Lys^8), 3.83 (m, 1H, αCH Lys^4), 3.73 (t, 2H, CH_2*m*-xylyl), 3.60 (t, 2H, CH_2*m*-xylyl), 3.12 (m, 1H, βCH Cys^6), 2.92 (s, 4H, εCH$_2$ Lys^{4,8}), 2.83 (m, 1H,βCH Cys^2), 2.74 (m, 1H,βCH Cys^6), 2.63 (m, 1H, βCH Cys^2), 1.93 (s, 3H, CH_3 Ac), 1.81 (m, 1H, βCH Lys^8), 1.70 (m, 2H, βCH$_2$ Lys^4),1.57 (m, 1H, βCH Lys^8), 1.50 (s, 3H, βCH$_3$ Aib^7), 1.43 (s, 6H, 2 βCH$_3$ Aib^5),1.40 (s, 3H, βCH$_3$ Aib^3), 1.38 (s, 3H, βCH$_3$ Aib^7), 1.37 (s, 6H, 2 βCH$_3$ Aib^9), 1.36 (s, 6H, 2 βCH$_3$ Aib^1), 1.35 (m, 4H, δCH$_2$ Lys^{4,8}),1.33 (s, 3H, βCH$_3$ Aib^3), 1.22 (m, 4H, γCH$_2$ Lys^{4,8}).HRMS (ESI+) *m*/*z* calcd. for $C_{56}H_{88}N_{12}O_{14}S_2$ 1216.5984; found 1217.6124 $[M+H]^+$, 609.2972 $[M+2H]^{2+}$.

Ac-Aib-Cys(X)-Aib-Lys(Y)-Aib-Cys(X)-Aib-Lys(Y)-Aib-NH_2 (**3**, X, *meta*-xylyl; Y, *bis*-carbonyloxy-(*E*/*Z*)-but-2-ene). The monocyclic peptide (**2**) (44 mg, 0.036 mmol) was dissolved in 20 mL of dry CH_2Cl_2 in an N_2-flushed flask equipped with a water-cooled condenser. A solution of the 2nd-generation Grubbs catalyst (6 mg, 20 mol%) in 1 mL of dry CH_2Cl_2 was added and the mixture was heated at 50 °C. The progress of the reaction was monitored by HPLC analysis. After refluxing for about 1.5 h, heating was stopped and the reaction was quenched by adding 25 µL of ethylvinyl ether. Stirring was continued for 15 min, after which the solvent was evaporated under reduced pressure. The crude residue was directly and effectively purified by flash chromatography (silica gel) with a $CHCl_3$/MeOH solvent mixture, by increasing the polarity of the eluant from 93:7 to 85:15. The solvent

mixture was evaporated. The recovered material was dissolved in MeOH and diethyl ether was added. The resulting suspension was centrifuged and settled to obtain the bicyclic product as a solid material (15 mg, yield 31%).

^{1}H-NMR (400 MHz, 25 °C, DMSO-d_6) δ 8.60(s, 1H, NH Aib^1), 8.33 (d, 1H, NH Cys^2), 8.02 (m, 1H, Cys^6), 7.77 (s, 1H, NH Aib^3), 7.71 (s, 1H, NH Aib^5), 7.63 (s, 1H, NH Aib^7), 7.61 (s, 1H, NH Lys^4), 7.47 (d, 1H, NH Lys^8), 7.31 (s, 1H, NH Aib^9), 7.28 (m, 1H, Ar-*H* *m*-xylyl), 7.21 (m, 1H, Ar-*H* *m*-xylyl), 7.18 (s, 1H, ζNH Lys^4), 7.15 (m, 1H, Ar-*H* *m*-xylyl), 6.97 (s, 1H, ζNH Lys^8), 6.97 (s, 1H, C-terminal NH), 6.75 (s, 1H, C-terminal NH), 5.70 (s, 2H, 2 CH alkene), 4.45 (m, 2H, CH_2 former Aloc), 4.41 (d, 2H, CH_2 former Aloc), 4.20 (m, 1H, αCH Cys^2), 4.10 (m, 1H, αCH Cys^6), 3.86 (m, 1H, αCH Lys^8), 3.80 (m, 1H, αCH Lys^4), 3.73 (m, 2H, CH_2 *m*-xylyl), 3.60 (m, 2H, CH_2 *m*-xylyl), 3.05 (m, 1H, βCH Cys^6), 2.90 (s, 2H, εCH$_2$ Lys^8), 2.88 (s, 2H, εCH$_2$ Lys^4), 2.84 (m, 1H, βCH Cys^2), 2.75 (m, 1H, βCH Cys^6), 2.60 (m, 1H, βCH Cys^2), 1.94 (s, 3H, CH_3 Ac), 1.85 (m, 1H, βCH Lys^8), 1.70 (m, 2H, βCH$_2$ Lys^4), 1.63 (s, 1H, βCH Lys^8), 1.52 (s, 3H, βCH$_3$ Aib^5), 1.43 (s, 6H, 2 βCH$_3$ Aib^7), 1.41 (s, 3H, βCH$_3$ Aib^3), 1.39 (s, 6H, 2 βCH$_3$ Aib^1), 1.38 (s, 6H, 2 βCH$_3$ Aib^9), 1.37 (s, 3H, βCH$_3$ Aib^5), 1.34 (m, 4H, δCH$_2$ Lys^{4,8}), 1.32 (s, 3H, βCH$_3$ Aib^3), 1.24 (m, 4H, γCH$_2$ Lys^{4,8}). HRMS (ESI+) *m*/*z* calcd. for $C_{54}H_{84}N_{12}O_{14}S_2$ 1188.5671; found 1189.5785 $[M+H]^+$, 595.2837 $[M+2H]^{2+}$.

b) Light-mediated modulation of screw-sense communication in helical foldamers

Fumaric acid derivatives

H-L-(αMe)Val-O^{t}Bu.[30] H-L-(αMe)Val-OH (500 mg, 3.8 mmol) was dissolved in *tert*-butyl acetate (10 mL) and the solution cooled to 0 °C. $HClO_4$ 70% (750 μL, 5.8 mmol) was added dropwise and the reaction mixture was stirred at r.t. overnight. The solution was washed with H_2O (30 mL) and HCl 1 M (15 mL). The resultant aqueous solution was treated with $K_2CO_{3(aq)}$ 10% until pH= 9 and then extracted with CH_2Cl_2 (3x25 mL). The combined organic phases were dried over $MgSO_4$, filtered and concentrated under reduced pressure. The product was recovered as a colorless oil (380 mg, 53% yield).
^{1}H NMR (400 MHz, $CDCl_3$) δ 1.94 (m, *J* = 6.8 Hz, 1H, βCH), 1.45 (s, 9H, O*t*Bu), 1.44 (s, 2H, NH_2), 1.20 (s, 3H, βCH_3), 0.90 (d, *J* = 6.9 Hz, 3H, γCH_3), 0.85 (d, *J* = 6.9 Hz, 3H, γCH_3). Data consistent with that reported in the literature.[31]

OEt-Fum-(αMe)Val-O^{t}Bu (**4a**). *Mono*ethyl fumarate (390 mg, 2.7 mmol) and HOAt (365 mg, 2.7 mmol) were dissolved in CH_2Cl_2. The suspension was cooled to 0 °C and EDC·HCl (500 mg, 2.7 mmol) was added. After complete dissolution H-(αMe)Val-OtBu (350 mg, 1.87 mmol) and TEA (400 μL, 2.9 mmol) were added and the reaction mixture stirred overnight at r.t. The solvent was removed under reduced pressure and the residue dissolved in EtOAc. The organic phase was washed with $KHSO_{4(aq)}$ 5%, $NaHCO_{3(aq)}$ 5%, brine, dried over $MgSO_4$, filtered and concentrated. The crude was purified *via* flash chromatography (eluant: petroleum ether/EtOAc increasing the solvent mixture polarity from 9:1 to 8:2). The product was obtained as a colorless oil (500 mg, 85 % yield).
HRMS (ES^+, MeOH) *m/z* calcd. for $C_{16}H_{27}NO_5Na$ ($[M+Na]^+$) 336.1787, found 336.1783. $[\alpha]_D^{20}$ = -36.3 (c 1, MeOH). FT-IR $\bar{\upsilon}_{max}$ 3351, 2977, 1727, 1682, 1259, 1368, 1296, 1272, 1150 cm^{-1}. ^{1}H NMR (400 MHz, $CDCl_3$) δ 6.91 (d, *J* = 15.3 Hz, 1H, CH Fum), 6.75 (d, *J* = 15.3 Hz, 1H, CH Fum), 6.60 (s, 1H, NH), 4.24 (q, *J* = 7.1 Hz, 2H, CH_2 Et), 2.42 (hept, *J* = 6.9 Hz, 1H, βCH), 1.63 (s, 3H, βCH_3), 1.47 (s, 9H, O*t*Bu), 1.31 (t, *J* = 7.1 Hz, 3H, CH_3 Et), 1.01 (d, *J* = 7.0 Hz, 3H, γCH_3), 0.90 (d, *J* = 6.9 Hz, 3H, γCH_3). ^{13}C NMR (101 MHz, $CDCl_3$) δ 172.57, 165.74, 162.55, 137.31, 130.19, 82.56, 64.33, 61.29, 34.17, 28.08, 19.28, 17.75, 17.67, 14.29.

OEt-Fum-Val-OtBu (**4b**). *Mono*ethyl fumarate (1.0 g, 6.9 mmol) and HOAt (940 mg, 7 mmol) were dissolved in 15 mL of dry CH_2Cl_2. The suspension was cooled to 0 °C and EDC·HCl (1.3 g, 6.9 mmol) was added. H-Val-OtBu·HCl (1 g, 4.8 mmol) and TEA (2 mL, 14

mmol) were dissolved in 10 mL of dry CH_2Cl_2 and added to the active ester solution. The reaction mixture was stirred overnight at r.t. The solvent was removed under reduced pressure and the residue dissolved in EtOAc. The organic phase was washed with $KHSO_{4(aq)}$ 5%, $NaHCO_{3(aq)}$ 5%, brine, dried over $MgSO_4$, filtered and concentrated. The crude was purified *via* flash chromatography (eluant: petroleum ether/EtOAc increasing the solvent mixture polarity from 95:5 to 9:1). The product was obtained as a white solid (1.2 g, 84 % yield).
HRMS (ES^+, MeOH) *m/z* calcd. for $C_{15}H_{25}NO_5K$ ($[M+K]^+$) 338.1370, found 338.1361. $[\alpha]_D^{20}$ = -32.5 (c 1, MeOH). Mp 105-107 °C. FT-IR $\bar{\upsilon}_{max}$ 3310, 2971, 1728, 1667, 1645, 1538, 1368, 1299, 1225, 1158 cm^{-1}. ^1H NMR (400 MHz, $CDCl_3$) δ 6.97 (d, *J* = 15.4 Hz, 1H, CH Fum), 6.82 (d, *J* = 15.4 Hz, 1H, CH Fum), 6.42 (d, *J* = 8.6 Hz, 1H, NH), 4.55 (dd, *J* = 8.7, 4.4 Hz, 1H, αCH), 4.24 (q, *J* = 7.1 Hz, 2H, CH_2 Et), 2.28-2.12 (m, 1H, βCH), 1.47 (s, 9H, OtBu), 1.31 (t, *J* = 7.1 Hz, 3H, CH_3 Et), 0.93 (dd, *J* = 9.6, 7.0 Hz, 6H, 2x γCH_3). ^{13}C NMR (101 MHz, $CDCl_3$) δ 170.89, 165.62, 163.48, 136.13, 130.97, 82.59, 61.35, 57.68, 31.80, 28.15, 18.97, 17.79, 14.28.

OH-Fum-(αMe)Val-O^{t}Bu (**5a**). **4a** (500 mg, 1.6 mmol) was dissolved in 30 mL of THF and a solution of LiOH (260 mg, 10.8 mmol) in 10 mL of H_2O was added. The solution was stirred at r.t. until TLC indicated complete consumption of the starting material. The organic solvent was removed under reduced pressure and the aqueous residue was diluted with 10 mL of H_2O. The aqueous solution was acidified with HCl 1M and extracted with EtOAc (3v). The combined organic phases were washed with $KHSO_{4(aq)}$ 5%, brine, dried over $MgSO_4$, filtered and concentrated under reduced pressure. The compound was recovered as a white solid (400 mg, 88 % yield).
HRMS (ES^+, MeOH) *m/z* calcd. for $C_{14}H_{23}NO_5Na$ ($[M+Na]^+$) 308.1474, found 308.1477. $[\alpha]_D^{20}$ = -38.4 (c 1, MeOH). Mp 213-215 °C. FT-IR $\bar{\upsilon}_{max}$ 3297, 2975, 1727, 1640, 1534, 1368, 1276, 1147 cm^{-1}. ^1H NMR (500 MHz, MeOD) δ 8.42 (s, 1H, NH), 7.11 (d, *J* = 15.5 Hz, 1H, CH Fum), 6.64 (d, *J* = 15.5 Hz, 1H, CH Fum), 2.13-2.03 (m, 1H, βCH), 1.44 (s, 9H, O*t*Bu), 1.42 (s, 3H, βCH_3), 1.01 (d, *J* = 6.9 Hz, 3H, γCH_3), 0.95 (d, *J* = 6.9 Hz, 3H, γCH_3). ^{13}C NMR (101 MHz, MeOD) δ 173.48, 168.52, 165.68, 137.85, 131.35, 82.35, 64.55, 35.87, 28.20, 17.71, 17.53, 17.50.

OH-Fum-Val-OtBu (**5b**). **4b** (1.1 g, 3.8 mmol) was dissolved in 30 mL of THF and a solution of LiOH (560 mg, 23 mmol) in 10 mL of H_2O was added. The solution was stirred at r.t. until TLC indicated complete consumption of the starting material. The organic solvent was removed under reduced pressure and the aqueous residue was diluted with water. The

aqueous solution was acidified with HCl 1M. The successive day, the compound crystalized from the solution was recovered by filtration as a white solid (849 mg, 85 % yield).
HRMS (ESI^+, MeOH) *m/z* calcd. for $C_{13}H_{21}NO_5Na$ ($[M+Na]^+$) 294.1317, found 294.1331. $[\alpha]_D^{20}$ = -36 (c 1, MeOH). Mp 170-172 °C. FT-IR $\bar{\upsilon}_{max}$ 3302, 2971, 1716, 1664, 1542, 1369, 1151 cm^{-1}. ^1H NMR (400 MHz, $CDCl_3$) δ 7.10 (d, *J* = 15.4 Hz, 1H, CH Fum), 7.02 (d, *J* = 9.0 Hz, 1H, NH), 6.85 (d, *J* = 15.4 Hz, 1H, CH Fum), 4.63 (dd, *J* = 9.0, 4.4 Hz, 1H, αCH), 2.26-2.18 (m, 1H, βCH), 1.48 (s, 9H, OtBu), 0.94 (dd, *J* = 12.6, 6.9 Hz, 6H, 2x γCH_3). ^{13}C NMR (101 MHz, $CDCl_3$) δ 171.93, 169.18, 163.66, 137.97, 130.16, 83.28, 57.73, 31.86, 28.14, 19.03, 17.68.

Aib oligomers

N_3-Aib-O*t*Bu. *tert*-Butyl *α*-bromo*iso*butyrate (12.5 mL, 67 mmol) was dissolved in dry DMF (65 mL) under N_2 atmosphere. Sodium azide (6.65 g, 102 mmol) was added and the resulting solution stirred at r.t. for 72 h. The reaction mixture was diluted with water (30 mL), acidified to pH = 2 with HCl 1 M and extracted with *tert*-butyl methyl ether (2x 75 mL). The combined organic phase was washed with HCl 1 M (4x 20 mL), dried over $MgSO_4$, filtered and concentrated under reduced pressure. The pure product was recovered as a pale yellow oil (9.8 g, 80%). ^1H NMR (500 MHz, $CDCl_3$) 1.49 (9H, s, O*t*Bu), 1.41 (6H, s, 2x βCH_3). All other data consistent with that previously reported in the literature.

H-Aib-O*t*Bu. N_3AibO*t*Bu (9.8 g, 53 mmol) was dissolved in MeOH (50 mL) under a N_2 atmosphere. Pd/C (850 mg) was carefully added and the reaction mixture stirred under an H_2 atmosphere for 24 h. The mixture was filtered through a pad of Celite, washed with MeOH and the filtrate concentrated under reduced pressure. The compound was recoverd as a pale yellow oil (7.35 g, 87%). ^1H NMR (500 MHz, CDCl3) δ 1.62 (s, 1H, NH_2), 1.43 (s, 9H, OtBu), 1.27 (s, 6H, 2x βCH_3). All other spectroscopic data consistent with that previously reported in the literature.[32]

N_3-Aib-OH. α-Bromo*iso*butyric acid (15 g, 90 mmol) was dissolved in dry DMF (80 mL) under N_2 atmosphere. Sodium azide (8.7 g, 134 mmol) was added and the resulting solution stirred at r.t. for 72 h. The reaction mixture was diluted with water (30 mL), acidified to pH = 2 with HCl 1 M and extracted with *tert*-butyl methyl ether (2x 75 mL). The combined organic phase was washed with HCl 1 M (4x 20 mL), dried over $MgSO_4$, filtered and concentrated under reduced pressure. The pure product was recovered as a colourless oil (10.2 g, 88%). ^1H

NMR (400 MHz, $CDCl_3$) δ 10.47 (1H, br s, OH), 1.49 (s, 6H, 2x βCH$_3$). All other data consistent with that previously reported in the literature.[24]

α-Azido*iso*butyryl chloride (**AzibCl**).[10b] N_3Aib-OH (7 g, 54 mmol) was dissolved in dry CH_2Cl_2 (12 mL). $SOCl_2$ (7.8 mL, 107 mmol) was added dropwise and the resulting solution stirred at reflux for 3 h. The mixture was concentrated and then distilled under reduced pressure to give the acid chloride as a colourless oil (6.15 g, 78%), that was used immediately.

N_3-Aib$_2$-O*t*Bu.[10b] H-AibO*t*Bu (6 g, 37.7 mmol) was dissolved in dry CH_2Cl_2 under N_2 atmosphere (25 mL) and TEA (7 mL, 50 mmol) was added. The solution was cooled to 0 °C and a solution of freshly distilled AzibCl (6.15 g, 41.7 mmol) in dry CH_2Cl_2 (8 mL) was added dropwise. The mixture was stirred at r.t. for 24 h. The reaction mixture was concentrated under reduced pressure. The residue was dissolved in EtOAc, washed with $KHSO_{4(aq)}$ 5%, $NaHCO_{3(aq)}$ 5% and brine. The organic phase was dried over $MgSO_4$, filtered and concentrated. The crude was purified *via* flash chromatography (eluant: petroleum ether/EtOAc 95:5). The product was obtained as a waxy solid (8.5 g, 84 % yield).
^{1}H NMR (400 MHz, $CDCl_3$) δ 7.04 (1H, s, NH), 1.45 (12H, s, 4x βCH$_3$), 1.39 (9H, s, 3x CH$_3$ O*t*Bu). Data consistent with that reported in the literature.[10b]

H-Aib$_2$-O*t*Bu.[10b] N_3Aib$_2$O*t*Bu (7.18 g, 26.5 mmol) was dissolved in EtOH (50 mL) under a N_2 atmosphere. Pd/C (10%, 650 mg) was carefully added and the reaction mixture stirred under an atmosphere of H_2 for 24 h. The mixture was filtered through a pad of Celite, washed with EtOH and the filtrate concentrated under reduced pressure. The compound was recovered as a white solid (6.2 g, 96%). ^{1}H NMR (500 MHz, $CDCl_3$) δ 8.07 (1H, s, NH), 1.53 (2H, br s, NH_2), 1.50 (6H, s, 2x βCH$_3$), 1.44 (9H, s, 3x CH$_3$ O*t*Bu), 1.33 (6H, s, 2x βCH$_3$). Data consistent with that reported in the literature.[10b]

N_3-Aib$_3$-O*t*Bu.[10b] H-Aib$_2$O*t*Bu (4.15 g, 17 mmol) was dissolved in dry CH_2Cl_2 under N_2 atmosphere (25 mL) and TEA (4 mL, 28.7 mmol) was added. The solution was cooled to 0 °C and a solution of freshly distilled AzibCl (3 g, 20.3 mmol) in dry CH_2Cl_2 (8 mL) was added dropwise. The mixture was stirred at r.t. for 24 h. The reaction mixture was concentrated under reduced pressure. The residue was dissolved in EtOAc, washed with $KHSO_{4(aq)}$ 5%, $NaHCO_{3(aq)}$ 5% and brine. The organic phase was dried over $MgSO_4$, filtered and concentrated. The crude was purified *via* flash chromatography using as eluent the solvent mixture petroleum ether/EtOAc 9:1 → 8:2. The product was obtained as a white solid (4.2 g, 70 % yield).

^{1}H NMR (500 MHz, $CDCl_3$) δ 7.19 (1H, s, NH), 6.97 (1H, s, NH), 1.55 (6H, s, 2x βCH$_3$), 1.53 (6H, s, 2x βCH$_3$), 1.52 (6H, s, 2x βCH$_3$), 1.45 (9H, s, O*t*Bu). Data consistent with that reported in the literature.[10b]

H-Aib$_3$-O*t*Bu.[10b] N_3Aib$_3$O*t*Bu (4.14 g, 11.7 mmol) was dissolved in EtOH (50 mL) under a N_2 atmosphere. Pd/C (10%, 450 mg) was carefully added and the reaction mixture stirred under an atmosphere of H_2 for 24 h. The mixture was filtered through a pad of Celite, washed with EtOH and the filtrate concentrated under reduced pressure. The compound was recovered as a white solid (3.7 g, 96%). ^{1}H NMR (500 MHz, $CDCl_3$) δ 8.16 (1H, s, NH), 7.46 (1H, s, NH), 1.73 (2H, br s, NH_2), 1.53 (6H, s, 2x βCH$_3$), 1.49 (6H, s, 2x βCH$_3$), 1.44 (9H, s, O*t*Bu), 1.36 (6H, s, 2x βCH$_3$). Data consistent with that reported in the literature.[10b]

N$_3$-Aib$_4$-O*t*Bu.[10b] H-Aib$_3$-O*t*Bu (3.83 g, 11.7 mmol) was dissolved in dry CH_2Cl_2 under N_2 atmosphere (15 mL) and TEA (3 mL, 21.5 mmol) was added. The solution was cooled to 0 °C and a solution of freshly distilled AzibCl (2.7 g, 18.2 mmol) in dry CH_2Cl_2 (8 mL) was added dropwise. The mixture was stirred at r.t. for 24 h. The reaction mixture was concentrated under reduced pressure. The residue was dissolved in EtOAc, washed with $KHSO_{4(aq)}$ 5%, $NaHCO_{3(aq)}$ 5% and brine. The organic phase was dried over $MgSO_4$, filtered and concentrated. The residue was triturated in cold Et_2O and the pure product was obtained as a white solid (4.2 g, 82 % yield).
^{1}H NMR (500 MHz, $CDCl_3$) δ 7.02 (1H, s, NH), 6.97 (1H, s, NH), 6.47 (1H, s, NH), 1.52 (6H, s, 2x βCH$_3$), 1.51 (6H, s, 2x βCH$_3$), 1.50 (6H, s, 2x βCH$_3$), 1.47 (6H, s, 2x βCH$_3$), 1.43 (9H, s, O*t*Bu). Data consistent with that reported in the literature.[10b]

N$_3$-Aib$_4$-OH.[10b] N_3-Aib$_4$-O*t*Bu (1 g, 2.3 mmol) was treated with a 1:1 mixture of TFA/CH_2Cl_2 (10 mL). After stirring for 1 h, the solution was concentrated under reduced pressure and the residue suspended in Et_2O. The compound was recovered by filtration as a white solid (790 mg, 91%). ^{1}H NMR (400 MHz, $CDCl_3$) δ 7.41 (s, 1H, NH), 7.04 (s, 1H, NH), 6.51 (s, 1H, NH), 1.56 (s, 6H, 2x βCH$_3$), 1.53 (s, 6H, 2x βCH$_3$), 1.49 (s, 6H, 2x βCH$_3$), 1.45 (s, 6H, 2x βCH$_3$). Data consistent with that reported in the literature.[10b]

N$_3$-Aib$_4$-GlyNH$_2$.[10a] N_3-Aib$_4$-OH (400 mg, 1 mmol) and HOAt (136 mg, 1 mmol) were dissolved in dry CH_2Cl_2. The resulting solution was cooled to 0 °C and EDC·HCl (192 mg, 1 mmol) was added. Then H-Gly-NH_2·HCl (230 mg, 2 mmol) and TEA (300 μL, 2 mmol) were added and the reaction mixture was stirred at r.t. for 4 d. The mixture was diluted with CH_2Cl_2 washed with $KHSO_{4(aq)}$ 5%, $NaHCO_{3(aq)}$ 5%, brine, dried over $MgSO_4$, filtered and

concentrated under reduced pressure. The organic phase was washed with $KHSO_{4(aq)}$ 5%, $NaHCO_{3(aq)}$ 5%, brine, dried over $MgSO_4$, filtered and concentrated. After purification *via* flash chromatography (eluent: CH_2Cl_2/MeOH 95:5, the product was obtained as a white solid (345 mg, 78 % yield).

^{1}H NMR (500 MHz, $CDCl_3$) δ 7.76 (1H, t, *J*=6.5, NH Gly), 7.44 (1H, s, NH), 7.42 (1H, br s, NH), 6.93 (1H, s, NH), 6.34 (1H, s, NH), 5.42 (1H, br s, NH), 3.92 (2H, d, *J*=6.5, CH_2 Gly), 1.53 (6H, s, 2x βCH_3 Aib), 1.52 (6H, s, 2x βCH_3 Aib), 1.48 (6H, s, 2x βCH_3 Aib), 1.41 (6H, s, 2x βCH_3 Aib). Data consistent with that reported in the literature.[10a]

H-Aib$_4$-GlyNH$_2$.[10a] N_3Aib$_4$-GlyNH$_2$ (200 mg, 0.45 mmol) was dissolved in EtOH (20 mL) under a N_2 atmosphere. Pd/C (10%, 30 mg) was carefully added and the reaction mixture stirred under an atmosphere of H_2 for 24 h. The mixture was filtered through a pad of Celite, washed with EtOH and the filtrate concentrated under reduced pressure. The compound was recovered as a white solid (181 mg, 97%). ^{1}H NMR (400 MHz, MeOD) δ 3.79 (2H, s, CH_2 Gly), 1.60 (6H, s, 2x βCH_3 Aib), 1.49 (6H, s. 2x βCH_3 Aib), 1.44 (6H, s, 2x βCH_3 Aib), 1.39 (6H, s, 2x βCH_3 Aib). Data consistent with that reported in the literature.[10a]

N$_3$-Aib$_4$-OMe. N_3-Aib$_4$-OH (400 mg, 1 mmol) was dissolved in 7.5 mL of THF/MeOH 3:2 solution and a solution of $TMSCHN_2$ 2M in hexane (1.2 mL, 2.4 mmol) was added dropwise. The solution was stirred at r.t. for 3 h. Few drops of acetic acid were added and the solvent was removed under reduced pressure. The residue was dissolved in EtOAc, then washed with $NaHCO_{3(aq)}$ and 5%, brine. The organic phase was dried over $MgSO_4$, filtered and concentrated. The crude was purified *via* flash chromatography (eluant: EtOAc/petroleum ether 65:35). The product was recovered as a white solid (300 mg, 72% yield).

^{1}H NMR (400 MHz, $CDCl_3$) δ 7.15 (s, 1H, NH), 6.90 (s, 1H, NH), 6.24 (s, 1H, NH), 3.69 (s, 3H, OMe), 1.53 (s, 6H, 2x βCH_3 Aib), 1.50 (s, 12H, 4x βCH_3 Aib), 1.47 (s, 6H, 2x βCH_3 Aib). Data consistent with that reported in the literature.[33]

H-Aib$_4$-OMe. N_3-Aib$_4$-OMe (300 mg, 0.75 mmol) was dissolved in 10 mL of EtOH under a nitrogen atmosphere. Pd/C (30 mg) was carefully added and the reaction mixture stirred under H_2 atmosphere until TLC indicated complete conversion (24 h). The catalyst was removed by filtration through a pad of Celite and the filtrate concentrated under reduced pressure to yield the product as a white solid (270 mg, 97% yield).

HRMS (ES^+, MeOH) *m/z* calcd. for $C_{17}H_{33}N_4O_5$ ($[M+H]^+$) 373.2451, found 373.2438. Mp 150-151 °C. FT-IR $\bar{\upsilon}_{max}$ 3314, 2985, 1732, 1650, 1507, 1418, 1154 cm^{-1}. ^{1}H NMR (400 MHz, $CDCl_3$) δ 8.13 (s, 1H, NH), 7.42 (s, 1H, NH), 6.37 (s, 1H, NH), 3.69 (s, 3H, OMe), 1.79 (s br,

2H, NH_2), 1.51 (s, 6H, 2x βCH$_3$ Aib), 1.48 (s, 6H, 2x βCH$_3$ Aib), 1.46 (s, 6H, 2x βCH$_3$ Aib), 1.37 (s, 6H, 2x βCH$_3$ Aib). ^{13}C NMR (101 MHz, $CDCl_3$) δ 178.05, 175.46, 173.60, 172.78, 56.70, 56.65, 56.09, 55.06, 52.35, 28.93, 25.51, 25.24, 24.83.

N_3-Aib$_8$-OMe. N_3-Aib$_4$-OH (150 mg, 0.4 mmol) was dissolved in 5 mL of dry CH_2Cl_2 and EDC·HCl (75 mg, 0.4 mmol) was added. The solution was stirred at r.t. for 1 h. The solvent was removed under reduced pressure and the residue dissolved in EtOAc. The organic solution was washed with $KHSO_4$, brine, dried over $MgSO_4$, filtered and concentrated under reduced pressure. The crude oxazolone was then placed under high vacuum before being dissolved in dry CH_3CN. Then H-Aib$_4$-OMe (140 mg, 0.37 mmol) was added. The reaction was stirred under reflux for 5 d under N_2. The white precipitated was collected by filtration, yielding the compound as a white solid (170 mg, 60% yield).
^{1}H NMR (400 MHz, $CDCl_3$) δ 7.56 (s, 1H, NH), 7.52 (s, 1H, NH), 7.48 (s, 1H, NH), 7.45 (s, 1H, NH), 7.34 (s, 1H, NH), 6.92 (s, 1H, NH), 6.15 (s, 1H, NH), 3.71 (s, 3H, OMe), 1.56 (s, 6H, 2x βCH$_3$), 1.53 (s, 6H, 2x βCH$_3$), 1.52 (s, 6H, 2x βCH$_3$), 1.50 (s, 6H, 2x βCH$_3$), 1.48 (s, 6H, 2x βCH$_3$), 1.46 (s, 12H, 4x βCH$_3$), 1.43 (s, 6H, 2x βCH$_3$).

Functionalized Aib oligomers

OtBu-(αMe)Val-Fum-Aib$_4$-Gly-NH_2 (6a). **5a** (140 mg, 0.49 mmol) and HOAt (70 mg, 0.51 mmol) were dissolved in CH_2Cl_2. The suspension was cooled to 0 °C and EDC·HCl (94 mg, 0.49 mmol) was added. After complete dissolution H-Aib$_4$-Gly-NH_2 (150 mg, 0.36 mmol) and DIPEA (100 µL, 0.57 mmol) were added and the reaction mixture stirred overnight at r.t. The solvent was removed under reduced pressure and the residue dissolved in EtOAc. The organic phase was washed with $KHSO_{4(aq)}$ 5%, $NaHCO_{3(aq)}$ 5%, brine, dried over $MgSO_4$, filtered and concentrated. The crude was purified *via* flash chromatography (eluant: CH_2Cl_2/MeOH 92:8). The product was obtained as a white solid (190 mg, 77% yield).
HRMS (ES$^+$, MeOH) *m/z* calcd. for $C_{32}H_{55}N_7O_9Na$ ([M+Na]$^+$) 704.3959, found 704.3976. $[\alpha]_D^{20}$ = -8.5 (c 1, MeOH). Mp 263-265 °C. FT-IR $\bar{\upsilon}_{max}$ 3293, 2930, 1654, 1537, 1468, 1383, 1364 cm^{-1}. ^{1}H NMR (500 MHz, CD_3CN) δ 7.80 (s, 1H, NH Aib^3), 7.79 (t, *J* = 6.5 Hz, 1H, NH Gly), 7.64 (s, 1H, NH Aib^4), 7.43 (s, 1H, NH Aib^1), 7.14 (s, 1H, NH Aib^2), 7.11 (s br, 1H, NHa GlyNH_2), 6.95 (d, *J* = 15.0 Hz, 1H, CH Fum), 6.90 (s, 1H, NH αMeVal), 6.85 (d, *J* = 15.0 Hz, 1H, CH Fum), 5.65 (s, 1H, NHb GlyNH_2), 3.67 (d, *J* = 6.4 Hz, 2H, CH_2 Gly), 2.10-2.06 (m, 1H, βCH αMeVal), 1.45 (s, 6H, 2x βCH$_3$ Aib), 1.44 (s, 6H, 2x βCH$_3$ Aib), 1.43 (s, 6H, 2x βCH$_3$ Aib), 1.41 (s, 9H, O*t*Bu), 1.40 (s, 3H, βCH$_3$ αMeVal), 1.35 (s, 5H, 2x βCH$_3$ Aib), 0.99 (d, *J* = 6.9 Hz, 3H, γCH$_3$ αMeVal), 0.92 (d, *J* = 6.9 Hz, 3H, γCH$_3$ αMeVal). ^{13}C

NMR (101 MHz, CD_3CN) δ 177.07, 176.60, 176.27, 175.30, 173.24, 172.59, 165.62, 164.18, 134.74, 132.98, 81.41, 64.04, 57.72, 57.54, 57.51, 57.48, 43.60, 35.49, 28.07, 25.54, 25.21, 25.10, 24.91, 17.67, 17.55, 17.44.

Synthesis of OtBu-(αMeVal)-Fum-Aib$_8$-Gly-NH$_2$ (6b). OtBu-(αMe)Val-Mal-Aib$_4$-OH (100 mg, 0.16 mmol) was dissolved in 4 mL of dry CH_2Cl_2 and EDC·HCl (38 mg, 0.2 mmol) was added. The solution was stirred at r.t. for 1 h. The solvent was removed under reduced pressure and the residue dissolved in EtOAc. The organic solution was washed with $KHSO_4$, brine, dried over $MgSO_4$, filtered and concentrated under reduced pressure The crude oxazolone was then placed under high vacuum before being dissolved in CH_3CN. Then H-Aib$_4$-Gly-NH_2 (100 mg, 0.24 mmol) was added. The reaction was stirred under reflux for 5 d. The solution was diluted with CH_2Cl_2 and the precipitate was recovered by filtration. After purification by flash chromatography (eluant: CH_2Cl_2/MeOH 95:5), the pure product was recovered as a white solid (55 mg, 33 % yield).
HRMS (ES$^+$ MeOH) *m/z* calcd. for $C_{48}H_{83}N_{11}O_{13}Na$ ([M+Na]$^+$) 1044.6064, found 1044.6060. $[\alpha]_D^{20}$ = -5.3 (c 1, MeOH). Mp decompose >270 °C. FT-IR $\bar{\upsilon}_{max}$ 3289, 2981, 1657, 1539, 1384, 1363, 1228 cm^{-1}. ^{1}H NMR (500 MHz, CD_3CN) δ 7.84 (m, 2H, 2x NH), 7.81 (s, 1H, NH), 7.79 (m, 3H, NH), 7.66 (s, 1H, NH), 7.51 (s, 1H, NH), 7.20 (s, 1H, NH), 7.12 (s, 1H, NH), 6.96 (d, *J* = 15.0 Hz, 1H, CH Fum), 6.91 (s, 1H, NH), 6.87 (d, *J* = 15.0 Hz, 1H, CH Fum), 5.65 (s, 1H, NH), 3.67 (d, *J* = 5.7 Hz, 2H, CH_2 Gly), 2.08 (m, 1H, βCH αMeVal), 1.48 (s, 6H, 2x βCH_3 Aib), 1.45 (s, 6H, 2x βCH_3 Aib), 1.44 (s, 18H, 6x βCH_3 Aib), 1.43 (s, 6H, 2x βCH_3 Aib), 1.42 (s, 6H, 2x βCH_3 Aib), 1.41 (s, 9H, O*t*Bu), 1.40 (s, 3H, βCH_3 αMeVal), 1.36 (s, 6H, 2x βCH_3 Aib), 0.99 (d, *J* = 6.9 Hz, 3H, γCH_3 αMeVal), 0.92 (d, *J* = 6.9 Hz, 3H, γCH_3 αMeVal). ^{13}C NMR (101 MHz, CD_3CN) δ 177.32, 177.09, 176.98, 176.95, 176.94, 176.30, 175.39, 173.22, 172.56, 165.66, 164.18, 134.75, 132.99, 81.44, 64.07, 57.72, 57.57, 57.48, 57.43, 57.33, 57.30, 57.27, 43.61, 35.47, 28.06, 25.19, 17.76, 17.53, 17.42.

OtBu-Val-Fum-Aib$_4$-Gly-NH$_2$ (6c). **5b** (65 mg, 0.24 mmol) and HOAt (35 mg, 0.26 mmol) were dissolved in dry CH_2Cl_2. The suspension was cooled to 0 °C and EDC·HCl (46 mg, 0.24 mmol) was added. After complete dissolution H-Aib$_4$-Gly-NH_2 (50 mg, 0.12 mmol) and DIPEA (60 µL, 0.34 mmol) were added and the reaction mixture stirred overnight at r.t. The solvent was removed under reduced pressure and the residue dissolved in EtOAc. The organic phase was washed with $KHSO_{4(aq)}$ 5%, $NaHCO_{3(aq)}$ 5%, brine, dried over $MgSO_4$, filtered and concentrated. The crude was purified *via* flash chromatography (eluant: CH_2Cl_2/EtOH,

increasing the solvent mixture polarity from 95:5 to 9:1). The product was obtained as a white solid (40 mg, 50% yield).

HRMS (ES^+, MeOH) *m/z* calcd. for $C_{31}H_{53}N_7O_9K$ ($[M+K]^+$) 706.3542, found 706.3536. $[\alpha]_D^{20}$ = -3 (c 1, MeOH). Mp 249-250 °C. FT-IR $\bar{\upsilon}_{max}$ 3292, 2932, 1642, 1537, 1472, 1420, 1363 cm^{-1}. ^{1}H NMR (500 MHz, MeOD) δ 7.15 (d, *J* = 15.1 Hz, 1H, CH Fum), 6.99 (d, *J* = 15.1 Hz, 1H, CH Fum), 4.30 (d, *J* = 5.8 Hz, 1H, αCH Val), 3.87-3.80 (m, 2H, AB system Gly), 2.21-2.15 (m, 1H, βCH Val), 1.52 (s, 3H, βCH_3 Aib), 1.51 (s, 3H, βCH_3 Aib), 1.50 (s, 6H, 2x βCH_3 Aib), 1.48 (s, 9H, OtBu), 1.47 (s, 6H, 2x βCH_3 Aib), 1.39 (s, 6H, 2x βCH_3 Aib), 0.98 (d, *J* = 6.9 Hz, 6H, 2x γCH_3 Val). ^{13}C NMR (126 MHz, MeOD) δ 178.10, 177.81, 176.22, 175.39, 171.96, 166.79, 166.24, 134.39, 134.00, 82.95, 60.29, 58.17, 58.07, 57.83, 57.78, 43.72, 31.81, 28.28, 25.69, 25.55, 25.16, 25.07, 19.51, 18.43.

OtBu-(αMe)Val-Fum-Aib-OMe (**8a**). **5a** (35 mg, 0.12 mmol) and HOAt (17 mg, 0.12 mmol) were dissolved in dry CH_2Cl_2. The suspension was cooled to 0 °C and EDC·HCl (23 mg, 0.12 mmol) was added. After complete dissolution H-Aib-OMe·HCl (37 mg, 0.24 mmol) and DIPEA (65 μL, 0.37 mmol) were added and the reaction mixture stirred overnight at r.t. The solvent was removed under reduced pressure and the residue dissolved in EtOAc. The organic phase was washed with $KHSO_{4(aq)}$ 5%, $NaHCO_{3(aq)}$ 5%, brine, dried over $MgSO_4$, filtered and concentrated. The product was obtained as a white solid after precipitation from EtOAc/petroleum ether (40 mg, 85% yield).

HRMS (ES^+ MeOH) *m/z* calcd. for $C_{19}H_{33}N_2O_6$ ($[M+H]^+$) 385.2333, found 385.2403. Mp 149-152 °C. FT-IR $\bar{\upsilon}_{max}$ 3351, 2978, 1730, 1649, 1533, 1367, 1335, 1283, 1152 cm^{-1}.

^{1}H NMR (500 MHz, CD_3CN) δ 7.09 (s, 1H, NH Aib), 6.87 (d, *J* = 15.1 Hz, 1H, CH Fum), 6.80 (s, 1H, NH αMeVal), 6.75 (d, *J* = 15.1 Hz, 1H, CH Fum), 3.62 (s, 3H, OMe), 2.05 (dt, *J* = 13.8, 6.9 Hz, 1H, βCH αMeVal), 1.44 (s, 6H, 2x βCH_3 Aib), 1.40 (s, 9H, OtBu), 1.38 (s, 3H, βCH_3 αMeVal), 0.97 (d, *J* = 6.9 Hz, 3H, γCH_3 αMeVal), 0.90 (d, *J* = 6.9 Hz, 3H, γCH_3 αMeVal). ^{13}C NMR (101 MHz, CD_3CN) δ 175.24, 172.67, 164.38, 134.40, 132.99, 81.43, 64.06, 56.93, 52.78, 35.51, 28.15, 25.21, 17.87, 17.60, 17.47.

OtBu-(αMe)Val-Fum-Aib$_2$-OMe (**8b**). **5a** (35 mg, 0.12 mmol) and HOAt (17 mg, 0.12 mmol) were dissolved in dry CH_2Cl_2. The suspension was cooled to 0 °C and EDC·HCl (23 mg, 0.12 mmol) was added. After complete dissolution H-Aib_2-OMe (48 mg, 0.24 mmol) and DIPEA (22 μL, 0.12 mmol) were added and the reaction mixture stirred overnight at r.t. The solvent was removed under reduced pressure and the residue dissolved in EtOAc. The organic phase was washed with $KHSO_{4(aq)}$ 5%, $NaHCO_{3(aq)}$ 5%, brine, dried over $MgSO_4$, filtered and

concentrated. The product was obtained as a white solid after precipitation from EtOAc/petroleum ether (45 mg, 80% yield).

HRMS (ES^+ MeOH) *m/z* calcd. for $C_{23}H_{40}N_3O_7$ ($[M+H]^+$) 470.2871, found 470.2853. Mp 89-90 °C. FT-IR $\bar{\upsilon}_{max}$ 3356, 2980, 1733, 1652, 1532, 1367, 1277, 1151 cm^{-1}. ^1H NMR (500 MHz, CD_3CN) δ 7.02 (s, 1H, NH Aib^1), 6.96 (s, 1H, NH Aib^2), 6.88 (d, *J* = 15.0 Hz, 1H, CH Fum), 6.81 (d, *J* = 15.1 Hz, 2H, CH Fum and NH αMeVal), 3.60 (s, 3H, OMe), 2.05 (dt, *J* = 13.7, 6.8 Hz, 1H, βCH αMeVal), 1.42 (s, 6H, 2x βCH_3 Aib), 1.40 (s, 9H, OtBu), 1.39 (s, 3H, βCH_3 αMeVal), 1.37 (s, 6H, 2x βCH_3 Aib), 0.97 (d, *J* = 6.9 Hz, 3H, γCH_3 αMeVal), 0.91 (d, *J* = 6.8 Hz, 3H, γCH_3 αMeVal). ^{13}C NMR (101 MHz, CD_3CN) δ 175.78, 174.25, 172.67, 164.49, 164.46, 133.95, 133.89, 81.45, 64.07, 57.88, 56.77, 52.59, 35.54, 28.16, 25.23, 25.21, 17.88, 17.60, 17.47.

OtBu-(αMe)Val-Fum-Aib_4-OMe (**8c**). **5a** (230 mg, 0.81 mmol) and HOAt (110 mg, 0.81 mmol) were dissolved in dry CH_2Cl_2. The suspension was cooled to 0 °C and EDC·HCl (155 mg, 0.81 mmol) was added. After complete dissolution H-Aib_4-OMe (200 mg, 0.54 mmol) and DIPEA (140 μL, 0.81 mmol) were added and the reaction mixture stirred overnight at r. t. The solvent was removed under reduced pressure and the residue dissolved in EtOAc. The organic phase was washed with $KHSO_{4(aq)}$ 5%, $NaHCO_{3(aq)}$ 5%, brine, dried over $MgSO_4$, filtered and concentrated. The crude was purified *via* flash chromatography using as eluent 94:6 CH_2Cl_2/MeOH. The product was obtained as a white solid (280 mg, 81% yield).

HRMS (ES^+, MeOH) *m/z* calcd. for $C_{31}H_{54}N_5O_9$ ($[M+H]^+$) 640.3916, found 640.3922. $[\alpha]_D^{20}$ = -8.1 (c 1, MeOH). Mp 136-137 °C. FT-IR $\bar{\upsilon}_{max}$ 3309, 2983, 1728, 1645, 1530, 1457, 1385, 1365, 1273, 1222, 1151, 732 cm^{-1}.

^1H NMR (500 MHz, CD_3CN) δ 7.42 (s, 1H, NH Aib^4), 7.37 (s, 1H, NH Aib^1), 7.34 (s, 1H, NH Aib^3), 7.01 (s, 1H, NH Aib^2), 6.93 (d, *J* = 15.0 Hz, 1H, CH Fum), 6.89 (s, 1H, NH αMeVal), 6.84 (d, *J* = 15.0 Hz, 1H, CH Fum), 3.58 (s, 3H, OMe), 2.06 (dq, *J* = 13.7, 6.9 Hz, 1H, βCH αMeVal), 1.42 (s, 6H, 2x βCH_3 Aib^3), 1.42 (s, 6H, 2x βCH_3 Aib^1), 1.40 (s, 9H, OtBu), 1.39 (s, 9H, 2x βCH_3 Aib^4 and βCH_3 αMeVal), 1.31 (s, 6H, 2x βCH_3 Aib^2), 0.98 (d, *J* = 6.9 Hz, 3H, γCH_3 αMeVal), 0.92 (d, *J* = 6.9 Hz, 3H, γCH_3 αMeVal). ^{13}C NMR (101 MHz, $CDCl_3$) δ 175.85, 174.80, 173.66, 173.02, 172.43, 164.97, 163.10, 135.26, 131.82, 82.14, 64.12, 57.48, 57.03, 56.92, 55.98, 52.32, 34.37, 29.85, 28.12, 25.65, 25.39, 25.05, 24.98, 18.65, 17.70, 17.67, 1.17.

OtBu-(αMe)Val-Fum-Aib_8-OMe (**8d**). **5a** (100 mg, 0.35 mmol) and HOAt (50 mg, 0.37 mmol) were dissolved in dry CH_2Cl_2. The suspension was cooled to 0 °C and EDC·HCl (70

mg, 0.36 mmol) was added. After complete dissolution, H-Aib$_8$-OMe (obtained after catalytic hydrogenation of N_3-Aib$_8$-OMe and immediately used, 140 mg, 0.2 mmol) and DIPEA (60 μL, 0.36 mmol) were added and the reaction mixture stirred overnight at r.t. The solvent was removed under reduced pressure and the residue dissolved in EtOAc. The organic phase was washed with $KHSO_{4(aq)}$ 5%, $NaHCO_{3(aq)}$ 5%, brine, dried over $MgSO_4$, filtered and concentrated. The product was obtained as a white solid after precipitation from EtOAc/petroleum ether (150 mg, 77% yield).

HRMS (ES^+ MeOH) *m/z* calcd. for $C_{47}H_{82}N_9O_{13}$ ($[M+H]^+$) 980.6027, found 980.6179. Mp 172-175 °C. FT-IR $\bar{\upsilon}_{max}$ 3310, 2986, 2942, 1733, 1659, 1535, 1467, 1458, 1385, 1364, 1229, 1152 cm^{-1}. ^1H NMR (400 MHz, $CDCl_3$) δ 7.92 (s, 1H, NH), 7.85 (s, 1H, NH), 7.80 (s, 1H, NH), 7.75 (s, 2H, 2x NH), 7.72 (s, 1H, NH), 7.49 (s, 1H, NH), 7.27 (s, 1H, NH), 7.08 (s, 1H, NH), 6.95-6.73 (m, 2H, AB system CH_2 Fum), 3.69 (s, 3H, OMe), 2.34 (dt, *J* = 14.1, 6.9 Hz, 1H, βCH αMeVal), 1.78 (s, 12H, 4x βCH_3 Aib), 1.57 (s, 3H, βCH_3 αMeVal), 1.52 (s, 12H, 4x βCH_3 Aib), 1.49 (s, 12H, 4x βCH_3 Aib), 1.47 (s, 15H, OtBu and 2x βCH_3 Aib), 1.41 (s, 6H, 2x βCH_3 Aib), 1.02 (d, *J* = 6.8 Hz, 3H, γCH_3 αMeVal), 0.93 (d, *J* = 6.8 Hz, 3H, γCH_3 αMeVal). ^{13}C NMR (101 MHz, $CDCl_3$) δ 176.49, 176.18, 176.09, 175.72, 175.22, 175.19, 174.69, 172.47, 165.44, 81.97, 64.11, 57.41, 56.99, 56.87, 56.73, 56.70, 56.26, 52.42, 34.47, 28.16, 25.12, 24.93, 18.83, 17.76.

OtBu-(αMe)Val-Mal-Aib$_4$-Gly-NH$_2$ (**7a**). A solution of **6a** (30 mg, 0.044 mmol) in 3 mL of MeOH was irradiated in a quartz cuvette at 254 nm for 2 h. The solvent was removed under reduced pressure obtaining the crude product. Pure compound **7a** was obtained by semipreparative HPLC, after freeze-drying as a white solid.

FT-IR $\bar{\upsilon}_{max}$ 3289, 2922, 1650, 1539, 1468, 1383, 1364 cm^{-1}. ^1H NMR (500 MHz, CD_3CN) δ 8.61 (s, 1H, NH Aib^2), 7.84 (s, 1H, NH Aib^3), 7.82 (t, *J* = 6.2 Hz, 1H, NH Gly), 7.70 (s, 1H, NH Aib^4), 7.46 (s, 1H, NH Aib^1), 7.10 (s br, 1H, GlyNH_2), 7.05 (s, 1H, NH αMeVal), 6.29 (d, *J* = 12.0 Hz, 1H, CH Mal), 6.20 (d, *J* = 12.0 Hz, 1H, CH Mal), 5.64 (s, 1H, GlyNH_2), 2.11-2.06 (m, 1H, βCH αMeVal), 1.44 (s, 12H, O*t*Bu and βCH_3 Aib), 1.43 (s, 3H, βCH_3 Aib), 1.42 (s, 3H, βCH_3 Aib), 1.41 (s, 6H, 2x βCH_3 Aib), 1.38 (s, 3H, βCH_3 αMeVal), 1.36 (s, 6H, 2x βCH_3 Aib), 1.35 (s, 3H, βCH_3 Aib), 0.99 (d, *J* = 6.9 Hz, 3H, γCH_3 αMeVal), 0.92 (d, *J* = 6.9 Hz, 3H, γCH_3 αMeVal). ^{13}C NMR (101 MHz, CD_3CN) δ ppm 177.35, 176.93, 176.30, 175.88, 173.26, 172.31, 168.69, 164.53, 136.05, 126.97, 81.63, 64.05, 57.71, 57.57, 57.33, 43.60, 35.46, 28.19, 26.43, 26.17, 26.06, 24.66, 24.46, 24.33, 24.26, 17.52, 17.40, 17.37.

Maleamide derivatives

OH-Mal-(αMe)Val-OtBu (***Z*5a**). H-(αMe)Val-O*t*Bu (150 mg, 0.8 mmol) was dissolved in 2 mL of dry CH_3CN and TEA (100 μL, 0.71 mmol) were added. Maleic anhydride (70 mg, 0.71 mmol) was dissolved in 1 mL of dry CH_3CN and added to the solution of the amino acid. The reaction mixture stirred overnight at r.t. The solvent was removed under reduced pressure and the residue dissolved in EtOAc. The organic phase was washed with $KHSO_{4(aq)}$ 5% and brine, dried over Na_2SO_4, filtered and concentrated. The product was obtained as a white solid (170 mg, 74% yield).

HRMS (ES^+, MeOH) *m/z* calcd. for $C_{14}H_{24}NO_5$ ($[M+H]^+$) 286.1649, found 286.1703. Mp 156-159 °C. FT-IR $\bar{\upsilon}_{max}$ 3306, 3002, 2980, 1727, 1712, 1632, 1593, 1558, 1490, 1368, 1147, 858 cm^{-1}. ^1H NMR (500 MHz, $CDCl_3$) δ 7.28 (s, 1H, NH), 6.36 (d, *J* = 12.8 Hz, 1H, CH Mal), 6.29 (d, *J* = 12.9 Hz, 1H, CH Mal), 2.50-2.37 (m, 1H, βCH), 1.65 (s, 3H, βCH_3), 1.49 (s, 9H, OtBu), 1.04 (d, *J* = 7.0 Hz, 3H, γCH_3), 0.92 (d, *J* = 6.9 Hz, 3H, γCH_3). ^{13}C NMR (101 MHz, $CDCl_3$) δ 171.71, 165.22, 164.68, 136.95, 131.52, 83.40, 65.32, 33.84, 27.88, 18.82, 17.53.

OtBu-(αMe)Val-Mal-Aib-OMe (**9a**). **5a** (50 mg, 0.17 mmol) and HOAt (23 mg, 0.17 mmol) were dissolved in dry CH_2Cl_2. The suspension was cooled to 0 °C and EDC·HCl (33 mg, 0.17 mmol) was added. After complete dissolution H-Aib-OMe·HCl (54 mg, 0.35 mmol) and DIPEA (90 μL, 0.52 mmol) were added and the reaction mixture stirred overnight at r.t. The solvent was removed under reduced pressure and the residue dissolved in EtOAc. The organic phase was washed with $KHSO_{4(aq)}$ 5%, $NaHCO_{3(aq)}$ 5%, brine, dried over $MgSO_4$, filtered and concentrated. The product was obtained as an oil (50 mg, 75% yield).

HRMS (ES^+, MeOH) *m/z* calcd. for $C_{19}H_{33}N_2O_6$ ($[M+H]^+$) 385.2333, found 385.2435. FT-IR $\bar{\upsilon}_{max}$ 3280, 2978, 1748, 1729, 1671, 1620, 1578, 1548, 1368, 1286, 1263, 1149, 854 cm^{-1}.

^1H NMR (500 MHz, CD_3CN) δ 8.94 (s, 1H, NH Aib), 8.70 (s, 1H, NH αMeVal), 6.12 (d, *J* = 13.4 Hz, 1H, CH Mal), 6.06 (d, *J* = 13.4 Hz, 1H, CH Mal), 3.62 (s, 3H, OMe), 2.02 (dt, *J* = 13.7, 6.9 Hz, 1H, βCH αMeVal), 1.44 (s, 3H, βCH_3 Aib), 1.43 (s, 3H, βCH_3 Aib), 1.40 (s, 9H, OtBu), 1.36 (s, 3H, βCH_3 αMeVal), 0.98 (d, *J* = 6.9 Hz, 3H, γCH_3 αMeVal), 0.91 (d, *J* = 6.9 Hz, 3H, γCH_3 αMeVal). ^{13}C NMR (101 MHz, CD_3CN) δ 175.15, 165.20, 134.14, 132.84, 81.36, 64.09, 56.86, 52.76, 35.73, 28.15, 25.16, 25.08, 17.67, 17.61, 17.43.

Carboxylic acids

OtBu-(αMe)Val-Fum-Aib$_4$-OH (**10a**). **8c** (320 mg, 0.54 mmol) was dissolved in 15 mL of THF and a solution of LiOH (85 mg, 3.5 mmol) in 5 mL of water was added. The solution was stirred at 40°C for 24 h, until complete conversion (TLC). The organic solvent was

removed under reduced pressure and the aqueous phase was acidified with HCl 1M. The compound was extracted using EtOAc (3v). The organic phase was washed with $KHSO_{4(aq)}$ 5% and brine, dried over $MgSO_4$, filtered and concentrated under reduced pressure. The product was obtained as a white solid (230 mg, 73% yield).

HRMS (ES^+, MeOH) *m/z* calcd. for $C_{30}H_{51}N_5O_9Na$ ($[M+Na]^+$) 648.3579, found 648.3584. $[\alpha]_D^{20}$ = -8 (c 1, MeOH). Mp 152-154 °C. FT-IR $\bar{\upsilon}_{max}$ 3305, 2982, 1728, 1650, 1534, 1458, 1385, 1260, 1225, 1151 cm^{-1}. ^1H NMR (400 MHz, $CDCl_3$) δ 8.01 (s, 1H, NH), 7.89 (s, 1H, NH), 7.87 (s, 1H, NH), 7.23 (s, 1H, NH), 6.97 (s, 1H, NH), 6.87 (m, 2H, AB system CH_2 Fum), 2.40 (m, 1H, βCH αMeVal), 1.59 (s, 3H, βCH_3 αMeVal), 1.56 (s, 6H, 2x βCH_3 Aib), 1.52 (s, 6H, 2x βCH_3 Aib), 1.50 (s, 6H, 2x βCH_3 Aib), 1.47 (s, 9H, OtBu), 1.43 (s, 6H, 2x βCH_3 Aib), 1.01 (d, *J* = 6.7 Hz, 3H, γCH_3 αMeVal), 0.91 (d, *J* = 6.7 Hz, 3H, γCH_3 αMeVal). ^{13}C NMR (101 MHz, $CDCl_3$) δ 176.78, 175.75, 175.56, 174.53, 172.66, 165.39, 163.86, 133.74, 133.07, 82.43, 64.30, 57.33, 56.97, 56.91, 34.21, 29.85, 28.11, 25.19, 24.85, 18.98, 17.78, 17.73.

OtBu-α-MeVal-Fum-Aib$_8$-OH (**10b**). **8d** (120 mg, 0.12 mmol) was dissolved in 10 mL of THF and a solution of LiOH (20 mg, 0.86 mmol) in 5 mL of water was added. The solution was stirred at 60 °C for 48 h, The solution was diluted with CH_2Cl_2 and the aqueous phase was acidified with HCl 1M. The compound was extracted using CH_2Cl_2 (3v). The organic phase was washed with $KHSO_{4(aq)}$ 5% and brine, dried over $MgSO_4$, filtered and concentrated under reduced pressure. The crude was purified *via* flash chromatography (eluant: CH_2Cl_2/MeOH 93:7→8:2). The product was obtained as a white solid (80 mg, 68% yield).

HRMS (ES^+ MeOH) *m/z* calcd. for $C_{46}H_{80}N_9O_{13}$ ($[M+H]^+$) 966.5870, found 966.6056. Mp 190-193 °C. FT-IR $\bar{\upsilon}_{max}$ 3309, 2985, 2939, 1728, 1659, 1535, 1385, 1365, 1228 cm^{-1}.

^1H NMR (400 MHz, MeOD) δ 7.10 (d, *J* = 15.1 Hz, 1H, CH Fum), 6.92 (d, *J* = 15.1 Hz, 1H, CH Fum), 2.09 (dt, *J* = 13.6, 6.7 Hz, 1H, βCH αMeVal), 1.52 (s, 6H, 2x βCH_3 Aib), 1.51 (s, 6H, 2x βCH_3 Aib), 1.49 (s, 6H, 2x βCH_3 Aib), 1.48 (s br, 24H, 4x βCH_3 Aib), 1.44 (s, 9H, O*t*Bu), 1.42 (s, 3H, βCH_3 αMeVal), 1.40 (s, 6H, 2x βCH_3 Aib), 1.01 (d, *J* = 6.7 Hz, 3H, γCH_3 αMeVal), 0.96 (d, *J* = 6.7 Hz, 3H, γCH_3 αMeVal). ^{13}C NMR (101 MHz, MeOD) δ 177.63, 177.48, 177.42, 177.15, 177.01, 176.74, 176.21, 173.54, 166.31, 166.02, 134.67, 133.75, 82.33, 64.57, 57.95, 57.89, 57.83, 57.79, 57.73, 35.86, 28.24, 25.49, 25.14, 17.72, 17.69, 17.56.

Helix-helix

OEt-Fum-Aib$_4$-Gly-NH$_2$. *Mono*ethyl fumarate (90 mg, 0.62 mmol) and HOAt (85 mg, 0.62 mmol) were dissolved in dry CH_2Cl_2. The suspension was cooled to 0 °C and EDC·HCl (120 mg, 0.62 mmol) was added. After complete dissolution, H-Aib$_4$-Gly-NH$_2$ (130 mg, 0.31 mmol) and TEA (90 μL, 0.65 mmol) were added and the reaction mixture stirred for 48 h at r.t. The precipitate collected and washed with CH_2Cl_2. The product was recovered after precipitation from MeOH/Et_2O obtaining a white solid (100 mg, 60% yield).
HRMS (ES$^+$, MeOH) *m/z* calcd. for $C_{24}H_{40}N_6O_8Na$ ([M+Na]$^+$) 563.2805, found 563.2794.
Mp 274-275 °C. FT-IR $\bar{\upsilon}_{max}$ 3264, 2985, 1720, 1652, 1533, 1455, 1386, 1363, 1281, 1223, 1172 cm^{-1}. ^{1}H NMR (400 MHz, MeOD) δ 7.10 (d, *J* = 15.4 Hz, 1H, CH Fum), 6.74 (d, *J* = 15.5 Hz, 1H, CH Fum), 4.26 (q, *J* = 7.1 Hz, 2H, CH_2 Et), 3.83 (s, 2H, CH_2 Gly), 1.50 (s, 6H, 2x βCH$_3$ Aib), 1.49 (s, 6H, 2x βCH$_3$ Aib), 1.47 (s, 6H, 2x βCH$_3$ Aib), 1.39 (s, 6H, 2x βCH$_3$ Aib), 1.31 (t, *J* = 7.1 Hz, 3H, CH_3 Et). ^{13}C NMR (101 MHz, MeOD) δ 178.09, 178.05, 177.81, 176.09, 175.40, 166.79, 165.65, 137.58, 131.26, 62.32, 58.14, 58.03, 57.88, 57.79, 43.68, 25.58, 25.27, 14.45.

OH-Fum-Aib$_4$-Gly-NH$_2$ (**16**). OEt-Fum-Aib$_4$-Gly-NH$_2$ (70 mg, 0.13 mmol) was dissolved in 6 mL of THF and a solution of LiOH (22 mg, 0.92 mmol) in 4 mL of water was added. The solution was stirred at r.t. for 1 h. The organic solvent was removed under reduced pressure and the aqueous phase was acidified with HCl 1M. After 24 h, the compound precipitated from the solution was recovered by filtration. The product was obtained as a white solid (50 mg, 73% yield).
HRMS (ES$^+$, MeOH) *m/z* calcd. for $C_{22}H_{36}N_6O_8Na$ ([M+Na]$^+$) 535.2492, found 535.2493. Mp 274-275 °C. FT-IR $\bar{\upsilon}_{max}$ 3300, 2986, 1659, 1537, 1386, 1224 cm^{-1}.
^{1}H NMR (400 MHz, MeOD) δ 7.07 (d, *J* = 15.4 Hz, 1H, CH Fum), 6.71 (d, *J* = 15.4 Hz, 1H, CH Fum), 3.83 (s, 2H, CH_2 Gly), 1.50 (s, 6H, 2x βCH$_3$ Aib), 1.49 (s, 6H, 2x βCH$_3$ Aib), 1.47 (s, 6H, 2x βCH$_3$ Aib), 1.39 (s, 6H, 2x βCH$_3$ Aib). ^{13}C NMR (101 MHz, MeOD) δ 178.17, 178.12, 178.11, 178.09, 177.92, 176.14, 175.41, 168.38, 165.86, 137.55, 131.85, 58.23, 58.14, 57.85, 57.81, 43.68, 25.58, 25.30, 25.08.

N$_3$-Aib$_4$-Ala-OtBu. N$_3$-Aib$_4$-OH (230 mg, 0.6 mmol) and HOAt (106 mg, 0.77 mmol) were dissolved in dry CH_2Cl_2. After cooling to 0 °C EDC·HCl (120 mg, 0.6 mmol) was added. Then H-Ala-OtBu·HCl (217 mg, 1.2 mmol) and TEA (250 μL, 1.8 mmol) were added and the reaction mixture stirred for 48 h at r.t. The reaction mixture was diluted with CH_2Cl_2 and washed with $KHSO_{4(aq)}$ 5%, $NaHCO_{3(aq)}$ 5%, brine. The organic phase was dried over $MgSO_4$,

filtered and concentrated. The crude was purified *via* flash chromatography (eluant: CH_2Cl_2/MeOH 93:7), yielding the product as a white solid (260 mg, 85 % yield).

HRMS (ES^+, MeOH) *m/z* calcd. for $C_{23}H_{41}N_7O_6Na$ ($[M+Na]^+$) 534.3016, found 534.3008. $[\alpha]_D^{20}$ = -53.1 (c 1, MeOH). Mp 164-166 °C. FT-IR $\bar{\upsilon}_{max}$ 3325, 2982, 2112, 1732, 1655, 1519, 1457, 1382, 1365, 1223, 1152 cm^{-1}.

^1H NMR (400 MHz, MeOD) δ 4.19 (q, *J* = 7.3 Hz, 1H, αCH Ala), 1.53 (s, 3H; βCH_3 Aib), 1.52 (s, 6H, 2x βCH_3 Aib), 1.49 (s, 3H, βCH_3 Aib), 1.44 (s, 6H, 2x βCH_3 Aib), 1.44 (s, 9H, OtBu), 1.42 (d, *J* = 7.4 Hz, 3H, βCH_3 Ala), 1.39 (s, 3H, βCH_3 Aib), 1.35 (s, 3H, βCH_3 Aib). ^{13}C NMR (101 MHz, MeOD) δ 177.21, 176.35, 176.25, 174.61, 173.64, 82.13, 64.75, 57.97, 57.94, 57.80, 50.77, 28.22, 27.41, 26.74, 25.52, 24.53, 24.46, 24.17, 24.12, 23.91, 17.10.

H-Aib$_4$-Ala-OtBu (**17**). N_3-Aib$_4$-Ala-OtBu (210 mg, 0.41 mmol) was dissolved in 8 mL of EtOH under a nitrogen atmosphere. Pd/C catalyst (30 mg) was carefully added and the reaction mixture stirred under H_2 atmosphere for 24 h. The catalyst was removed by filtration through a pad of Celite and the filtrate concentrated under reduced pressure to yield the product as a white solid (170 mg, 85% yield).

HRMS (ES^+, MeOH) *m/z* calcd. for $C_{23}H_{43}N_5O_6Na$ ($[M+Na]^+$) 508.3111, found 508.3114. $[\alpha]_D^{20}$ = -52.3 (c 1, MeOH). Mp 179-181 °C. FT-IR $\bar{\upsilon}_{max}$ 3308, 2981, 1730, 1653, 1525, 1456, 1382, 1363, 1226, 1165 cm^{-1}. ^1H NMR (400 MHz, MeOD) δ 4.20 (q, *J* = 7.3 Hz, 1H, αCH Ala), 1.52 (s, 3H, βCH_3 Aib), 1.50 (s, 3H, βCH_3 Aib), 1.44 (s, 15H, O*t*Bu and 2x βCH_3 Aib), 1.42 (d, *J* = 7.4 Hz, 3H, βCH_3 Ala), 1.40 (s, 3H, βCH_3 Aib), 1.36 (s, 3H, βCH_3 Aib), 1.33 (s, 3H, βCH_3 Aib), 1.32 (s, 3H, βCH_3 Aib). ^{13}C NMR (101 MHz, MeOD) δ 179.61, 177.26, 176.62, 176.49, 173.66, 82.13, 57.96, 57.74, 57.40, 55.67, 50.75, 28.54, 28.23, 28.08, 27.43, 26.83, 25.70, 24.20, 24.17, 24.00, 17.12.

OtBu-Ala-Aib$_4$-Fum-Aib$_4$-Gly-NH$_2$ (**18**). **16** (33 mg, 0.062 mmol) and HOAt (10 mg, 0.073 mmol) were dissolved in dry CH_2Cl_2. After cooling to 0 °C EDC·HCl (12 mg, 0.062 mmol) was added. Then **17** (35 mg, 0.072 mmol) and DIPEA (20 μL, 0.11 mmol) were added and the reaction mixture stirred for 48 h at r.t. The solid was recovered and washed with CH_2Cl_2. The crude product was purified *via* flash chromatography (eluant: CH_2Cl_2/MeOH 90:15). The product was recovered as a white solid (20 mg, 33 % yield).

HRMS (ES^+, MeOH) *m/z* calcd. for $C_{45}H_{78}N_{11}O_{13}$ ($[M+H]^+$) 980.5781, found 980.5770. $[\alpha]_D^{20}$ = +11 (c 0.1, MeOH). Mp >267 °C decompose. FT-IR $\bar{\upsilon}_{max}$ 3295, 2985, 1656, 1537, 1384, 1364, 1226 cm^{-1}.^1H NMR (500 MHz, MeOD) δ 7.08 (s, 2H, CH_2 Fum), 4.22 (q, *J* = 7.3 Hz, 1H, αCH Ala), 3.83 (s, 2H, CH_2 Gly), 1.53 (s, 3H, βCH_3 Aib), 1.52 (s, 3H, βCH_3 Aib), 1.51

(s, 12H, 4x βCH$_3$ Aib), 1.50 (s, 3H, βCH$_3$ Aib), 1.47 (s, 3H, βCH$_3$ Aib), 1.47 (s, 6H, 2x βCH$_3$ Aib), 1.46 (s, 6H, 2x βCH$_3$ Aib), 1.45 (s, 9H, OtBu), 1.44 (s, 3H, βCH$_3$ Aib), 1.43 (d, *J* = 7.4 Hz, 3H, βCH$_3$ Ala), 1.38 (s, 3H, βCH$_3$ Aib), 1.37 (s, 3H, βCH$_3$ Aib), 1.34 (s, 3H, βCH$_3$ Aib).

Diastereoselection experiments

Reactions of 5(4*H*)oxazolones with H-D,L-Val-OMe were performed in CH_3CN or CH_2Cl_2 at controlled temperature using a thermostatic oil bath (20, 35, 45 and 70 °C).

The carboxylic acid (**10a-b** or **11a-b**) (0.05 mmol) was suspended in 5 mL of the appropriate solvent and EDC·HCl (0.06 mmol) was added, and the solution stirred for 10 min at r.t. The quantitative formation of the oxazolone (**12a-b** or **13a-b**) was controlled by HPLC.

Separately H-D,L-Val-OMe·HCl (0.31 mmol) and DIPEA (0.31 mmol) were suspended in 1 mL of the appropriate solvent.

In a typical experiment, the oxazolone solution (500 μL, 1 equiv.) and the racemate solution (125 μL, 8 equiv.) were mixed and the resulting solution was maintained under stirring in a thermostatic oil bath. The reaction was monitored by HPLC, by following the disappearance of the oxazolone accompanied by the formation of the two diastereomeric products. The formation of the two resulting peptides **15a-d** (*Z* isomer) can be quantified directly by HPLC. Whereas in the case of **14a-d** (*E* isomer), after the disappearance of the oxazolone reactant, the product mixture was irradiated at 254 nm and successively analyzed by HPLC. The independent preparation of each diastereomer was performed by reaction of the oxazolone with either D or L H-Val-OMe.

Table S1. Crystal data and structure refinement for **6a**.

Identification code	mc262b	
Empirical formula	$C_{32}\ H_{55}\ N_7\ O_9$	
Formula weight	681.83	
Temperature	293(2) K	
Wavelength	1.54178 Å	
Crystal system	Orthorhombic	
Space group	$P\ 2_1\ 2_1\ 2_1$	
Unit cell dimensions	a = 9.01420(14) Å	α = 90°.
	b = 10.94112(14) Å	β = 90°.
	c = 38.4416(6) Å	γ = 90°.
Volume	3791.32(10) $Å^3$	
Z	4	
Density (calculated)	1.195 Mg/m^3	
Absorption coefficient	0.724 mm^{-1}	
F(000)	1472	
Crystal size	0.25 × 0.20 × 0.05 mm^3	
Theta range for data collection	2.299 to 70.959°.	
Index ranges	$-11 \le h \le 10, -13 \le k \le 12, -47 \le l \le 41$	
Reflections collected	33257	
Independent reflections	7272 [R(int) = 0.0326]	
Completeness to theta = 67.679°	100.0 %	
Absorption correction	Semi-empirical from equivalents	
Max. and min. transmission	1.00000 and 0.22453	
Refinement method	Full-matrix least-squares on F^2	
Data / restraints / parameters	7272 / 0 / 433	
Goodness-of-fit on F^2	1.031	
Final R indices [I>2sigma(I)]	R_1 = 0.0406, wR_2 = 0.1098	
R indices (all data)	R_1 = 0.0438, wR_2 = 0.1126	
Absolute structure parameter	0.01(6)	
Largest diff. peak and hole	0.269 and -0.225 $e.Å^{-3}$	

Table S2. Selected torsion angles [°] for **6a**.

Torsion angle	
C1F-N6-C6A-C6	-58.4(3)
N6-C6A-C6B1-C6G1	174.5(2)
N6-C6A-C6B1-C6G2	-61.3(3)
CT1-OT-C6-C6A	178.9(2)
N6-C6A-C6-OT	-47.9(3)
C6A-N6-C1F-C2F	-171.0(2)
N6-C1F-C2F-C3F	159.6(3)
C1F-C2F-C3F-C4F	-174.6(3)
C2F-C3F-C4F-N1	169.1(3)
C3F-C4F-N1-C1A	-176.2(2)
C4F-N1-C1A-C1	-54.3(3)
N1-C1A-C1-N2	-31.4(3)
C1A-C1-N2-C2A	-172.9(2)
C1-N2-C2A-C2	-48.6(3)
N2-C2A-C2-N3	-33.5(3)
C2A-C2-N3-C3A	-176.9(2)
C2-N3-C3A-C3	-51.1(3)
N3-C3A-C3-N4	-40.4(3)
C3A-C3-N4-C4A	-172.8(2)
C3-N4-C4A-C4	-66.1(3)
N4-C4A-C4-N5	-23.3(3)
C4A-C4-N5-C5A	178.2(2)
C4-N5-C5A-C5	66.2(4)
N5-C5A-C5-NT	-135.8(3)

Table S3. Hydrogen bonds for **6a** [Å and °].

D-H...A	d(D-H)	d(H...A)	d(D...A)	<(DHA)
N3-H3...O2F	0.86	2.45	3.292(3)	168
N4-H4...O1	0.86	2.15	2.947(3)	155
N5-H5...O2	0.86	2.29	3.069(3)	151
N6-H6...O6#1	0.86	2.15	2.989(3)	164
N1-H1...O3#2	0.86	2.32	3.142(2)	161
N2-H2...O5#3	0.86	2.29	2.906(3)	128
NT-HT1...O3#4	0.86	2.37	3.197(4)	160
NT-HT2...O2#4	0.86	2.50	3.061(4)	124

Symmetry transformations used to generate equivalent atoms:

#1 -x+2, y-1/2, -z+1/2; #2 x, y+1, z; #3 x+1/2, -y+1/2, -z; #4 x-1/2, -y-1/2, -z

References

[1] (a) B. N. Bullock, A. L. Jochim, P. S. Arora, *J. Am. Chem. Soc.*, **2011**, *133*, 14220-14223; (b) V. Azzarito, K. Long, N. S. Murphy, A. J. Wilson, *Nat. Chem.*, **2013**, 5, 161-173.

[2] M. A. Klein, *ACS Med. Chem. Lett.*, **2014**, *5*, 838−839.

[3] Y. Heng Lau, P. de Andrade, Y. Wu, D. R. Spring, *Chem. Soc. Rev.*, **2015**, *44*, 91-102.

[4] A. K. Boal, I. Guryanov, A. Moretto, M. Crisma, E. L. Lanni, C. Toniolo, R. H. Grubbs, D. J. O'Leary, *J. Am. Chem. Soc.*, **2007**, *129*, 6986–6987.

[5] A. Moretto, M. Crisma, F. Formaggio, L. A. Huck, D. Mangion, W. J. Leigh, C. Toniolo, *Chem. Eur. J.*, **2009**, *15*, 67–70.

[6] D. Mazzier, C. Peggion, C. Toniolo, A. Moretto *Biopolymers (Pept. Sci.)*, **2014**, *102*, 115-123.

[7] (a) S. H. Gellman, *Acc. Chem. Res.*, **1998**, *31*, 173-180; (b) D. J. Hill, M. J. Mio, R. B. Prince, T. S. Hughes, J. S. Moore, *Chem. Rev.*, **2001**, *101*, 3893-4012; (c) G. Guichard, I. Huc *Chem. Commun.*, **2011**, *47*, 5933–5941.

[8] (a) J. Clayden, *Chem. Soc. Rev.*, **2009**, *38*, 817–829; (b) C. P. Johnston, M. D. Smith, *Angew. Chem. Int. Ed.* **2014**, *53*, 3315-3317.

[9] J. Venkatraman, S. C. Shankaramma, P. Balaram, *Chem. Rev.*, **2001**, *101*, 3131-3152.

[10] (a) R. A. Brown, T. Marcelli, M. De Poli, J. Solà, J. Clayden, *Angew. Chem., Int. Ed.*, **2012**, *51*, 1395-1399; (b) J. Clayden, A. Castellanos, J. Solà, G. A. Morris, *Angew. Chem., Int. Ed.*, **2009**, *48*, 5962-5965; (c) J. Solà, G. A. Morris, J. Clayden, *J. Am. Chem. Soc.*, **2011**, *133*, 3712-3715; (d) L. Byrne, J. Solà, T. Boddaert, T. Marcelli, R. W. Adams, G. A. Morris, J. Clayden, *Angew. Chem., Int. Ed.*, **2014**, *53*, 151-155; (e) M. De Poli, L. Byrne, R. A. Brown, J. Solà, A. Castellanos, T. Boddaert, R. Wechsel, J. D. Beadle, J. Clayden, *J. Org. Chem.*, **2014**, *69*, 4659-4675; (f) T. Boddaert, J. Clayden, *Chem. Commun.*, **2012**, *48*, 3397-3399; (g) S. J. Pike, M. De Poli, W. Zawodny, J. Raftery, S. J. Webb, J. Clayden, *Org. Biomol. Chem.*, **2013**, *11*, 3168-3176; (h) J. Solà, S. P. Fletcher, A. Castellanos, J. Clayden, *Angew. Chem., Int. Ed.*, **2010**, *49*, 6836-6839; (i) M. De Poli, M. De Zotti, J. Raftery, J. A. Aguilar, G. A. Morris, J. Clayden, *J. Org. Chem.*, **2013**, *78*, 2248-2255.

[11] B. A. F. Le Bailly, J. Clayden, *Chem. Commun.*, **2014**, *50*, 7949-7952.

[12] L. Byrne, J. Solà, J. Clayden, *Chem. Commun.*, **2015**, *51*, 10965-10968.

[13] (a) L. A. Carpino, *J. Am. Chem. Soc.*, **1993**, *115*, 4397–4398; (b) L. A. Carpino, El- A. Faham, C. A. Minor, F. Albericio, *J. Chem. Soc. Chem. Commun.*, **1994**, 201–203.

[14] H. Jo, N. Meinhardt, Y. Wu, S. Kulkarni, X. Hu, K. E. Low, P. L. Davies, W. F. DeGrado, D. C. Greenbaum, *J. Am. Chem. Soc.*, **2012**, *134*, 17704-17713.

[15] S. Beychok, *Poly-α-Amino-Acids: Protein Models for Conformational Studies*, G. D. Fasman, Ed.; Dekker: New York, NY, **1967**, 293–337.

[16] (a) M. C. Manning, R. W. Woody, *Biopolymers*, **1992**, *31*, 569–586; (b) C. Toniolo, A. Polese, F. Formaggio, M. Crisma, J. Kamphuis, *J. Am. Chem. Soc.*, **1996**, *118*, 2744–2745; (c) F. Formaggio, M. Crisma, P. Rossi, P. Scrimin, B. Kaptein, Q. B. Broxterman, J. Kamphuis, *Chem. Eur. J.*, **2000**, *6*, 4498–4504.

[17] M. Rance, O. W. Sørensen, G. Bodenhausen, G. Wagner, R. R. Ernst, K. Wüthrich, *Biochem. Biophys. Res. Commun.*, **1983**, *117*, 479–485.

[18] C. Griesinger, G. Otting, K. Wüthrich, R. R. Ernst, *J. Am. Chem. Soc.*, **1988**, *110*, 7870–7872.

[19] C. W. Lee, R. H. Grubbs, *Org. Lett.*, **2000**, *2*, 2145–2147.

[20] K. Wüthrich, *NMR of Proteins and Nucleic Acids*, Wiley, New York, **1986**.

[21] (a) C. E. Schafmeister, J. Po, G. L. Verdine, *J. Am. Chem. Soc.*, **2000**, *122*, 5891–5892; (b) T. K. Sawyer, *Chem. Biol. Drug. Des.*, **2009**, *73*, 3–6; (c) Z. Guo, U. Mohanty, J. Noehre, T. K. Sawyer, W. Sherman, G. Krilov, *Chem. Biol. Drug. Des.*, **2010**, *75*, 348–359.

[22] (a) E.R. Kay, D.A. Leigh, F. Zerbetto, *Angew. Chem. Int. Ed.*, **2007**, *46*, 72-191; (b) A. Moretto, I. Menegazzo, M. Crisma, E.J. Shotton, H. Nowell, S. Mammi, C. Toniolo, *Angew. Chem. Int. Ed.*, **2009**, *48*, 8986-8989.

[23] (a) F. G. Gatti, S. Leó, J. K. Y. Wong, G. Bottari, A. Altieri, M. A. Farran Morales, S. J. Teat, C. Frochot, D. A. Leigh, A. M. Brouwer, F. Zerbetto, *Proc. Natl. Acad. Sci. U.S.A.*, **2003**, *100*, 10-14; (b) A. Altieri, G. Bottari, F. Dehez, D. A. Leigh, J. K. Y. Wong, F. Zerbetto, *Angew. Chem. Int. Ed.*, **2003**, *42*, 2296-2300; (c) G. Bottari, D. A. Leigh, E. M. Perez, *J. Am. Chem. Soc.*, **2003**, *125*, 13360-13361.

[24] M. Meldal, M. A. Juliano, A. M. Jansson, *Tetrahedron Lett.*, **1997**, *38*, 2531-2534.

[25] J. Solà, M. Helliwell, J. Clayden, *J. Am. Chem. Soc.*, **2010**, *132*, 4548-4549.

[26] (a) A. Polese, F. Formaggio, M. Crisma, G. Valle, C. Toniolo, G. M. Bonora, Q. B. Broxterman, J. Kamphuis, *Chem. Eur. J.*, **1996**, *2*, 1104–1111; (b) M. Crisma, C. Toniolo, *Biopolymers (Pept. Sci.)*, **2015**, *104*, 46–64.

[27] (a) T. Li, K.-H. Budt, Y. Kishi, *J. Chem. Soc., Chem. Commun.*, **1987**, 1817–1819; (b) M. Crisma, A. Moretto, F. Formaggio, B. Kaptein, Q. B. Broxterman, C. Toniolo, *Angew. Chem., Int. Ed.*, **2004**, *43*, 6695–6699; (c) A. Moretto, C. Peggion, F. Formaggio, M. Crisma, B. Kaptein, Q. B. Broxterman, C. Toniolo, *Chirality*, **2005**, *17*, 481–487.

[28] M.C. Burla, R. Caliandro, B. Carrozzini, G.L. Cascarano, C. Cuocci, C. Giacovazzo, M. Mallamo, A. Mazzone, G. Polidori, *J. Appl. Crystallogr.*, **2015**, *48*, 306-309.

[29] G.M. Sheldrick, *Acta Crystallogr. C*, **2015**, *71*, 3-8.

[30] H. Chen, Y. Feng, Z. Xub, T. Ye *Tetrahedron*, **2005**, *61*, 11132-11140.

[31] C. Toniolo, M. Crisma, G. M. Bonora, B. Klajc, F. Lelj, P. Grimaldi, A. Rosa, S. Polinelli, E. M. Meijer, H. E. Schoemaker, J. Kamphuis, *Int. J. Pept. Protein Res.*, **2009**, *38*, 242–252.

[32] D. Leibfritz, E. Haupt, N. Dubischar, H. Lachmann, R. Oekonomopulos, G. Jung, *Tetrahedron*, **1982**, *38*, 2165-2181.

[33] S. J. Pike, J. Raftery, S. J. Webb, J. Clayden, *Org. Biomol. Chem.*, **2014**, *12*, 4124-4131.

3. Functionalized helical polypeptides: synthesis and self-assembly properties

The construction of supramolecular architectures characterized by well-distinct shapes and functions is a relevant target in areas such as materials science, nanochemistry and biomimetic chemistry.[1] The self-assembly process of polymers through non-covalent interactions, such as hydrogen bonding, van der Waals interactions, π–π stacking and hydrophobic interactions, has a great potential for creating such supramolecular architectures.[2] Synthetic polypeptides are fascinating and unique for their ability to self-assemble into ordered structures, making them attractive in those many applications where well-organized architectures are essential to accomplish a function.[3] In fact they can self-organize into highly ordered secondary structures, such as α-helix and β-sheets in solution phase or in solid state, same as those typically observed in proteins or peptides but inaccessible in other synthetic polymeric materials. Since in the past decade substantial progresses have been made in the synthesis of polypeptides *via N*-carboxyanhydrides (NCAs),[4] recently several innovative polypeptide-based materials have been produced and studied.[5] We chose the well-known rod-like α-helical polypeptide poly(γ-benzyl-L-glutamate) (PBLG)[6] and we explored the possibility to create self-assembled microstructures with different characteristics, shapes and functions from different PBLG-conjugates. In this chapter the results obtained after the functionalization of PBLG with carbon nanostructures, such as fullerene (C_{60})[7] and carbon quantum dots (CQDs) will be discussed.[8] Moreover the possibility to create "smart" supramolecular architectures was examined by the insertion of photoisomerizabile azobenzene moieties in PBLG systems.[9]

3.1 Poly(γ-Benzyl-L-Glutamate)-fullerene conjugates (PBLG-C_{60})

Recently, thiol-ene click chemistry was successfully employed to prepare C_{60} (fullerene) polystyrene conjugates obtaining only the mono-addiction product.[10] With the aim to synthesize *mono* and *bis* C_{60}-PBLG conjugates (respectively **4** and **7**, Scheme 3.1) and to study their self-assembly properties in water, we decided to apply a similar approach to functionalize PBLG *via* thiol-ene reaction.

The first step of these studies was the synthesis of the PBLG with the thiol-group at the C-terminus (**1**, Scheme 3.1). Thus BLG-NCA (**1**, 4 mmol) was polymerized in dioxane for 24 h at room temperature, using Trt-cysteamine **2** (Trt, triphenylmethyl) as initiator (0.04 mmol) (Scheme 3.1). Polymer **3** was obtained after precipitation with methanol in an 81% yield. Subsequently, the Trt-protecting group was removed under acidic conditions and the resulting polymer (0.01 mmol) was dissolved in DMF and added to toluene. Then, fullerene (0.05 mmol) and AIBN (0.15 mmol) were added to the previous solution and the subsequent homogeneous mixture was heated at 90°C under stirring for 5 hrs. Subsequently, the solvent was removed and the resulting solid was suspended in DMF, passed through a 20 μm filter, and then precipitated by addition of methanol, giving polymer **4** as a brown solid in 85% yield.

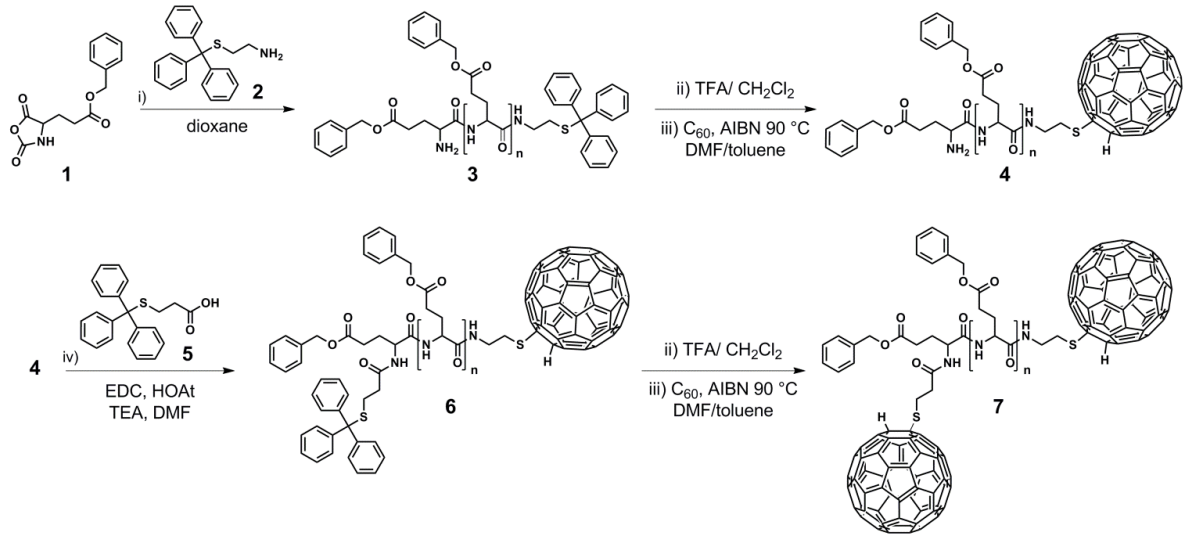

Scheme 3.1 Synthesis of polymers NH_2-PBLG-C_{60} (**4**) and C_{60}-PBLG-C_{60} (**7**). Reagents and Conditions: i) (tritylsulfanyl)ethanamine (**2**), dioxane, r.t., 24 h. ii) 50% TFA in CH_2Cl_2, TIS, r.t., 20 min. iii) C_{60}, AIBN, DMF/toluene 2:8 (v/v), 90 °C, 5 h. iv) Trt-*mercapto*propionic acid (**5**), EDC·HCl, TEA, DMF, r.t. 48 h.

Moreover, polymer **4** was successively N-end capped with a large excess of pre-activated Trt-mercaptopropionic acid (**5**), yielding polymer **6**. Polymer **6** was C-terminus Trt-deprotected and placed to react in the same conditions described above for the synthesis of polymer **4**, thus to generate the *bis*- conjugate C_{60}-PBLG-C_{60}, polymer **7** in 78 % yield.
Since all the synthetized polymers possess the same PBLG part (as it comes from polymer **3**), the differences in M_Ws determined by SEC constitute a first evidence for the addition of one or two fullerenes (Figure 3.1).

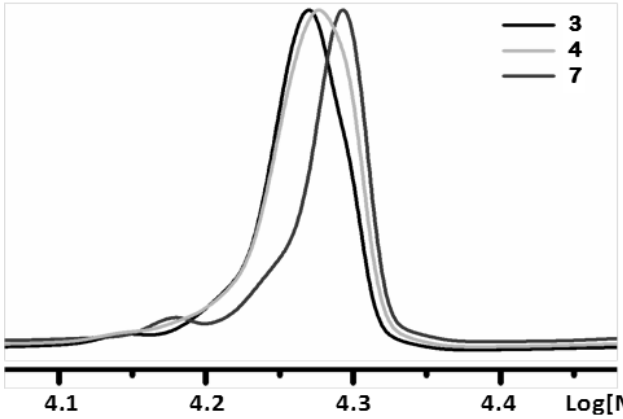

polymer	M_W	PDI
3	19100	1.11
4	19550	1.09
7	20300	1.11

Figure 3.1 Left: SEC traces of polymers **3**, **4** and **7** in DMF solution. Right: table with molecular weights (M_w) and polydispersity index (PDI) determined for polymers **3**, **4** and **7**.

A second evidence for the covalent attachment of fullerenes arises from the absorption spectra of **3**, **4** and **7**, which were recorded in THF solution (Figure 3.2 A). The observed patterns are close to that of fullerene, which shows high UV absorptions around λ=287, 330 nm and tails spanning over the 600 nm region. We assign the observed UV absorptions of *mono* (**4**) and *bis* (**7**) fullerene-conjugates to the fullerene moiety[10] considering the small differences in the resonance frequencies with respect to the isolated fullerene due to perturbations of the electronic structure caused by the bonding with the PBLG polymer. The third indication of the formation of PBLG-conjugated fullerenes come from the thermal stability of **3**, **4** and **7** that was investigated *via* thermogravimetric analysis (TGA; 100-700 °C) under nitrogen flow with a heating rate of 10 °C min^{-1} (Figure 3.2 B). Accordingly, PBLG polymers undergo a thermal decomposition between 250-350 °C, whereas the thermally stable fullerene component keeps its stability up to almost 600 °C.[10] The weight percentages of the components (polymer **4**, C_{60}/PBLG 4:96 %; polymers **7**, C_{60}/PBLG 7:93 %) determined by TGA are in agreement to those of SEC analysis. All of the experimental results suggested an average number of BLG amino acids, for polymer unit, close to 85. The secondary structure

of polymers **3**, **4** and **7** was analyzed by CD (circular dichroism), which confirmed the preservation of the α-helical conformation for all the synthesized compounds (Figure 3.3), that in turn implies the rod-like shape of the polymers.

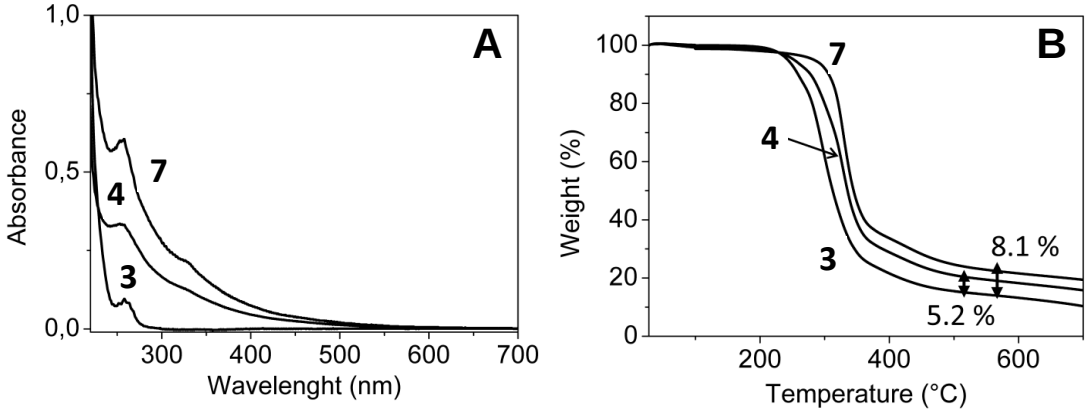

Figure 3.2 (**A**) UV/Vis spectra of polymers **3**, **4** and **7** in THF solution (concentration: 0.01 mg/mL). (**B**) Thermogravimetric analysis comparison of polymers **3**, **4** and **7**.

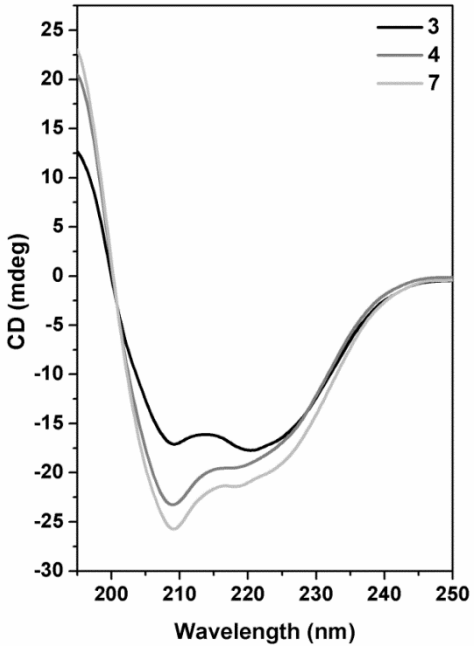

Figure 3.3 Comparison of CD spectra of polymers **3**, **4** and **7** in HFIP solution.

From polymer **4**, doughnut-like morphologies were generated, in form of milk-like suspension, starting from a 20 mg (3:7, v/v) DMF/THF solution (10 mL) dialyzed (membrane cutoff, 12 KD) against ultrapure water for 48 hours (Figure 3.4). TEM (transmission electron microscopy) images showed toroidal shapes with an external diameter ranging between 200 nm and 650 nm (Figures 3.4 A-B, stained and unstained samples, respectively), additionally confirmed by SEM (scanning electron microscopy) analysis (Figure 3.4 C). Moreover, AFM (atomic force microscopy) details of the selected nanodoughnut reported in Figure 3.4 D,

revealed a diameter of 200 nm, a thickness of 70 nm and a hole of 30 nm (Figure 3.4 E). Additionally, after running the same self-assembly process but starting from a more dilute solution of **4** (2-5 mg in 10 mL), smaller but uniform in size (60 nm diameter) toroidal nanostructures were obtained as detected by AFM (Figure 3.4 F).

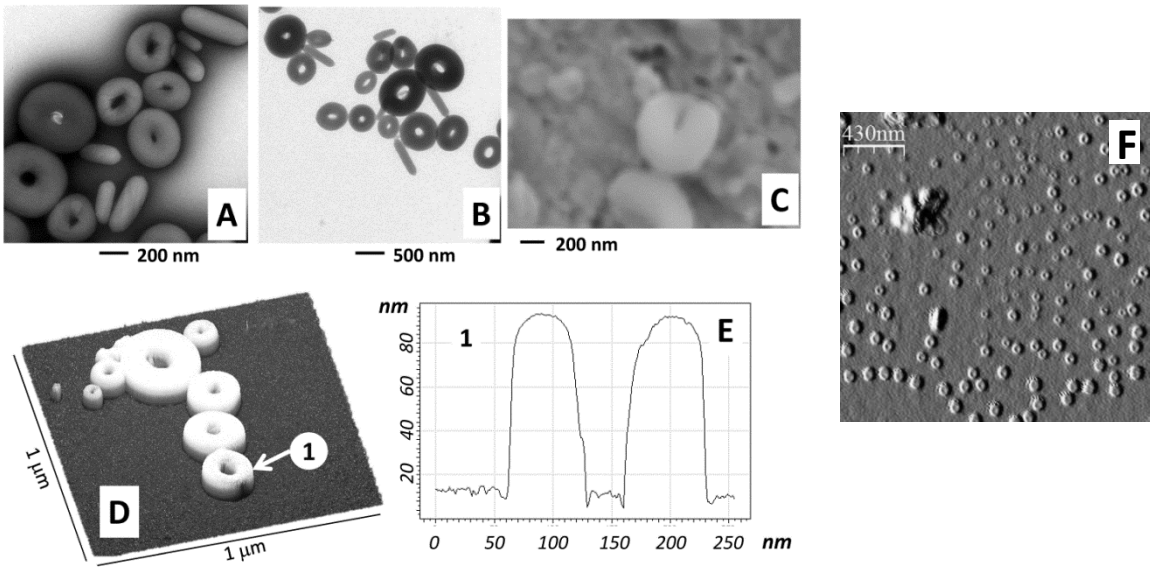

Figure 3.4 TEM (**A** stained and **B** unstained, respectively) and SEM (**C**) images of the resulting self-assembled nanostructures obtained from polymer **4**. (**D** and **E**) AFM micrograph and high-profile of the selected (1) toroidal nanostructure. (**F**) AFM image of toroid, obtained from a diluted solution of **4**.

Sphere-shaped aggregates were generated from polymer **7** under the same conditions described above for polymer **4** (Figure 3.5). TEM revealed the formation of deep-dark round morphologies (Figure 3.5 A) with diameters ranging between 250-700 nm. Moreover, these aggregates displayed an internal cavity as shown from the TEM image reported in Figure 3.5 B; thus, the observed spherical morphologies can be attributed to hollow vesicle-like microstructures. These results were additionally confirmed by AFM (Figure 3.5 C) and SEM analyses (Figure 3.5 D). While polymers **4** and **7** were able to self-assemble into ordered structures, polymer **3**, bearing a Trt group instead of fullerene, did not give any specific nano-structuration under similar conditions. To get polymer **4** from **3**, the Trt protecting group was removed in acidic conditions, thus in polymer **4** the N-terminus amine is protonated (NH_3^+). Importantly, when NaOH 0.2 M was added to a solution containing the toroidal objects obtained by self-assembly of **4**, an immediate precipitation of the polymer was achieved. On the other hand, the addition of HCl 0.2 M did not affect the self-assembled structures, since doughnut-like structures could still be detected by TEM. This information suggested that: (i)

fullerene is necessary for the formation of ordered nanostructures and (ii) the NH_3^+ group is mandatory for the formation of the toroid-shaped structures.

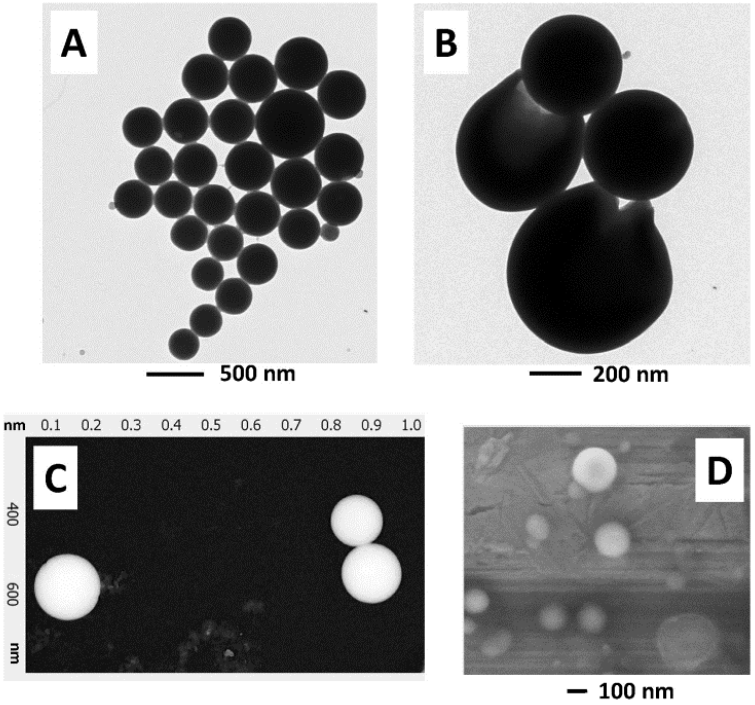

Figure 3.5 (**A** and **B**) TEM (unstained) images of the resulting self-assembled nanostructures obtained from polymer **7**. (**C** and **D**) AFM and SEM images, respectively, from the very same sample used for TEM analysis.

Since, at fixed volume, a toroidal shape exposes a larger surface with respect to a spherical shape, our hypothesis is that in order to generate self-assembled toroid forms in water (starting from the hydrophobic polymer **4**) the single polymer chain may firstly undergo a tail-to-tail dimerization and successively a large scale, coil-coil spiral-like, self-assembly process. According to this hypothesis, all of the fullerenes could be aligned along an internal axle, thus to result buried by the PBLG hydrophobic helices, while the charged NH_3^+ groups may be exposed to water solution in accordance with previously reported similar, but much smaller, structures.[11] This hypothesis is in agreement with the pH-depending experiments described above.

In collaboration with Dr. M. Zerbetto (University of Padova), who performed the molecular dynamic simulations, calculus was used to support experimental observations and in particular to investigate the atomistic structure of the vesicles formed by polymer **7**.

To this purpose a bottom-up coarse graining protocol with the intent to set up a simulation able to independently recover the experimental observations was employed. To limit the computational weight of the whole procedure, a set of molecules of polymer **7** constituted by 25 BLG units was used as a model. The coarse-graining representation sees each of the BLG

units and the two terminal moieties as single beads. Differently from other systems, in which a balance between attractive and repulsive forces of the building blocks drives the assembly, here the driving force of the self-assembly is the low affinity of the hydrophobic PBLG molecules with water. Thus, in these simulations the medium needs to be included explicitly to observe aggregation of polymer **7** molecules. A coarse-grained 4-water model for the solvent was employed, in which one bead is used to represent a cluster of 4 water molecules. A system containing 1600 polymer molecules and 1600608 water beads was simulated. In the starting configuration, the polymer molecules are randomly placed and oriented in space (Figure 3.6 A).

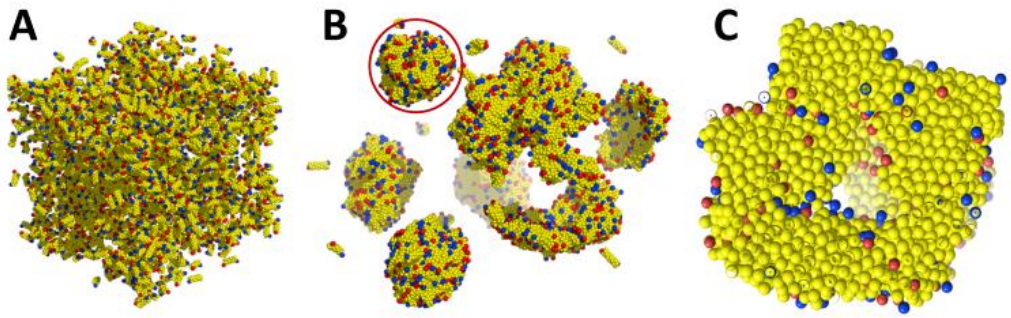

Figure 3.6 (**A**) Initial random configuration of the 1600 PBLG molecules constituted by 25 BLG amino acids. (**B**) Final configuration of the system after 5 ns of simulation time. (**C**) Details of a selected spherical aggregate with front and rear clipping planes applied to highlight the hollow part of the spherical aggregate. Water molecules have been omitted for clarity. The color scheme is: yellow to represent BLG beads, red for the N-terminal group, and blue for C-terminal group.

After 5 ns of simulation time, the simulation box results populated by a small number of aggregates with different shapes (Figure 3.6 B). Most of them are spherical aggregates of dimensions ranging from 15 to 20 nm of diameter. However, a couple of assemblies are present showing a bent layer of about 4 nm of thickness (very close to the length of one polymer molecule) that can be thought to be a piece of a larger vesicle that could not be formed in this simulation due to an insufficient number of polymer molecules. A number of important observations can be drawn from the simulations. The first and most important observation reflecting the experiments is that in water the polymer molecules aggregate into ordered structures instead of creating an amorphous precipitate. Second, all the aggregates are formed by layers of limited size ranging from 4 to 6 nm, which is in the order of the length of the polymers. Third, the layer is not structured in a simple way as it happens in phospholipids: couples of polymers form coiled-coil super structures, which in turn create a network giving

origin to the layer, with the C_{60} termini preferentially exposed to the solvent. We shall also notice that, while being quite compact, the spherical structures obtained in the simulation are hollow (Figure 3.6 C). The obtained aggregates are in quite good accord with those observed experimentally.

Conclusions

We reported the one-pot synthesis of two novel PBLG-polymers C- and C/N-terminus capped with fullerenes, by means of thiol-ene chemistry. The self-assembly in water of such rod-like systems led to the formation of bulky, toroid-like or vesicle-like, nanostructures depending on the fullerene position over the main chain of the polymer. In conclusion, such polymer-fullerene conjugates may be interesting systems to prepare organized, at nanoscale level, fullerene-based devices.

3.2 Poly(γ-Benzyl-L-Glutamate)-Carbon Quantum Dots conjugates (PBLG-CQDs)

Carbon Quantum Dots (CQDs) are water-soluble carbon nanomaterials that show peculiar photoluminescence (PL) properties, such as multi-colour emission that varies with the excitation wavelength.[12] Several procedures to prepare CQDs have been reported, according both to bottom-up[13] and top-down[14] approaches. Starting from natural precursors (e.g. carbohydrates, peanut skin, soy milk) and nitrogen-rich organic compounds using hydrothermal treatment it is possible to obtain CQDs with particular photoluminescence properties. CQDs can be prepared also from amino acids, which are abundant and inexpensive natural compounds, by microwave-assisted hydrothermal treatment.[15]

We synthesized the starting CQDs by using arginine and 1,2-ethylendiamine precursors in order to maximize the number of available amine moieties with the aim to grow polymeric structures on the surface of CQDs (Figure 3.7 A). TEM analysis of the products (Figure 3.7 C) revealed round particles of uniform size and a diameter of 1.4 ± 0.2 nm. High resolution TEM analysis (Figure 3.7 D) and Fast Fourier Transform (FFT) (Figure 3.7 D, inset) highlight an interplanar distance of 0.21 nm, compatible with the (0001) graphite facet. Elemental analysis yield 71.47% for C, 5.05% for H, 17.09% for N and 5.39% residual elements.

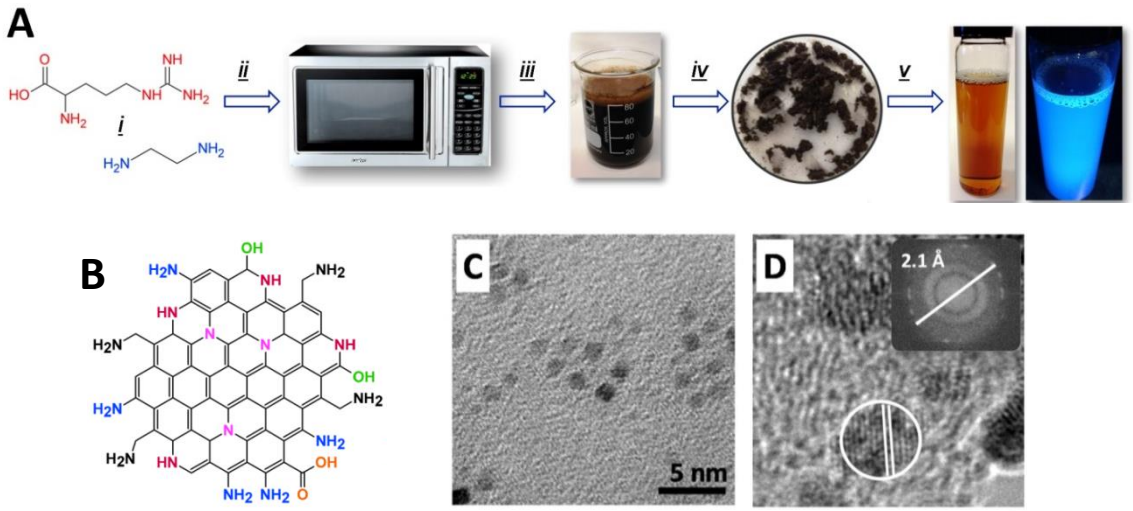

Figure 3.7 (**A**) Schematic representation of CQDs synthesis. Reagents and conditions: (i) arginine and 1,2-ethylendiamine (1:1 mol/mol) in ultrapure water; (ii) domestic microwave, 700 watt; (iii) dissolution in ultrapure water and centrifugation; (iv) lyophilisation; (v) dissolution in ultrapure water (left: under irradiation, visible-light; right: under irradiation, UV-light at 365 nm). (**B**) Hypothetic representation for the chemical structure of a single CQD. (**C** and **D**) TEM and HRTEM images of CQDs.

MALDI analysis displayed a M_W dispersion, as expected from the random combination of different atoms, centred at 1150 Da. Solid state FT-IR data are consistent with the presence of amines. XPS measurements were carried out to provide a deeper insight on the different chemical species introduced by the synthesis. The XPS survey spectrum reported in Figure 3.8 A shows the C 1s, N 1s and O 1s photoemission lines centred at a binding energy (BE) of 284.9 eV, 399.8 eV and 531.6 eV, respectively. The observed elemental composition (C 74.3 %, N 18.8 % and O 6.9%) is in good agreement with that of the previous elemental analysis. The detailed scans of C 1s and N 1s lines were deconvoluted into single chemically-shifted components (Figures 3.8 B-C).

The multicomponent analysis of the C 1s line confirms the presence of C-N bonds (285.2 eV) as well as that of several oxygen-bearing functional groups, such as C-O (286.5 eV), C=O (288.0 eV) and O-C=O (288.9 eV).[16] The weak component on the low BE slope of the main peak can be attributed to C atoms around vacancy sites (283.8 eV).[17] The fit of the N 1s line, on the other hand, shows five different chemical components centred at BEs of 398.0 eV, 399.1 eV, 400.2 eV, 401.3 eV and 402.2 eV, corresponding to pyridinic, amine, pyrrolic, graphitic and pyridine oxide groups, respectively. In particular, the ratios between these last functional groups suggest that, on the average, each CQD contains 8-10 $–NH_2$ groups (either aliphatic or aromatic, see Figure 3.7 B for a schematic representation).

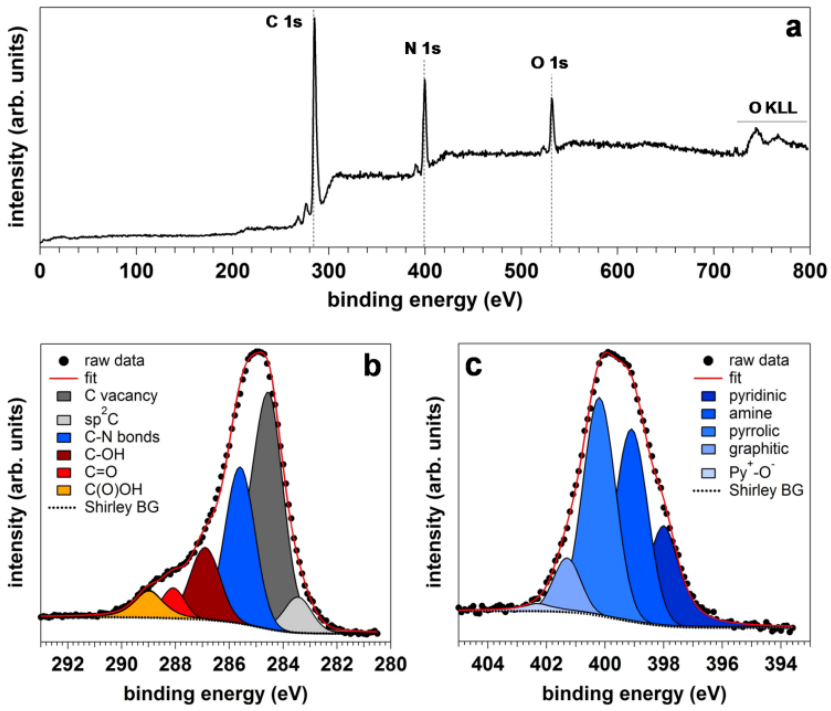

Figure 3.8 (**A**) XPS survey scan. (**B**) Multipeak analysis for the Carbon 1s and (**C**) Nitrogen 1s photoemission lines.

The UV-Vis absorption spectrum of the as-prepared CQDs shows an absorption shoulder around 350 nm, typical of aromatic structures (Figure 3.9 A). Non-Normalized emission spectra are shown in Figure 3.9 B and display the distinctive features of CQDs, such as the dependence of the emission maxima on the excitation wavelength (normalized spectra, Figure 3.9 B, inset). We evaluated the emission quantum yield upon 360 nm excitation as 30.1% using quinine sulphate as a reference, in line with data reported earlier by similar synthetic methods.[12a,18]

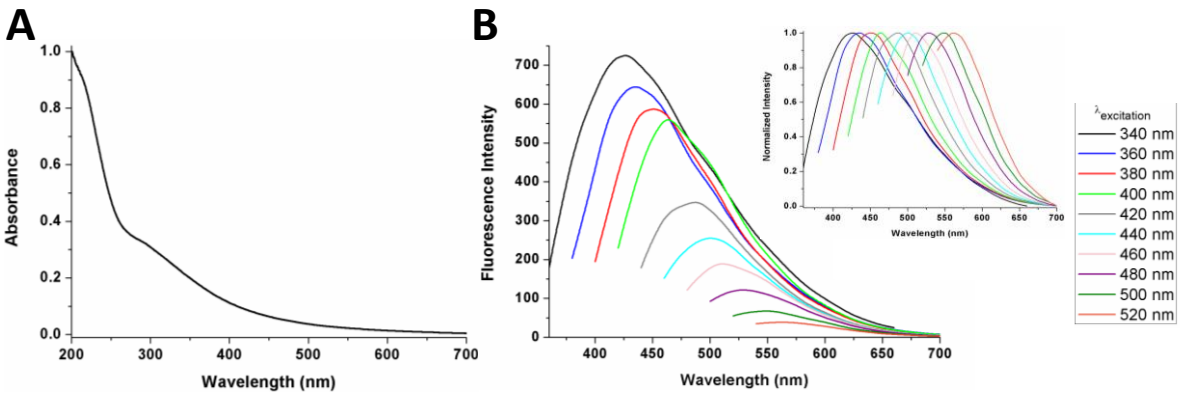

Figure 3.9 (**A**) UV-Vis absorption spectrum of CQDs in water. (**B**) Non-normalized and normalized (inset) fluorescence emission spectra of CQDs in water obtained by excitation at different wavelengths.

Primary amines can be used to promote controlled NCA-ROP processes.[4] Thus, BLG-NCA was polymerized using CQDs as the amino-group-bearing initiator (Figure 3.10).

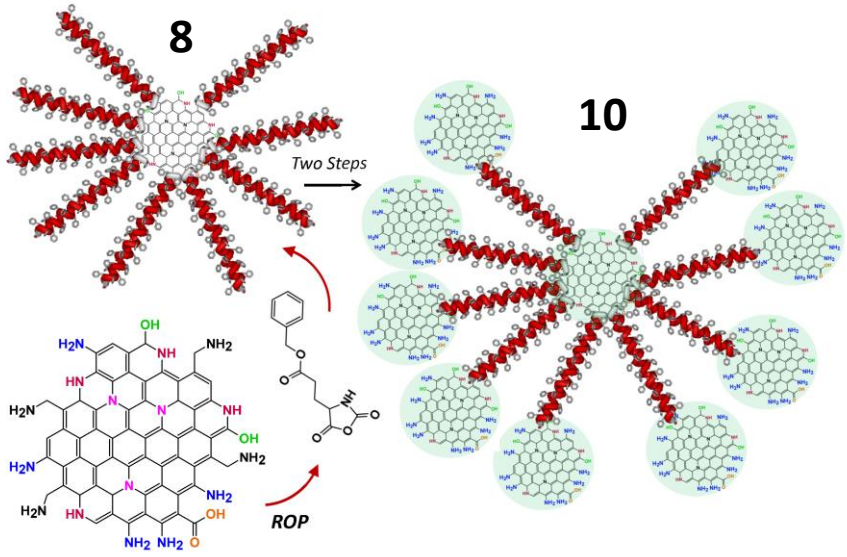

Figure 3.10 Schematic representation of the synthesis of **8** and successive modification to obtain **10**. Polymer **8**: polymerization conditions: BLG-NCA, DMSO, 96 h, r.t., yield 78 %); polymer **10**: (i) DMF, succinic anhydride, TEA, 40°C, 24 h; (ii) CQDs, DMF, DPPA, TEA, 40°C, 24 h.

The formation of PBLG arms from the CQDs core (hybrid material **8**, Figure 3.10) was confirmed by NMR, FT-IR and circular dichroism (CD) spectra. CD data being related to the secondary, rod-like, α-helical, structure of PBLG (Figure 3.11 A). Size exclusion chromatography (SEC) showed an average MW of around 45 KDa (Figure 3.11 B). Termogravimetric analysis (TGA) yields a BLG:CQDs weight ratio of 97:3 (Figure 3.12). Like pristine CQD, **8** shows a dependence of its emission spectra on λ_{ex} (Figure 3.13 B).

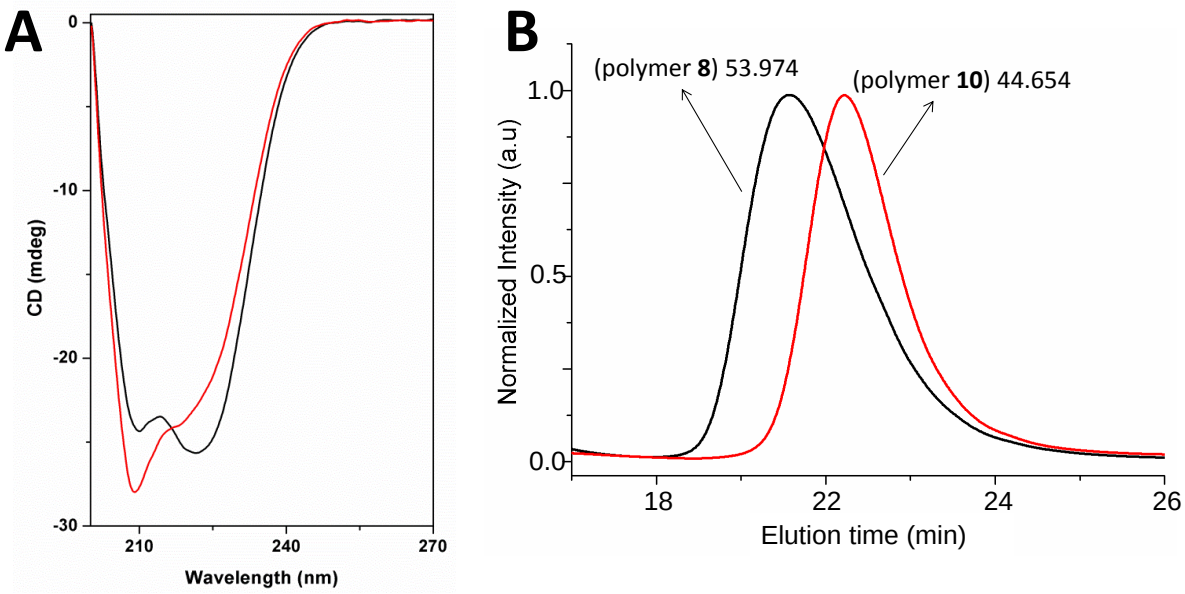

Figure 3.11 (**A**) CD spectra of polymers **8** (red line) and **10** (black line) in HFIP solution (concentration 2 mg/mL). (**B**) SEC traces of polymers **8** (red line) and **10** (black line) in DMF.

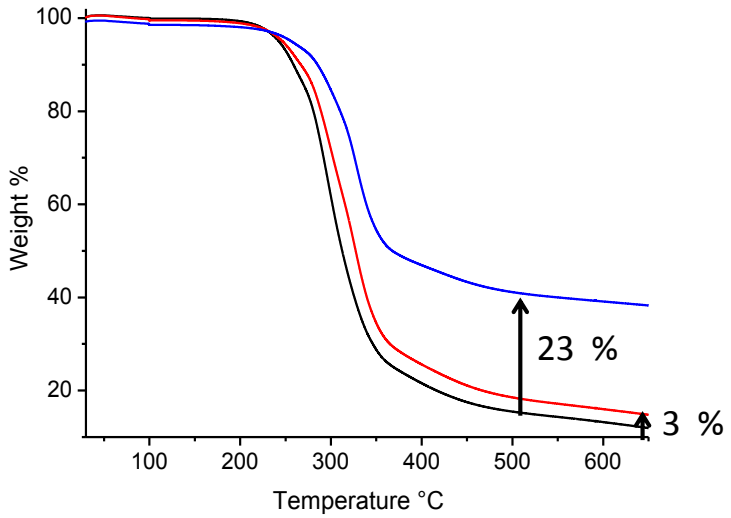

Figure 3.12 Thermogramivetric analysis comparison of a reference PBLG (black line), polymer **8** (red line) and polymer **10** (blue line).

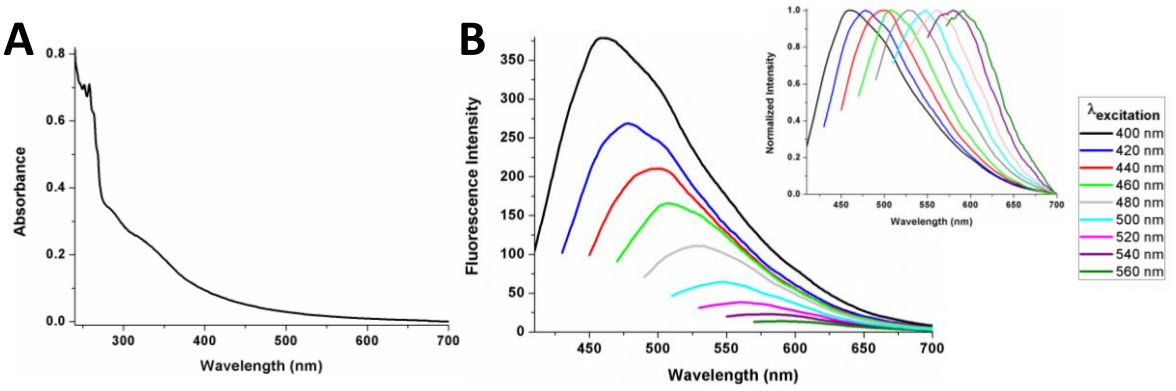

Figure 3.13 (**A**) UV-Vis absorption spectrum of **8** in THF. (**B**) Non-normalized and normalized (inset) fluorescence emission spectra of **8** in THF obtained by excitation at different wavelengths.

The CQD-PBLG-NH_2 structure of **8** was further modified in its N-terminus position by reaction with a large excess of succinic anhydride in order to obtain the corresponding carboxylic derivative, CQD-PBLG-COOH (**9**). A negative Kaiser test (ninhydrin) confirmed the absence of primary amine groups upon reaction with the anhydride. The carboxylic groups of this intermediate were further derivatized, by activation with diphenylphosphoryl azide and reaction with a large excess of CQDs. The SEC trace of the resulting material **10** confirmed the addition of several CQDs per core, by showing an increase of the M_W, in comparison to **8**, of ca. 10 KDa (Figure 3.11 B). TGA analysis corroborated this finding, indicating a 22% increase of the CQDs abundance with respect to PBLG in comparison to hybrid **8** (Figure 3.12). By assuming a M_W of 1150 Da for CQDs, we estimate a covalent attachment of an average of nine peripheral CQDs per core for hybrid **10**.

In order to observe the structure of **10**, we exploited the electron-donating capabilities of photoexcited CQDs, that enable the reduction of silver salts to the corresponding silver nanoparticles (AgNPs) on the surface of the CQDs themselves.[19] To this end, a THF solution of **10** was photoexcited with ultraviolet irradiation in presence of silver nitrate. The formation of AgNPs brought a change in color from yellow to brown (Figure 3.14, upper part). AgNPs are expected to form on the surface of the external layer of **10**, which is composed by CQDs. TEM analysis of the resulting organic-inorganic hybrid **11** shows the formation of star-shaped nanostructures with sizes in the 30-60 nm range, carrying several 5 nm AgNPs (Figure 3.14). According to previous studies,[19] the templating and clustering effect of CQD supports has a dramatic effect on the plasmonic properties of the NPs. This is demonstrated by a broad surface plasmon resonance peak in the UV-Vis absorption spectrum of **11**, between 400 and 520 nm (Figure 3.13). The remarkable broadening of the UV-Vis spectrum of **11** compared to

that of free-standing AgNPs in a similar size range (with a sharp absorption peak at 400 nm), is due to the compact arrangement of the AgNPs in **11**, that results in strong plasmonic coupling interactions.[20]

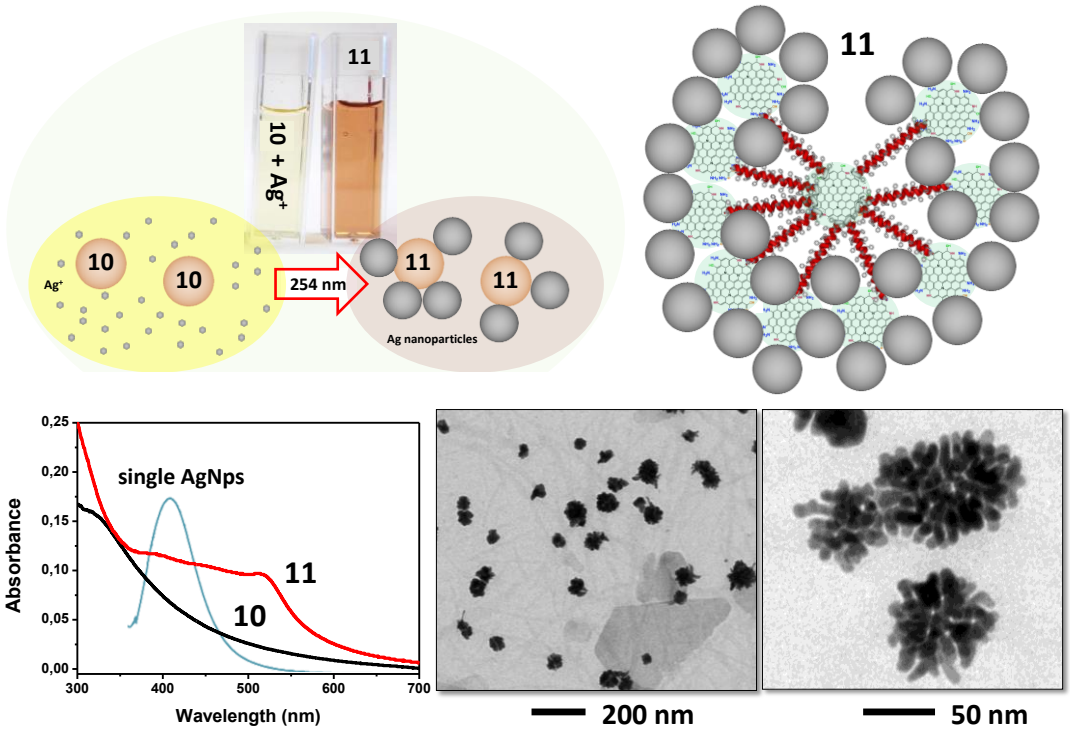

Figure 3.14 Upper part: schematic representation of the photoreaction to generate **11**. Bottom part left: UV-Vis absorption spectra for **10**, **11** and single AgNPs. Bottom part right: Two TEM images of single units of **11**.

Finally, we made use of the self-aggregation properties of PBLG to generate self-assembled microstructures from hybrids **8** and **10**. To this end, we solubilized **8** or **10** in a THF/DMF mixture and dialyzed against water for 48 h. The resulting milky, light-brown (**8**) and dark-brown (**10**) solutions were submitted to a size exclusion gel-filtration (water as eluant) and the main fractions were collected and examined by TEM (without uranyl-acetate staining) and SEM (Figure 3.15). In both cases spherical aggregates with diameters ranging from 100 to 300 nm were observed. When **8** was used, the surfaces of the aggregates showed a smooth profile (Figure 3.15 A), whereas in the case of **10** the surfaces appear rough, with limited flat areas (Figure 3.15 B). This is compatible with the exposure of the hydrophilic CQDs on the surface of the aggregate formed by **10**. Furthermore, the aggregated structures obtained in this last case, still displayed the multicolour emission characteristics described previously for CQDs and hybrids **8** and **10**. We were able to picture it directly in the fluorimeter by using a digital camera, as shown on the top of Figure 3.15.

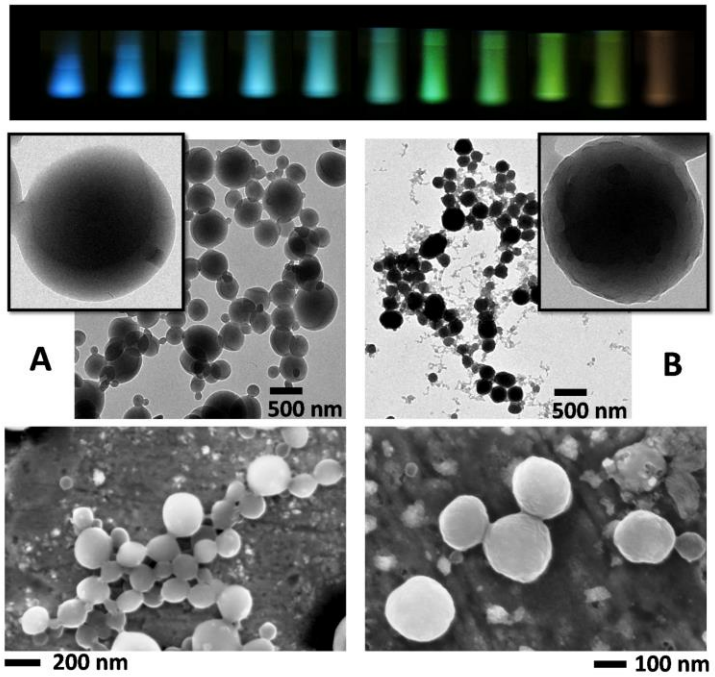

Figure 3.15 (**A**) and (**B**) TEM and SEM images of microstructures generated by self-assembling of **8** and **10**, respectively. Upper part: emission colours occurring from **10** microstructures.

Conclusions

In conclusion, we reported the synthesis and characterization of CQDs bearing amino groups at their edges, as demonstrated by elemental and XPS analyses. Functionalization of dots with poly-γ-benzyl-L-glutamate gave the first reported CQD/polypeptide polymeric systems of star shaped fashion that were further decorated with an outer shell of CQDs. We tracked the spectroscopic properties of the materials throughout the syntheses, and exploited the electron-donating capabilities of photoexcited CQDs to grow silver nanoparticles. These, in turn, allowed visualization of the structure of the resulting hybrid materials by TEM imaging thanks to their contrasting effect. Finally, we assembled supramolecular aggregates of spherical shape with evidence of rough surfaces profile in the case of CQD-capped hybrid materials, which may indicated the presence of aggregated areas of CQDs on the external layer. These microstructures are able to retain the characteristic emission properties of the native CQDs. The approach developed in this study is a facile, but highly efficient approach to the synthesis of fluorescent, peptide-based materials, attractive for many applications including optical sensing, biolabelling, imaging, targeted drug delivery/tracking and even UV protection for optical devices.

3.3 Poly(γ-benzyl-L-glutamate)-azobenzene conjugates

With the aim to obtain "smart" supramolecular architectures with light-responsive behavior we decided to incorporate a photoresponsive moiety in the polypeptide chain. In addition to study the effect of geometry (*cis*/*trans* isomerization) on the response behavior of azobenzene-functionalized PBLG microstructures, bifunctional (Scheme 3.2) or trifunctional (Scheme 3.3) initiators with C_2- or C_3- type symmetry were exploited.

The synthetic strategy to obtain the *bis*-aminoester (**16**) (initiator of the C_2-symmetry) followed a modification of the reported protocol.[21] The synthesis involved condensation of two L-Phe derivatives, bearing an amino (**13**) and a nitroso (**14**) moiety, respectively (Scheme 3.2). After Boc-protection of the N-terminus of H-L-Phe(*p*NO_2)-OMe (**12**), the following catalytic hydrogenation yielded the *p*-amino derivative (**13**). Nitroso derivative (**14**), obtained upon reduction of **12** with Zn dust and subsequent treatment with $FeCl_3$, was immediately condensed with **13** in acetic acid (AcOH), yielding the Boc-protected *bis*-azo-L-Phe compound (**15**). Finally, compound **16** was obtained by a TFA treatment of **15**.

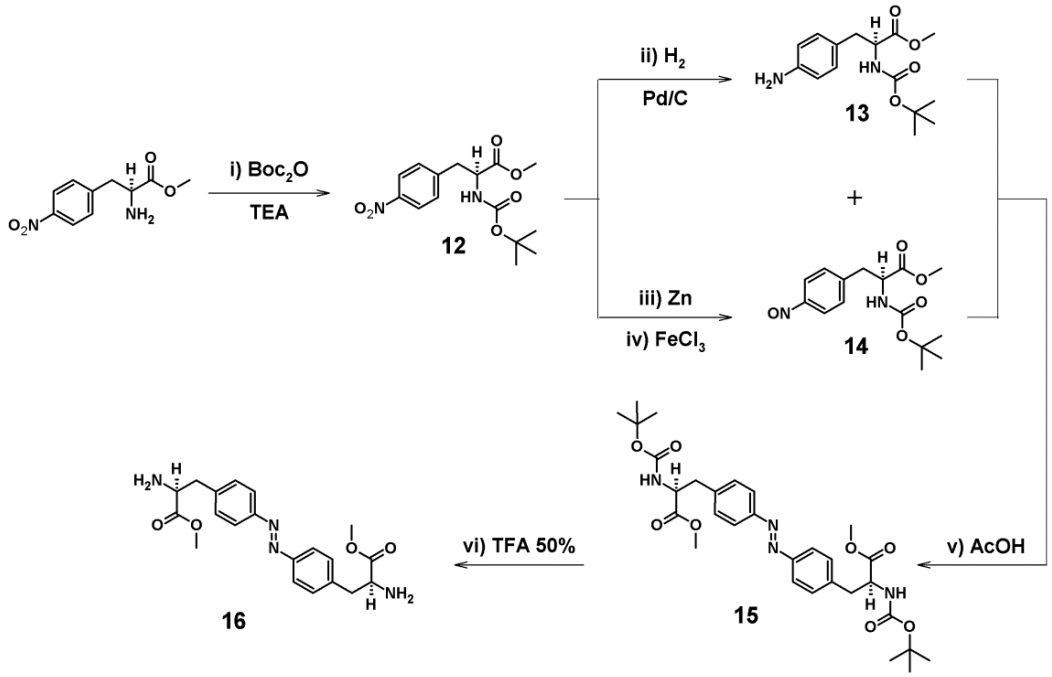

Scheme 3.2 Synthesis of H-*bis*azo-L-Phe-OMe (**16**), C_2-Symmetry initiator. Reagents and Conditions: i) Boc_2O, TEA, 1:1 CH_3CN/H_2O, r.t., 18 h. ii) Pd/C, H_2, MeOH, r.t., 40 min. iii) Zn, NH_4Cl, 5:1 $EtOH/H_2O$, r.t., 2 h. iv) $FeCl_3$, 5:1 $EtOH/H_2O$, 0 ºC, 30 min. v) AcOH, r.t., 24 h. vi) 50% TFA in CH_2Cl_2, r.t., 40 min.

The synthesis of the initiator with C_3-symmetry (**22**) initially involved the preparation of the azo compound (**19**)[22] (Scheme 3.2). The amino group of *p*-nitrobenzylamine was Boc-protected (**17**) and then the nitroso moiety of **18** was prepared *via* Zn/Fe redox treatment. The

condensation of **18** with *p*-aminobenzoic acid in AcOH afforded **19**. The C_3- platform (**20**) was easily obtained *via* thiol-ene "click" chemistry starting from the *tris*-alkene core 2,4,6-triallyloxy-1,3,5-triazine and 2-β-mercaptoethanol, by UV irradiaton (λ= 365 nm) and using DMPA as photoinitiator. Condensation of compounds **19** and **20** using the EDC/DMAP C-activation protocol yielded the amino-protected compound (**21**), which after acidic treatment (50% TFA) gave the trifunctional amine initiator (**22**).

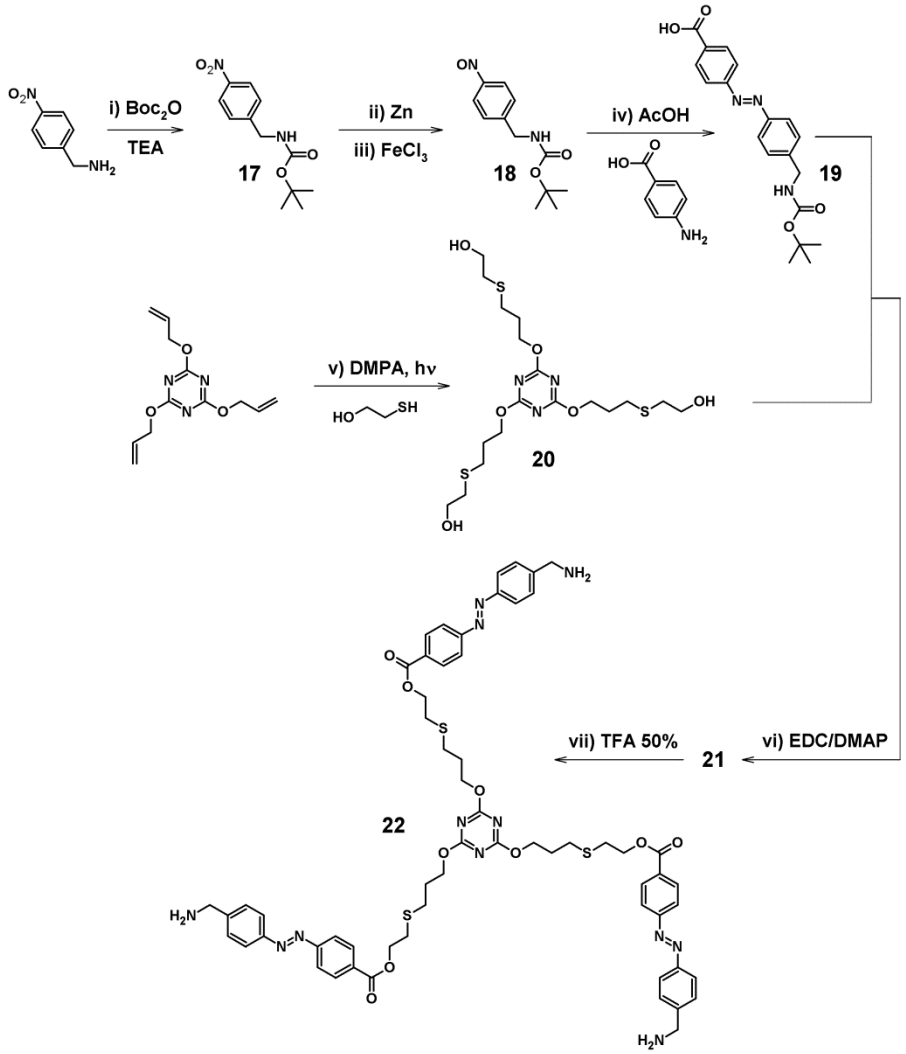

Scheme 3.3 Synthesis of C_3-symmetry initiator (**22**). Reagents and conditions: i) Boc_2O, TEA, 1:1 CH_3CN/H_2O, r.t., 18 h. ii) Zn, NH_4Cl, 5:1 $EtOH/H_2O$, r.t., 2 h. iii) $FeCl_3$, 5:1 $EtOH/H_2O$, 0 ºC, 40 min. iv) AcOH, *p*-aminobenzoic acid, r.t., 48 h. v) 10% mol DMPA, 2-mercaptoethanol, λ=365 nm, 40 min. vi) EDC, DMAP, DMF, r.t., 18 h. vii) 50% TFA in CH_2Cl_2, r.t., 2 h.

The photo-isomerization of the two initiators (**16**) and (**22**) in solution was monitored by UV-Vis absorption spectroscopy and HPLC (Figure 3.16). Compound **16** can efficiently isomerize in the *cis* form by irradiation with light at 365 nm for 40 s (Figure 3.16 B). In Figure 3.16 C

we show the four isomers expected from the photoisomerization of **22** and the co-presence of the four species can be detected by HPLC (Figure 3.15 D). A more prolonged irradiation at 365 nm is able to quantitatively isomerize the *trans* form to the *cis* form.

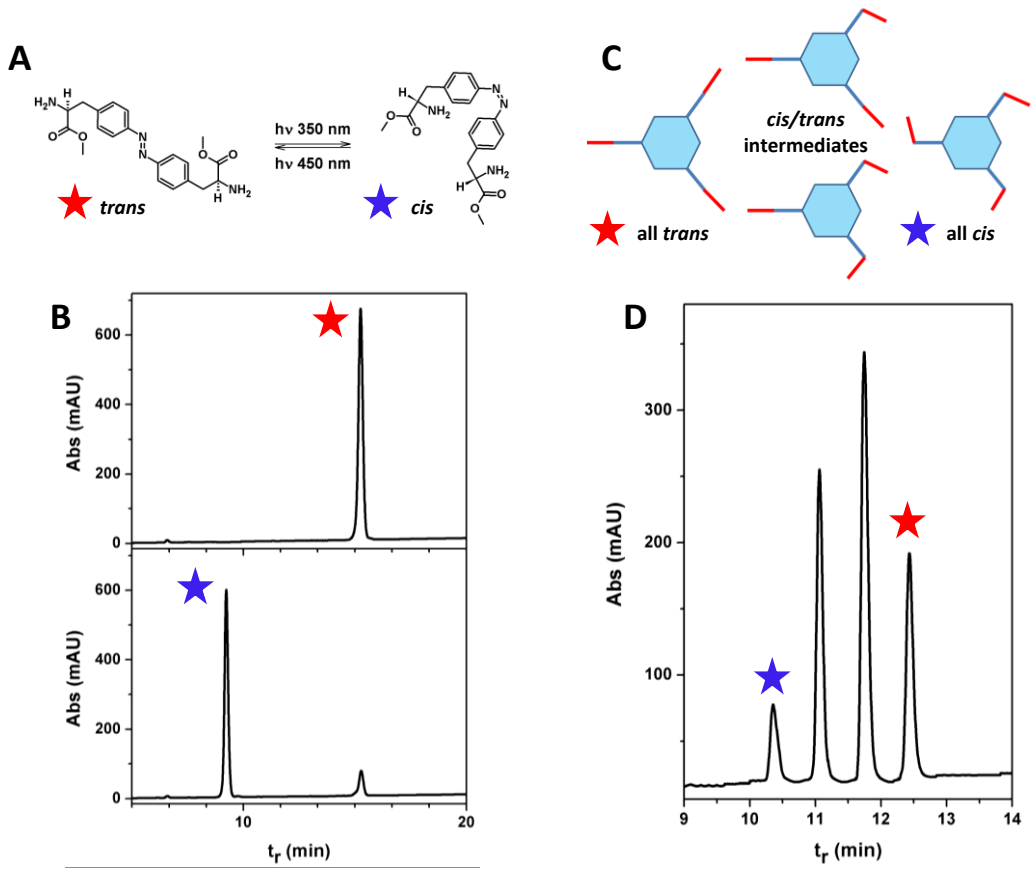

Figure 3.16 (**A**) Schematic representation of the light-driven, reversible photoisomerization process occurring for **16**. (**B**) HPLC profiles of a solution of **16** before (top) and after (bottom) irradiation at 365 nm. (**C**) Schematic representation of the light-driven, reversible photoisomerization process occurring for **22**. (**D**) HPLC profile of solution of **22** irradiated at 365 nm for 40 s, which revealed formation of all (four) of its possible isomers.

The PBLG hybrids with C_2- and C_3-symmetries were obtained *via* NCA-ROP (ring opening polymerization) using compounds **16** and **22**, respectively, as the initiators. The polymerizations using BLG-NCA were performed in 1,4-dioxane or DMF. The solid PBLG hybrids, obtained after precipitation with MeOH, were characterized by SEC analysis. We obtained a M_W distribution of 63,500 Da, PDI 1.16 (C_2-symmetry PBLG) and 46,800 Da, PDI 1.56 (C_3-symmetry PBLG).

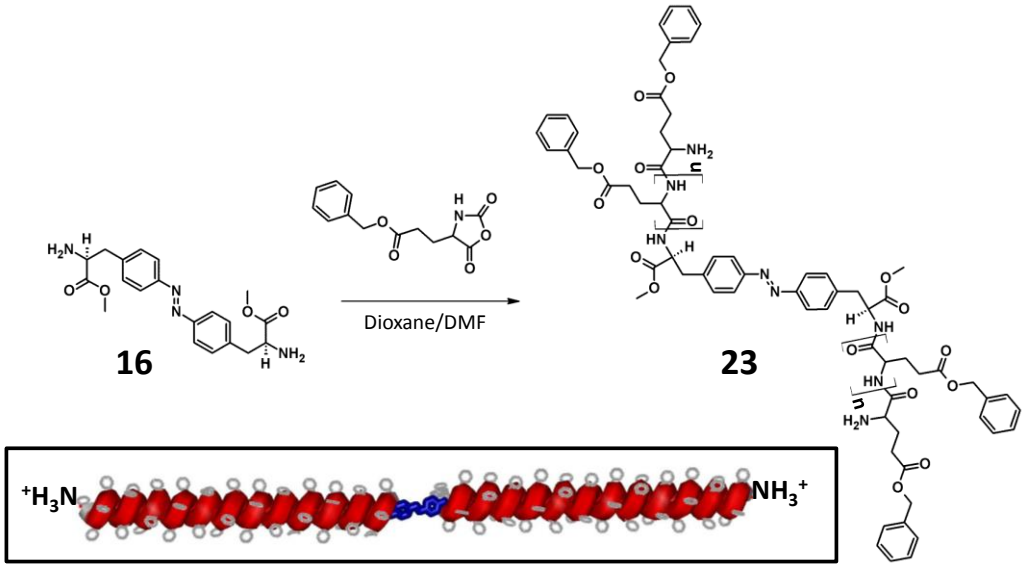

Scheme 3.4 Synthesis of PBLG Hybrid with C_2-Symmetry (**23**). Inset: schematic representation of polymer **23**.

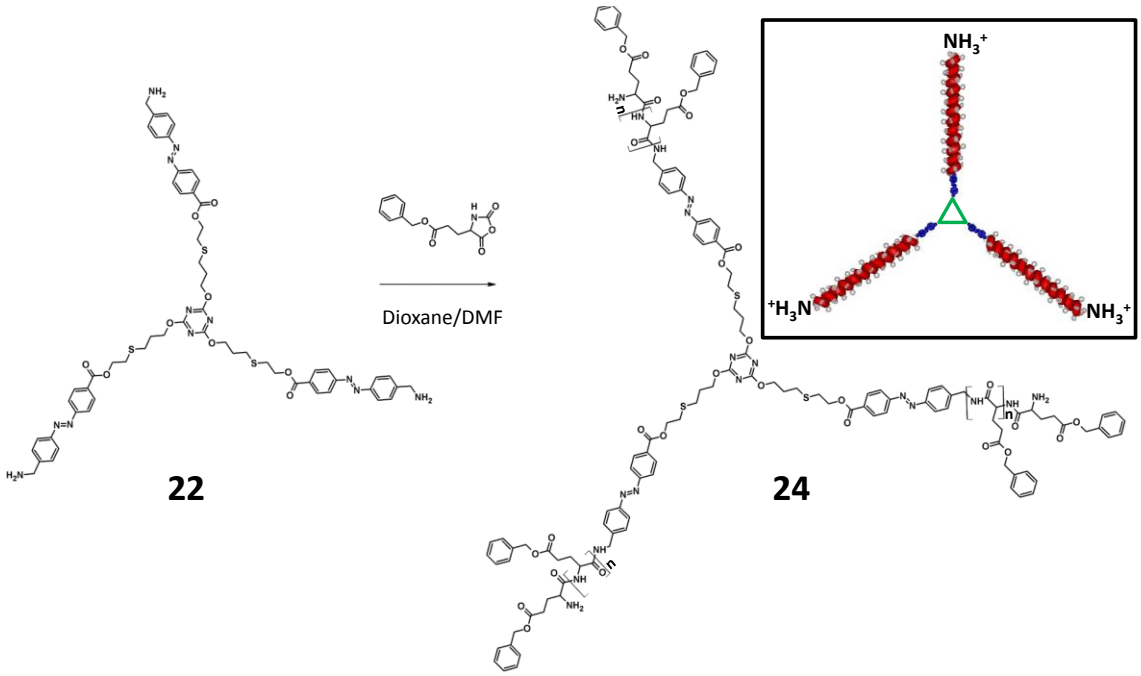

Scheme 3.5 Synthesis of PBLG Hybrid with C_3-Symmetry (**24**). Inset: schematic representation of polymer **24**.

The C_2-symmetry PBLG hybrid (**23**) was studied in terms of photoresponsive behavior (Figure 3.17 A). After UV irradiation at λ= 365 nm of a PBLG hybrid solution in THF, isomerization of the azobenzene moiety from *trans*-to-*cis* was observed, as indicated by the decrease of the π-π* transition band at 328 nm and the concomitant increase of the n-π* transition band at 440 nm (Figure 3.17 B). This process was found reversible for several cycles (repeated irradiation at 365 and 420 nm).

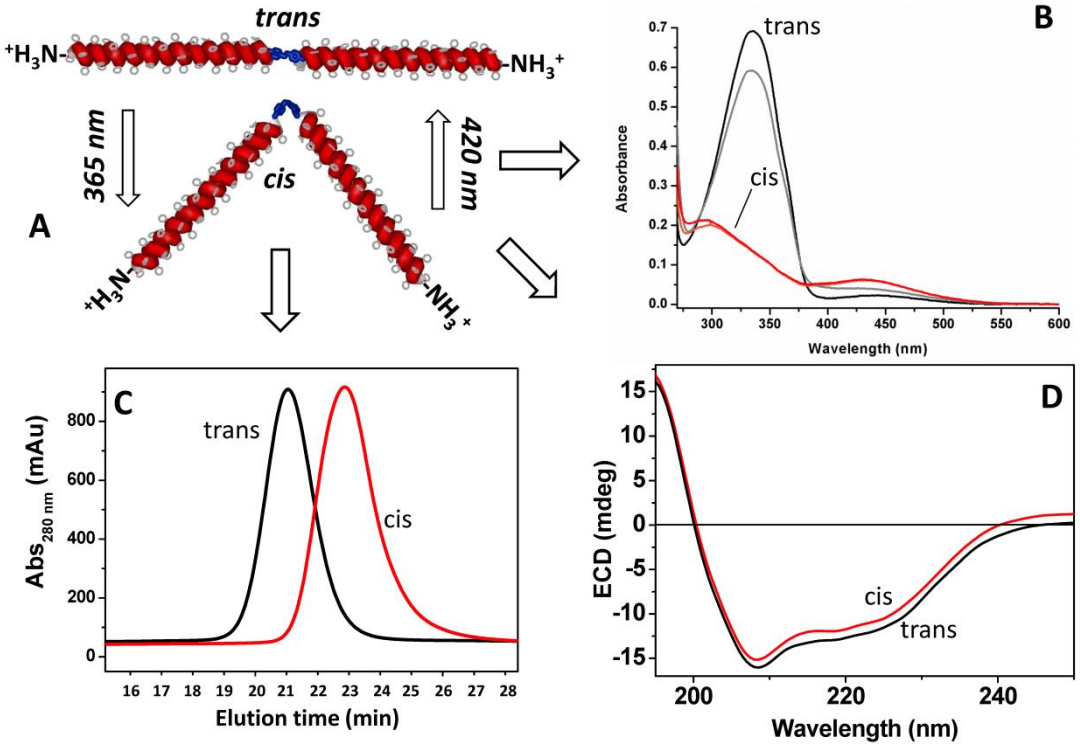

Figure 3.17 (**A**) Schematic representation of the *cis*/*trans* photoisomerization underwent by the C_2-symmetry PBLG hybrid (**23**). (**B**) UV-Vis absorption spectra of the *cis* and *trans* isomers of the C_2-symmetry PBLG hybrid in THF solution, two cycles of irradiation are represented. (**C**) SEC analysis which shows different elution profiles occurring for the *cis* and the *trans* forms of the C_2-symmetry PBLG hybrid. (**D**) CD spectra of the *cis* and *trans* isomers of the C_2-symmetry PBLG hybrid in HFIP solution (the *cis* red trace was slightly shifted up for clarity).

Interestingly, the *cis* and *trans* isomers can be differentiated by SEC analysis (Figure 3.17 C). Specifically, the *cis* form is characterized by a longer elution time, indicative of a more compact 3D-shape, with respect to the *trans* form. Conversely, as expected, *cis*/*trans* isomerization does not affect the polypeptide secondary structure of the PBLG hybrid, the CD spectra of which are almost identical for both isomers and indicative of an overwhelmingly prevailing α-helical conformation (Figure 3.17 D).

The self-assembly properties of the C_2-symmetry PBLG hybrid were investigated in aqueous environment.[5b] Starting from a solution of this hybrid in an organic solvent mixture (20 mg in 10 mL of 3:7 DMF/THF *v*/*v*), a milk-like suspension was obtained after dialysis against ultrapure water for 48 h (membrane cutoff, 12 KD). Few drops of this suspension, examined by TEM and SEM revealed formation of aggregates which display polydisperse spherical morphologies with diameters of 100-500 nm (Figures 3.18 A-B). The relative high and positive value of the Z-potential function (+30 mV)[23] (related to the degree of electrostatic repulsion between adjacent, similarly charged particles) obtained from these experiments

provides evidence for the presence of electrostatic net charges, due to the protonated N-terminal amino groups, present at least in the outer layer of these microstructures. Moreover, high Z-potential values are often associated to double-layer systems, such as vesicles. Indeed, our rod-like PBLG hybrid, largely hydrophobic but carrying protonated amino groups at both termini, might give rise to a vesicle-like self-assembly (Figure 3.18 C). By considering that this hybrid has an average M_W of 63,500, which corresponds to about 280 BLG units, and the elevation per residue in the α-helix is 0.15 nm,[24] the wall thickness of the vesicles might be of the order of 40 nm.

Upon UV irradiation (λ= 365 nm) of the suspension, a rapid and progressive collapse of these ordered structures was observed, most likely driven by the change in 3D-geometry of few polymeric molecules as a consequence of the azobenzene isomerization from *trans* to *cis* (Figures 3.18 D-G).

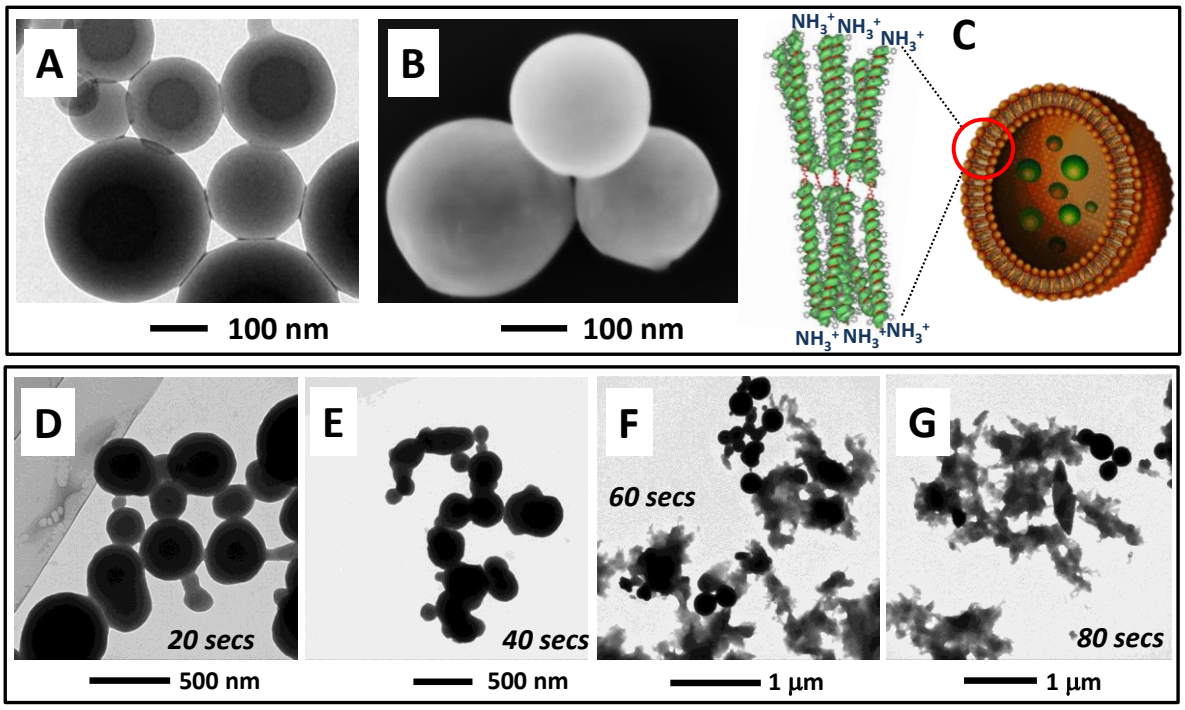

Figure 3.18 TEM (**A**) and SEM (**B**) images of the self-assembled structures obtained from the C_2-symmetry PBLG hybrid (**23**) in aqueous suspension. (**C**) Tentative model of the self-assembled structures. (**D-G**): TEM images of the microstructure transitions occurring after different irradiation times under UV light at λ= 365 nm (20, 40, 60 and 80 sec, respectively).

Evidence for the vesicular nature of the self-assembled structures was obtained by the carboxyfluorescein (CF)-entrapped technique.[25] The self-assembly process described above was repeated in the presence of CF in the starting organic medium. After dialysis, the resulting suspension was submitted to SEC, thus allowing removal of the non-entrapped CF and the isolation of a red-orange colored main fraction, consisting of spherical self-assembled structures, homogeneous in size (200 nm), according to a TEM and DLS analyses (Figure 3.19, upper part).

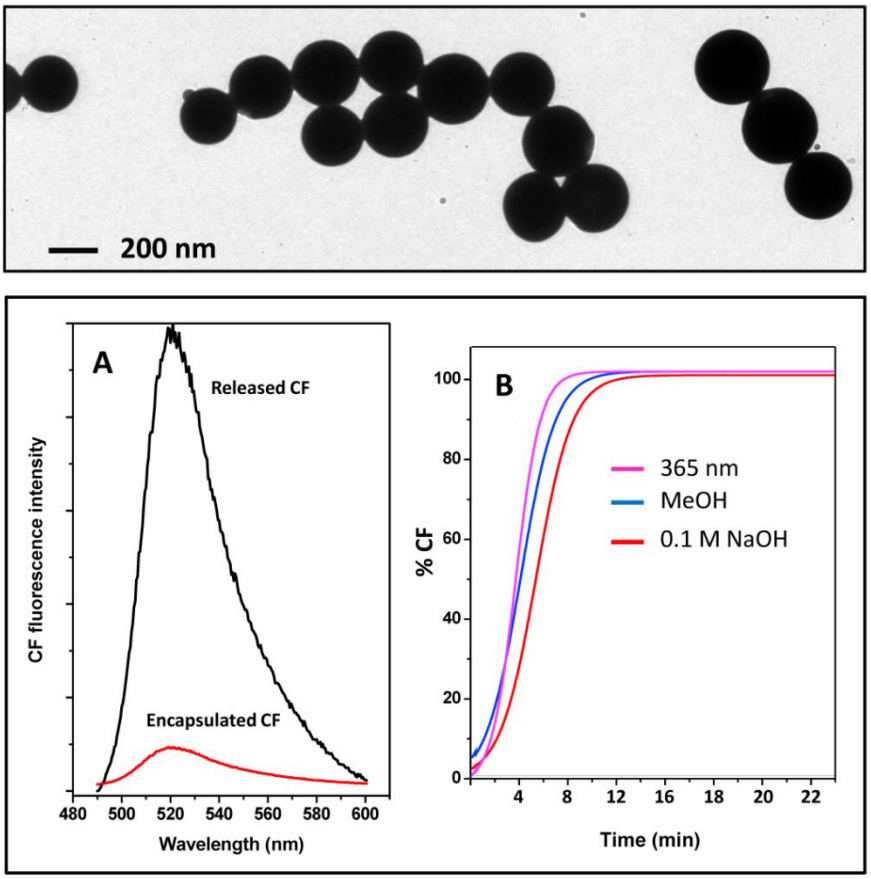

Figure 3.19 Upper part: TEM image spherical aggregates of the C_2-symmetry PBLG hybrid (**23**) formed in the presence of CF. Lower part: (**A**) Comparison of the fluorescence emission spectra of the CF-encapsulated aggregates before (red line) and after (black line) UV irradiation at 365 nm. (**B**) Time evolution of the release of CF from the spherical aggregates as a result of either UV irradiation (365 nm) or denaturation by addition of 10 % MeOH (v/v) or 5% 0.1 M NaOH (v/v).

We recorded the fluorescence spectra of a diluted water solution of the spherical aggregates prior and after exposure to UV light at λ= 365 nm (Figure 3.19 A). The UV-induced collapse of the aggregates (demonstrated above) is accompanied by a dramatic enhancement in the CF fluorescence. This result strongly supports the view that our spherical aggregates of the C_2-symmetry PBLG hybrid are indeed vesicles, hosting in their inner cavity CF molecules at

relatively high concentration. This phenomenon gives rise to a low fluorescence emission owing to the self-quenching effect. Upon disruption of the vesicles, diluted CF is released in the medium, fully restoring its strong fluorescence. As shown in Figure 3.19 B, the maximum fluorescence intensity is reached after 6 min irradiation at 365 nm. This represents a much longer time than the 20-80 sec required for the collapse of the empty vesicles reported in Figure 3.18. Such a discrepancy might be rationalized by observing that CF absorbs part of the irradiating light. Beside *via* UV-induced *trans-cis* isomerization, the disruption/destabilization of the vesicles leading to CF release within a few minutes can be achieved also by addition to the aqueous suspension of either MeOH (it dissolves the polymeric vesicles) or a diluted NaOH solution (it removes the positive charges on the surface of the vesicle that are fundamental to prevent the aggregation effect of this colloidal form) as shown in Figure 3.19 B.

We also investigated the self-assembly properties of the C_3-symmetry PBLG hybrid (**24**) in aqueous environment. The microstructures formed starting from an organic solution upon dialysis against water are characterized by an oval shape and dimensions of 100-400 nm (Figure 3.20).

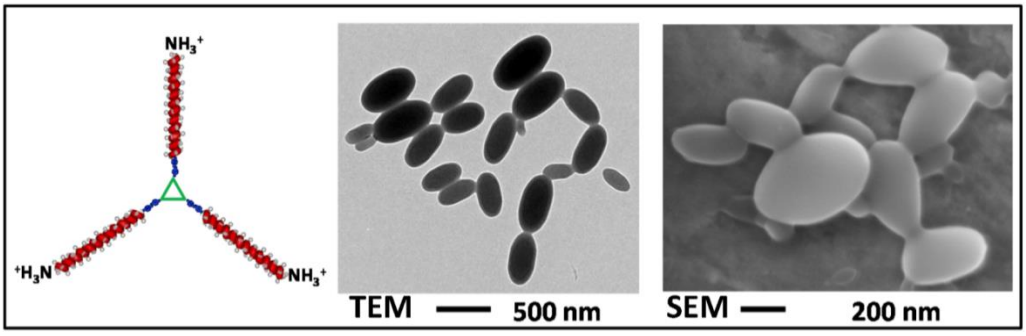

Figure 3.20 TEM (left) and SEM (right) images of the self-assembled structures obtained from the C_3-symmetry PBLG hybrid (**24**) in aqueous suspension.

After UV irradiation for increasing times up to 30 min, we observed the reorganization of the microstructures in smaller aggregates as detected by TEM analyses (Figures 3.21 A-F). In particular, after 5 min of irradiation a partial disassembling of the oval aggregates was detected, whereas prolonged irradiation (up to 20-30 min) led to the formation of smaller organizations of spherical nature (20-40 nm) as showed by SEM experiments (Figure 3.21, lower part). Since each molecule of the hybrid contains three azobenzene units, in all probability the disassembly of the large, oval aggregates is related to a partial conversion to the *cis* form. Upon prolonged irradiation the *all-cis* hybrid is formed, which can reorganize into novel, smaller microstructures.

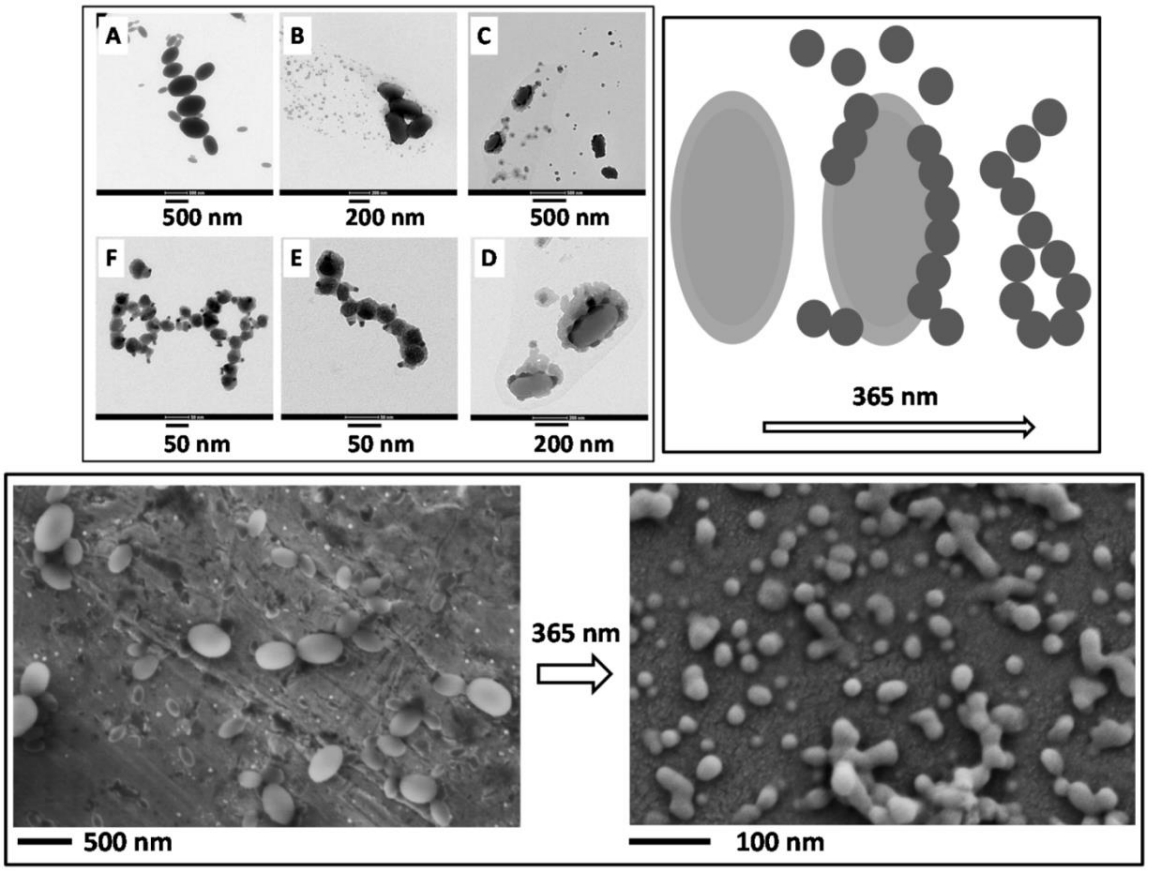

Figure 3.21 Upper part, left: TEM images of the microstructures obtained from the C_3-symmetry PBLG hybrid (**24**) in water after UV irradiation (λ= 365 nm) for different times (**A**, no irradiation; **B**, 5 min; **C** and **D**, 10 min; **E**, 20 min; **F**, 30 min). Central part right: Schematic representation of the light-induced microstructure reorganization. Lower part: SEM images showing the microstructures before (left) and after (right) 30 min UV irradiation.

Finally, we investigated the photoresponsive behavior of a C_3-symmetry PBLG hybrid characterized by a higher M_W (154,000 Da). In this case, the self-assembly process obtained upon dialysis against water led again to the formation of oval microstructures. At variance with the lower M_W polypeptide, however, no variation of morphology could be detected even after prolonged UV irradiation. Therefore, inspired by a recent publication on electrospun α-helical PBLG fibers[26] and considering the characteristics of our C_3-symmetry PBLG hybrid (it has a M_W comparable to that reported in ref. 26), we decided to process our high M_W C_3-symmetry PBLG hybrid via the electrospinning technique. The characterization of the resulting material is illustrated in Figure 3.22. The densely packed fibrillar network detected by SEM (Figure 3.22 A) corresponds, to the macroscopic level, to a solid layer (Figure 3.22 B). We tested the photoresponsive behavior of this solid layer under UV irradiation. The fibers, originally remarkably homogenous in shape, tend to progressively "swell" into larger

domains after 30-60 min of irradiation (Figures 3.22 C-D). A total collapse of the fiber morphology was achieved after 200 min UV irradiation (Figure 3.22 E).

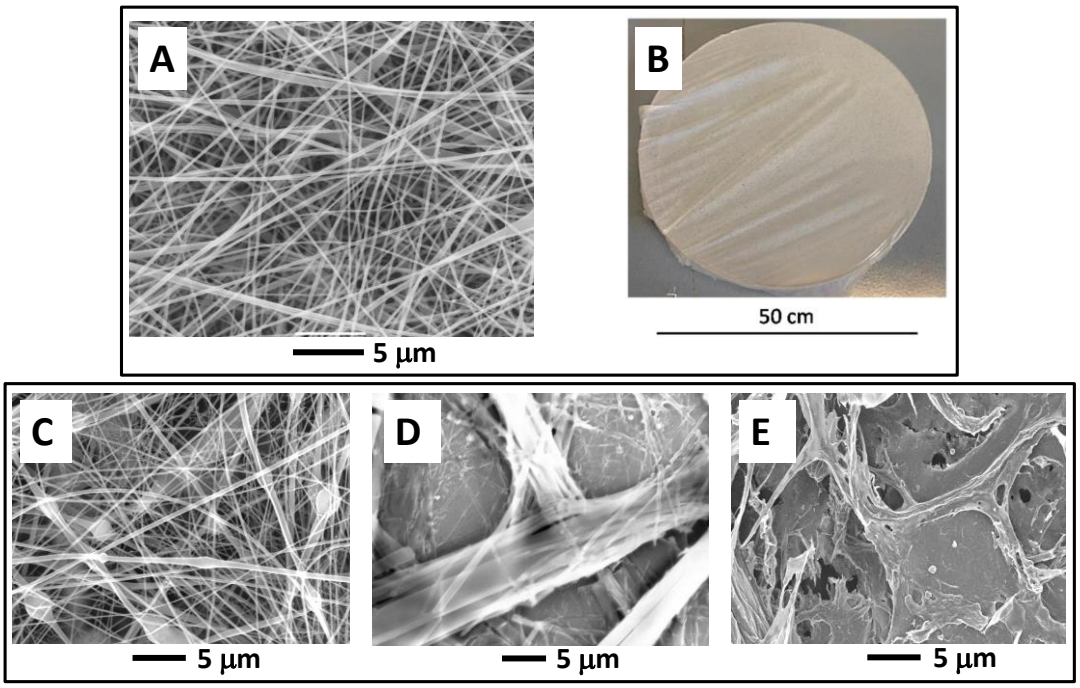

Figure 3.22 (**A**) SEM image of the fibers obtained from the high MW C_3-symmetry PBLG hybrid after processing by the electrospinning technique. (**B**) Imagine showing the macroscopic material collected by electrospinning. (**C-E**) SEM images of the microstructure transition occurring at different irradiation time at λ= 365 nm (30, 60, and 200 min, respectively).

Interestingly, application of the electrospinning technique to the C_2-symmetry PBLG hybrid also led to the formation of a fibrillar network. In this case, however, the fiber morphology did not change even after prolonged UV irradiation (up to 3 h). In all probability, the packing of polypeptide chains within the fibers of this linearly organized material is tighter than in the case of the C_3-symmetry PBLG hybrid.

Conclusions

We took advantage from two azobenzene-based amino acids as polymerization initiators for the construction of "smart" supramolecular systems endowed with photoswitchable behavior. The two starting materials are an N^{α}-protected derivative of the (4-aminomethyl)phenylazobenzoic acid (**19**)[22] and the azo-bridged di-α-amino-diester 4,4'-diazenediyldi-L-Phe (**16**).[21] In particular, the NCA polymerization methodology was utilized to prepare two PBLG hybrid molecules characterized by either C_2- or C_3-symmetry. In the

first case, the *bis*-initiator was the di-α-amino-diester (**16**) itself, while in the second case the *tris*-initiator was the three-branched compound **22** with a triazinic central core.

These azobenzene-containing compounds and materials were reversibly *trans*-to-*cis* photoisomerized, and the micro- and macroscopic changes in their 3D-structures, self-aggregation properties and overall characteristics were carefully analyzed by chromatography and UV-Vis/CD spectroscopies as well as by TEM/SEM nanomaterial techniques. In particular, the results reported here clearly indicate that the morphology of the self-aggregated systems can be finely tuned by a geometric (*trans vs. cis*) modification of one (azobenzene) of the building blocks.

3.4 Experimental Section

Instruments and Methods

Nuclear Magnetic Resonance. ^{1}H and ^{13}C NMR spectra were recorded at room temperature on a Bruker AC-200 (200 MHz) instrument using TMS (tetramethylsilane) as the internal reference. The multiplicity of a signal is indicated as s, singlet; d, doublet; t, triplet; m, multiplet, br, broad. Chemical shifts (δ) are expressed in ppm.

Fourier Transform-Infrared Spectroscopy. FT-IR absorption spectra in KBr disc were recorded with a Perkin-Elmer 1720X spectrophotometer. The $\bar{\upsilon}$ maxima for the main absorption bands are given.

High-Resolution Mass Spectroscopy. Mass spectra were obtained by electrospray ionization (ESI) on a Perseptive Biosystem Mariner ESI-ToF 5220 spectrometer. Data were collected in the positive mode.

UV-Vis Absorption. Absorption spectra were recorded using a Shimadzu model UV-2501 PC spectrophotometer. A 1-cm path length quartz cell was used.

Circular Dicroism. CD measurements were carried out at room temperature using a Jasco J-715 spectropolarimeter. Fused quartz cells of 1-mm or 0.2-mm path length (Hellma) were used.

Dynamic Light Scattering. DLS measurements were carried out at 25 °C on a Malvern Zetasizer Nano-S instrument using a He- Ne laser (633 nm) and a scattering angle of 176°.

Transmission Electron Microscopy. Samples were analyzed on a Jeol 300PX instrument. Samples were prepared immediately before use, by dilution of the dialyzed solutions with MilliQ water. A small drop of solution was floated on a glow discharged carbon coated grid and excess was removed by #50 hardened Whatman filter paper. For the samples with negative staining, the grid was then floated on 2% uranyl acetate solution for 10 seconds, and the excess was removed by #50 hardened Whatman filter paper.

Scanning Electron Microscopy. A Carl Zeiss Merlin field emission SEM operating at 5 kV accelerating voltage was used. A small drop of the suspension was placed on a microscope glass cover slip and allowed to dry overnight.

Atomic Force Microscopy. AFM experiments were performed on Agilent Technologies 5500 scanning probe microscope, operating in acoustic AC AFM mode (tapping mode) with a silicon Asylum Reasearch high frequency cantilever displaying a resonance frequency of 305

kHz. A small drop of sample was placed on a mica or silicon surface and allowed to dry in air for at least 60 min before measurement.

Size Exclusion Chromatography. SEC analyses were performed on a Agilent 1260 Infinity system equipped with 1260 isopump, 1260 TCC, 1260 VWD VL, 1260 RID, Phenogel 5u linear/mixed guard column (30 × 4.6 mm), followed by Phenomenex Phenogel 5u 10^4 Å (300 × 4.6 mm) column working at 60 °C. DMF was used as eluant at a flow rate of 1 mL/min. Before SEC analysis, the samples were filtered through a 0.2 μm PTFE filter (15 mm, Phenomenex). The M_Ws were calculated according to calibration using polystyrene standards.

MALDI-TOF. Mass spectra were recorded with an AB SCIEX 4800 MALDI TOF/TOF Analyzer (AB SIEX Pte Ltd, Massachusetts, USA), using reflector mirror and positive ion detection. A dual microchannel plate reflector detector was used. LDI was performed with the 355 nm (3-7 ns) pulses of a Nd:YAG laser at a repetition rate of 200 Hz. We used 70% of maximum laser power for all measurements. Each spectrum was averaged over 400 laser shots and analyzed with the AB SCIEX 4000 Series Explorer Software (AB SCIEX Pte Ltd, Massachusetts, USA). Matrix: 2,5-dihydroxybenzoic acid 1 M in 1:1 methanol/water solution.

X-ray photoemission spectroscopy. XPS measurements were carried out on dialysed and lyophilised CQDs powder. Core level photoemission spectra were taken on a VG ESCALAB MKII spectrometer using Mg anode of a conventional non-monochromatized X-ray source (Kα=1253.6 eV). The electron analyser pass energy was set to 50 eV for the survey wide scans and to 20 eV for the single spectral region. The measurements were taken at r.t. with a detection direction perpendicular to the sample surface. The calibration of the binding energy (BE) scale was carried out using Au 4f as reference. In order to characterize the chemical states of carbon and nitrogen, the C 1s and N 1s peaks were de-convoluted into individual components (after Shirley background removal) using a Doniach-Šunjić shape for the C sp^2 component and symmetrical Voigt functions for the fitting of the molecular-like components. The χ^2 minimization was ensured by the use of the nonlinear least squares routines.

Microstructures Preparation. Typically, 20 mg of polymer were dissolved in 10 mL of a DMF/THF 3:7 (*v*/*v*) solvent mixture. This solution was put into a cellulose dialysis tubing with a M_W cutoff of 12 KD (flat width 35 mm, Sigma). The dialysis process was carried out against deionized water for 48 h.

High-Performance Liquid Chromatography. The HPLC measurements were performed on an Agilent 1200 apparatus equipped with a UV detector at 226 nm. Conditions: Phenomenex C_{18} (100Å) (stationary phase), 5-80% B, 25 min, 1 mL/min (eluants: A=9:1 H_2O/CH_3CN, 0.05% TFA; B= 1:9 H_2O/CH_3CN, 0.05% TFA).

Electrospinning of PBLG Fibres. Three solutions at different concentrations (4, 8, and 12 wt%) were prepared by dissolving PBLG in dicloroacetic acid at 50°C. A 2 mL SGE syringe with stainless steel needle was used as an electrode. Syringes with 8 mL of each concentration were loaded in a syringe pump (Genei™ Plus Syringe pump, Kent Scientific), to control the flow rate of the polypeptide solutions. Electrospinning was performed at ambient conditions with a constant applied voltage of +8 kV at needle and −5 kV at collector with the flow rate set at 0.01 mL/min to maintain a constant size of droplet at the tip of the syringe needle. A circular aluminium plate was used as a collector. The tip to collector distance was kept at 15 cm. Electrospinning was performed for about 2 h to obtain a non-woven, continuous fibre mat. All fibres were dried prior to use for the photostimuli experiments.

Materials

γ-Benzyl-L-glutamate (BLG), succinic anhydride, arginine, *p*-nitrobenzylamine and 4-dimethylaminopyridine (DMAP) were obtained from Fluka. 1-Ethyl-3-(3-dimethylaminopropyl)carbodiimide hydrochloride (EDC·HCl) and 1-hydroxy-7-aza-1,2,3-benzotriazole (HOAt) was purchased from GL Biochem (Shanghai). Triphosgene, triisopropylsilane (TIS), cysteamine hydrochloride, triphenylmethanol, 1,2-ethylendiamine, diphenylphosphoryl azide (DPPA), di-*tert*-butyl dicarbonate (Boc_2O), triethylamine (TEA), *p*-aminobenzoic acid, 2,2'-dimethoxy-2-phenylacetophenone (DMPA), 2-mercaptoethanol, *p*-nitro-L-phenylalanine methyl ester hydrochloride [H-L-Phe(*p*NO_2)-OMe·HCl], 2,4,6-triallyloxy-1,3,5-triazine, trifluoroacetic acid (TFA), and α-pinene were obtained from Sigma-Aldrich. The deuterated solvents $CDCl_3$ and DMSO-d_6 were purchased from Euriso-Top. Catalyst 10% Pd/C was obtained from Acros-Janssen. All other chemicals and solvents are Sigma-Aldrich, Fluka or Acros products and were used as provided without further purification. Dialysis tubes with molecular weight cutoff 1 KD were obtained from Spectrum Labs and 12 KD cutoff from Sigma-Aldrich.

Synthesis and Characterization

γ-Benzyl-L-glutamate *N*-carboxyanhydride (BLG-NCA, **1**).[27] BLG (5.05 g, 21.3 mmol) and α-pinene (6.64 g, 48.7 mmol) were dissolved in EtOAc (70 mL) in a three-neck flask and heated under reflux. Triphosgene (4.24 g, 14.2 mmol) was dissolved in EtOAc (25 mL) and added slowly with a dropping funnel once the reflux started. After 4h of reaction, heating was interrupted and most of the solvent was evaporated under reduced pressure. The compound was precipitated by addition of petroleum ether and the recovered solid was recrystallized twice, subsequently filtered and washed with petroleum ether. BLG-NCA was recovered as a white solid (4.6 g, 84%).

^{1}H-NMR (200 MHz, $CDCl_3$): δ 7.35 (s, 5H, ArH), 6.61 (s, 1H, NH), 5.14 (s, 2H, Ar-CH_2-), 4.37 (t, *J*= 6 Hz, 1H, αCH), 2.59 (t, *J*= 6.8 Hz, 2H, γCH_2), 2.36-2.02 (m, 2H, βCH_2). Data consistent with that previously reported in the literature.[27]

a) Synthesis of PBLG-C_{60} conjugates

2-(tritylsulfanyl)ethanamine (**2**).[28] A solution of cysteamine hydrochloride (1.04 g, 9.17 mmol) and triphenylmethanol (2.18 g, 8.37 mmol) in TFA (5 mL) was stirred at room temperature for 1 h. After co-evaporation with acetonitrile the residue was dissolved in ethyl acetate and washed with $NaOH_{(aq)}$ 1 M, water and brine. The organic layer was dried over Na_2SO_4, filtered and the solvent was evaporated under reduced pressure. The compound was recovered as white solid (2.4 g, yield 89 %).

^{1}H NMR (200 MHz, $CDCl_3$) δ 7.48-7.43 (m, 7H, ArH), 7.35-7.23 (m, 8H, ArH), 2.61 (t, 2H, CH_2), 2.35 (t, 2H, CH_2), 1.42 (s, 2H, NH_2). Data consistent with that previously reported in the literature.[28]

3-(tritylsulfanyl)propanoic acid (**5**). To a suspension of triphenylmethanol (2.6 g, 10 mmol) in 10 mL of TFA was added 3-mercaptopropionic acid (1.4 g, 13 mmol). The mixture was stirred for 1 h at room temperature. After that the TFA was removed under vacuum and the residue was dissolved in ethyl acetate and washed with $NaHCO_{3(aq)}$ 5%, $KHSO_{4(aq)}$ 10%,water and brine. The organic layer was dried over Na_2SO_4, filtered and the solvent was evaporated under reduced pressure. The compound was recovered as white solid (3.05 g, yield 88 %).

^{1}H NMR (200 MHz, $CDCl_3$) δ 7.47-7.40 (m, 6H, ArH), 7.35-7.22 (m, 9H, ArH), 2.49 (t, 2H, CH_2), 2.25 (t, 2H, CH_2). Data consistent with that previously reported in the literature.[29]

PBLG derivatives

NH_2-PBLG-S-Trt (**3**). BLG-NCA (**1**) (1 g, 3.8 mmol) was dissolved in 3 mL of dry dioxane under N_2 atmosphere and the flask was cooled with a MeOH/ice bath. Then (tritylsulfanyl)ethanamine (**2**) (12 mg, 0.038 mmol) dissolved in 500 µL of dry dioxane was added to the solution and the cool bath was removed. The reaction was stirred at 25 °C for one day, until the mixture became very viscous. The product was precipitated by adding MeOH to the solution, the polymer was filtered and dried in vacuo. The polymer was recovered as a white fibrous solid (810 mg, recovered yield 81 %).
SEC M_W: 19100 (PDI 1.11). ^{1}H NMR (200 MHz, $CDCl_3$) δ 7.27 (s, 5H), 5.05 (s, 2H), 3.94 (s, 1H), 2.57 (s, 2H), 2.26 (s, 2H). ^{13}C NMR (50 MHz, $CDCl_3$) δ 175.54, 172.20, 136.11, 128.60, 128.26, 66.29, 30.95, 25.67.

NH_2-PBLG-C_{60} (**4**). The removal of Trt protective group was performed by treatment of polymer **1** (200 mg, 10.5 µmol) with 4 mL of a solution 50% TFA in CH_2Cl_2 with TIS for 20 min. The solvent was evaporated under reduced pressure and the residue was suspended in Et_2O, filtered and washed with Et_2O. The resulting polymer was dissolved in 10 mL of a solution of DMF/toluene 2:8 v/v. Then fullerene (37 mg, 0.052 mmol) and AIBN (24 mg, 0.16 mmol) were added. The reaction mixture was heated at 90 °C for 5 h, after that the solvent was removed under reduced pressure. The residue was suspended in DMF and filtered through a 20 µm filter to eliminate the non-reacted fullerene. The polymer was precipitated from the filtrate solution by adding MeOH. The solid was filtered and washed several times with MeOH and acetone to remove the fullerene by-products. The polymer **3** was recovered as brown solid (171 mg, yield 85 %).
SEC M_W: 19550 (PDI 1.09). ^{1}H NMR (200 MHz, $CDCl_3$) δ 7.27 (s, 5H), 5.05 (s, 2H), 3.95 (s, 1H), 2.55 (s, 2H), 2.27 (s, 2H). ^{13}C NMR (50 MHz, $CDCl_3$) δ 175.53, 172.24, 136.08, 128.59, 128.24, 66.29, 30.94, 25.72.

Trt-S-PBLG-C_{60} (**6**). Trt-*mercapto*propionic acid (**5**) (60 mg, 0.17 mmol) and HOAt (24 mg, 0.17 mmol) were dissolved in 3 mL of anhydrous DMF, cooled at 0 °C and then EDC·HCl (33 mg, 0.17 mmol) was added. The mixture was stirred for 15 min at 0 °C. Polymer **3** (90 mg, 4.6 µmol) was dissolved in 2 mL of DMF and added with TEA (50 µL, 0.36 mmol) to the solution of active ester. After stirring the solution at r.t. for 48 h, the

polymer was precipitated by adding MeOH, then filtered and washed several times with MeOH. The polymer was dry to obtain a brown solid (92 mg, yield 98%).

C_{60}-PBLG-C_{60} (**7**). Polymer **4** (75 mg, 3.8 μmol) was treated with 4 mL of a solution 50% TFA in CH_2Cl_2 with TIS for 20 min. The solvent was evaporated under reduced pressure and the residue was suspended in Et_2O, filtered and washed with Et_2O. The obtained compound was dissolved in 5 mL of a solution of DMF/toluene 2:8 v/v. Successively fullerene (15 mg, 0.021 mmol) and AIBN (10 mg, 0.061 mmol) were added. The mixture was heated at 90 °C for 5 h, after that the solvent was removed under reduced pressure. The residue was suspended in DMF and filtered through a 20 μm filter. To the filtrated solution MeOH was added to precipitate the polymer. The compound was filtered and washed several times with MeOH and acetone. The compound was obtained as a brown solid (60 mg, yield 78 %). SEC M_W: 20300 (PDI 1.11).

^{1}H NMR (200 MHz, $CDCl_3$) δ 7.28 (s, 5H), 5.05 (s, 2H), 3.95 (s, 1H), 2.56 (s, 2H), 2.28 (s, 2H). ^{13}C NMR (50 MHz, $CDCl_3$) δ 175.52, 172.21, 136.14, 128.61, 128.27, 66.32, 31.07, 25.61.

b) Synthesis of PBLG-CQDs conjugates

CQDs. Arginine·HCl (5.6 g, 26.6 mmol) and 1,2-ethylendiamine (1.78 mL, 26.6 mmol) were dissolved in 13.3 mL of ultrapure water. The solution was placed in a domestic microwave oven and heated at 700 W for 180 s. The brown-burned resulting solid was suspended in 50 mL of ultrapure water and centrifuged several times. The water solution was placed in a dialysis sack (1 KD cutoff) and dialyzed against ultrapure water for 24 h. Finally the aqueous solution was lyophilized giving 1.2 g of solid CQDs.
FT-IR absorption: ῡ 3399, 2934, 1623, 1451, 1382 cm^{-1}.

PBLG derivatives

Polymer 8. BLG-NCA (450 mg, 1.7 mmol) was dissolved in 1 mL of dry DMSO under N_2 atmosphere. Then CQDs (20 mg) dissolved in 2 mL of DMSO were added to the NCA solution. The reaction was left to stir at r.t. for 96 h. The polymer was precipitated by adding MeOH to the solution. The polymer was filtered, washed several times with MeOH and Et_2O, and dried *in vacuo*. The polymer was recovered as a brown solid (350 mg, yield 78%).
FT-IR absorption: ῡ 3298, 3063, 3034, 2952, 1735, 1651, 1545, 1161 cm^{-1}. ^1H NMR (200 MHz, $CDCl_3$): δ ppm 7.24 (s, 5H, ArH), 6.61 (s, 1H, NH), 5.00 (s, 2H, Ar-CH_2), 3.56 (s, 1H, αCH), 3.56 (t, 2H, γCH_2), 2.19 (br s, 2H, β CH_2).

COOH-PBLG-CQD (intermediate, **9**). Polymer **8** (160 mg) was dissolved in 2 mL of dry DMF. Succinic anhydride (100 mg, 1 mmol) was dissolved in 1 mL of dry DMF and added to the solution of the polymer together with TEA (50 μL, 0.36 mmol). After 24 h under stirring at 40 °C, aqueous acetic acid (1 mL) was added to the reaction mixture. Then the polymer was precipitated by adding MeOH and washed several times with MeOH and Et_2O. The polymer was recovered as a brown solid (140 mg).
FT-IR absorption: ῡ 3294, 3064, 3034, 2952, 1735, 1650, 1545, 1452, 1158 cm^{-1}.

Polymer 10. Polymer **9** (100 mg) was dissolved in dry DMF and activated with DPPA (200 μL, 0.93 mmol) and TEA (250 μL, 1.8 mmol). CQDs (50 mg) were added to this mixture and maintained at 40 °C under stirring for 24 h. The polymer was precipitated from the mixture by adding acidic water and MeOH, washed several times and obtained as a brown solid (80 mg).
FT-IR absorption: ῡ 3295, 3063, 3033, 2951, 1735, 1651, 1545, 1452, 1160 cm^{-1}.

Functionalization with silver nanoparticles[19]

Compound 11. CQDs and $AgNO_3$ blend solution (1:4, w/w) in EtOH was prepared at a concentration of 2 mg/mL and placed in a UV quartz cuvette (1×1×5 cm). This solution was exposed to UV light with wavelength of 254 nm for 30 min using a 6W UV (mineralight lamp, Model UVGL-54). The cell was kept 3 cm apart from the light source. After UV irradiation for few minutes, the color of solution start to change from light yellow to dark brown, implying the reduction of Ag ions and the formation of Ag nanoparticles.

Silver nanoparticles (**AgNPs**). $AgNO_3$ was dissolved in N-methyl-2-pyrrolidone at a concentration of 4 mg/mL. This solution was treated with same procedure as **11**, but UV irradiation was carried out for 1 h. Free AgNPs prepared in this manner had an average diameter of 3 nm, equal to the diameters of AgNPs synthesized using CQDs.

c) Synthesis of PBLG-Azobenze conjugates

H-bisazo-L-Phe-OMe (16), C_2-symmetry initiator[21]

Boc-L-Phe(*p*NO_2)-OMe (**12**). H-L-Phe(*p*NO_2)-OMe·HCl (4.9 g, 18.8 mmol) was dissolved in an 1:1 CH_3CN/H_2O solvent mixture (20 mL) and TEA was added to pH = 9. Then, Boc_2O (5.50 g, 25.2 mmol), dissolved in CH_3CN (10 mL), was added. The mixture was stirred at r.t. for 18 h. The mixture was concentrated under reduced pressure and the residue was diluted with EtOAc. The organic layer was washed with 5% $KHSO_{4(aq)}$, 5% $NaHCO_{3(aq)}$, and brine. After drying over Na_2SO_4, the solvent was removed under reduced pressure and the compound was obtained as solid (5.9 g, 97%).
FT-IR absorption: ῡ 3358, 2985, 1732, 1689, 1524, 1346 cm^{-1}. HRMS (ESI+): *m/z* calcd. for $C_{15}H_{20}N_2O_6$ 324.1321, found 325.3298 $[M+H]^+$. ^1H NMR (200 MHz, $CDCl_3$): δ 1.40 (s, 9H), 3.11 (dd, *J*=13.7, 6.2 Hz, 1H), 3.27 (dd, *J*=13.7, 6.2 Hz, 1H), 3.73 (s, 3H), 4.58-4.68 (m, 1H), 5.06 (d, *J*=7.7 Hz, 1H), 7.31 (d, *J*=8.7 Hz, 2H), 8.6 (d, *J*=8.7 Hz, 2H).

Boc-L-Phe(*p*NH_2)-OMe (**13**). Boc-L-Phe(*p*NO_2)-OMe (2.40 g, 7.4 mmol) was dissolved in MeOH (50 mL) and N_2 was bubbled in the solution for 10 min. Then, Pd/C (300 mg) was added and the mixture was stirred at r.t. under an atmospheric pressure of H_2 gas for 1 h. The catalyst was removed by filtration through celite. The solvent was evaporated and the residue was purified *via* flash chromatography (eluant: EtOAc/hexane 1:1). The product was recovered as a solid (2.1 g, 96%).
FT-IR absorption: ῡ 3397, 3374, 3232, 1741, 1690, 1515 cm^{-1}. HRMS (ESI+): *m/z* calcd. for $C_{15}H_{22}N_2O_4$ 294.1579, found 295.1732 $[M+H]^+$. ^1H NMR (200 MHz, $CDCl_3$): δ 1.40 (s, 9H), 2.96 (d, *J*=5.7 Hz, 2H), 3.44 (s br, 2H), 3.70 (s, 3H), 4.45-4.55 (m, 1H), 4.95 (d, *J*=7.9 Hz, 1H); 6.61 (d, *J*=8.4 Hz, 2H), 6.89 (d, *J*=8.4 Hz, 2H).

Boc-L-Phe(*p*NO)-OMe (**14**). Boc-L-Phe(*p*NO_2)-OMe (1.07 g, 3.3 mmol) and NH_4Cl (790 mg, 14.8 mmol) were dissolved in a 5:1 $EtOH/H_2O$ (42 mL) solvent mixture. Then, Zn dust (600 mg, 9.2 mmol) was added. The resulting suspension was stirred at r.t. for 2 h, then filtered through celite, and washed with a cold mixture of 5:1 $EtOH/H_2O$ (40 mL) to remove the excess of Zn. The filtrate was cooled to 0 ºC and a cold solution of $FeCl_3·6H_2O$ (6.33 g, 23.4 mmol) in 5:1 $EtOH/H_2O$ (35 mL) was added. The mixture was stirred at 0 ºC for 30 min, diluted with brine and extracted with EtOAc. The combined organic phases were washed with brine, dried over anhydrous Na_2SO_4, and filtered. The solvent was removed under reduced pressure and the residue was purified rapidly *via* flash chromatography (eluant: CH_2Cl_2/EtOH

30:1). Compound **14** was obtained as a green oil (910 mg, 89%), which was immediately used for the next synthetic step.

Boc-*bis*-azo-L-Phe-OMe (**15**). A solution of freshly prepared compound **13** (1.0 g, 3.4 mmol) in glacial AcOH (15 mL) was added to a solution of compound **14** (1.15 g; 3.7 mmol) in glacial AcOH (15 mL). The mixture was stirred at r.t. for 24 h. The solvent was evaporated and the crude product was purified *via* flash chromatography (eluant: 50:1 CH_2Cl_2/EtOH). After precipitation from EtOAc/hexane, compound **15** was recovered as an orange solid (830 mg, 43%).

FT-IR absorption: ῡ 3356, 1752 1735, 1688, 1520 cm^{-1}. HRMS (ESI+): *m/z* calcd. for 584.2846, found 585.2832 $[M+H]^+$. ^1H NMR (200 MHz, $CDCl_3$): δ 1.42 (s, 18H), 3.14-3.20 (m, 4H), 3.73 (s, 6H), 4.58-4.68 (m, 2H), 5.03 (d, *J*=7.27 Hz, 2H), 7.27 (d, *J*=8.3 Hz, 4H), 7.84 (d, *J*=8.3 Hz, 4H).

H-*bis*-azo-L-Phe-OMe (**16**). The removal of the Boc protecting group was obtained by treating Boc-*bis*-azo-L-Phe-OMe (175 mg, 0.29 mmol) with an 1:1 TFA/CH_2Cl_2 mixture (10 mL) at r.t. under stirring for 40 min. Then, the solvent was evaporated and the residue suspended in water and lyophilized. Product **16** was obtained as an orange solid (170 mg, 98%).

FT-IR absorption: ῡ 3425, 3007, 1748, 1674 cm^{-1}. HRMS (ESI+): *m/z* calcd. for 384.1797, found 385.2035 $[M+H]^+$. ^1H NMR (200 MHz, DMSO-d_6): δ 3.21 (d, *J*=5.3 Hz, 4H), 3.70 (s, 6H), 4.42 (t, 2H), 7.46 (d, *J*=8.4 Hz, 4H), 7.86 (d, *J*=8.4 Hz, 4H), 8.59 (s br, 4H). ^{13}C NMR (50 MHz, DMSO-d_6) δ 169.41, 151.22, 138.51, 130.66, 122.84, 53.05, 52.81, 35.82.

Compound (22), C_3-symmetry initiator

Boc-*p*-nitrobenzylamine (**17**). Solid Boc_2O (4.5 g, 20.8 mmol) was added to a solution of *p*-nitrobenzylamine (2 g, 10.6 mmol) and TEA (2 mL, 14.4 mmol) in CH_2Cl_2 (45 mL) cooled to 0 °C. The mixture was stirred at r.t. for 18 h. Then, the mixture was diluted with CH_2Cl_2 and washed with 5% $KHSO_{4(aq)}$ and brine. The organic phase was dried over $MgSO_4$, filtered, and concentrated under reduced pressure. After precipitation from CH_2Cl_2/petroleum ether, compound **17** was recovered as a solid (1.8 g, 67%).

FT-IR absorption: ῡ 3325, 2984, 2935, 2914, 1688, 1520, 1165 cm^{-1}. HRMS (ESI+): *m/z* calcd. for $C_{12}H_{16}N_2O_4$ 252.1110, found 197.0652 $[M-t\text{Bu}+H]^+$. ^1H NMR (200 MHz, $CDCl_3$): δ 1.46 (s, 9H), 4.40 (d, *J*=6.2 Hz, 2H), 4.98 (s br, 1H), 7.44 (d, *J*=8.7 Hz, 2H), 8.19 (d, *J*=8.7 Hz, 2H).

Boc-4-(aminomethyl)phenylazobenzoic acid (**19**).[22] Boc-*p*-nitrobenzylamine (1 g, 4 mmol) and NH_4Cl (690 mg, 13 mmol) were dissolved in 5:1 EtOH/H_2O (25 mL). Then, Zn dust (940 mg, 14.4 mmol) was added and the obtained suspension was stirred at r.t. for 2 h. The suspension was filtered through celite, the filtrate was cooled to 0 ºC and a cold solution of $FeCl_3 \cdot 6H_2O$ (6.33 g, 23.4 mmol) in 5:1 EtOH/H_2O (35 mL) was added. The mixture was stirred at 0 ºC for 30 min, diluted with brine, and extracted with EtOAc. The combined organic phases were washed with brine, dried over anhydrous Na_2SO_4, and filtered. The solvent was evaporated and the crude was rapidly purified *via* flash chromatography (eluant: 100:1 CH_2Cl_2/MeOH), affording compound (**18**) as a green solid (880 mg), which was immediately used for the next synthetic step. This compound was dissolved in glacial AcOH (10 mL) and a solution of *p*-aminobenzoic acid (0.746 g, 5.4 mmol) in glacial AcOH (5 mL) was added. After 48 h under stirring at r.t., the mixture was concentrated and diluted with EtOAc. The organic solution was washed with 5% $NaHCO_{3(aq)}$, 5% $KHSO_{4(aq)}$, and brine. After drying over $MgSO_4$, the filtrate was concentrated and the crude purified *via* flash chromatography (eluant: CH_2Cl_2/EtOAc, increasing the solvent mixture polarity from 9:1 to 1:1). The compound was obtained as an orange solid after precipitation from EtOAc/petroleum ether (370 mg, 28%).
FT-IR absorption: $\bar{\upsilon}$ 3343, 2980, 1682, 1507, 1426, 1168 cm^{-1}. HRMS (ESI+): *m/z* calcd. for $C_{19}H_{21}N_3O_4$ 355.1532, found 356.1691 $[M+H]^+$. ^1H NMR (200 MHz, DMSO-d_6): δ 1.41 (s, 9H), 4.24 (d, *J*=6 Hz, 2H), 7.47 (d, *J*=8.4 Hz, 2H), 7.88-7.97 (m, 4H), 8.14 (d, *J*=8.4 Hz, 2H), 13.18 (s, 1H).

Compound (**20**). 2,4,6-Triallyloxy-1,3,5-triazine (5.03 g, 20.2mmol), 2-mercaptoethanol (8.66 g, 110.8 mmol) and DMPA (2,2-dimethoxy-2-phenyl-acetophenone) (376 mg, 1.5 mmol) were mixed in a becker and stirred under irradiation at 365 nm with a UV lamp for 40 min. The mixture was diluted with MeOH (10 mL) and Et_2O was added until the precipitation of an oily compound took place. The supernatant was removed and the oily compound was washed twice with Et_2O. Compound **20** was recovered as a colorless oil (8.2 g, 84%).
FT-IR absorption: $\bar{\upsilon}$ 3389, 2920, 1567, 1417, 1332, 1140 cm^{-1}. HRMS (ESI+): *m/z* calcd. for $C_{18}H_{33}N_3O_6S_3$ 483.1531, found 484.1626 $[M+H]^+$. ^1H NMR (200 MHz, $CDCl_3$): δ 2.00-2.13 (m, 6H), 2.30 (s br, 3H), 2.65-2.75 (m, 12H), 3.72 (t, *J*=6.2 Hz, 6H), 4.49 (t, *J*=6.2 Hz, 6H).

Compound (**21**). To a solution of compound **19** (320 mg, 0.91 mmol), compound **20** (120 mg, 0.25 mmol) and DMAP (36 mg, 0.29 mmol) in 10 mL of anhydrous DMF cooled to 0 °C, EDC·HCl (190 mg, 0.97 mmol) was added and the reaction mixture was stirred at r.t. for 48

h. The solvent was removed under reduced pressure, the residue dissolved in CH_2Cl_2 and washed with 5% $KHSO_{4(aq)}$ and brine. After drying over $MgSO_4$, the filtrate was concentrated and the crude was purified *via* flash chromatography (eluant: CH_2Cl_2/MeOH, increasing the solvent mixture polarity from 60:1 to 40:1). Compound **21** was recovered as an orange solid (270 mg, 70%).

FT-IR absorption: ῡ 3335, 2975, 1716, 1684, 1513, 1167 cm^{-1}. HRMS (ESI+): *m/z* calcd. for $C_{75}H_{90}N_{12}O_{15}S_3$ 1494.5810, found 1495.6822 $[M+H]^+$. ^1H NMR (200 MHz, $CDCl_3$): δ 1.48 (s, 27H), 2.01-2.20 (m, 6H), 2.78 (t, *J*=7.1 Hz, 6H), 2.90 (t, *J*=7.1 Hz, 6H), 4.39 (s, 6H), 4.46-4.53 (m, 12H), 4.95 (s br, 3H), 7.43 (d, *J*=8.4 Hz, 6H), 7.89-7.85 (m, 12H), 8.17 (d, *J*=8.6 Hz, 6H).

Compound (**22**). The removal of the Boc protecting group was obtained by treating compound **21** (61 mg, 0.041 mmol) with an 1:1 TFA/CH_2Cl_2 mixture (4 mL) at r.t. under stirring for 2 h. The solvent mixture was evaporated, the residue suspended in water and lyophilized. Product **22** was obtained as an orange solid (47 mg, 96%).

FT-IR absorption: ῡ 3423, 2955, 1715, 1561, 1271 cm^{-1}. HRMS (ESI+): *m/z* calcd. for $C_{60}H_{66}N_{12}O_9S_3$ 1194.4237, found 1195.5364 $[M+H]^+$. ^1H NMR (200 MHz, DMSO-d_6): δ 1.95-2.01 (m, 6H), 2.67-2.74 (m, 6H), 2.89-2.85 (m, 6H), 4.17 (s, 6H), 4.34-4.48 (m, 12H), 7.70 (m, 6H), 7.98 (m, 12H), 8.13-8.17 (m, 6H), 8.41 (s, 12H). ^{13}C NMR (50 MHz, DMSO-d_6): δ 172.52, 164.92, 154.38, 151.69, 149.90, 138.19, 131.66, 130.58, 130.01, 122.98, 122.75, 66.34, 64.17, 59.30, 41.88, 32.56, 29.67, 28.17, 27.64.

PBLG derivatives

C_2-Symmetry PBLG Hybrid (**23**). BLG-NCA (1.10 g, 4.2 mmol) was dissolved in dry 1,4-dioxane (2 mL) under an N_2 atmosphere and the solution was cooled to 0 °C. Then, a solution of compound (**5**) (5 mg, 0.013 mmol) in 2:1 1,4-dioxane/DMF (600 µL) solvent mixture was added and the mixture was stirred at 25 °C for 48 h. The mixture was diluted with 1,4-dioxane and the polypeptide hybrid was precipitated by adding MeOH. The obtained solid was filtered, washed with MeOH and Et_2O, and dried *in vacuo*. The polypeptide hybrid was recovered as a light yellow solid (680 mg, 62%).

SEC M_W: 63500 (PDI 1.16). FT-IR absorption: ῡ 3295, 3003, 2951, 1734, 1653, 1546, 1163, cm^{-1}.

C_3-Symmetry PBLG Hybrid (**24**). BLG-NCA (1.00 g, 3.81 mmol) was dissolved in dry 1,4-dioxane (2.3 mL) under an N_2 atmosphere and the solution was cooled to 0 °C . Then, a

solution of compound **22** (12 mg, 0.010 mmol) in DMF (1 mL) was added and the mixture was stirred at 25 °C for 72 h. The mixture was diluted with 1,4-dioxane and the polypeptide hybrid was precipitated by adding MeOH. The obtained solid was filtered, washed with MeOH and Et_2O, and dried *in vacuo*. The polypeptide hybrid was recovered as a light yellow solid (750 mg, 76%).

SEC M_W: 46800 (PDI 1.56). FT-IR absorption: ῡ 3331, 3064, 2940, 1734, 1653, 1545, 1161 cm^{-1}.

This synthesis was repeated under similar conditions by using a higher monomer/initiator ratio (500:1) and a prolonged reaction time (5 d). The polypeptide hybrid was recovered as a light yellow solid (550 mg, 56%).

SEC MW: 154000 (pdi 1.66). FT-IR absorption: ῡ 3329, 3062, 2941, 1732, 1651, 1542, 1161 cm^{-1}.

References

[1] (a) A. R. Hirst, B. Escuder, J. F. Miravet, D. K. Smith, *Angew. Chem. Int. Ed.*, **2008**, *47*, 8002-8018; (b) G. M. Whitesides, M. Boncheva, *Proc. Natl. Acad. Sci. USA*, **2002**, *99*, 4769-4774.

[2] (a) G. M. Whitesides, B. Grzybowski, *Science*, **2002**, *295*, 2418-2421; (b) O. Ikkala, G. ten Brinke, *Science*, **2002**, *295*, 2407-2409; (c) J. A. A. W. Elemans, A. E. Rowan, R. J. M. Nolte, *J. Mater. Chem.*, **2003**, *13*, 2661-2670.

[3] (a) K. Numata, *Polymer Journal*, **2015**, *47*, 537-545; (b) J. Guo, Y. Huang, X. Jing, X. Chen, *Polymer* **2009**, *50*, 2847–2855; (c) F. Segura-Sánchez, V. Montembault, L. Fontaine, M. E. Martínez-Barbosa, K. Bouchemal, G. Ponchel, *Int. J. Pharm.* **2010**, *387*, 244–252.

[4] (a) H. Lu, J. Wang, Z. Song, L. Yin, Y. Zhang, H. Tang, C. Tu, Y. Lin, J. Cheng, *Chem. Commun.*, **2014**, *50*, 139-155; (b) N. Hadjichristidis, H. Iatrou, M. Pitsikalis, G. Sakellariou, *Chem. Rev.*, **2009**, *109*, 5528-5578. (c) H. R. Kricheldorf, *Angew. Chem. Int. Ed.*, **2006**, *45,* 5752-5784. (d) Y. Shen, X. Fu, W. Fu, Z. Li *Chem. Soc. Rev.*, **2015**, *44*, 612-622.

[5] (a) M. Zelzer, R. V. Ulijn, *Chem. Soc. Rev.*, **2010**, *39*, 3351-3357; (b) J. Huang, A. Heise, *Chem. Soc. Rev.*, **2013**, *42*, 7373-7390.

[6] H. Block, *Poly(γ-benzyl-L-glutamate) and Other Glutamic Acid Containing Polymers*; Gordon and Breach: New York, NY, **1983**.

[7] D. Mazzier, M. Mba, M. Zerbetto, A. Moretto, *Chem. Commun.*, **2014**, *50*, 4571-4574.

[8] D. Mazzier, M. Favaro, S. Agnoli, S. Silvestrini, G. Granozzi, M. Maggini, A. Moretto, *Chem. Commun.*, **2014**, *50*, 6592-6595.

[9] D. Mazzier, M. Maran, O. Polo Perucchin, M. Crisma, M. Zerbetto, V. Causin, C. Toniolo, A. Moretto, *Macromolecules*, **2014**, *47*, 7272-7283.

[10] B. Iskin, G. Yilmaz, Y. Yagci, *Chem. Eur. J.*, **2012**, *18*, 10254-10257.

[11] Y. Kim, W. Li, S. Shin, M. Lee, *Acc. Chem. Res.*, **2013**, *46*, 2888-2897.

[12] (a) S. N. Baker, G. A. Baker, *Angew. Chem. Int. Ed.*, **2010**, *49*, 6726-6744; (b) S. Y. Lim, W. Shen, Z. Gao, *Chem. Soc. Rev.*, **2015**, *44*, 362-381.

[13] (a) H. P. Liu, T. Ye, C. D. Mao, *Angew. Chem. Int. Ed.*, **2007**, *46*, 6473-6475; (b) K. Linehan, H. Doyle, *RSC Adv.*, **2014**, *4*, 18-21; (c) L. Tian, D. Ghosh, W. Chen, S. Pradhan, X. Chang, S. Chen, *Chem. Mater.*, **2009**, *21*, 2803-2809; (d) J. Hou, J. Yan, Q. Zhao, Y. Li, H. Ding, L. Ding, *Nanoscale*, **2013**, *5*, 9558-9561; (e) R. L. Liu, D. Q. Wu, S. H. Liu, K. Koynov, W. Knoll, Q. Li, *Angew. Chem.*, **2009**, *121*, 4668-4671; *Angew. Chem. Int. Ed.*, **2009**, *48*, 4598-4601; (f) W. Kwon, J. Lim, J. Lee, T. Park, S-W. Rhee, *Mater. Chem. C*, **2013**, *1*, 2002-2008; (g) J. Zhou, X. Shan, J. Ma, Y. Gu, Z. Qian, J. Chena, H. Feng, *RSC Adv*., **2014**, *4*, 5465-5468.

[14] (a) L. Cao, X. Wang, M. J. Meziani, F. S. Lu, H. F.Wang, P. J. G. Luo,Y. Lin, B. A. Harruff, L. M. Veca, D. Murray, S. Y. Xie, Y. P. Sun, *J. Am. Chem. Soc.*, **2007**, *129*, 11318-11319; (b) S. L. Hu, K. Y. Niu, J. Sun, J. Yang, N. Q. Zhao, X.W. Du, *J. Mater. Chem.*, **2009**, *19*, 484-488; (c) Y. P. Sun, X. Wang, F. S. Lu, L. Cao, M. J. Meziani, P. J. G. Luo, L. R. Gu, L. M. Veca, *J. Phys. Chem. C*, **2008**, *112*, 18295-18298; (d) X. Wang, L. Cao, F. S. Lu, M. J. Meziani, H. Li, G. Qi, B. Zhou, B. A. Harruff, F. Kermarrec, Y. P. Sun, *Chem. Commun.*, **2009**, *25*, 3774-3776; (e) J. Peng, W. Gao, B. K. Gupta, Z. Liu, R. Romero-Aburto, L. Ge, L. Song, L. B. Alemany, X. Zhan, G. Gao, S. A. Vithayathil, B. A. Kaipparettu, A. A. Marti, T. Hayashi, J-J. Zhu, P. M. Ajayan, *Nano Lett.*, **2012**, *12*, 844-849.

[15] J. Jiang, Y. He, S. Li, H. Cui, *Chem. Commun.*, **2012**, *48*, 9634-9636.

[16] (a) Y. Li, Y. Zhao, H. Cheng, Y. Hu, G. Shi, L. Dai, L. Qu, *J. Am. Chem. Soc.*, **2012**, *134*, 15-18; (b) L. Li, G. Wu, G. Yang, J. Peng, J. Zhao, J-J. Zhu, *Nanoscale*, **2013**, *5*, 4015-4039.

[17] M. Favaro, S. Agnoli, C. Di Valentin, C. Mattevi, M. Cattelan, L. Artiglia, E. Magnano, F. Bondino, S. Nappini, G. Granozzi, *Carbon*, **2014**, *68*, 319-329.

[18] P. Zhang, W. Li, X. Zhai, C. Liu, L. Dai, W. Liu, *Chem. Commun.*, **2012**, *48*, 10431-10433.

[19] H. Choi, S-J. Ko, Y. Choi, P. Joo, T. Kim, B. R. Lee, J.-W. Jung, H. J. Choi, M. Cha, J-R. Jeong, I-W. Hwang, M. H. Song, B-S. Kim, J. Y. Kim, *Nat. Photonics*, **2013**, *7*, 732-738.

[20] P. K. Jaina, M. A. El-Sayed, *Chem. Phys. Lett.*, **2010**, *487*, 153-164.

[21] (a) J. Juodaityte, N. Sewald, *J. Biotechnol.* **2004**, *112*, 127-138; (b) P. Fatás, J. Bachl, S. Oehm, A. I. Jiménez, C. Cativiela, D. Díaz Díaz, *Chem. Eur. J.*, **2013**, *19*, 8861-8874.

[22] R. Behrendt, M. Schenk, H. J. Musiol, L. Moroder, *J. Pept. Sci.*, **1999**, *5*, 519-529.

[23] H. Robson Marsden, J.-W. Handgraaf, F. Nudelman, N. A. J. M. Sommerdijk, A. Kros, *J. Am. Chem. Soc.*, **2010**, *132*, 2370-2377.

[24] M. Crisma, F. Formaggio, A. Moretto, C. Toniolo, *Biopolymers (Pept. Sci.)*, **2006**, *84*, 3-12.

[25] M. El Hajji, S. Rebuffat, T. Le Doan, G. Klein, M. Satre, B. Bodo, *Biochim. Biophys. Acta*, **1989**, *978*, 97-104.

[26] Farrar, D.; Ren, K.; Cheng, D.; Kim, S.; Moon, W.; Wilson, W. L.; West, J. E.; Yu, S. M. *Adv. Mater*., **2011**, *23*, 3954-3958.

[27] G. J. M. Habraken, M. Peeters, C. H. J. T. Dietz, C. E. Koning, A. Heise, *Polym. Chem.*, **2010**, *1*, 514-524.

[28] K. Görmer, M. Bürger, J. A. W. Kruijtzer, I. Vetter, N. Vartak, L. Brunsveld, P. I. H. Bastiaens, R. M. J. Liskamp, G. Triola, H. Waldmann, *Chem Bio Chem*, **2012**, *13*, 1017-1023.

[29] A. Polidori, N. Michel, A. S. Fabiano, B. Pucci, *Chem. Phys. Lipids*, **2005**, *136*, 23-46.

4. Self-assembling short peptides: synthesis and nanostructures formation

The generation of many biological nanostructures, that plays a fundamental role in nature, occurs through the self-assembly process. Taking inspiration from nature, the bottom-up self-assembly strategy has emerged as one of the most applicable approaches to create ordered structures from small molecule arrangements.[1] The self-assembly process is mediated through a combination of intramolecular/intermolecular interactions including van der Waals, electrostatic, hydrogen bonding, and stacking interactions.[2] The creation of ordered aggregates characterized by discrete 3D-architectures with specific shapes, dimensions and functions finds application in areas ranging from chemistry to materials science and medicine. In this connection, peptides offer important advantages as building blocks for the construction of self-assembled nanostructures[3] because of their biocompatibility and structural/functional diversity.

Nanotubes and nanofibers predominate as molecular architectures among the self-assemblies formed by short peptides[4] of which the phenylalanine homo-dipeptide H-Phe-Phe-OH is the most extensively investigated example.[5] Conversely, spherical nanostructures based exclusively on low molecular-weight peptides are much less common.[6]

The chemical diversity of peptides may be further expanded with the use of non-proteinogenic α-amino acid residues. In the group where I carried out my PhD, a symmetrically α,α-disubstituted glycine, *bis*[*p*-(phenylazo)benzyl]glycine (*p*azoDbg), that contains two side-chain azobenzene moieties and undergoes reversible *cis-trans* isomerization upon exposure to light of the appropriate wavelength, has been already described[7]. In this chapter, the synthesis and self-assembly properties of derivatives and short peptides containing this photoswitchable α-amino acid will be presented.[8]

In addition the self-assembly behaviour of a hydrophobic, terminally protected dipeptide Boc-L-Leu-L-Cys(Me)-OMe and of its diacetylene derivative will be discussed.[9] These compounds revealed the formation of nano-, micro- and macroscale complex architectures in different conditions.

4.1 Photocontrolled self-assembly of azobenzene-containing peptides

Intermolecular π-π stacking interactions involving aromatic side chains are a potent driving force for peptide self-assembly.[6] Phe-Phe has been recognized as the minimal self-assembling peptide sequence.[5,10] The Fmoc protected derivative (Fmoc-Phe-Phe-OH) usually self-assembles in supramolecular nanostructures with fibrillar shape due to the additional aromatic interactions that involve the Fmoc group.[11] We started our investigation with the substitution of one Phe residue with the photoswitchable α-amino acid *p*azoDbg, obtaining the dipeptide **1** (Fmoc-Phe-*p*azoDbg-OH, Figure 4.1 A). Compound **1** was synthesized by solution-phase methods. The reversible isomerization between the all *trans* (*t*) and all *cis* (*c*) forms [(*t*)**1**↔(*c*)**1**] upon irradiation with UV (350 nm) or Vis (450 nm) light was studied in MeOH solution by HPLC, CD, and UV-Vis absorption experiments (Figures 4.1 B-D and 4.2).

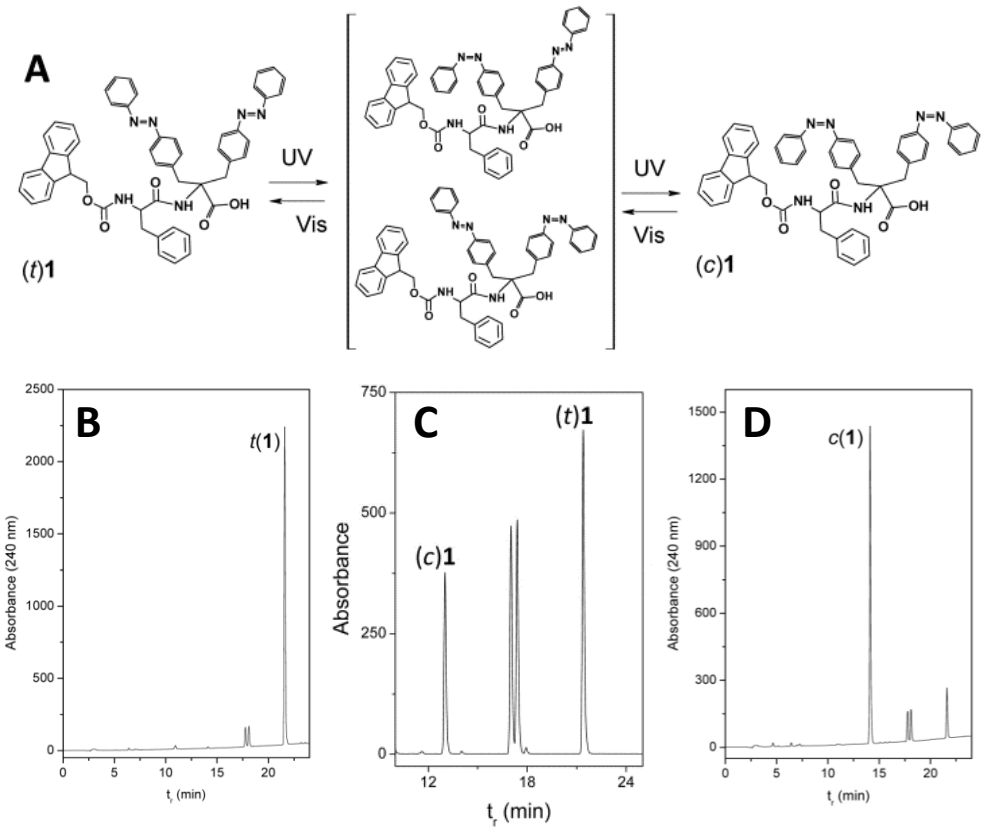

Figure 4.1 (**A**) Chemical structures of Fmoc-Phe-*p*azoDbg-OH (**1**); the all *trans* (*t*), *cis*/*trans* and *trans*/*cis*, and all *cis* (*c*) forms are shown. HPLC profiles of (*t*)**1** solution (1 mM in MeOH) before irradiation (**B**), and after irradiation at 350 nm for 1 min (**C**) and 3 min (**D**).

The (*t*)**1**→(*c*)**1** conversion was complete within 3 minutes. The HPLC profile obtained after 1-minute UV irradiation of (*t*)**1** (Figure 4.1 C) shows the presence of intermediate species in which only one azobenzene group has isomerized (note that *p*azoDbg becomes chiral in this state[7]). The UV-Vis absorption and CD spectra of (*t*)**1** and (*c*)**1** exhibit significant differences in the region above 220 nm (Figure 4.2) that we assigned primarily to different relative dispositions of the aromatic ring in the chiral Phe residue with respect to those in the achiral *p*azoDbg for the (*c*)**1** and (*t*)**1** forms, which allow for a more effective chirality transfer in (*t*)**1**. However, it should be noted that also the Fmoc chromophore is known to contribute to the electronic absorption and CD above 250 nm.[12]

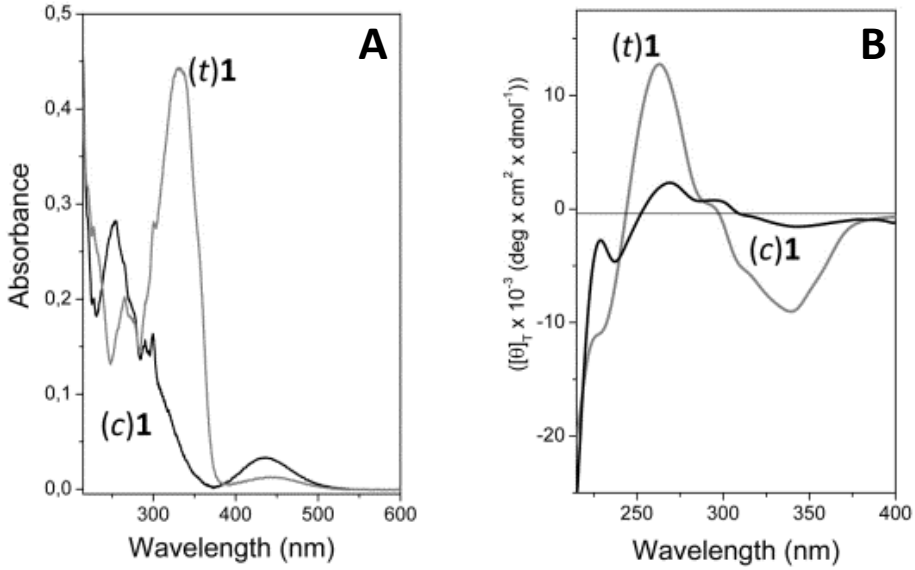

Figure 4.2 (**A**) UV-Vis absorption spectra of (*t*)**1** and (*c*)**1** (0.1 mM solution in MeOH). (**B**) CD spectra of (*t*)**1** and (*c*)**1** (1 mM solution in MeOH).

The self-assembly properties of **1** were investigated in an aqueous environment. The lyophilized dipeptide was dissolved in DMSO at a concentration of 50 mg/mL. A 20 μL aliquot of this solution was dropped into 1980 μL of water and vortexed for a few seconds.[10] The resulting suspension was submitted to size-exclusion chromatography by gel filtration (Sephadex G75) and eluted with water. Dynamic light scattering (DLS), transmission electron microscopy (TEM), scanning electron microscopy (E-SEM, FE-SEM), and atomic force microscopy (AFM) revealed that (*t*)**1** forms spherical vesicle-like nanostructures with diameters of 50-200 nm (Figure 4.3).

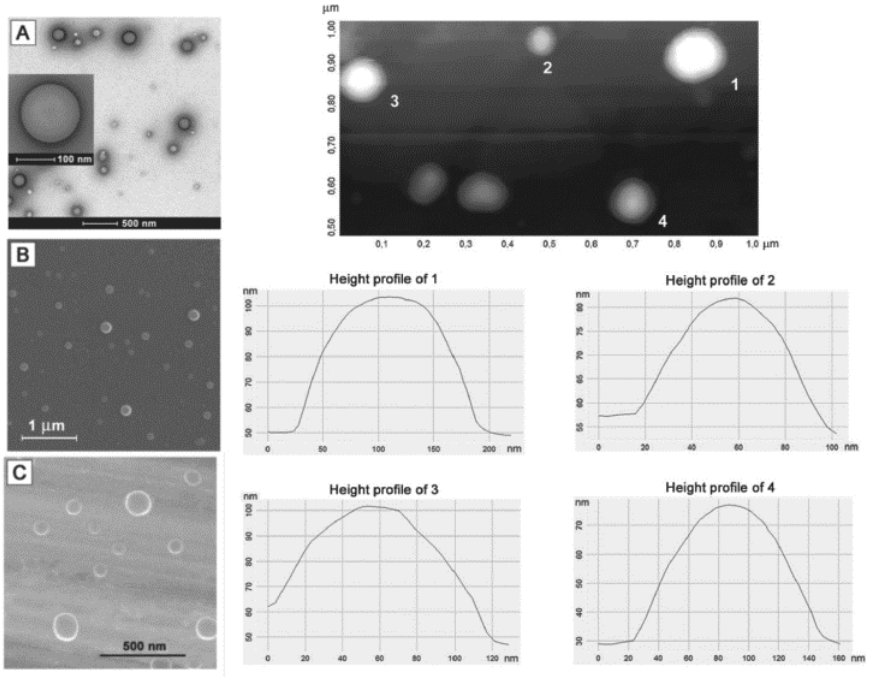

Figure 4.3 Left: TEM (unstained, **A**) and SEM (**B**, field emission; **C**, environmental) images of the nanostructures formed by (*t*)**1** in water. Right (top): AFM image of the (*t*)**1** nanostructures; the brightest spots correspond to the highest parts of the surface. Bottom: height profiles of selected nanospheres.

The close similarity of the microscopy images obtained after the sample was let to stand at room temperature for several weeks indicates a high stability for the system. Irradiation at 350 nm for 5 minutes to generate (*c*)**1** resulted in deformation of the nanospheres to yield elongated shapes (Figure 4.4). This morphological change proved to be reversible as the spherical assemblies were recovered after illumination with Vis light [(*c*)**1**→(*t*)**1**]. The reversibility of the isomerization process was also confirmed by UV-Vis absorption spectroscopy along two cycles. Longer UV irradiation times resulted in complete disruption of the vesicles (Figure 4.4). These latter results suggest that the (*t*)**1**→(*c*)**1** isomerization is somewhat hindered in the assembled structure (note that a 3-minute exposure to UV light allowed for complete isomerization in solution, Figure 4.1 C). Accordingly, the *trans*-to-*cis* isomerization of only a fraction of azobenzene moieties induces a slight rearrangement of the assembly, but the intermolecular attractive forces are still capable of essentially preserving the three-dimensional self-assembled structure. However, when the ratio of azobenzene moieties in the non-planar *cis* form reaches a certain level, the intermolecular packing mode is so strongly perturbed (due to shape change and less effective π-π stacking) that the ordered supramolecular architecture is not maintained and the spherical assemblies are transformed into amorphous aggregates.

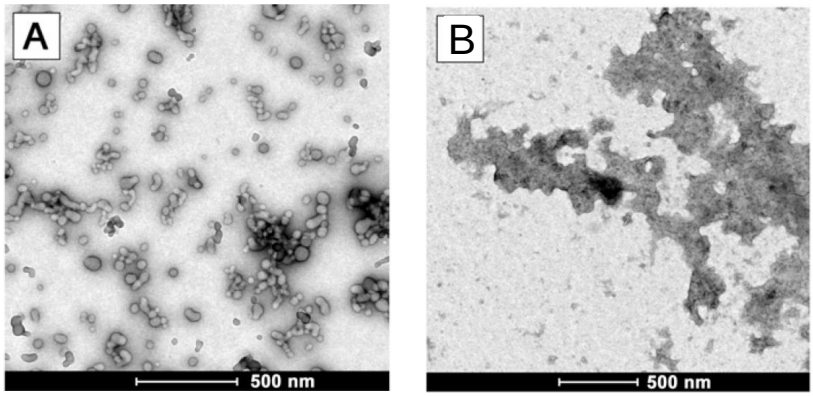

Figure 4.4 TEM images (unstained) showing the morphological modification of the *t*(**1**) nanospheres upon exposure to UV light for 5 min (**A**, elongated spheres) or 15 min (**B**, disruption of the vesicles).

A potential application of this photosensitive process to induce the controlled release of substances entrapped in the nanoassemblies was evaluated. A 20 μL aliquot of the above mentioned solution of (*t*)**1** in DMSO was mixed with 1980 μL of a 10 mg/mL aqueous solution of gold nanoparticles (GNps, 2 nm size) coated with a helical undecapeptide.[13] After a short vortex agitation, the suspension obtained was submitted to gel filtration and thus separated from the non-encapsulated peptide-coated GNps. Microscopy studies revealed the presence of nanostructures similar in morphology to those formed by (*t*)**1** in the absence of GNps. UV irradiation of the gel-filtered sample (10 min) resulted in partial disruption of the vesicles with concomitant release of the encapsulated peptide-coated GNps, as detected by TEM (Figure 4.5).

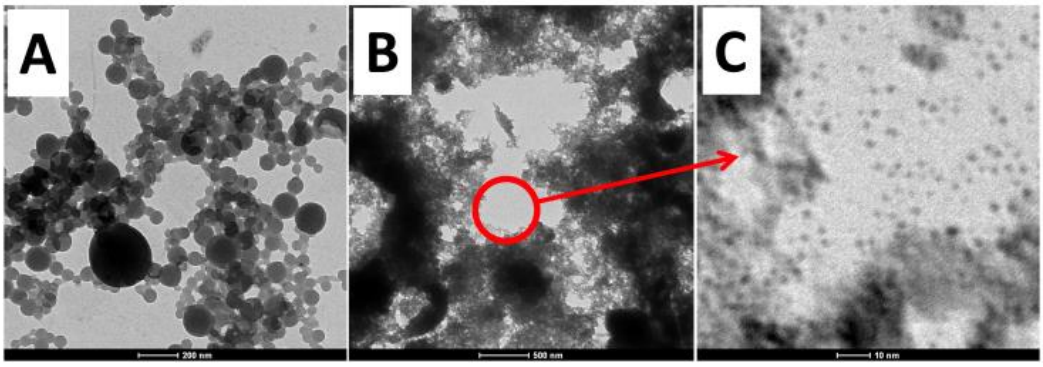

Figure 4.5 TEM images (unstained) showing: (**A**) nanospheres formed by (*t*)**1** and peptide-coated GNps; (**B**) the nanospheres disassembly induced by UV irradiation; (**C**) details of released GNps (black dots).

Recently, novel, stimulus-responsive supramolecular structures in the form of fibers, gels, and spheres, derived from an azobenzene-containing benzenetricarboxamide derivative, were described by Kim and coworkers.[14] Therefore, we next decided to conjugate H-(*p*azoDbg)-OEt to 1,3,5-trichlorotriazine with the aim at exploring the supramolecular stimuli response of a novel C_3-symmetrical *tris*-azobenezene system (compound **2**, Figure 4.6 A). H-(*p*azoDbg)-OEt, 1,3,5-trichlorotriazine and triethylamine were mixed in a DMF solution for 48 hours, affording **2** in 69 % yield. All six azobenzene units were able to switch reversibly in a MeOH solution from the (*t*)↔(*c*) states (Figure 4.6 A) under appropriate irradiation. The intermediates were detected by HPLC.

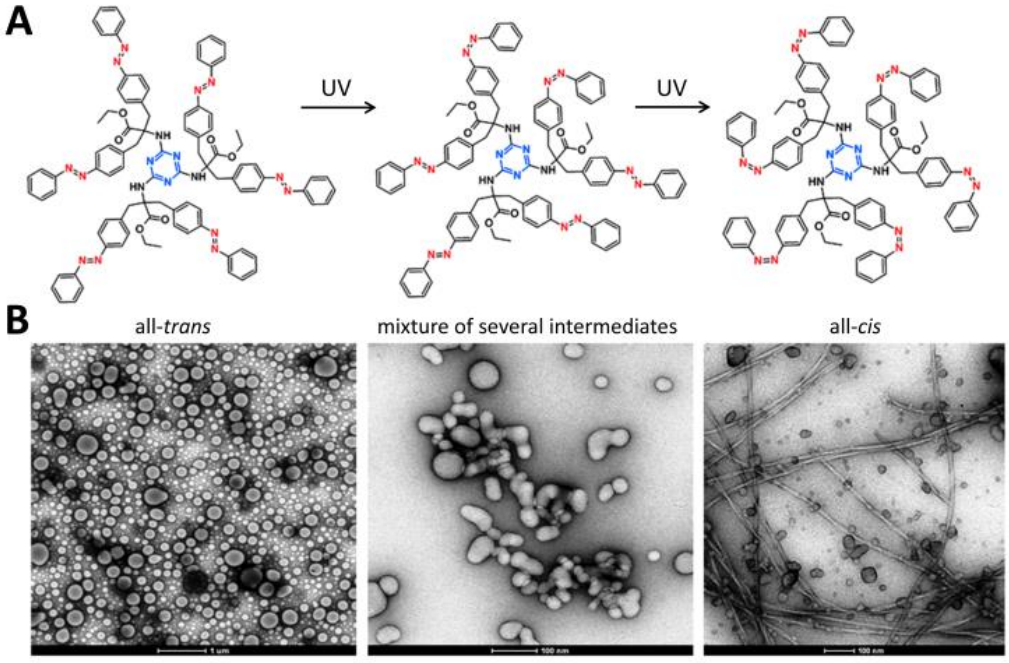

Figure 4.6 (**A**) Chemical structure and isomerization process of compound **2** formed by our *p*azoDbg-containing building block *tris*-conjugated to the 1,3,5-triazine template. (**B**) TEM images of the light-driven, microstructure morphological transition of this system, generated from a DMSO/H_2O suspension.

Spherical microstructures were generated (in form of milk-like suspension) from a 15 mM (1:7) DMF/THF solution dialyzed (membrane cutoff, 1 KD) against ultrapure water (48 h) (Figure 4.6 B, left). Under (20 min) UV irradiation, a morphological transition from the suspension to gel was observed. We recorded TEM images over different times of irradiation. The analysis revealed a conversion from spheres to elongated spheres (5 min), and eventually to a mixture of spherical/elongated fibers (20 min) (Figure 4.6 B, center and right, respectively). Irradiation of the gel with Vis light resulted in gel disruption, followed by precipitation of the obtained amorphous aggregates which do not undergo light-induced

conversion any further. The formation of vesicles and hydrogel microstructures was also confirmed by AFM analysis (Figure 4.7).

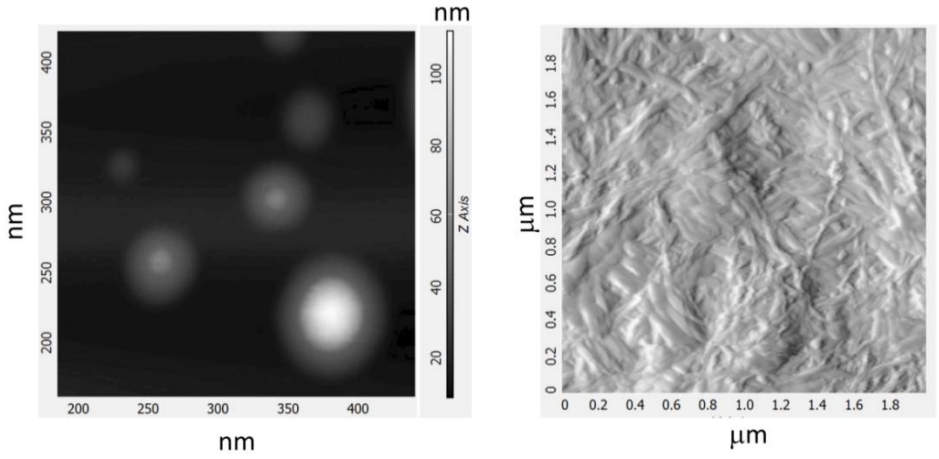

Figure 4.7 AFM images of vesicles (left) and fibers (hydrogel, right) obtained from **2**.

Finally, we expanded the use of our *p*azoDbg amino acid to the synthesis of the "octopus" system **3** (Figure 4.8 A) to generate photoresponsive C_4-symmetrical, dendrimeric-like, multiazobenzene systems. Tfa-(*p*azoDbg)-OH (Tfa, trifluoroacetyl), reacted with pentaerythritol in presence of N,N'-diisopropylcarbodiimide and N,N-dimethylaminopyridine afforded **3** in a remarkable 90 % yield. The resulting system is characterized by as many as eight azobenzene moieties and can be viewed as a central core surrounded by a shell of azobenzene groups at the periphery.

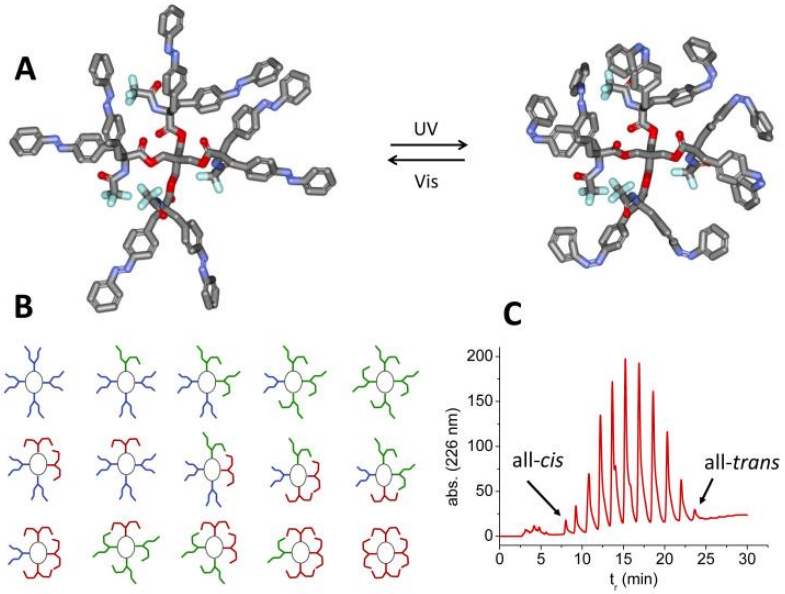

Figure 4.8 (**A** and **B**) Chemical structure and isomerization process of the system (**3**) formed by our *p*azoDbg-containing building block tetra-conjugated to the pentaerythritol template. (**C**) HPLC profile of a solution in MeOH of **3** irradiated at 350 nm for 3 min.

Up to eleven (out of the possible fifteen, Figure 4.8 B) discrete states produced by *trans*-to-*cis* isomerizations of the individual azobenzene units were observed by reverse-phase HPLC depending on the time of exposure of **3** (in a MeOH solution) to the UV light (Figure 4.8 C). This process is fully reversible (*cis*-to-*trans*) under Vis light irradiation for several cycles.
Moreover, this system shows a high propensity to self-assemble in a variety of organic (DMF, DMSO, THF, MeOH, CH_3CN)/aqueous solutions (even at low concentration, below 1 mM) to generate supramolecular vesicles as revealed by TEM experiments (Figure 4.9 A). These vesicles were able to rearrange, depending on the exposure time to UV light, to: (i) a sponge-like microstructure (10 min) (Figure 4.9 B and inset) and (ii) to fibers (40 min) (Figure 4.9 C). These microstructure rearrangement was reversibly controlled under exposure to Vis light, which produced sponge-like microstructures (20 min) (Figure 4.9 D), followed by a mixture of fiber, sponge-like and spherical microstructures (1 h) (Figure 4.9 E) and finally by almost only spherical microstructures (2 h) (Figure 4.9 F).

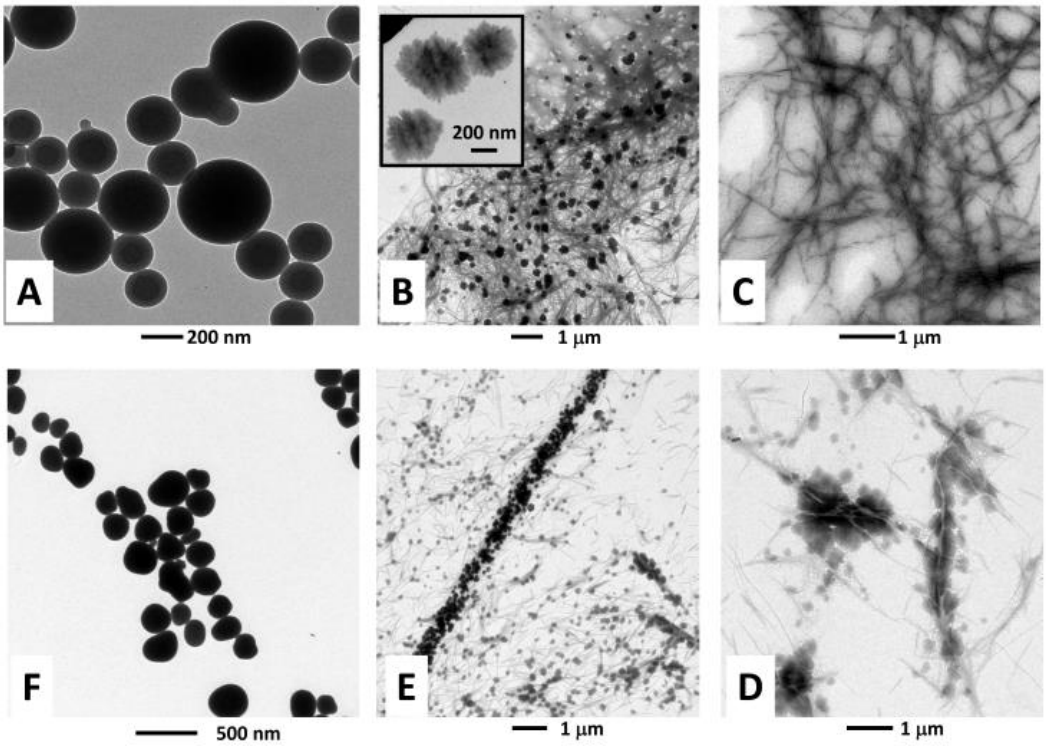

Figure 4.9 TEM images of the light-driven, reversible, vesicle-to-sponge-to-fiber microstructure transitions underwent by **3**.

The vesicle-to-sponge-to-fiber microstructure transition occurring for **3** was additionally studied by AFM. Vesicles and fibers are reported, respectively, in Figures 4.10 A and B. The sponge-like microstructures (Figure 4.10 C) were characterized in a mixture with fiber, under

same conditions as those reported for Figure 9B. The height profiles of selected sponges reveal the irregular 3D-morphology present on their surface.

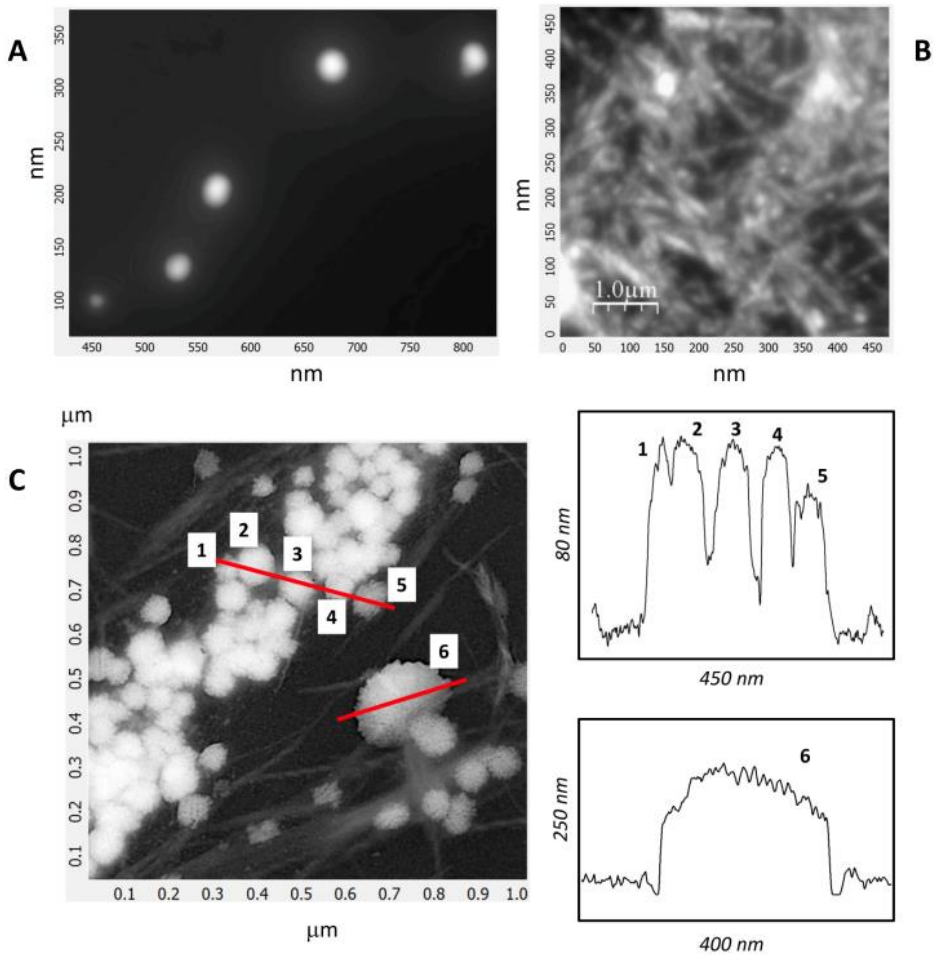

Figure 4.10 AFM images of vesicles (**A**) and fibers (**B**) from **3**. (**C**) AFM image of a mixture of sponges and fibers from **3**, and height profiles of selected nano-sponges.

Conclusions

In summary, the compounds described, containing the photoresponsive amino acid *p*azoDbg and characterized by different geometries, are able to promote the formation of well-ordered supramolecular nanostructures in water. Moreover the presence of the light-responsive azobenzene moieties renders photoresponsive the microstructures, thus allowing triggering of reversible transitions between different morphologies transition upon irradiation with light at the appropriate wavelength.

4.2 Self-assembled architectures from a hydrophobic dipeptide

Molecular architectures obtained by the self-assembly of short unprotected peptides predominate in the field of peptide supramolecular chemistry.[4] Conversely, only a few examples of terminally-protected peptides, the crystal structures of which are characterized by a nanotube architecture, were reported, but their self-assembly properties have not been further explored.[15] In this context, we synthetized a hydrophobic, terminally protected dipeptide Boc-L-Cys(Me)-L-Leu-OMe (**4**) (where Boc is tert-butoxycarbonyl, Cys(Me) is S-methyl cysteine, and OMe is methoxy) (Figure 4.11 A) that is able to self-assemble producing nano-, micro- and macroscale complex architectures.

The X-ray diffraction structure of **4** was determined on a single crystal grown from MeOH (Figure 4.11 B). The conformation adopted by both α-amino acid residues is *semi*extended, and the N-H groups of Cys and Leu point to opposite directions. In the packing mode (Figure 4.11 C), the N1-H group is intermolecularly H-bonded to the (*y*, -*x*+*y*, *z*+1/6) symmetry equivalent of the (urethane carbonyl) O0 atom, and the N2-H group is H-bonded to the (*x*-*y*, *x*, *z*-1/6) symmetry equivalent of the (amide) O1 atom. As a result, H-bonded molecules wrap around the sixfold screw axis along the *c* direction, each molecule being connected to the next by two H-bonds. The left-handed, supramolecular sixfold helix thus generated is characterized by a very narrow internal lumen, about 2.5 Å in diameter (Figure 4.11 C, bottom).

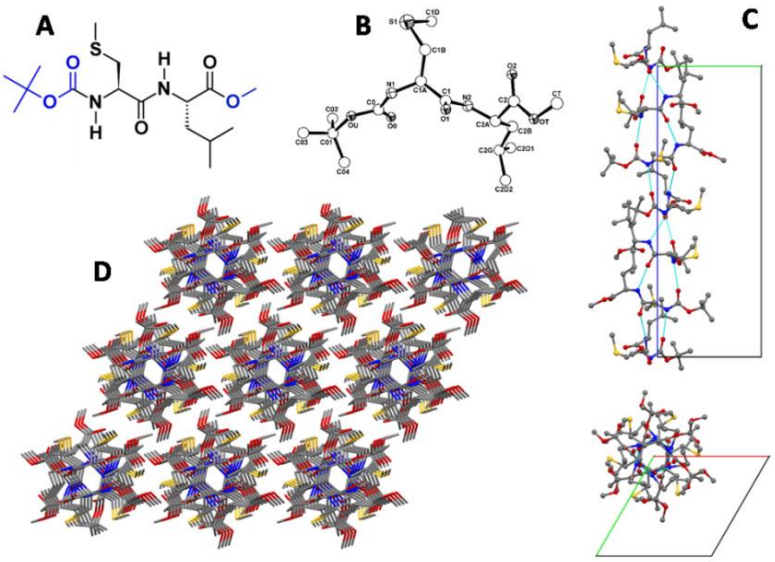

Figure 4.11 (**A**) Chemical formula of dipeptide **4**. (**B**) X-Ray diffraction structure of **4** with atom numbering. (**C**) Packing mode of **4** in the crystal. A single helical row of molecules is shown as viewed perpendicularly (upper part) and down (lower part) the sixfold screw axis. Intermolecular H-bonds are indicated by dashed lines. (**D**) Overall packing of **4** molecules as viewed nearly down the *c* axis. Carbon, grey; nitrogen, blue; oxygen, red; sulphur, yellow.

The Cys(Me) and Leu side chains, as well as the N- and C-terminal Boc and OMe groups of each molecule are located on the external surface. Each helical row of molecules is surrounded by six counterparts (Figure 4.11 D). Lateral stabilization between rows is provided, in addition to van der Waals interactions, by C-H···O interactions taking place between the (Boc) C02-H02B group and the (*x*-1, *y*-1, *z*) symmetry equivalent of the (methyl ester) OT atom.

Dipeptide **4** is able to adopt a well-organized, micro 3D arrangement when allowed to self-assemble under appropriate conditions. As a first experiment, upon slow evaporation of a concentrated solution of **4** in 1,1,1,3,3,3-hexafluoroisopropanol (HFIP), flower-like microstructures, homogenous in size and characterized by large and empty cavities were obtained (SEM images, Figure 4.12).

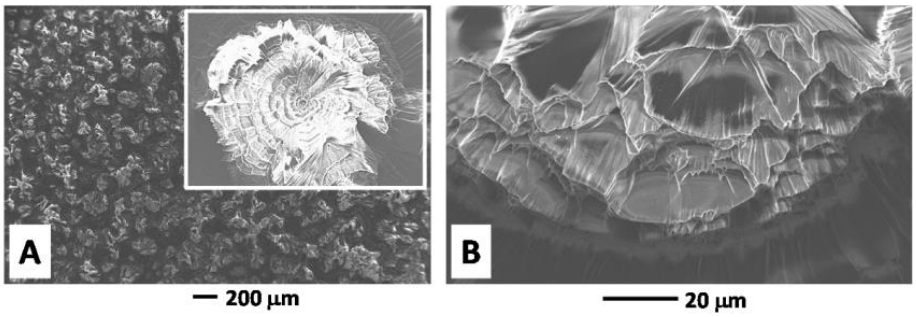

Figure 4.12 (**A**) SEM image of **4** after slow evaporation from HFIP solution. Inset: frontal detail of one flower-like microstructure. (**B**) SEM detail (lateral view) of one flower-like microstructure.

Conversely, the slow evaporation of concentrated solutions of **4** in either EtOAc, CH_3CN or acetone led to the formation of long, aligned rods (up to 10 cm in length) as shown in Figures 4.13 A and B. Interestingly, such are rods characterized by an overall parallelepiped shape that present an empty inner cavity (Figure 4.13 B). Smaller and packed rods of **4** (at the microscale level) were obtained by interfacial crystallization between water and EtOAc, as revealed by SEM images (Figure 4.13 C). Moreover, by adding a diluted solution of **4** in MeOH to a large excess of water, formation of micrometric, isolated rods was observed (Figure 4.13 D). According to a SEM analysis (Figures 4.13 E and F), even at this microscale level, the rods are characterized by an empty inner cavity while maintaining the overall parallelepiped shape found at the macroscale level.

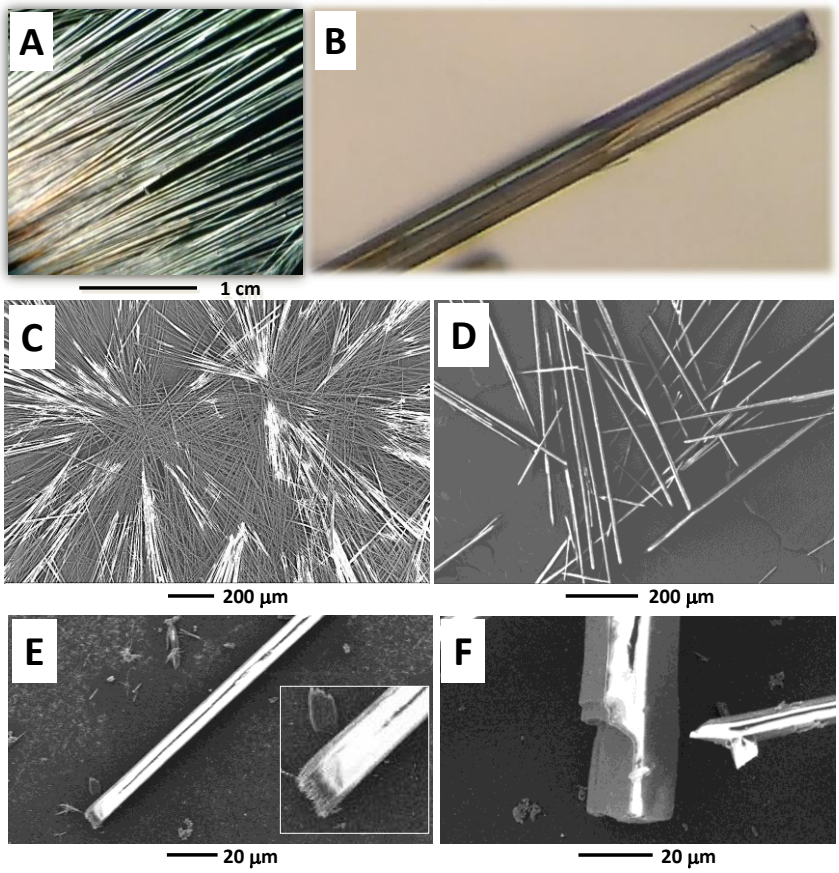

Figure 4.13 (**A**) Camera picture of macroscopic rods from **4** obtained after evaporation from a concentrated solution in CH_3CN. (**B**) Camera picture showing details of a macroscopic rod obtained from a CH_3CN solution. (**C**) SEM image of micrometric rods from **4** obtained from a water/EtOAc interfacial crystallization. (**D**) SEM image of micrometric rods from **4** obtained from a water/MeOH solution. (**E**,**F**): SEM images showing details of the rods (obtained from a water/MeOH solution).

Peptide **4** was further studied by circular dichroism in CH_3CN solution and as solid-state rods obtained after evaporation from the same solvent (Figures 4.14 A and B). Notably, **4** shows a strong aggregation propensity in CH_3CN solution at concentrations above 1 mg/mL (Figure 4.14 A). This conclusion is justified by the change of the Cotton effect near 195 nm from weakly positive at 0.3 mg/mL concentration to strongly negative at concentrations in the range 2-10 mg/mL, accompanied by a marked increase in ellipticity of the positive Cotton effect at about 218 nm. The CD spectra of the most concentrated solutions nicely resemble the spectrum obtained in the solid state (Figure 4.14 B), i.e. that of the rod structure, although the latter would be entirely red-shifted, albeit slightly.

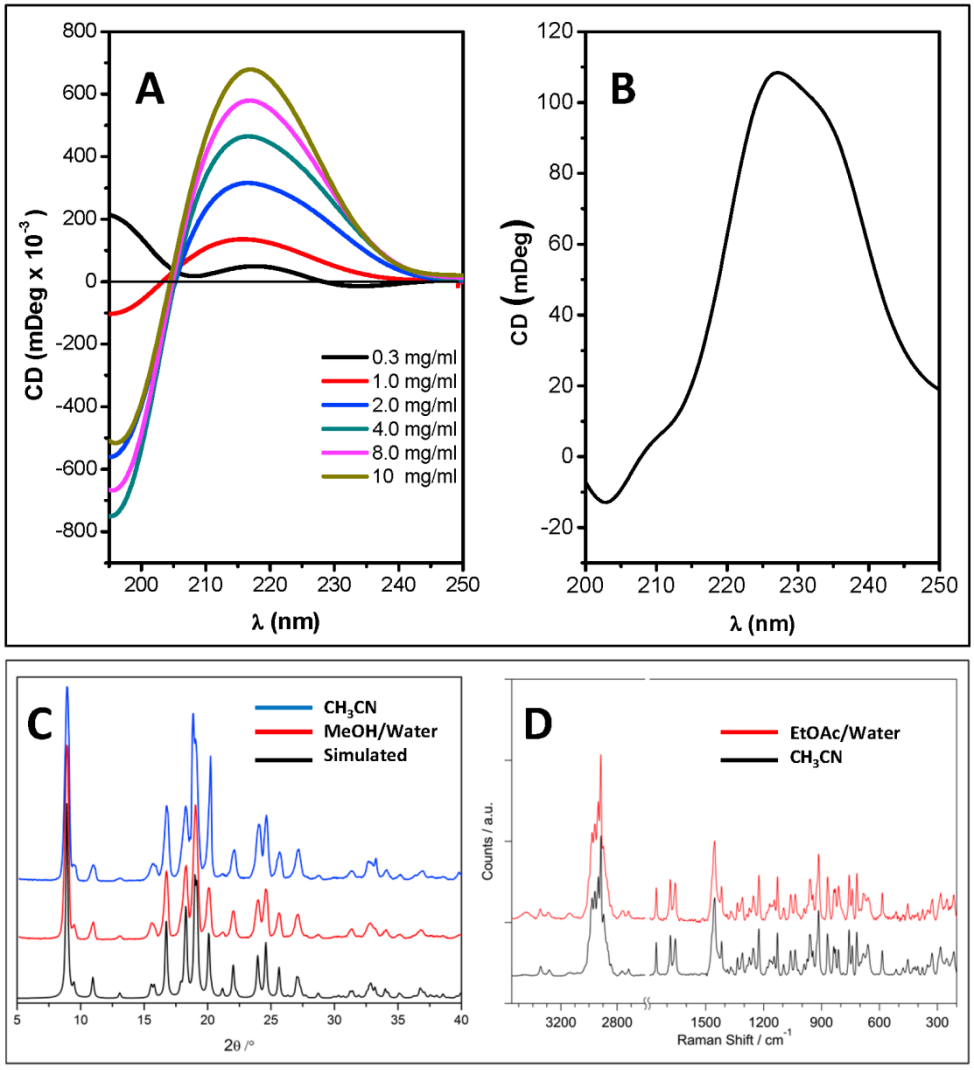

Figure 4.14 (**A**) CD spectra of **4** at different concentrations in CH_3CN solution. (**B**) Solid-state CD spectra of rods obtained from CH_3CN. (**C**) Comparison of simulated PXRD measurements (from single-crystal X-ray diffraction) with experimental results on rods obtained from the CH_3CN and MeOH/water preparation methods. (**D**) Comparison of Raman spectra of the rods obtained from the EtOAc/water and CH_3CN preparation methods.

The powder X-ray diffraction (PXRD) technique was exploited in order to check whether formation of rods characterized by an empty cavity at the macro- and microscale level (prepared from CH_3CN and MeOH/water, respectively) could be ascribed to a supramolecular organization different from that determined at the single crystal level. The PXRD patterns of the rods prepared by the two methods (CH_3CN and MeOH/water) are identical to each other all over the 2θ range investigated, and virtually overlapping to the simulated pattern of the single crystal X-ray diffraction sample (Figure 4.14 C). In addition, the values of the unit cell parameters extracted from the two experimental PXRD patterns are in excellent agreement

with those of the single crystal. These results clearly indicate that, although different preparation methods lead to different morphologies, the 3D-supramolecular organization adopted by **4** in the crystal state is shared by the micro- and macro-hollow rods. Similar conclusions were extracted from a Raman study (Figure 4.14 D). Indeed, the rods obtained from the EtOAc/water and CH_3CN preparation methods exhibit identical Raman signatures.

To gain in-depth information on the nature of the rod architectures, we investigated the mother liquor remained after the MeOH/water preparation method. The transmission electron microscopy (TEM) analysis of this mixture carried out on stained (uranyl acetate) samples showed the presence of nano- and micrometric rods (Figure 4.15 A).

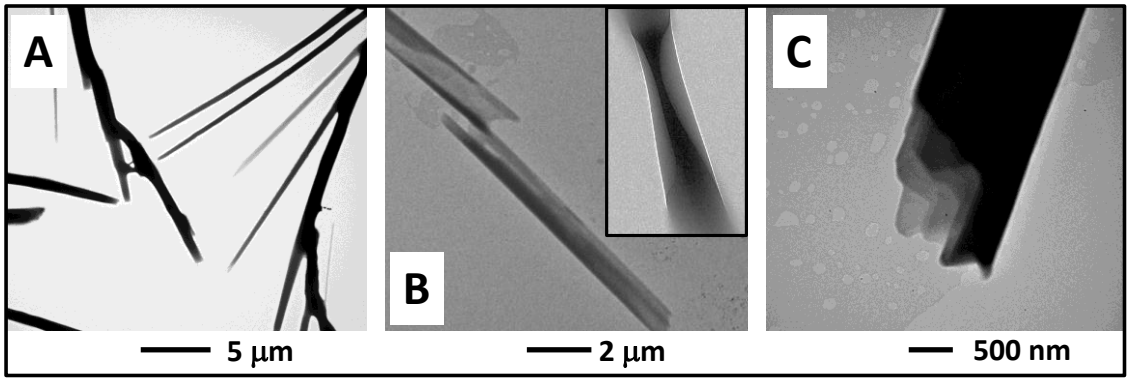

Figure 4.15 (**A**) Stained TEM image after filtration of the macroscopic rods from a MeOH/water solution of **4**. (**B**) Stained TEM image showing details of the self-assembled rods. (**C**) Stained TEM image showing details of the multiwall nature of a nanoscopic rod.

A more detailed investigation of these samples revealed two interesting features. First, we observed the presence of "incompletely folded" rods, which confirmed the tubular nature of such type of architecture (Figure 4.15 B). Second (Figure 4.15 C), we noticed a multilayer structure of the external part of the rod. In a few cases, our TEM analysis of the same, but non-stained, sample (Figure 4.16 A) revealed the typical structure of a multiwall nanotube characterized by two parallel, dark lines, associated to a higher material density, occurring at the boundaries of the rods. Interestingly, these images are similar to those that can be obtained from the TEM analysis performed on multi-walled carbon nanotubes samples.[16] To prove the existence of such a type of hollow superstructure, we made use of citrate-passivated (water soluble) gold nanoparticles (10-nm diameter)[17] which were added to the MeOH/water solution. After the self-assembly process, the results of TEM analysis (non-stained samples, Figure 4.16 B), energy-dispersive X-ray spectroscopy (EDX) (Figure 4.16 C), and optical microscopy (polarized light, Figures 4.16 D and E) clearly showed that the gold nanoparticles are incorporated into the rod structures.

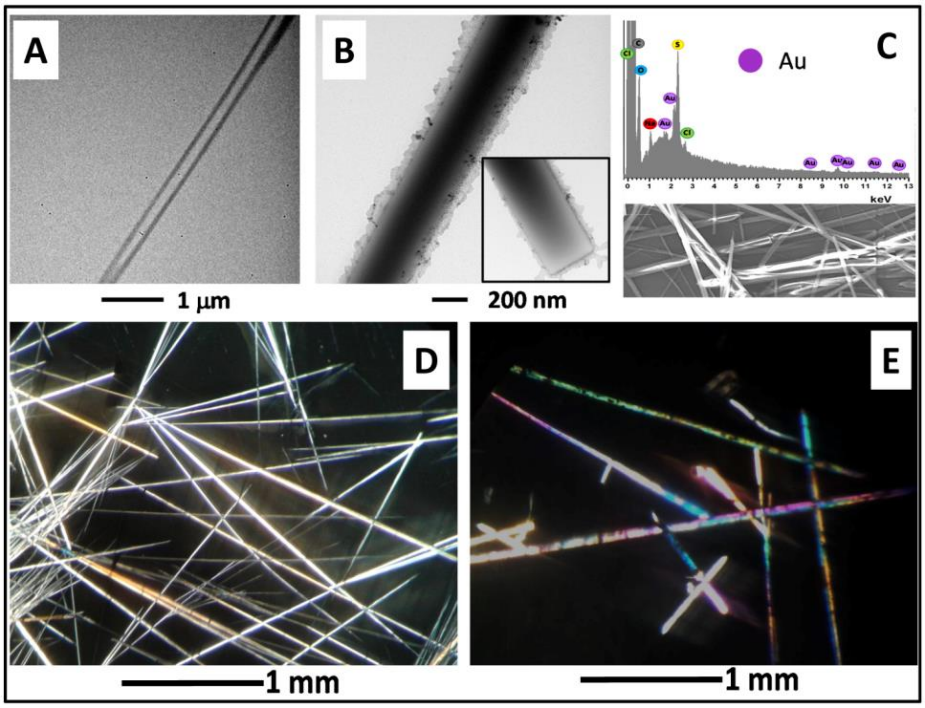

Figure 4.16 (**A**) Non-stained TEM image of a nanorod from **4**. (**B**) Non-stained TEM image showing the encapsulation of water-soluble gold nanoparticles into a rod. (**C**) SEM image and EDX pattern of the **4**-nanotube/gold nanoparticles hybrid rods. (**D**) Optical microscopy image of **4**-rods prepared from MeOH/water under polarized light. (**E**) Optical microscopy image of co-assembled **4**-rods/gold nanoparticles under polarized light.

Interestingly, the positional isomer of peptide **4**, Boc-L-Leu-L-Cys(Me)-OMe (**5**, Figure 4.17), turned out to be also amenable to a single-crystal X-ray diffraction analysis. Peptide **5** crystallizes in the orthorhombic space group $P2_12_12_1$. The packing mode of **5** is characterized by the occurrence of two intermolecular H-bonds, namely between the N1-H group and the (x+1, y, z) translational equivalent of the (urethane carbonyl) O0 atom, and between the N2-H group and the (x-1, y, z) translational equivalent of the (peptide) O1 atom. Although the H-bond donor and acceptor atoms are the same as in the intermolecular H-bonding scheme of **4**, the different symmetry operators involved result in a completely different overall packing arrangement. Indeed, at variance with the helical packing of **4**, the packing mode of **5** can be described as a highly corrugated arrangement of molecules in the *bc* plane, with the intermolecular H-bonds connecting molecules along the *a* direction (Figure 4.17 C).

However, **5** was unable to generate any superstructure, thus suggesting a strong connection between packing mode and self-assembly behaviour. Interestingly, quite recently a strictly related observation was published, namely that sequence exchange in an *unprotected* dipeptide (Val-Ala *vs.* Ala-Val) strongly affects its molecular structure and the related self-assembly tendency.[18]

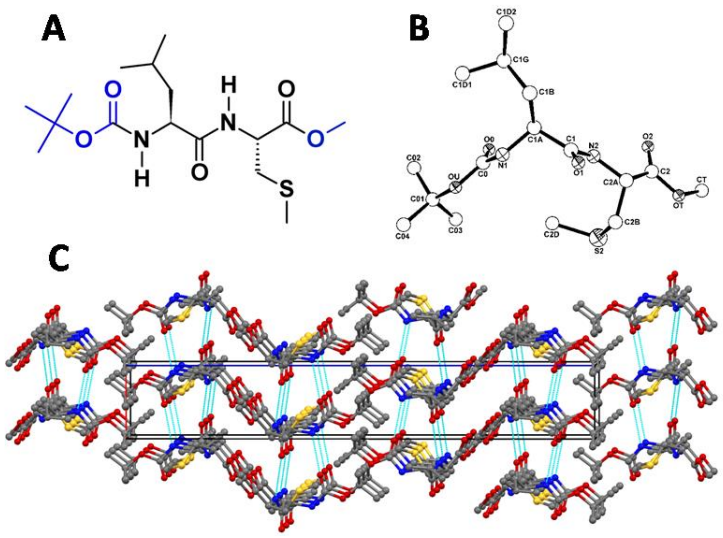

Figure 4.17 (**A**) Molecular formula of **5**. (**B**) X-Ray diffraction structure of **5** with atom numbering. Only the major occupancy site for the disordered Leu side chain is shown. (**C**) Overall packing of **5** as viewed nearly down the *b* axis. The intermolecular H-bonds are indicated by dashed lines.

Subsequently, we decided to chemically modify **4**, to explore effects of the modifications on its self-assembly propensity. To this aim **4** was first converted to **6** *via* transamination with propargylamine in the presence of catalytic DBU (Scheme 1).[19]

Then the corresponding diacetylene **7** was prepared *via* Ni-catalyzed oxidative homocoupling reaction of terminal alkynes (Scheme 4.1).[20]

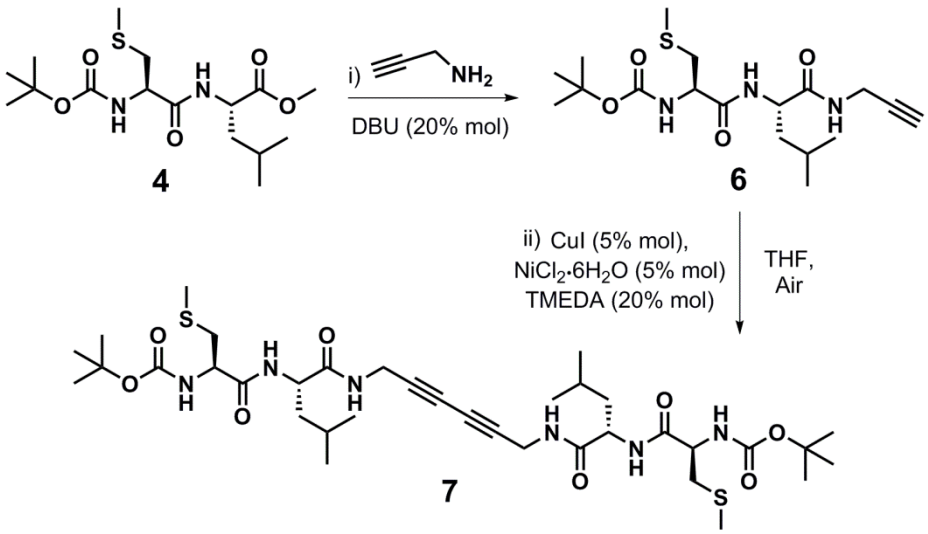

Scheme 4.1 Synthesis of **6** and **7**. Reagents and conditions: i) propargylamine, DBU (20% mol), r.t., 48 h; ii) CuI (5% mol), $NiCl_2 \cdot H_2O$ (5% mol), TMEDA(20% mol), THF, r.t., 48 h.

Compound **7** showed different propensity to aggregate compared to **4**, in fact it is able to form an organogel in CH_2Cl_2 (Figure 4.18, right).

It is known that diacetylenes undergo radical polymerization by heating or under UV-light irradiation without the need for chemical initiators or catalysts.[21] The polydiacetylenes thus obtained are π-conjugated polymers that have alternating ene–yne backbone structures. These conjugated polymers generally have intense color and several intriguing properties indeed they have received much attention as conductive and non-linear optical materials. Howecer, a necessary condition for the topochemical polymerization of diacetylenes is that the diacetylene groups are aligned and placed in the appropriate spatial proximity. To test the possibility to obtain the polydiacetilene from derivative **7**, we applied UV light at 254 nm to the organogel (Figure 4.18, bottom). A polymeric orange film was then obtained, confirming that the proximity condition was satisfied.

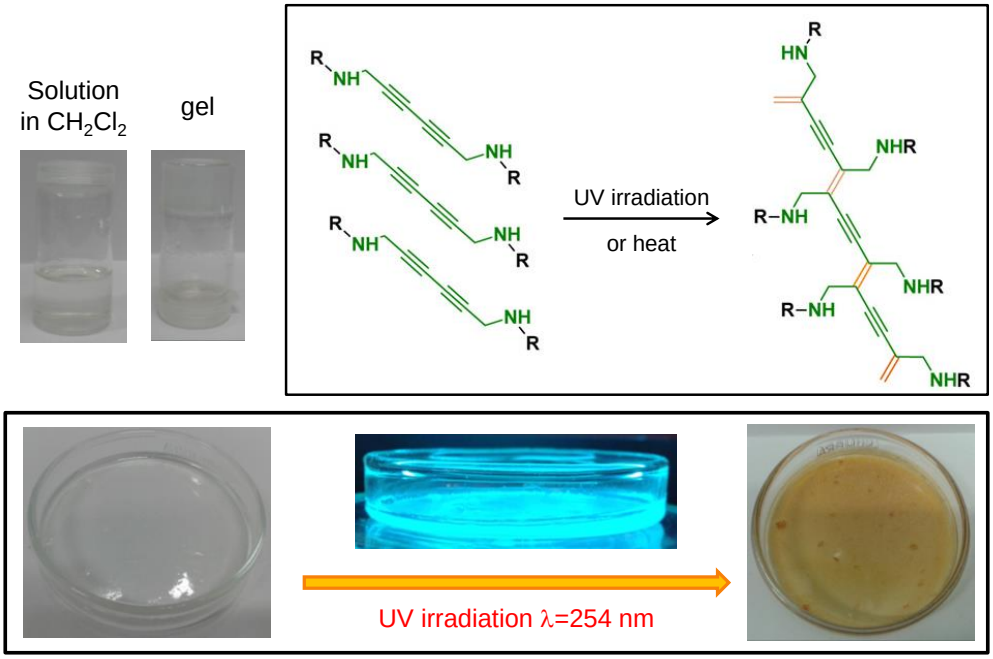

Figure 4.18 Top: images of solution and organogel obtained from **7** in CH_2Cl_2 (20 mg/mL); left: Schematic representation of light induced polymerization occurring for diacetylenes. Bottom: Images of the organogel obtained from **7** in CH_2Cl_2 before, during and after UV-light irradiation.

TEM, SEM and AFM analysis of the organogel revealed the formation of a dense network of small fibers (Figures 4.19 A, D and E). Successively, TEM and AFM analysis of the sample irradiated with UV light showed that the dense network of small fibers was almost replaced by longer and larger new structures (Figures 4.19 B, C and F).

Compound **7** is also able to self-assemble forming sponge-like 3D microstructures upon slow evaporation of a concentrated solution in MeOH. These microstructures are homogenous in size (5-10 μm) and shape (SEM images, Figures 4.20 A-C). The polymerization was obtained

after irradiation even in these objects, obtaining red polydiacetilene spheres (Figures 4.20 E-F).

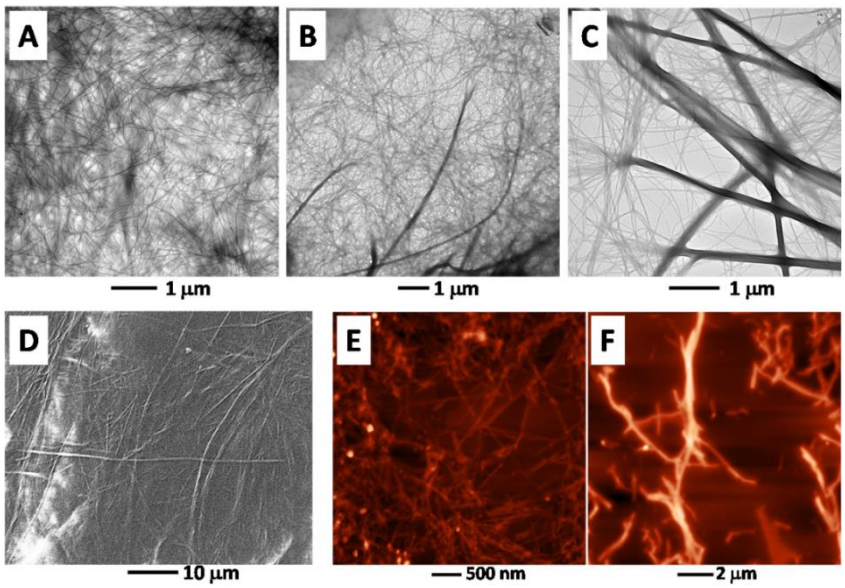

Figure 4.19 TEM images of organogel obtained from **7** in CH_2Cl_2 (**A**), after irradiation for 30 min (**B**) and for 1 h (**C**). (**D**) SEM images of the organogel. AFM images of the organogel before (**E**) and after (**F**) irradiation for 1 h.

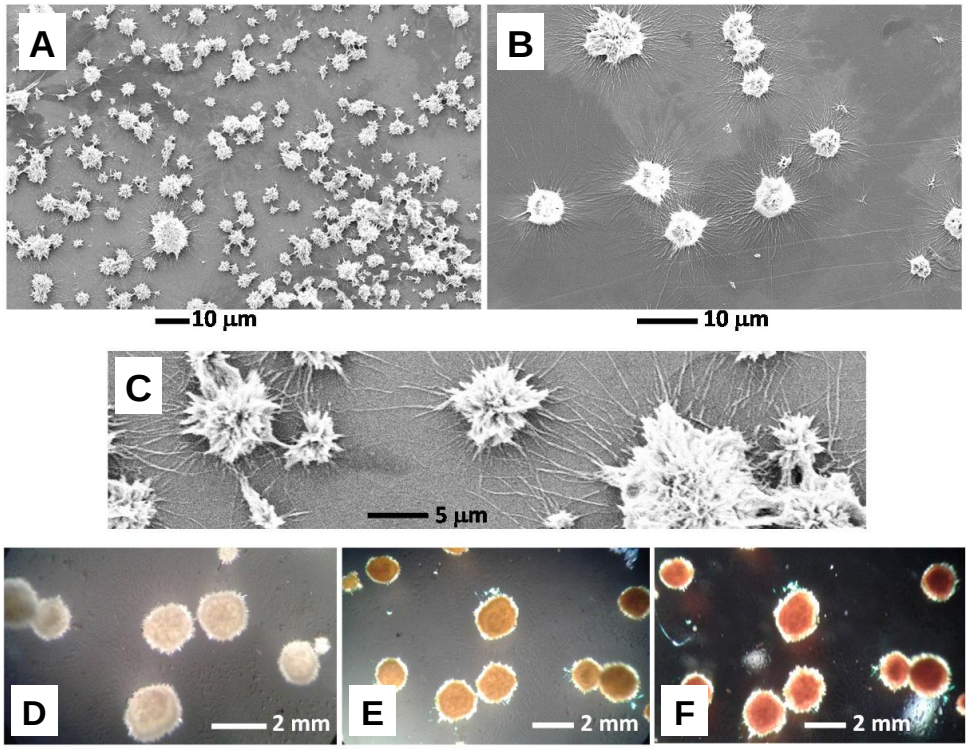

Figure 4.20 (**A-C**) SEM images of microstructures obtained from slow evaporation of methanolic solution of **7**. Optical microscopy images of microstructures obtained from slow evaporation of methanolic solution of **7** before (**D**) and after irradiation at 254 nm for 1 h (**E**) and 2 h (**F**).

Conclusions

To summarize, we showed that a terminally protected, hydrophobic dipeptide, Boc-L-Cys(Me)-L-Leu-OMe (**4**), is able to hierarchically self-assemble in well-defined structures. In particular, evaporation from organic solvents (*e.g.*, EtOAc, CH_3CN, acetone) or interfacial (EtOAc/water and MeOH/water) crystallizations led to the formation of hollow rods ranging from the nano- to the macroscale. In addition, the diacetylene derivative (**7**) obtained by chemical modification of (**4**) is able to assemble in an organogel in CH_2Cl_2 or to form sponge-like spheres by slow evaporation from MeOH. After irradiation of these microstructures it is possible to obtain the orange polydiacetylene derivative.

4.3 Experimental Section

Instruments and Methods

Nuclear Magnetic Resonance. ^{1}H and ^{13}C NMR spectra were recorded at room temperature on a Bruker AC-200 (200 MHz) and Bruker AC-300 (300 MHz) instruments using the partially deuterated solvent as the internal reference. Chemical shifts (δ) are expressed in ppm. The multiplicity of a signal is indicated as: br - broad, s - singlet, d - doublet, t - triplet, m - multiplet, etc.

High resolution Mass Spectrometry.. Mass spectra were obtained by electrospray ionization (ESI) on a Perseptive Biosystem Mariner ESI-ToF spectrometer (Foster City, CA). Data were collected in positive mode.

Fourier Transform-Infrared Spectroscopy. FT-IR absorption spectra in KBr disc were recorded with a Perkin-Elmer 1720X spectrophotometer. The $\bar{\upsilon}$ maxima for the main absorption bands are given.

High-Performance Liquid Chromatography. HPLC was performed on an Agilent 1200 series apparatus equipped with a UV detector at variable wavelengths. Conditions: Phenomenex C_{18} (100Å) (stationary phase), 45-100% B in 25 min, 1 mL/min (eluants: A=9:1 H_2O/CH_3CN, 0.05%TFA; B=1:9 H_2O/CH_3CN, 0.05% TFA).

UV-Vis Absorption. The UV-Vis absorption spectra were recorded using a Shimadzu model UV-2501 PC spectrophotometer. A 1-cm path length quartz cell was used.

Circular Dicroism. CD measurements were carried out at room temperature using a Jasco J-715 spectropolarimeter. A fused quartz cell of 0.2-mm path length (Hellma) was used.

Transmission Electron Microscopy. Samples were analyzed on a Jeol 300 PX instrument. Samples were prepared immediately before use. A small drop of solution was floated on a glow discharged carbon coated grid and excess was removed by #50 hardened Whatman filter paper. For the samples with negative staining, the grid was then floated on 2% uranyl acetate solution for 10 seconds, and the excess was removed by #50 hardened Whatman filter paper.

Field Emission Scanning Electron Microscope. A Carl Zeiss Merlin FE-SEM operating at 5 kV accelerating voltage was used. A small drop of the aqueous suspension was placed on a microscope glass cover slip and allowed to dry overnight.

Environmental Scanning Electron Microscope. Samples were analyzed on a Quanta FEG 250 E-SEM operating at 10–20 kV and using a gaseous secondary electron detector. Measurements were carried out in the wet mode (52–100% humidity) at 1 °C.

Atomic Force Microscopy. A small drop of sample was placed on a mica or silicon surface and allowed to dry in air for at least 60 min before measurement. AFM experiments were performed on two different instruments:

(i) Ntegra Aura (NT-MDT) instrument operating in tapping mode at 200−400 kHz drive frequency and using a single crystal silicon tip coated with TiN (NSG01/TiN, 0.01-0.025 Ω-cm, antimony dope).

(ii) Agilent Technologies 5500 scanning probe microscope, operating in acoustic AC AFM mode (tapping mode) with a silicon Asylum Research high frequency cantilever displaying a resonance frequency of 305 kHz.

Dynamic Light Scattering (DLS). Particle size analyses were carried out at 25 °C on a Malvern Zetasizer Nano-S instrument using a He-Ne laser (633 nm) and a scattering angle of 176°.

X-Ray diffraction. Single crystals of Boc-L-Cys(Me)-L-Leu-OMe (**4**) and Boc-L-Leu-L-Cys(Me)-OMe (**5**) were grown by slow evaporation from MeOH. Relevant crystal data, structure refinement parameters and details specific to the individual structures are given below (Tables S1-5). CCDC-1057628 and 1057629 contain the supplementary crystallographic data. These data can be obtained from The Cambridge Crystallographic Data Centre

(i) Single crystal X-ray diffraction data were collected with an Agilent Technologies Gemini E four-circle kappa diffractometer equipped with a 92 mm EOS CCD detector, using graphite monochromated Cu Kα radiation (λ = 1.54178 Å). Data collection and reduction were performed with the CrysAlisPro software (version 1.171.36.28; Agilent Technologies). A semi-empirical absorption correction based on the multi-scan technique using spherical harmonics, implemented in the SCALE3 ABSPACK scaling algorithm, was applied. The structures were solved by ab initio procedures of the SIR 2002 program,[22] and refined by full-matrix least-squares on F^2 using all data, by application of the SHELXL-97 program,[23]

with anisotropic displacement parameters for all of the non-H atoms. H-Atoms were calculated at idealized positions and refined using a riding model.

(ii) Powder X-ray diffraction measurements (PXRD) were carried out by means of a Bruker D8 Advance diffractometer equipped with a Göbel mirror and a Cu Kα source (40 kV, 40 mA). Powder pattern indexing was performed by use of the N-TREOR[24] software in the framework of the EXPO2013[25] package.

Materials

1-hydroxy-7-aza-1,2,3-benzotriazole (HOAt) was purchased from GL Biochem (Shanghai) Ltd. H-Cys(Me)-OH, H-Leu-OMe·HCl, Boc-Leu-OH, Fmoc-Phe-OH and N-(3-Dimethylaminopropyl)-N′-ethylcarbodiimide hydrochloride (EDC·HCl) were obtained from Iris Biotech (Germany). Trifluoroacetic anhydride, N,N'-diisopropylcarbodiimide (DIC), 2,4,6-trichloro-1,3,5-triazine, 4-(dimethylamino)pyridine (DMAP), di-tert-butyl dicarbonate (Boc_2O), thionyl chloride, propargylamine, 1,8-Diazabicyclo[5.4.0]undec-7-ene (DBU), Triethylamine (TEA), N,N,N′,N′-Tetramethylethylenediamine (TMEDA), copper(I) iodide and nickel(II) chloride hydrate were obtained from Sigma-Aldrich. The deuterated solvent DMSO-d_6, $CDCl_3$ was purchased from Euriso-Top (France). All other chemicals and solvents were purchased from Sigma-Aldrich, Fluka or Acros products and used as provided without further purifications.

H-*p*azoDbg-OH and H-*p*azoDbg-OEt have been previously synthesized in our laboratory.[7]

Synthesis and Characterizations

a) Synthesis of azobenzene-containing peptides

Tfa-*p*azoDbg-OH. To a 1:1 solution of trifluoroacetic anhydride/CH_2Cl_2 (8 mL), solid HCl·H-*p*azoDbg-OH was added. The mixture was allowed to stir under reflux for 12 h. The solvent was removed under reduced pressure and the obtained residue was dissolved in EtOAc, washed successively with 10% $KHSO_{4(aq)}$ and water, dried over Na_2SO_4, and EtOAc evaporated to dryness, giving Tfa-*p*azoDbg-OH in 90 % yield.

HRMS (ESI+): *m/z* calcd. for $C_{30}H_{24}F_3N_5O_3$ 559.1831, found 560.2048 $[M+H]^+$. FT-IR absorption: ῡ 3327, 3060, 2938, 1719, 1602, 1519 cm^{-1}. ^1H NMR ($CDCl_3$, 200 MHz) δ 3.44 (d, 2H, *J*=11.8 Hz), 3.65 (s br, 2H), 7.19 (d, 6H, *J*=7.4 Hz), 7.41-7.38 (m, 7H), 7.66-7.74 (m, 8H). ^{13}C NMR ($CDCl_3$, 50 MHz) δ 40.26, 67.89, 112.64, 118.64, 122.66, 123.14, 123.79, 129.11, 130.72, 131.34, 139.03, 151.75, 152.33, 157.00, 177.11.

Fmoc-L-Phe-*p*azoDbg-OH *t*(1). Fmoc-Phe-OH (250 mg, 0.65 mmol) and HOAt (88 mg, 0.65 mmol) were dissolved in dry DMSO (8 mL) at 0 °C. N,N'-diisopropylcarbodiimide (DIC) (79 μL, 0.65 mmol) was added and the resulting mixture was vigorously stirred for 30 min. Next, a solution of H-*p*azoDbg-OH (300 mg, 0.65 mmol) in DMSO (2 mL) was added, followed by TEA (180 μL, 1.3 mmol), and the mixture was stirred at 50 °C for 2 days. The reaction mixture was diluted with water and the resulting suspension was centrifuged. The residue obtained was taken up in EtOAc and washed successively with 10% $KHSO_{4(aq)}$, water, 5% $NaHCO_{3(aq)}$, 0.5 M HCl and water, dried over $Na_2SO_{4(aq)}$ and evaporated to dryness. Purification by flash chromatography (eluant: $CHCl_3$/MeOH 95:5) afforded pure *t*(**1**) in 78% yield.

HRMS (ESI+): *m/z* calcd. for $C_{52}H_{44}N_6O_5$ 832.3373, found 833.3887 $[M+H]^+$. FT-IR absorption: ῡ 3393, 3053, 2932, 1715, 1673, 1602, 1499 cm^{-1}. ^1H NMR (DMSO-d_6, 300 MHz) δ 2.72 (dd, 1H, *J*=15.0, 3.0Hz), 3.04 (dd, 1H, *J*=15.0, 12.0 Hz), 3.20–3.50 (m, 2H), 3.71 (d, 1H, *J*=12.5 Hz), 3.81 (d, 1H, *J*=13.0 Hz), 3.90–4.20 (m, 4H), 7.05–7.95 (m, 31H). ^{13}C NMR (DMSO-d_6, 75 MHz) δ 37.91, 47.14, 58.67, 66.65, 66.98, 120.69, 122.67, 123.09, 125.94, 126.22, 126.99, 127.79, 128.25, 128.89, 129.65, 129.95, 130.07, 130.14, 131.06, 131.79, 131.97, 139.50, 141.30, 144.55, 151.06, 151.24, 152.78, 156.36, 171.83, 172.72.

C_3 symmetrical system *t*(2). To a solution of 2,4,6-trichloro-1,3,5-triazine (39 mg, 0.16 mmol) and TEA (170 μl, 1.28 mmol) in anhydrous DMF (4 mL), solid HCl·H-*p*azoDbg-OEt (0.35 g, 0.64 mmol) was added. The mixture was allowed to stir at r.t. for 48 h. The solvent was removed under reduced pressure and the crude was purified by flash-chromatography

(eluant: $CHCl_3$/MeOH 95:5) giving ***t*(2)** as a red oil in 69 % yield.
HRMS (ESI+): *m/z* calcd. for $C_{93}H_{84}N_{18}O_6$ 1548.6821, found 1549.7334 $[M+H]^+$. FT-IR absorption: ῡ 3376, 3060, 2978, 2929, 1731, 1691, 1446 cm^{-1}. ^1H NMR (200 MHz, $CDCl_3$) δ 1.29 (t, 9H, *J* = 7.1 Hz), 2.79 (s, 3H), 3.01 (d, 6H, *J* = 13.1 Hz), 3.51 (d, 6H, *J* = 13.1 Hz), 4.18 (q, 6H, *J* = 7.1 Hz), 7.60-7.30 (m, 30H), 7.99-7.72 (m, 24H). ^{13}C NMR (200 MHz, $CDCl_3$) δ 14.38, 46.34, 61.47, 63.22, 122.58, 122.95, 123.76, 129.20, 131.14, 132.73, 137.44, 137.44, 152.73, 152.83, 175.68.

C_4 symmetrical system *t*(3). To a solution of pentaerythritol (25 mg, 0.18 mmol), Tfa-*p*azoDbg-OH (0.51 g, 0.92 mmol) and 4-(dimethylamino)pyridine (23 mg, 0.18 mmol) in 5 mL of anhydrous DMF, N,N'-diisopropylcarbodiimide (0.18 g, 1.44 mmol) was added and the reaction was allowed to stir at 50 °C for 4 days. The solvent was removed under reduced pressure and the crude was purified by flash-chromatography (eluant: CH_2Cl_2/EtOH 98:2) giving *t*(**3**) as a red glass-solid in 90 % yield.
HRMS (ESI+): *m/z* calcd. for $C_{125}H_{100}N_{20}O_{12}$ 2300.7638, found 1151.4121 $[M+2H]^{2+}$. FT-IR absorption: ῡ 3384, 3058, 2940, 1726, 1529 cm^{-1}. ^1H NMR ($CDCl_3$, 200 MHz) δ 3.30 (d, 8H, *J*= 14.0 Hz), 3.51 (d, 8H, *J*= 14.0 Hz), 3.83 (s, 8H), 6.82 (s, 4H), 7.04-7.08 (m, 16H), 7.40-7.47 (m, 24 H), 7.75-7.83 (m, 32 H). ^{13}C NMR ($CDCl_3$, 50 MHz) δ 40.71, 43.25, 63.04, 66.22, 67.13, 112.54, 118.28, 122.79, 123.26, 123.62, 124.01, 129.15, 130.48, 131.35, 137.11, 152.07, 152.55, 157.00, 170.22.

b) Synthesis of peptides containing Cys(Me)

Boc-Cys(Me)-OH. H-Cys(Me)-OH (5 g, 36.7 mmol) was dissolved in 80 mL of solvent mixture of CH_3CN/H_2O (1:1 v/v) with TEA (6 mL, 43 mmol). Boc_2O (8.4 g, 38.4 mmol) was dissolved in 25 mL of CH_3CN and added to the solution of amino acid. The mixture was stirred at r.t. for 18 h. The organic solvent was removed under reduced pressure and the aqueous residue was acidified with HCl 1M. The precipitate was extracted with EtOAc (3v), then the organic phase was washed with water (2v) and brine. The organic layer was dried over Na_2SO_4, filtered and evaporated to dryness under reduced pressure. The product was recovered as an oil (8.2 g, 94% yield).
HRMS (ESI+): *m/z* calcd. for $C_9H_{17}NO_4S$ 235.0878, found 236.1029 $[M+H]^+$. FT-IR absorption: ῡ 3318, 3103, 2979, 2924, 1716, 1510, 1394, 1368, 1249, 1164, 1056 cm^{-1}.
^1H NMR (200 MHz, $CDCl_3$) δ 7.60 (s br, 1H, COOH), 5.42 (d, *J* = 6.9 Hz, 1H, NH), 4.54 (d, *J* = 5.5 Hz, 1H, αCH), 2.97 (d, *J* = 4.6 Hz, 2H, βCH_2), 2.14 (s, 3H, SMe), 1.44 (s, 9H, $3CH_3$ Boc). ^{13}C NMR (50 MHz, $CDCl_3$) δ 175.52, 155.70, 80.74, 53.02, 36.46, 28.42, 16.39.

Boc-Cys(Me)-Leu-OMe (**4**). Boc-Cys(Me)-OH (6.76 g, 28.6 mmol) was dissolved in CH_2Cl_2 and activated with HOAt (3.9 g, 28.6 mmol) and EDC·HCl (5.48 g, 28.6 mmol). Separately H-Leu-OMe·HCl (10.4 g, 38.8 mmol) was dissolved in CH_2Cl_2 with addition of TEA (10 mL, 71.8 mmol) and the obtained solution was added to the active ester. The mixture was stirred at r.t. for 18 h. The solvent was removed under reduced pressure and the residue dissolved in EtOAc. The organic phase was washed with 5% $KHSO_{4(aq)}$ (4v), 5% $NaHCO_{3(aq)}$ (3v) and brine. The organic layer was dried over Na_2SO_4, filtered and evaporated under reduced pressure. The residue was dissolved in EtOAc and precipitated by addition of petroleum ether. After filtration and drying, the product was obtained as a white solid (8.35 g, 84% yield).
HRMS (ESI+): *m/z* calcd. for $C_{16}H_{30}N_2O_5S$ 362.1875, found 363.1966 $[M+H]^+$. FT-IR absorption: ῡ 3342, 3281, 3085, 2973, 2920, 1756, 1682, 1656, 1557, 1522, 1315, 1274, 1251, 1225, 1197, 1158, 1020 cm^{-1}. ^1H NMR (200 MHz, $CDCl_3$) δ 6.84 (d, *J* = 8.1 Hz, 1H, NH amide), 5.37 (d, *J* = 6.0 Hz, 1H, NH urethane), 4.66-4.55 (m, 1H, αCH), 4.30-4.20 (m, 1H, αCH), 3.73 (s, 3H, OMe), 2.98-2.67 (m, 2H, βCH_2 Cys), 2.17 (s, 3H, SMe), 1.68-1.60 (m, 3H, βCH_2 and γCH Leu), 1.46 (s, 9H, $3CH_3$ Boc), 0.93 (d, 6H, δCH_3 Leu). ^{13}C NMR (50 MHz, $CDCl_3$) δ 173.08, 170.68, 155.53, 80.65, 53.59, 52.46, 51.09, 41.63, 36.41, 28.40, 24.93, 22.92, 22.02, 16.04.

H-Cys(Me)-OMe·HCl. H-Cys(Me)-OH (5 g, 37 mmol) was suspended in 120 mL of dry MeOH and cooled in a MeOH/ice bath. Then $SOCl_2$ (10 mL) was added dropwise to the

mixture. After removal of the bath, the mixture was refluxed for 2 days. The residual solid was removed by filtration and the filtrate was evaporated under reduced pressure. The residue was dissolved in the minimal amount of MeOH and precipitated by addition of Et_2O. The product was recovered by filtration obtaining a white solid (4.8 g, 70% yield).
HRMS (ESI+): *m/z* calcd. for $C_5H_{11}NO_2S$ 149.0510, found 150.3091 $[M+H]^+$. FT-IR absorption: ῡ 3003, 2864, 2633, 2500, 1743, 1594, 1571, 1507, 1434, 1316, 1235, 1206, 1064 cm^{-1}. ^1H NMR (200 MHz, DMSO-d_6) δ 8.91 (s, 3H, NH_2·HCl), 4.23 (t, *J* = 5.8 Hz, 1H, αCH), 3.74 (s, 3H, OMe), 3.04 (d, *J* = 5.8 Hz, 2H, βCH_2), 2.11 (s, 3H, SMe). ^{13}C NMR (50 MHz, DMSO) δ 168.73, 52.82, 51.63, 33.37, 15.38.

Boc-Leu-Cys(Me)-OMe (**5**). Boc-Leu-OH (2 g, 8.65 mmol) was dissolved in 40 mL of CH_2Cl_2 and activated with HOAt (1.18 g, 8.67 mmol) and EDC·HCl (1.65 g, 8.64 mmol). Separately H-Cys(Me)-OMe·HCl (1.6 g, 8.62 mmol) was dissolved in CH_2Cl_2 with addition of TEA (2.4 mL, 10.7 mmol) and the solution was added to the active ester. TEA was added to the resulting mixture until basic pH. The mixture was stirred at r.t. for 48 h. The solvent was removed under reduced pressure and the residue dissolved in EtOAc. The organic phase was washed with 5% $KHSO_{4(aq)}$ (4v), 5% $NaHCO_{3(aq)}$ (3v) and brine. The organic layer was dried over Na_2SO_4, filtered and evaporated under reduced pressure. The residue was dissolved in EtOAc and precipitated by addition of petroleum ether. After filtration and drying, the product was obtained as a white solid (2 g, 64 % yield).
HRMS (ESI+): *m/z* calcd. for $C_{16}H_{30}N_2O_5S$ 362.1865, found 363.3309 $[M+H]^+$. FT-IR absorption: ῡ 3325, 2955, 2921, 1747, 1740, 1689, 1649, 1525, 1443, 1276, 1208, 1169 cm^{-1}.
^1H NMR (200 MHz, $CDCl_3$) δ 6.88 (d, *J* = 7.1 Hz, 1H, NH amide), 4.87 (d, 1H, NH urethane), 4.84 - 4.66 (m, 1H, αCH), 4.14 (d, *J* = 5.8 Hz, 1H, αCH), 3.76 (s, 3H, OMe), 2.95 (dd, 2H, βCH_2 Cys), 2.10 (s, 3H, SMe), 1.77-1.56 (m, 3H, βCH_2 and γCH Leu), 1.44 (s, 9H, 3 CH_3 Boc), 0.94 (dd, *J* = 6.1, 2.4 Hz, 6H, δCH_3 Leu). ^{13}C NMR (50 MHz, $CDCl_3$) δ 172.60, 171.23, 155.70, 80.33, 53.21, 52.74, 51.78, 41.25, 36.45, 28.42, 24.84, 23.05, 22.06, 16.32.

Boc-Cys(Me)-Leu-NH-CH_2-C≡CH (**6**). A mixture of Boc-Cys(Me)-Leu-OMe (500 mg, 1.38 mmol), propargylamine (1 mL, 15.6 mmol) and DBU (40 μL, 0.27 mmol) was stirred at r.t. for 48 h. The mixture was diluted with EtOAc and the organic phase was washed with 5% $KHSO_{4(aq)}$ (3v) and brine. The solution was dried over Na_2SO_4, filtered and the solvent was evaporated under reduced pressure. The product was obtained as a white solid (490 mg, 92 % yield).

HRMS (ESI+): *m/z* calcd. for $C_{18}H_{31}N_3O_4S$ 385.2035, found 386.2110 $[M+H]^+$. FT-IR absorption: ῡ 3283, 3079,2959, 2929, 2871, 1693, 1646, 1548, 1525, 1391, 1367, 1278, 1250, 1170 cm^{-1}. ^1H NMR (200 MHz, $CDCl_3$) δ 7.00 (s, 1H, NH amide), 6.70 (d, *J* = 8.2 Hz, 1H, NH amide), 5.41 (d, *J* = 6.2 Hz, 1H, NH urethane), 4.50 (m, 1H, αCH), 4.24 (m, 1H, αCH), 4.01 (m, 2H, CH_2 propargyl), 2.87 (d, *J* = 5.2 Hz, 2H, βCH_2 Cys), 2.19 (t, *J* = 2.5 Hz, 1H, -C≡CH), 2.14 (s, 3H, SMe), 1.91–1.52 (m, 3H, βCH_2 and γCH Leu), 1.45 (s, 9H, Boc), 0.92 (t, *J* = 6.2 Hz, 6H, δCH_3 Leu). ^{13}C NMR (50 MHz, $CDCl_3$) δ 171.42, 171.10, 155.92, 81.14, 79.46, 71.67, 54.07, 51.91, 40.61, 36.17, 29.34, 28.41, 24.92, 23.17, 21.81, 15.92.

[Boc-Cys(Me)-Leu-NH-CH_2-C≡C-]$_2$ (**7**). CuI (5 mol%) and $NiCl_2 \cdot H_2O$ (5 mol%) were dissolved in 500 μL of THF, then TMEDA (20 mol%) was added. The solution was stirred at r.t. under air for 2 min. Boc-Cys(Me)-Leu-NH-CH_2-C≡CH (500 mg, 1.30 mmol) was dissolved in 3 mL of THF. The mixture was stirred at r.t. under air for 48 h. The solvent was removed under reduced pressure and the residue was purified by flash chromatography (eluant: CH_2Cl_2/MeOH 97:3). The product was recovered as a white solid (260 mg, 50 % yield).

HRMS (ESI+): *m/z* calcd. for $C_{36}H_{60}N_6O_8S_2$ 768.3914, found 769.3878 $[M+H]^+$. FT-IR absorption: ῡ 3287, 2959, 2930, 2871, 1693, 1647, 1521, 1391, 1367, 1280, 1248, 1169 cm^{-1}. ^1H NMR (200 MHz, $CDCl_3$) δ 7.57 (t, 2H, NH amide), 7.07 (d, *J* = 8.2 Hz, 2H, NH amide), 5.51 (d, *J* = 6.9 Hz, 2H, NH urethane), 4.58 (m, 2H, αCH), 4.46–4.10 (m, 4H, αCH and CH_2 propargyl), 3.90 (m, 2H, CH_2 propargyl), 2.88 (d, *J* = 4.8 Hz, 4H, βCH_2 Cys), 2.14 (s, 6H, SMe), 1.87–1.52 (m, 6H, βCH_2 and γCH Leu), 1.46 (s, 18H, Boc), 0.92 (dd, *J* = 8.1, 6.0 Hz, 12H, δCH_3 Leu). ^{13}C NMR (50 MHz, $CDCl_3$) δ 171.65, 171.35, 155.88, 80.91, 74.39, 68.01, 54.03, 51.91, 40.71, 36.49, 30.08, 28.43, 24.93, 23.07, 21.94, 16.01.

Table S1. Crystal data and structure refinement for Boc-L-Cys(Me)-L-Leu-OMe (**4**).

Identification code	mc237f	
Empirical formula	$C_{16}H_{30}N_2O_5S$	
Formula weight	362.48	
Temperature	293(2) K	
Wavelength	1.54178 Å	
Crystal system	Hexagonal	
Space group	P 6_5	
Unit cell dimensions	a = 11.4458(2) Å	α= 90°.
	b = 11.4458(2) Å	β= 90°.
	c = 27.7551(5) Å	γ = 120°.
Volume	3148.95(10) $Å^3$	
Z	6	
Density (calculated)	1.147 Mg/m^3	
Absorption coefficient	1.580 mm^{-1}	
F(000)	1176	
Crystal size	0.20 × 0.05 × 0.01 mm^3	
Theta range for data collection	4.46 to 51.25°.	
Index ranges	$-11 \le h \le 11$, $-11 \le k \le 11$, $-27 \le l \le 27$	
Reflections collected	18290	
Independent reflections	2281 [R(int) = 0.0441]	
Completeness to theta = 51.25°	100.0 %	
Absorption correction	Semi-empirical from equivalents	
Max. and min. transmission	1.00000 and 0.81551	
Refinement method	Full-matrix least-squares on F^2	
Data / restraints / parameters	2281 / 31 / 217	
Goodness-of-fit on F^2	1.042	
Final R indices [I>2sigma(I)]	R_1 = 0.0403, wR_2 = 0.1040	
R indices (all data)	R_1 = 0.0468, wR_2 = 0.1083	
Absolute structure parameter	-0.01(3)	
Largest diff. peak and hole	0.307 and -0.145 e.$Å^{-3}$	

Table S2. Crystal data and structure refinement for Boc-L-Leu-L-Cys(Me)-OMe (**5**).

Identification code	mc238f	
Empirical formula	$C_{16}H_{30}N_2O_5S$	
Formula weight	362.48	
Temperature	293(2) K	
Wavelength	1.54178 Å	
Crystal system	Orthorhombic	
Space group	$P2_12_12_1$	
Unit cell dimensions	a = 5.08911(7) Å	α= 90°.
	b = 12.09583(13) Å	β= 90°.
	c = 32.4406(4) Å	γ = 90°.
Volume	1996.95(4) $Å^3$	
Z	4	
Density (calculated)	1.206 Mg/m^3	
Absorption coefficient	1.661 mm^{-1}	
F(000)	784	
Crystal size	0.80 × 0.06 × 0.02 mm^3	
Theta range for data collection	2.72 to 69.34°.	
Index ranges	$-5 \le h \le 4$, $-14 \le k \le 14$, $-39 \le l \le 38$	
Reflections collected	14108	
Independent reflections	3652 [R(int) = 0.0220]	
Completeness to theta = 69.34°	98.1 %	
Absorption correction	Semi-empirical from equivalents	
Max. and min. transmission	1.00000 and 0.63618	
Refinement method	Full-matrix least-squares on F^2	
Data / restraints / parameters	3652 / 50 / 245	
Goodness-of-fit on F^2	1.035	
Final R indices [I>2sigma(I)]	R_1 = 0.0391, wR_2 = 0.1077	
R indices (all data)	R_1 = 0.0406, wR_2 = 0.1091	
Absolute structure parameter	0.00(2)	
Largest diff. peak and hole	0.280 and -0.173 e.$Å^{-3}$	

Table S3. Selected backbone and side-chain torsion angles [°] for Boc-L-Cys(Me)-L-Leu-OMe (**4**) and Boc-L-Leu-L-Cys(Me)-OMe (**5**).

Boc-L-Cys(Me)-L-Leu-OMe			**Boc-L-Leu-L-Cys(Me)-OMe**		
Torsion angle			Torsion angle		
C01-OU-C0-N1	θ^1	179.0(3)	C01-OU-C0-N1	θ^1	-179.00(18)
OU-C0-N1-C1A	ω_0	-175.2(3)	OU-C0-N1-C1A	ω_0	-179.10(15)
C0-N1-C1A-C1	ϕ_1	-95.2(4)	C0-N1-C1A-C1	ϕ_1	-116.68(18)
N1-C1A-C1-N2	ψ_1	132.9(3)	N1-C1A-C1-N2	ψ_1	108.45(17)
C1A-C1-N2-C2A	ω_1	171.1(3)	C1A-C1-N2-C2A	ω_1	-173.14(15)
C1-N2-C2A-C2	ϕ_2	-66.3(4)	C1-N2-C2A-C2	ϕ_2	-159.11(15)
N2-C2A-C2-OT	ψ_2	158.5(3)	N2-C2A-C2-OT	ψ_2	-172.42(16)
C2A-C2-OT-CT	ω_T	176.6(5)	C2A-C2-OT-CT	ω_T	176.39(19
N1-C1A-C1B-S1	χ_1^1	-73.8(4)	N1-C1A-C1B-C1G	χ_1^1	-82.1(3) / -51.0(4)[a]
C1A-C1B-S1-C1D	χ_1^2	-74.4(4)	C1A-C1B-C1G-C1D1	$\chi_1^{2,1}$	65.9(5) / -58.7(9)[b]
N2-C2A-C2B-C2G	χ_2^1	-72.8(4)	C1A-C1B-C1G-C1D2	$\chi_1^{2,2}$	-171.3(3) / 178.5(6)[c]
C2A-C2B-C2G-C2D1	$\chi_2^{2,1}$	163.0(3)	N2-C2A-C2B-S2	χ_2^1	71.18(19)
C2A-C2B-C2G-C2D2	$\chi_2^{2,2}$	-74.7(4)	C2A-C2B-S2-C2D	χ_2^2	-80.84(18)

[a] Minor occupancy conformer N1-C1A-C1B-C1G'.

[b] Minor occupancy conformer C1A-C1B-C1G'-C1D3.

[c] Minor occupancy conformer C1A-C1B-C1G'-C1D4.

Table S4. Hydrogen bond parameters [Å and °] for Boc-L-Cys(Me)-L-Leu-OMe (**4**).

D-H...A	d(D-H)	d(H...A)	d(D...A)	<(DHA)
N1-H1...O0#1	0.86	2.09	2.929(4)	164
N2-H2...O1#2	0.86	2.01	2.868(4)	179
C02-H02B…OT#3	0.96	2.54	3.485(5)	168

Symmetry transformations used to generate equivalent atoms:

#1: y,-x+y,z+1/6; #2: x-y,x,z-1/6; #3: x-1, y-1, z

Table S5. Hydrogen bond parameters [Å and °] for Boc-L-Leu-L-Cys(Me)-OMe (**5**).

D-H...A	d(D-H)	d(H...A)	d(D...A)	<(DHA)
N1-H1...O0#1	0.86	2.12	2.965(2)	166.7
N2-H2...O1#2	0.86	2.25	3.093(2)	167.1

Symmetry transformations used to generate equivalent atoms:

#1: x+1,y,z; #2: x-1,y,z

References

[1] (a) J. M. Lehn, *Angew. Chem. Int. Ed.*, **1988**, *27*, 89-112; (b) J. M. Lehn, *Angew. Chem. Int. Ed.*, **1990**, *29*, 1304-1319; (c) J. M. Lehn, *Science*, **1993**, *260*, 1762-1763. (d) J. M. Lehn, *Science*, **2002**, *295*, 2400-2403.

[2] J. M. Lehn, *Proc. Natl. Acad. Sci. USA*, **2002**, *99*, 4763-4768.

[3] (a) S. Zhang, *Nature Biotechnology*, **2003**, *21*, 1171-1178; (b) R. de la Rica, H. Matsui, *Chem. Soc. Rev.*, **2010**, *39*, 3499–3509.

[4] (a) C. H. Görbitz, *Chem. Commun.*, **2006**, 2332-2334; (b) C. H. Görbitz, *Chem. Eur. J.*, **2007**, *13*, 1022-1031; (c) A. K. Das, D. Haldar, R. P. Hedge, N. Shamala, A. Banerjee, *Chem. Commun.*, **2005**, 1836-1838; (d) P. P. Bose, A. K. Das, R. P. Hedge, N. Shamala, A. Banerjee, *Chem. Mater.*, **2007**, *19*, 6150-6157.

[5] E. Gazit, *Chem. Soc. Rev.*, **2007**, *36*, 1263-1269.

[6] (a) Z. Luo, S. Zhang, *Chem. Soc. Rev.* **2012**, *41*, 4736-4754; (b) C. Valéry, F. Artzner, M. Paternostre, *Soft Matter* **2011**, *7*, 9583-9594; (c) X. Yan, P. Zhua, J. Li, *Chem. Soc. Rev.* **2010**, *39*, 1877-1890; (d) I. W. Hamley, *Angew. Chem. Int. Ed.*, **2007**, *46*, 8128-8147.

[7] P. Fatás, E. Longo, F. Rastrelli, M. Crisma, C. Toniolo, A. I. Jiménez, C. Cativiela, A. Moretto, *Chem. Eur. J.* **2011**, *17*, 12606-12611.

[8] M. Mba, D. Mazzier, S. Silvestrini, C. Toniolo, P. Fatás, A. I. Jiménez, C. Cativiela, A. Moretto *Chem. Eur. J.* **2013**, *19*, 15841-15846.

[9] D. Mazzier, F. Carraro, M. Crisma, M. Rancan, C. Toniolo, A. Moretto *Soft Matter*, **2015**, 10.1039/c5sm02189h.

[10] M. Reches, E. Gazit, *Science* **2003**, *300*, 625-627.

[11] (a) Y. Zhang, H. Gu, Z. Yang, B. Xu, *J. Am. Chem. Soc.* **2003**, *125*, 13680-13681; (b) S. Sutton, N. L. Campbell, A. I. Cooper, M. Kirkland, W. J. Frith, D. J. Adams, *Langmuir* **2009**, *25*, 10285-10291; (c) Z. Yang, H. Gu, D. Fu, P. Gao, J. K. Lam, B. Xu, *Adv. Mater.* **2004**, *16*, 1440-1444.

[12] (a) C.-D. Chang, M. Waki, M. Ahmad, J. Meienhofer, E. O. Lundell, J. D. Haug, *Int. J. Pept. Protein Res.* **1980**, *15*, 59-66; (b) H. Cao, X. Zhu, M. Liu, *Angew. Chem. Int. Ed.* **2013**, *52*, 4122-4126.

[13] I. M. Rio-Echevarria, R. Tavano, V. Causin, E. Papini, F. Mancin, A. Moretto, *J. Am. Chem. Soc.* **2011**, *133*, 8-11.

[14] S. Lee, S. Oh, J. Lee, Y. Malpani, Y.-S. Jung, B. Kang, J. Y. Lee, K. Ozasa, T. Isoshima, S. Y. Lee, M. Hara, D. Hashizume, J.-M. Kim, *Langmuir* **2013**, *29*, 5869-5877.

[15] (a) S. Ray, D. Haldar, M. G. B. Drew, A. Banerjee, *Org. Lett.*, **2004**, *6*, 4463–4465; (b) M. Crisma, C. Toniolo, S. Royo, A. I. Jiménez, C. Cativiela, *Org. Lett.*, **2006**, *8*, 6091–6094; (c) U. S. Raghavender, Kantharaju, S. Aravinda, N. Shamala, P. Balaram, *J. Am. Chem. Soc.*, **2010**, *132*, 1075–1086; U. S. Raghavender, B. Chatterjee, I. Saha, A. Rajagopal, N. Shamala, P. Balaram, *J. Phys. Chem. B*, **2011**, *115*, 9236–9243.

[16] A. Bianco, K. Kostarelos, C. D. Partidos, M. Prato, *Chem. Commun.*, **2005**, 571-577.

[17] G. Frens, *Nature Phys. Sci.*, **1973**, *241*, 20-22.

[18] H. Erdogan, E. Babur, M. Yilmaz, E. Candas, M. Gordesel, Y. Dede, E. E. Oren G. B. Demirel, M. K. Ozturk, M. S. Yavuz, G. Demirel, *Langmuir*, **2015**, *31*, 7337-7345.

[19] E. C. de Lima, C. C. de Souza, R. de O. Soares, B. Gontijo Vaz, M. N. Eberlin, A. G. Dias, P. R. R. Costa, *J. Braz. Chem. Soc.*, **2011**, *22*, 2186-2190.

[20] W. Yin, C. He, M. Chen, H. Zhang, A. Lei, *Org. Lett.*, **2009**, *11*, 709-712.

[21] R. Jelinek, M. Ritenberg *RSC Adv.*, **2013**, *3*, 21192-21201.

[22] M. C. Burla, M. Camalli, B. Carrozzini, G. L. Cascarano, C. Giacovazzo, G. Polidori, R. Spagna, *J. Appl. Crystallogr.*, **2003**, *36*, 1103.

[23] G. M. Sheldrick, *Acta Crystallogr.*, **2008**, *A64*, 112-122.

[24] A. Altomare, G. Campi, C. Cuocci, L. Eriksson, C. Giacovazzo, A. Moliterni, R. Rizzi, P.-E. Werner, *J. Appl. Crystallogr.*, **2009**, *42*, 768-775.

[25] A. Altomare, C. Cuocci, C. Giacovazzo, A. Moliterni, R. Rizzi, N. Corriero, A. Falcicchio, *J. Appl. Crystallogr.*, **2013**, *46*, 1231-1235.

List of Publications

[1] M. Mba, D. Mazzier, S. Silvestrini, C. Toniolo, P. Fatás, A. I. Jiménez, C. Cativiela, A. Moretto, *Chem. Eur. J.*, **2013**, *19*, 15841-15846;

[2] D. Mazzier, C. Peggion, C. Toniolo, A. Moretto, *Biopolymers (Pept. Sci.)*, **2014**, *102*, 115-123;

[3] D. Mazzier, M. Mba, M. Zerbetto, A. Moretto, *Chem. Commun.*, **2014**, *50*, 4571-4574;

[4] D. Mazzier, M. Favaro, S. Agnoli, S. Silvestrini, G. Granozzi, M. Maggini, A. Moretto, *Chem. Commun.*, **2014**, *50*, 6592-6595;

[5] D. Mazzier, M. Maran, O. Polo Perucchin, M. Crisma, M. Zerbetto, V. Causin, C. Toniolo, A. Moretto, *Macromolecules*, **2014**, *47*, 7272-7283;

[6] S. Bartocci, D. Mazzier, A. Moretto, M. Mba, *Org. Biomol. Chem.*, **2015**, *13*, 348-352;

[7] D. Mosconi, D. Mazzier, S. Silvestrini, A. Privitera, C. Marega, L. Franco, A. Moretto, *ACS Nano*, **2015**, *9*, 4156–4164;

[8] D. Mazzier, F. Carraro, M. Crisma, M. Rancan, C. Toniolo, A. Moretto, *Soft Matter*, **2016**, *12*, 238-245.

Ringraziamenti

Al termine di questi tre anni di dottorato desidero ringraziare tutte le persone che a vario titolo mi hanno accompagnata e sostenuta in questo percorso, rendendo possibile la realizzazione di questo progetto.

In primo luogo vorrei ringraziare il mio supervisore, il Prof. Alessandro Moretto, perché è proprio merito suo se ho deciso di avventurarmi nel mondo della ricerca. Gli sono grata per la sua costante disponibilità, per la fiducia riposta nelle mie capacità, per avermi coinvolta in molti progetti creativi e dinamici, e per tutte le cose che da lui ho potuto imparare.

I would like to thank Prof. Jonathan Clayden for giving me the opportunity to work in his research group as a visiting student. It has been a great experience working in his laboratory and being part of his group. The experience wouldn't have been the same without all the people that I had the pleasure to meet in Manchester.

Inoltre, un sentito ringraziamento va rivolto a tutte le persone che fanno parte del nostro gruppo di ricerca, in primis, ai Professori Claudio Toniolo e Fernando Formaggio per avermi permesso di crescere in un contesto scientifico altamente stimolante. Desidero esprimere la mia riconoscenza alle Dottoresse Cristina Peggion, Marta De Zotti e Miriam Mba per il supporto con gli esperimenti NMR più complessi; alla Dott.ssa Barbara Biondi per gli spettri di massa e al Dott. Renato Schiesari per gli spettri IR. Infine, ringrazio il Dott. Marco Crisma per la risoluzione delle strutture molecolari tramite diffrazione di raggi X e per tutti i preziosi suggerimenti che mi ha saputo dare.

Alcuni dei risultati discussi in questa Tesi e le pubblicazioni che ne sono state ricavate sono state possibili grazie a diverse collaborazioni all'interno del nostro dipartimento. Desidero quindi esprimere la mia gratitudine a tutti coloro che hanno contribuito a vario titolo, ringraziandoli idealmente uno ad uno.

Voglio, inoltre, ringraziare tutti i colleghi dottorandi e laureandi con cui ho condiviso non solo la vita di laboratorio ma che ho avuto il piacere di conoscere anche al di fuori dell'ambito accademico.

Un grazie enorme, infine, alla mia famiglia, a grandi e piccoli che ne fanno parte, per non avermi mai fatto mancare il fondamentale sostegno morale che mi ha permesso di raggiungere questo traguardo.